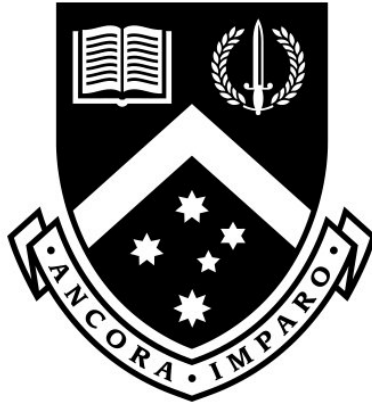# Mitochondrial damage control: delineating the mechanisms of mitochondrial repair

Louise Uoselis

BSc (Hons)

Biomedicine Discovery Institute

Department of Biochemistry and Molecular Biology

Monash University

A thesis submitted for the degree of Doctor of Philosophy

May 2022

Copyright notice

Declaration

This thesis is an original work of my research and contains no material which has been accepted for the award of any other degree or diploma at any university or equivalent institution and that, to the best of my knowledge and belief, this thesis contains no material previously published or written by another person, except where due reference is made in the text of the thesis.

Signature: ……………………

Print Name: Louise Uoselis

Date: 24th May 2022

Publications during enrolment

Padman, B.S., Nguyen, T.N., **Uoselis, L**. et al. LC3/GABARAPs drive ubiquitin-independent recruitment of Optineurin and NDP52 to amplify mitophagy. *Nat Commun* 10, 408 (2019).

Nguyen, T.N, Padman, B.S., Zellner, S., **Uoselis, L.**, Skulsuppaisarn, M., Watts, E.M., Behrends, C., Lazarou, M. (2021). Atg4 family proteins drive phagophore growth independently of the LC3/GABARAP lipidation system. *Mol Cell* 9, 81 (2021)

Acknowledgements

I would like to start by acknowledging my supervisory team. To Meagan, Georg and Thomas, thank you for making the PhD process painless and for your enthusiasm and interest in my work. Ralf, thank you for being the directional light at the end of the tunnel when I didn't know where I was going. Michael, please see below.

To Jo, thank you for your early mentorship during my undergraduate days. I always strived to reach the same level of your achievement and your knowledge, and that endeavour has helped propel me to where I am today.

To Ryan lab members, both past and present, thank you for being such great next-door neighbours. I must give a special mention to Marris and Felix who took me under their wing as the young, naïve PhD student on the block and showed me the ropes. Maddie too, thank you for indulging in our 'lab experiments' that some may call childish. I for one still remember those times fondly.

To Thanh and Ben – thank you for making me feel like a part of the team and not just a student. Discoveries take confidence and the environment you helped foster gave me that confidence and made it unwavering. Perhaps too unwavering. Grace, thank you for putting up with me. Emily and Marvin, thank you for being such great PhD lab mates and sharing in the tribulations that come with a PhD.

And now lastly, Michael – it seems wholly insufficient to try and summarise the support and guidance you've awarded me over the last 6 years in a short paragraph, but I will give it a go. Thank you for taking a chance on an undergraduate student with no special track record who messaged you out of the blue 6 years ago. Thank you for invigorating my love and passion for science that I had once lost before I found your work and your lab but is now lit by a flame I truly hope never goes out. Thank you for taking the time to then teach me your bench skills, your precision, and your work ethic. Thank you for teaching me the unscientific components of a career in science that are usually learnt through self-exposure. Thank you for giving me both the freedom and the guidance to grow into the researcher I am now. Thank you for trusting in me that I would use these lessons well. I am the researcher I am today because of your mentorship and for that I will forever be indebted to you for your support. They say we see further though standing on the shoulders of giants; what I achieve in the future will be through the foundations you helped me set, so in saying that, I hope I have done and will continue to make you proud of the career I hope is only beginning.

Lastly, thank you for creating such a great lab.

Abstract

Mitochondrial health is maintained in our cells through the actions of the mitochondrial quality control machinery. Two major mitochondrial quality control pathways function in mammals: the PINK1/Parkin mitophagy pathway and the mitochondrial unfolded protein response (UPR^{mt}). PINK1/Parkin mitophagy involves the sequestration and degradation of severely damaged mitochondria. In contrast, the UPR^{mt} repairs damaged mitochondria through the transcriptional upregulation of mito-protective factors. In comparison to our comprehensive mechanistic understanding of the PINK1/Parkin mitophagy pathway, comparatively little is understood about how the UPR^{mt} program is signalled, and how the UPR^{mt} protects and repairs mitochondrial proteostasis and function. Additionally, as PINK1/Parkin mitophagy and the UPR^{mt} have mostly been examined in isolation, we have minimal understanding of how cells balance between repairing and degrading damaged mitochondria, and whether signalling interactions between each pathway help facilitate this balance. The work in this thesis sought to improve our mechanistic understanding of the UPR^{mt} and to examine the interplay between PINK1/Parkin mitophagy and the UPR^{mt}. Analyses of mitochondria subjected to a protein folding stress revealed that the transcription factors CHOP, ATF4 and ATF5 each regulate independent arms of the UPR^{mt}. A novel method of analysing the functional proteostasis of the mitochondrial proteome using mass spectrometry was developed to allow for functional characterisation of the UPR^{mt}. Temporal analysis of mitochondrial proteostasis during an acute stress and then recovery from that stress revealed that each arm of the UPR^{mt}, driven by CHOP, ATF4 or ATF5, facilitates non-redundant, widespread protection of proteostasis across the mitochondrial proteome. Subsets of the mitochondrial proteome were highly sensitive to proteostatic damage including complex I, metabolism related proteins and the mitochondrial transcription and translation machinery. In particular, the UPR^{mt} was found to play essential roles in protecting the mitochondrial ribosome and facilitating repair of OXPHOS complexes to restore their function. Transcriptomic analyses of UPR^{mt} signalling demonstrated that each of CHOP, ATF4 and ATF5 undertake proteostasis protection and repair through unique transcriptional signatures with areas of interaction and overlap in the genes and pathways affected by each transcription factor. Integrated analysis of PINK1/Parkin mitophagy and UPR^{mt} activity revealed a unidirectional signalling relationship between the pathways and a novel role of the UPR^{mt} in sustaining PINK1/Parkin mitophagy activity during proteostasis repair. Taken together, this work has improved our mechanistic understanding of the UPR^{mt} and its interplay with PINK1/Parkin mitophagy and their fundamental roles in maintaining mitochondrial health.

Table of Contents

Abbreviations

~	Approximately
24 h R	24 hours recovery
48 h R	48 hours recovery
AARS2	Alanyl-tRNA synthase 2
ABCB10	ATP-binding cassette sub-family B member 10
ACN	Acetonitrile
ADP	Adenosine diphosphate
AFG3L2	AFG3-Like matrix AAA peptidase subunit 2
Ag85A	Diacylglycerol acyltranferase/mycolyltransferase
AGC	Automatic gain control
AI	Aggregation index
Ara-C	Cytosine β-D-arabinofuranoside
ATF	Activating transcription factor
ATF4	Activating transcription factor 4
ATF5	Activating transcription factor 5
ATFS-1	Stress activated transcription factor atfs-1
Atg8	Autophagy-related protein 8
ATP	Adenosine triphosphate
Bak	Bcl-2 homologous antagonist/killer
BAX	Bcl-2-like protien 4
BCA	Bicinchoninic assay
BCAA	Branched chain amino acids
BCKDHA	Branched Chain Keto Acid Dehydrogenase EI subunit alpha
BCKDHB	Branched Chain Keto Acid Dehydrogenase EI subunit beta
BCL2L13	BCL2-like 13
BME	Basal Medium Eagle
BP	Biological process

bp	base-pair
BSA	Bovine serum albumin
C. elegans	Caenorhabditis elegans
CAA	Chloroacetamide
cDNA	Complimentary DNA
CHOP	DNA damage-inducible transcript 3 protein
CI	Complex I
CID	Collision-induced dissociation
CII	Complex II
CIII	Complex III
CIV	Complex IV
CLPB	Caseinolytic peptidase B protein homolog
ClpP	Caseinolytic mitochondrial matrix peptidase proteolytic subunit
CRISPR	Clustered regularly interspaced short palindromic repeats
Ct	Cycle threshold
CTBP1	C-Terminal Binding Protein 1
CV	Complex V
Da	Dalton
DA neuron	Dopaminergic neuron
DARS2	Aspartyl-tRNA Synthase 2
DELE1	DAP3 Binding Cell Death Enhancer 1
DFCP1	Zinc finger FYVE domain-containing protein 1
DFP	Deferiprone
DIV	Days in vitro
DKK	Dickkopf genes
DMEM	Dulbecco's Modified Eagle Medium
DMSO	Dimethyl sulfoxide
DNA	Deoxyribonucleic acid
DPBS	Dulbecco's phosphate-buffered saline
DSS	Dextran sodium sulfate
DTT	Dithiothreitol
DVE-1	Defective proventriculus homologue
E Coli	Escherichia coli
EBSS	Earle's balanced salt solution
EDTA	Ethylenediaminetetraacetic acid

EP300	E1A Binding Protein P300
ER	Endoplasmic reticulum
ETC	Electron transport chain
EtOH	Ethanol
F	Forward
FA	Formic acid
FACS	Fluorescence activated cell sorting
FBS	Foetal bovine serum
FCCP	Carbonyl cyanide-4-(trifluoromethoxy)phenylhydrazone
FDR	False discovery rate
FOS	Cellular oncogene FOS
FOXO1	Forkhead box protein O1
GABARAP	Gamma-aminobutyric acid receptor-associated protein
gDNA	Genomic DNA
GFP	Green fluorescent protein
GO	Gene ontology
GRSF1	G-Rich GNA Sequence Binding Factor 1
G-TPP	Gamitrinib-triphenylphosphonium
GWAS	Genome-wide association study
h	Hours
HDAC1/2	Histone deacetylase 1 and 2
	Heme-Regulated Eukaryotic Initiation Factor EIF-2-Alpha
HRI	Kinase
HSP10	Heat shock protein 10
HSP60	Heat shock protein 60
HSP90	Heat shock protein 90
HtrA2	HtrA Serine Peptidase 2
IB	Immunoblot
IMM	Inner mitochondrial membrane
INDELs	Insertions/deletions
ISR	Integrated stress response
IT	Injection time
JUN	Jun Proto-oncogene
KD	Knockdown
kDa	Kilodalton

KO	Knockout
LB	Luria-Bertani media
LC3	Microtubule-associated protein 1A/1B-light chain 3
LONP1	Lon Peptidase 1
LRG4	Leucine Rich Repeat Containing G Protein-Coupled Receptor 4
LRPPRC	Leucine Rich Pentatricopeptide Repeat Cassette
LRRK2	Leucine Rich Repeat Kinase 2
m/z	mass/charge
MAS	Mitochondrial assay solution
MAX	MYC Associated Factor X
MeOH	Methanol
MET-2	Histone-lysine N-methyltransferase
METTL15	Methyltransferase Like 15
METTL15P1	Putative methyltransferase-like protein 15P1
MF	Molecular function
Mfn1/2	Mitofusin 1 and 2
min	Minutes
mito-proteome	Mitochondrial proteome
Mitoribosome	Mitochondrial ribosome
MPP	Mitochondrial processing peptidase
MRM2	Mitochondrial rRNA Methyltransferase 2
mRNA	Messenger RNA
MRPS27	Mitochondrial Ribosomal Protein S27
ms	Millisecond
mtDNA	Mitochondrial DNA
mtHSP90	Mitochondrial HSP90
mtKeima	Mitochondrial targeted keima
MTO1	Mitochondrial tRNA Translation Optimization 1
mTOR	Mammalian target of rapamycin
MTS	Mitochondrial targeting sequence
MW	Molecular weight
MXI1	MAX interactor 1
MYC	MYC Proto-Oncogene
NDP52	Nuclear dot protein 52 kDa
NDUFS1	NADH:Ubiquinone Oxidoreductase Core Subunit S1

NDUFS3	NADH:Ubiquinone Oxidoreductase Core Subunit S3
NFY	Nuclear Transcription Factor Y
NFYB	Nuclear Transcription Factor Y Subunit Beta
NFYC	Nuclear Transcription Factor Y Subunit Gamma
NGS	Next-Generation sequencing
NLS	Nuclear localisation sequence
NP-40	Nonidet P-40
Nrf2	Nuclear factor-erythriod factor 2-related factor 2
NSUN4	NOP2/Sun RNA Methyltransferase 4
O. faveolata	Orbicella faveolata
OA	Oligomycin/antimycin A
OMM	Outer mitochondrial membrane
OPA1	Optic-atrophy 1
OPTN	Optineurin
OTC	Ornithine transcarbamylase
OXPHOS	Oxidative phosphorylation
p62	sequestome-1
PAM	Presequence translocase-associated protein import motor
PARL	Presenilin Associated Rhomboid Like
PBS	Phosphate buffered saline
PCA	Principle component analysis
PCP	Planar cell polarity
PCR	Polymerase chain reaction
PD	Parkinson's disease
PDK4	Pyruvate dehydrogenase lipoamide kinase isozyme 4
PE	Phosphatidylethanolamine
PGAM5	Serine/threonine-protein phosphatase PGAM5
PGAM5-L	PGAM5 - long isoform
PGAM5-S	PGAM5 - short isoform
PI	Phosphatidylinositol
PI(3)P	Phosphatidylinositol-3-phosphate
PI3K	Phosphatidylinositol-3-kinase
PINK1	PTEN-induced kinase 1
pS65-Ub	Phosphorylated (S65) ubiquitin
PTM	Post translational modification

PVDF	Polyvinylidene difluoride
qRT-PCR	Quantitative reverse transcription PCR
R	Reverse
RNA	Ribonucleic acid
RNAi	RNA interference
ROS	Reactive oxygen species
rpm	Rotations per minute
rRNA	Ribosomal RNA
RT	Room temperature
S. cerevisiae	Saccharomyces cerevisiae
SATB1/2	Special AT-rich sequence binding protein-1 and 2
SDS	Sodium dodecyl sulfate
SDS-PAGE	Sodium dodecyl sulfate-polyacrylamide gel electrophoresis
sec	Seconds
SHMT2	Serine hydroxymethyltransferase-2
SMAD2	SMAD Family Member 2
SMAD3	SMAD Family Member 3
SNIP1	Smad Nuclear Interacting Protein 1
SPG7	Paraplegin
TAE	Tris-acetate EDTA
TAX1BP1	TAX1-binding protein 1
TCA	Trichloroacetic acid
TCEP	Tris(2-carboxyethyl)phosphine
TEA	Triethanolamine
TEAB	Triethylammonium bicarbonate
TFA	Trifluoroacetic acid
TIMM	Translocase of the inner mitochondrial membrane
TKO	CHOP/ATF4/ATF5 triple knockout
TMT	Tandem-mass tag
TOMM	Translocase of the outer mitochondrial membrane
tRNA	Transfer RNA
TUJ1	Neuron-specific class III beta-tubulin
TX-100	TritonX100
U	Unit
Ub	Ubiquitin

UBE2L3	Ubiquitin-conjugating enzyme E2 L3
UBL5	Ubiquitin Like 5
ULK1	Unc-51 Like Autophagy Activating Kinase 1
UPR	Unfolded protein response
UPRer	Endoplasmic reticulum unfolded protein response
UPRmt	Mitochondrial unfolded protein response
V	Volts
VCP	Valosin-containing protien
VDAC1/2	Voltage-dependent anion channel 1 and 2
WIPI2	WD repeat domain phosphoinositide-interacting protein 2
YFP	Yellow fluorescent protein
YME1L1	YME1 Like 1 ATPase
YY1	Yin Yang 1
ΔOTC	Mutated ornithine transcarbamylase

Chapter 1

Introduction

Among the many organelles in eukaryotic cells are mitochondria, the sites of a myriad of metabolic processes that are integral for proper cell function. Mitochondria are perhaps best known for their role as the major site of adenosine triphosphate (ATP) generation, the energy currency that drives most chemical processes in a cell (*1*). No less important though are the additional roles of mitochondria, including the biosynthesis of heme (*2*) and certain phospholipids (*3*) and nucleotides (*4*), production of metabolites involved in epigenetic regulation of gene expression (*5*), acting as signalling platforms for innate immune responses (*6*), and driving controlled cell death through the intrinsic pathway of apoptosis (*7*). Due to the diverse cellular roles played by mitochondria, mitochondrial dysfunction can cause catastrophic problems in multiple pathways throughout the cell (*8*). To counteract the development of mitochondrial dysfunction, intrinsic processes within mitochondria and dedicated mitochondrial quality control pathways continually monitor the health of mitochondria and respond with appropriate cellular programs to mitigate mitochondrial damage and maintain the health of the mitochondrial network.

1.1: Fundamentals of mitochondrial biology

Mitochondria are organised into dynamic interconnected networks which undergo continual cycles of fission and fusion (*9*). Highly conserved large GTPase proteins mediate fission and fusion of mitochondrial membranes to facilitate mitochondrial biogenesis, quality control, and adaptations to changing nutrient requirements of the cell (*10, 11*). Owing to their ancestral bacterial origin, mitochondria comprise two lipid-bilayer membranes that must fuse and divide; an outer mitochondrial membrane (OMM), and a separate inner mitochondrial membrane (IMM) that is

organised into a tightly folded structure termed the cristae which encapsulates the matrix of mitochondria (*12*). Housed in the cristae are the five protein complexes of the electron transport chain (ETC), Complexes I – V, which generate a proton gradient across the IMM through the reduction of oxygen (*13*). The electrochemical energy of the proton gradient is converted into chemical energy in the form of ATP by Complex V, which is then exported for use in nearly every energy-dependent cellular process (*14*).

Mitochondria contain DNA in the form of mitochondrial DNA (mtDNA) nucleoids in the mitochondrial matrix which is a relic of their bacterial origin (*15*). The mtDNA encodes both ribosomal RNA and transfer RNA molecules, as well as 13 key components of the mitochondrial respiratory chain that are transcribed and translated within the mitochondrial matrix (*16*). All protein components of mitochondrial ribosomes are encoded by DNA in the nuclear genome and must be imported into mitochondria and then assembled into mature protein complexes (*17*). Due to the double membrane structure of mitochondria, all nuclear DNA encoded proteins must be imported in their unfolded state (*18, 19*). Given that ~99% of mitochondrial proteins are encoded by the nuclear genome (*20*), this positions the protein import machinery and mitochondrial protein quality control pathways as central regulators of mitochondrial function. An overview of these fundamentals of mitochondrial biology can be found in Figure 1.1.
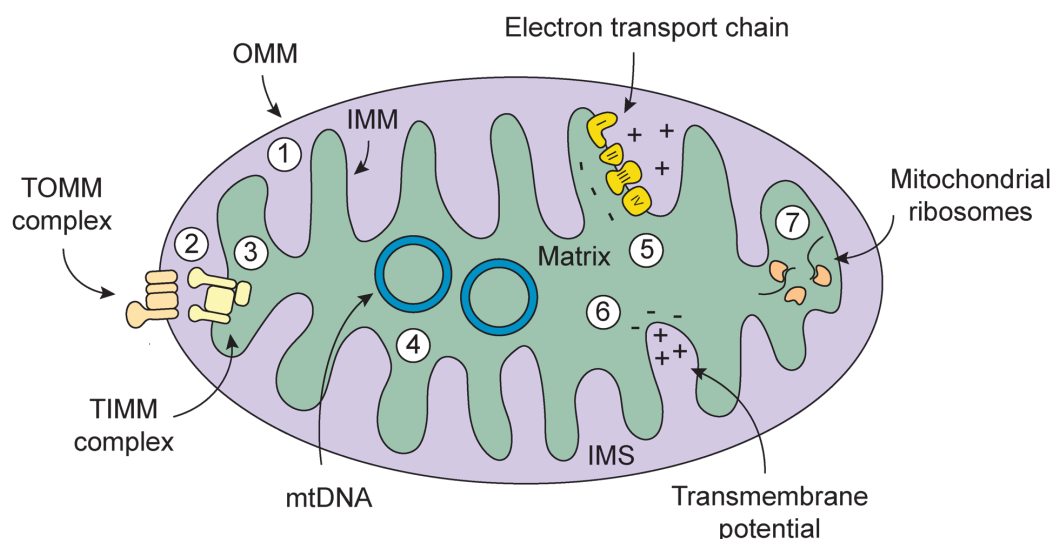
Figure 1.1 **Fundamentals of mitochondrial biology.** Key aspects of mitochondrial biology include **(1)** the two limiting phospholipid bilayer membranes, **(2)** the TOMM complex that mediates protein import through the OMM, **(3)** the TIMM complex that mediates protein import across the IMM, **(4)** mtDNA nucleoids that are present in varying numbers per organelle, **(5)** the electron transport chain (ETC) situated in the cristae, **(6)** the transmembrane potential across the IMM, and **(7)** mitochondrial ribosomes that translate mtDNA products. The area between the OMM and IMM is termed the intermembrane space (IMS), while the area encapsulated by the IMM is termed the matrix.

Proteins imported into mitochondria are typically targeted to the mitochondria by sequences of approximately 10 – 90 amino acids located at the N-terminus of the peptide chain, termed the mitochondrial targeting sequence (MTS) (*21, 22*). While MTS sequences do not share homology in their amino acid composition, they typically comprise a large number of positively charged and hydrophobic residues which form an α-helical structure that is recognised by the protein import machinery (*21, 23*). The translocase of the outer mitochondrial membrane (TOMM) complex mediates import of all nuclear encoded mitochondrial proteins across the OMM (*24*). Depending on the nature of their mitochondrial targeting sequence (MTS) composition, proteins will then be either inserted into the IMM, retained for assembly in the intermembrane space (IMS), or imported across the translocase of the inner mitochondrial membrane (TIMM) complex into the matrix (*24*). Transport through the TIMM complex is dependent on an intact trans-membrane potential across IMM which facilitates passage of the peptide chain through the TIMM channel by electrostatic attraction of the positively charged MTS with the electronegative matrix side of the IMM (*25, 26*). Proteins destined for the mitochondrial matrix require an additional translocation complex termed the presequence translocase-associated motor (PAM) that drives movement of the full peptide sequence into the matrix space through ATP hydrolysis (*27, 28*). The metallomembrane protease (MPP) then cleaves the MTS of matrix-destined proteins to allow for maturation and assembly of the peptide chain, either during PAM mediated translocation or shortly after its completion (*29*).

Assembly of peptide chains into their native forms and larger complexes in both the IMS and the matrix space is mediated by a host of mitochondrial protein folding chaperones and chaperonins. Chaperones in the mitochondria function similarly to their cytosolic and endoplasmic reticulum (ER) resident counterparts by binding to hydrophobic residues in peptide chains to maintain peptide solubility and prevent aggregation during formation of the native protein structure (*30, 31*). Mitochondrial chaperonins such as mitochondrial HSP90 (mtHSP90) also play integral roles in protein folding in the mitochondrial matrix by providing an isolated chamber for peptides to fold (*32, 33*). However, while chaperones can help facilitate correct folding, protein folding may still fail and peptide chains will then collapse and begin to aggregate, which is a fate estimated to occur to ~30% of all newly synthesised proteins (*34*). Removal of these aggregates is performed by the varied family of proteases that localise within various mitochondrial compartments (*31*). Every biological process within mitochondria relies on the correct translation, import, and assembly of proteins encoded by either mtDNA or nuclear DNA, so it is imperative that adequate pools of chaperones and proteases are present within mitochondria to provide a sufficient protein folding and quality control capacity to produce enough correctly assembled protein complexes.

The chaperones and proteases that comprise the mitochondrial protein folding machinery are summarised in Figure 1.2.
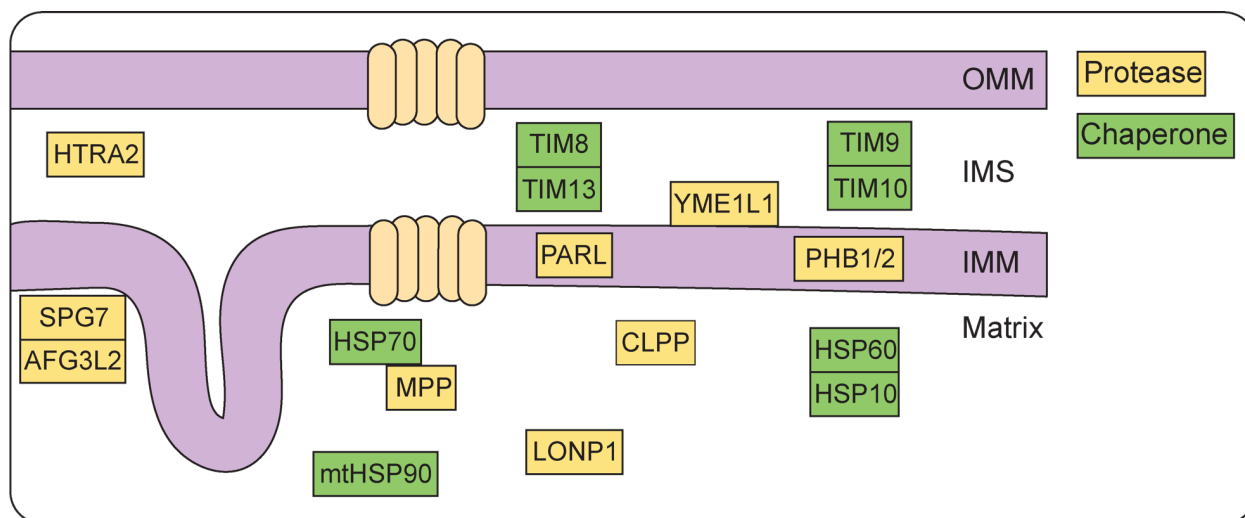
Figure 1.2 **Distribution of the mitochondrial protein folding machinery**. Distinct mitochondrial specific proteases (yellow) and chaperones (green) are located throughout the mitochondria to assist in compartment protein folding and quality control.

1.1.1: Mitochondrial damage

Like a well-oiled machine, healthy mitochondria function as a harmonious chain of biological processes that link together to provide the energy and metabolites required to power our cells. However, as with any system reliant on chain events, if any component of the chain fails, the effects will flow on to subsequent links and cause breakdown of the system. In the context of the mitochondrial machine, dysfunction of any component, such as mitochondrial import, can have systemic, cell wide effects on processes that rely on mitochondrial function including immune responses which use mitochondria as signalling platforms (*35*), cellular processes that utilise mitochondrial metabolites including nuclear DNA replication (*36*), and all biological processes that rely on the ATP or other metabolites generated by mitochondria (*37*). As mitochondria contain the factors that govern the intrinsic pathway of apoptosis, severe mitochondrial damage also risks triggering unwanted cell death if mitochondrial membranes were to rupture (*38*). To appreciate how important maintaining mitochondrial function is to our health, we simply need to look at the diverse disease pathologies associated with mitochondrial dysfunction, including but not limited to insulin resistance (*39*), metabolic syndrome (*40*), cardiomyopathy (*41*), neurodegeneration (*42*), aging (*43*) and cancer (*44*). Boosting mitochondrial function in various disease models, including

mouse models of Alzheimer's disease (*45*) and Duchenne muscular dystrophy (*46*), has been shown to prevent disease progression or reduce disease severity, demonstrating the central role mitochondrial health plays in these pathologies. To protect the integrity of our mitochondrial network and prevent the development of disease, dedicated mitochondrial quality control pathways monitor mitochondrial health and quickly attend to signs of dysfunction

1.2: Mitochondrial quality control pathways

Two major mitochondrial quality control pathways that monitor and respond to changes in mitochondrial health are a) PINK1/Parkin mitophagy and b) the mitochondrial unfolded protein response, which will be discussed in detail below.

1.2.1: PINK1/Parkin Mitophagy

Severe mitochondrial damage leads to the selective removal of individual mitochondria through a degradative pathway termed PINK1/Parkin mitophagy. Damaged mitochondria are sequestered by a double membrane vesicle termed an autophagosome which subsequently fuses with the lysosome where the mitochondrial cargo is degraded (*47*).

In healthy mitochondria, the serine/threonine kinase PINK1 is constitutively imported through the OMM and degraded by proteolytic cleavage in the IMS by the metalloprotease PARL (*48-50*). However, when mitochondrial import is disrupted through mitochondrial dysfunction or damage, PINK1 becomes trapped in the TOMM complex where it is thought to be laterally released into the OMM (*48*). Once stabilised on the OMM, PINK1 phosphorylates the S65 residue on resident ubiquitin (Ub) chains located on mitochondrial surface proteins (*51*). Phosphorylated S65 Ub (pS65-Ub) acts as a platform to recruit the E3 ubiquitin ligase, Parkin (*51, 52*). Once bound to pS65-Ub, Parkin undergoes a conformational change leading to partial activation of Parkin's Ub ligase activity (*53*). The conformational change also promotes Parkin phosphorylation by PINK1 at an analogous S65 residue within Parkin's ubiquitin like domain which results in maximal activation (*53-57*). Parkin conjugates Ub chains onto numerous OMM proteins thereby providing additional ubiquitin substrate for PINK1 to phosphorylate (*58*). This creates a positive feedback loop of Parkin recruitment and activation that amplifies the generation of pS65-Ub on the mitochondrial surface (*58, 59*). In addition to amplifying the damage-signal, ubiquitination of OMM proteins tags them for proteasomal degradation (*60, 61*). Although Parkin does not appear to have specific substrates, certain OMM substrates appear to be preferentially ubiquitinated and

degraded by the proteosome (*58*). Among these proteins are the mitochondrial fusion factor Mfn1/2 (*62*), and apoptosis related factors including BAX, Bak and VDAC1/2 (*62*). Degradation and inactivation of the fusion machinery serves to segregate severely damaged mitochondria from the wider mitochondrial network, preventing the transmission of pathogenic mitochondrial components to healthy mitochondria, such as ROS and protein aggregates. A summary of PINK1/Parkin mitophagy activation can be found in Figure 1.3.
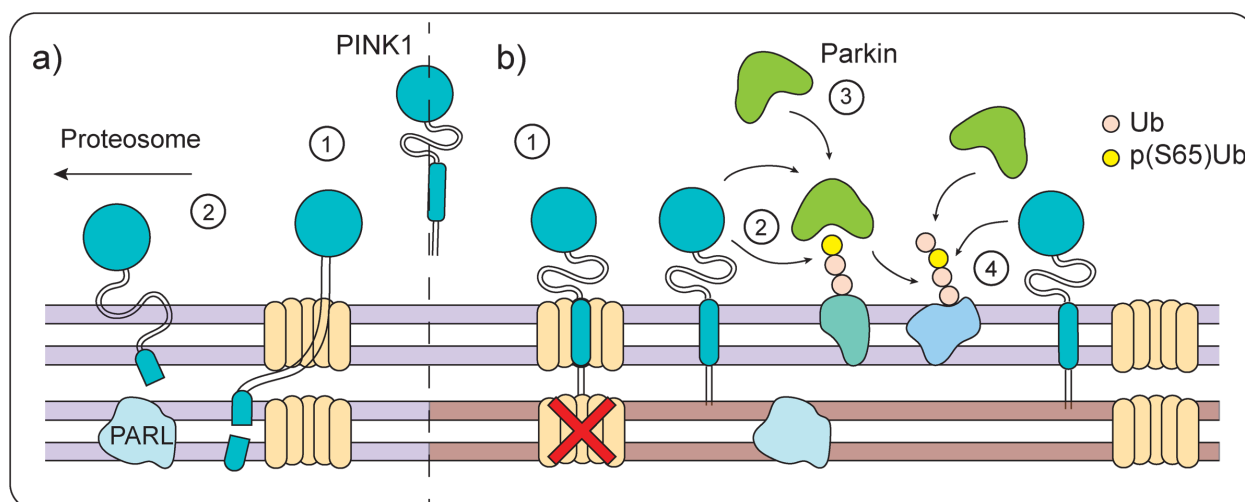
Figure 1.3 **PINK1/Parkin mitophagy**. **A**. 1 - In healthy mitochondria, PINK1 is constitutively imported through the TOMM channel. 2 - After import, cleavage by PARL releases PINK1 for degradation by the N-end rule in the proteasome. **B**. 1 - In damaged mitochondria with a disrupted IMM membrane potential, PINK1 import is arrested at the TOMM complex and PINK1 remains attached to the OMM. 2 – PINK1 phosphorylates resident Ub chains on the OMM. 3 – Phosphorylated Ub recruits Parkin, which is then phosphorylated by PINK1 to induce activation of Parkin Ub ligase activity. 4 – Activated Parkin on the OMM adds additional Ub chains to OMM proteins, providing additional Ub substrate for PINK1 to phosphorylate, generating a positive feedback cycle that amplifies the strength and speed of the mitophagy stress signal.

In addition to Parkin, pS65-Ub recruits the specialised mitophagy receptor proteins NDP52, OPTN and TAX1BP1 to the mitochondrial surface (*63*). These mitophagy receptors begin a recruitment cascade of the protein and lipid machinery required to construct autophagosomes around damaged mitochondria (*64*). Autophagy receptors initiate autophagosome biogenesis by binding a multi-subunit kinase complex referred to as the ULK1 kinase complex (*63, 65*). In turn, the ULK1 complex recruits and activates a phosphoinositol-3-kinase (PI3K) complex characterised by the catalytic subunit Vps34 (*66*). Phosphorylation of phosphatidyl-inositol (PI) to generate PI(3)P triggers the recruitment of various PI(3)P binding proteins including DFCP1 and WIPI2 to the growing membrane structure commonly known as the phagophore (*67, 68*). Both PI(3)P lipid and

WIPI2 then recruit sequential ubiquitin-like conjugation machineries that ultimately lead to the lipidation of the Atg8 family of LC3 and GABARAP proteins to phosphatidyl ethanolamine (PE) to facilitate the expansion of the growing autophagosome (*69-71*). Lipidated Atg8 proteins are capable of recruiting further mitophagy receptors to the growing autophagosome, creating an additional positive feedback loop that amplifies the speed at which damaged mitochondria become encapsulated by an autophagosome (*72*). Once the autophagosomal structure seals and sequesters the mitochondrion within its limiting membrane, the fully formed autophagosome fuses with a lysosome whereby the inner membrane is degraded, and the damaged mitochondrion is released to the hydrolytic environment of the lysosome where it is degraded (*47*). While detailed, this summary of autophagosome biogenesis is by no means complete. A schematic summary of autophagosome biogenesis during PINK1/Parkin mitophagy can be found in Figure 1.4.

Due to the continual fission and fusion of the mitochondrial network, mitophagy provides a way to remove dysfunctional and pathogenic components of a damaged mitochondrion from the mitochondrial pool. Without targeted removal of segments of severely damaged mitochondria, those components will instead diffuse throughout the mitochondrial network and presumably accumulate as the cell ages causing widespread mitochondrial network disruption. Accordingly,
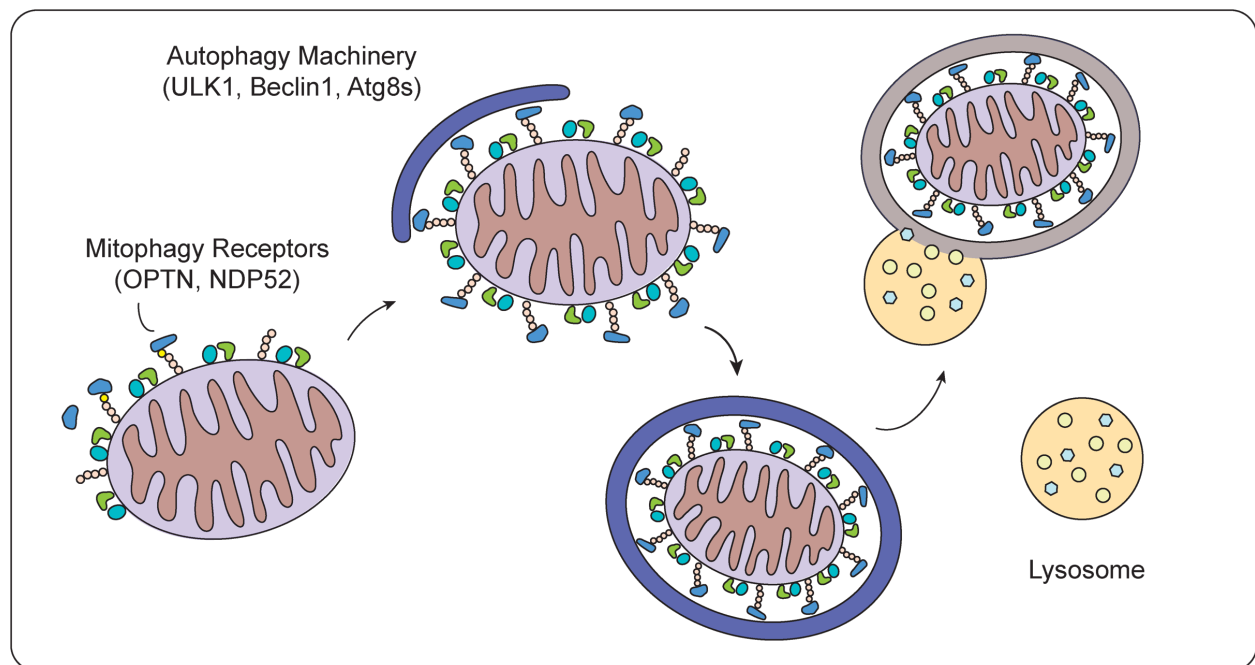
Figure 1.4 **Autophagosome biogenesis around damaged mitochondria**. Phosphorylated Ub recruits the mitophagy receptors OPTN and NDP52 that begin a sequential recruitment cascade of autophagosome biogenesis machinery to the mitochondrial surface. The damaged mitochondria becomes enveloped by a double membraned vesicle termed an autophagosome, which then fuses with a lysosome and delivers the damaged mitochondrial cargo to the hydrolytic environment of the lysosome for degradation.

decreases in mitophagy that correspond with decreases in mitochondrial respiratory capacity and an accumulation of mitochondrial DNA mutations are seen in ageing related pathogeneses (*73*), positioning mitophagy as a protective mechanism that, while energy intensive in the short-term, ensures cells retain the capacity to produce the required energy over an organism's life.

1.2.2: The mitochondrial unfolded protein response (UPR^mt)

Sources of mitochondrial dysfunction can be varied, and mitochondria are complex organelles that require considerable energy expenditure by the cell to construct. Degradation of entire organelles when select components of the mitochondrial machine are dysfunctional would be an inefficient way of restoring mitochondrial network homeostasis. Instead, the mitochondrial unfolded protein response (UPR^mt) pathway monitors and proactively repairs mitochondrial damage. The UPR^mt is a transcriptional program characterised by an increase in expression of mitochondrial chaperones and proteases in response to an accumulation of aggregated protein within mitochondria. A variety of stress stimuli can cause aggregation of mitochondrial proteins, including mutations to mtDNA (*74*), heat stress (*75*) and excess ROS generation (*76*).

1.2.2 - The UPR^mt (*C. elegans*)

While the UPR^mt pathway was initially identified in mammals by the Hoogenraad laboratory in 2002 (*77*), the majority of studies examining the UPR^mt have been performed in *Caenorhabditis elegans* (*C. elegans*). An elegant UPR^mt signalling pathway responding directly to the aggregation of proteins within the mitochondrial matrix has been delineated in the *C. elegans* model system. The UPR^mt pathway in *C. elegans* centres around a molecular sensor of mitochondrial proteostasis – the transcription factor termed ATFS-1, which contains both an MTS and a nuclear localisation sequence (NLS). In healthy mitochondria with a sufficient protein folding capacity, ATFS-1 is readily imported into the matrix space where it is then degraded by the Lon protease (*76*). However, when there are changes to the protein folding capacity of mitochondria, aggregated proteins accumulate and begin to be degraded by the protease ClpP (*78*). The short peptides generated by ClpP are exported through the IMM barrier by the Haf-1 transporter channel and are then thought to diffuse through the more permeable OMM to the cytosol (*79*). While it is unknown mechanistically how this next event occurs, the export of peptides by Haf-1 has been shown to directly result in inhibited mitochondrial import that biases ATFS-1 translocation to the nucleus (*79*).

Concurrently with the changes in ATFS-1 translocation, the export of peptides generated by ClpP leads to the nuclear localisation of LIN-65, a cofactor of the histone methyltransferase MET-2. Together, LIN-65 and MET-2 demethylate histone H3K9 which leads to selective compaction of specific areas of chromatin while leaving other areas loose and accessible (*80*). The nuclear transcription factor DVE-1 binds to the "loose" areas of DNA together with ATFS-1 to induce a selective upregulation in the transcription of not only mitochondrial chaperones and proteases, but also genes involved in global cellular pathways such as innate immunity and ROS defences that help boost cell fitness during mitochondrial stress (*78, 81*). A schematic summary of the UPR[mt] pathway in *C. elegans* is shown in Figure 1.5.

While a comparative analysis of transcripts induced within *C. elegans* with abrogated ATFS-1 expression compared to *C. elegans* with abrogated DVE-1 expression has not been published, many observations in the literature indicate that ATFS-1 and DVE-1 control two distinct UPR[mt] pathways. Firstly, although ClpP expression is required for LIN-65 and DVE-1 redistribution, the peptide transporter Haf-1 that is critical for ATFS-1 signalling is in fact dispensable (*79, 80*). Additionally, ATFS-1 suppression through RNAi enhances LIN-65 nuclear localisation and does not affect mitochondrial protein folding stress mediated chromatin reorganisation (*80*). Suppression of either ATFS-1 or LIN-65/MET-2 by RNAi also only leads to partial suppression of the UPR[mt] program induced in wild-type *C. elegans* undergoing mitochondrial protein folding stress (*76, 80, 82, 83*). Lastly, it is well documented that mitochondrial protein folding stress during early development of *C. elegans* leads to lifespan extension through UPR[mt] activation (*82, 84*). Abrogation of ATFS-1 in multiple studies only partially supresses the early mitochondrial stress induced lifespan extension (*80, 85*). Work from the Dillin laboratory has shown that abrogation of both ATFS-1 and MET-2 is required for a full abolition of lifespan extension induced by early mitochondrial stress (*80*). While the signalling events that mediate transmission of an unfolded protein stress signal at the mitochondria to the LIN-65/MET-2/DVE-1 axis in the nucleus are unclear, there is still strong evidence to suggest that ATFS-1 and LIN-65/MET-2/DVE-1 function in independent pathways during the UPR[mt] in *C. elegans*.
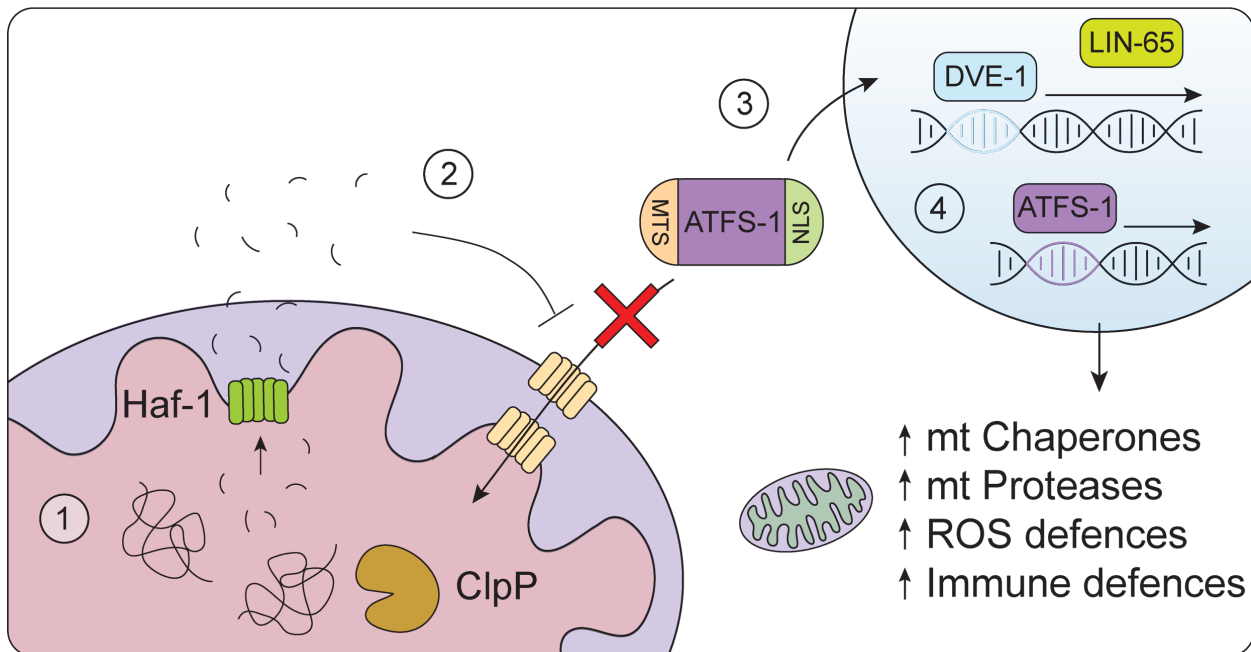
Figure 1.5 *C. elegans* **UPR^mt pathway.** 1 – Protein aggregates within the matrix are digested by ClpP to generate peptide fragments. 2 – Peptide fragments are exported to the cytosol, where they inhibit mitochondrial import. 3 – ATFS-1 is no longer constitutively imported into the mitochondria and degraded. Instead, atfs-1 translocates to the nucleus. 4 – ATFS-1, together with DVE-1 and LIN-65 mediate chromatin rearrangement and induction of mitochondrial protein folding machinery, ROS defences and immune pathways, together boosting mitochondrial health and cellular defences to allow for mitochondrial repair.

1.2.2 - The UPR^mt (mammals)

Analysis of cellular responses to mitochondrial protein folding stress in mammalian systems has illustrated that, similar to *C. elegans*, the mammalian UPR^mt is characterised by a mitochondrial protein-folding stress-specific induction of mitochondrial chaperones and proteases (*86*). However, global responses to mitochondrial protein folding stress, such as the alterations in metabolic and immune related pathways seen in *C. elegans,* have not yet been investigated in a mammalian system, therefore the extent of conservation in the pathways induced during the mammalian and *C. elegans* UPR^mt is unclear. To date, most research into the mammalian UPR^mt pathway has focussed on attempting to identify homologues to main factors in the *C. elegans* pathway, but conflicting information has instead emerged to suggest that considerable evolutionary divergence in UPR^mt signalling has occurred between *C. elegans* and mammals.

The most upstream UPR^mt related factor in *C. elegans* is the protease ClpP. Homologous proteases to ClpP are present in mammals, however, their central role in the UPR^mt pathway is controversial. Cell-based studies using murine intestinal epithelial cells have demonstrated that suppression of ClpP activity using a small molecule inhibitor of ClpP is sufficient to abolish HSP60 induction

during dextran sodium sulphate (DSS) treatment, and these findings have been reinforced in ClpP knockout (KO) C2C12 cells undergoing protein folding stress through aberrant decreases in mitochondrial translation (*87, 88*). However, studies examining the white adipose tissue of ClpP-/- mice revealed elevated levels of UPR^mt specific markers such as HSP60, HSP40 and Lon in adipose tissue, suggesting a constitutive activation of the UPR^mt may occur in the absence of ClpP (*89*). Similarly, a loss of ClpP in mice with defective mitochondria translation through ablation of DARS2 expression (a mitochondrial tRNA synthase) did not alter UPR^mt signalling in heart tissue (*90*). Ablation of ClpP expression in HEK293T cells also did not affect UPR^mt signalling during inhibition of the SPG7 protease (*90*), questioning whether ClpP is required for the mammalian UPR^mt.

ABCB10, a member of the ABC transporter family in mitochondria has been proposed as a mammalian orthologue of Haf-1. Depletion of ABCD10 in two separate studies produced a marked decrease in mRNA levels of UPR^mt related proteins including HSP60, HSP90 and LONP1 (*91, 92*). However, ABCB10 depletion did not alter the peptide efflux from mitochondria, so the mechanism by which it may be participating in UPR^mt signalling is unclear (*91*). It is worth noting that ABCB10 plays a critical role in heme biosynthesis which is required as a metabolic cofactor during OXPHOS and many other cellular processes (*93, 94*). Decreases in heme in ABCB10 KO models may be additional sources of mitochondrial and cellular stress that are not isolated to mitochondrial protein aggregation stimuli, making it difficult to ascertain whether signalling events in ABCB10 KO models are representative of an isolated UPR^mt signalling pathway.

The sparse conservation of the mammalian and *C. elegans* UPR^mt pathway extends to the signalling molecules driving the nuclear portion of the UPR^mt. Three main transcription factors, CHOP, ATF4 and ATF5, have been independently identified to drive the mammalian UPR^mt program. ATF5 has been identified as a homologue of the central *C. elegans* UPR^mt signalling factor, ATFS-1. The mammalian transcription factor ATF5 has both an NLS and an MTS, and quite remarkably has been shown to be capable of rescuing the loss of ATFS-1 in *C. elegans* (*95*). Knockdown of ATF5 in human cells was reported to prevent induction of HSP60, mtHSP70 and LONP1 in response to mitochondrial unfolded protein stress, supporting the notion that ATF5 plays a central role in the mammalian UPR^mt (*95*). However, knockdown of a key component of the mitochondrial import machinery, Tim23, leads to negligible induction of ATF5 expression, while still leading to the induction of other UPR^mt related factors such as HSP10 and ClpP (*96*). The lack of ATF5 induction with import disruption suggests that while ATF5 is capable of functioning synonymously to ATFS-1 in *C. elegans*, a different, non-import dependent method of UPR^mt induction may exist in mammals. Both DVE-1 and UBL-5 (a cofactor of DVE-1 required

during the UPR^{mt} (*97*)) have mammalian homologues in SATB1/2 and UBL5 respectively. Like DVE-1, SATB1/2 demonstrates similar preferential localisation to "loose" regions of chromosomes (*98, 99*). However, no studies at this time of writing have examined the role of the mammalian homologues to the DVE-1 mediated arm of *C. elegans* in the mammalian UPR^{mt}.

The main transcription factor that has reproducibly been shown to be induced during mitochondrial unfolded protein stress in mammals is CHOP. Promoter regions of mitochondrial proteases ClpP, YME1L1 and MPPβ have CHOP consensus sequences, as does the mitochondrial chaperone HSP60 (*86, 91*). Mutation of the DNA binding domain of CHOP prevents HSP60 upregulation during mitochondrial protein folding stress, suggesting that CHOP upregulation is a core component of the UPR^{mt} program (*91*). However, there is no apparent homologue of CHOP in *C. elegans*, reinforcing that there is a limit to the knowledge we can gain regarding the mammalian UPR^{mt} through studying the *C. elegans* system. The identification of an UPR^{mt} related role of CHOP further complicates our understanding of the UPR^{mt} pathway in mammals. Historically, CHOP is most well characterised as an integrated stress response (ISR) related factor (*100*) (a summary of the ISR can be found in Figure 1.6), and the ISR can be triggered by generalised mitochondrial damage (*101*). Additionally, the canonical ISR-related transcription factor, ATF4, is upregulated during mitochondrial protein folding stress in mammals (*102*). No role of atf-4 in driving the UPR^{mt} in *C. elegans* has been identified to date. Accordingly, it remains to be seen whether the UPR^{mt} represents a distinct signalling pathway in mammals, similar to the endoplasmic reticulum UPR (UPR^{er}), or whether it is simply an extension of the ISR. Activation of the ISR related kinase GCN-2 is observed during mitochondrial protein folding stress in *C. elegans*, but its activation occurs by mechanisms independent of UPR^{mt} activation, indicating the UPR^{mt} and ISR pathways are delineated in *C. elegans* (*103*). It remains to be seen whether this delineation is a point of conservation in mammals.

Recent genome-wide CRISPR screens looking for drivers of transcription factor expression during mitochondrial stress have identified the IMM/IMS resident protein DELE1 as a key molecule required for the transmission of the stress signal to the nucleus (*104, 105*). During mitochondrial stress, DELE1 is cleaved by OMA1, and the cleaved form of DELE1 is released into the cytosol where it interacts with the ISR-related enzyme HRI that drives stress response pathway activation through phosphorylation of the cytosolic ribosome subunit eIF2α (*104, 105*). Although DELE1 is a mitochondrial protein, and DELE1 activity is required for CHOP and ATF4 induction during mitochondrial stress, it is not yet understood how the stress response signal is tailored to mitochondrial stress. The mechanism of eIF2α phosphorylation that DELE1 uses to relay the
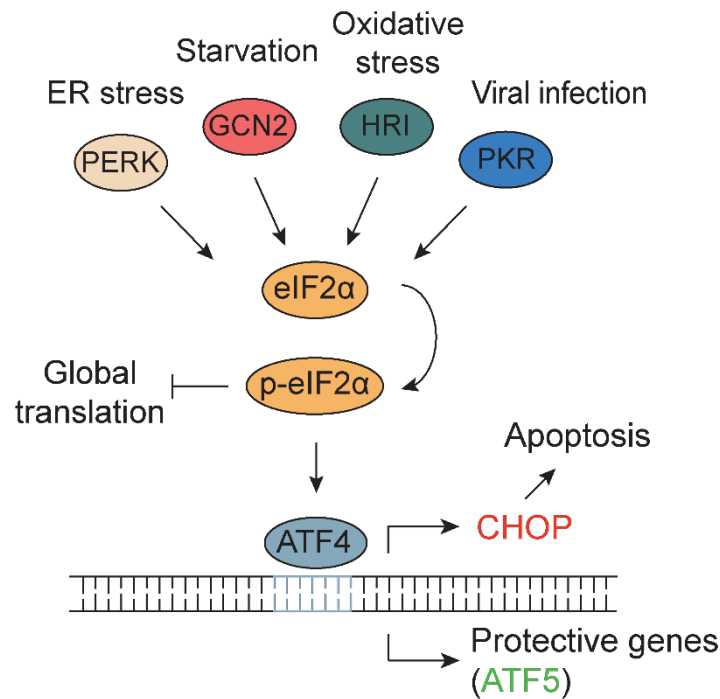
Figure 1.6 **The Integrated Stress Response (ISR)**. The integrated stress response is a transcriptional program that is activated in response to a wide variety of different stressors. Each stressor leads to the homodimerization and activation of a kinase complex (PERK, GCN2, HRI or PKR) that then phosphorylates the eIF2α component of the ribosome assembly complex required for cap-dependent translation (*106*). Phosphorylation of eIF2α inhibits global translation (*107, 108*), while allowing for select translation of stress related proteins with inhibitory upstream open reading frames in their mRNA transcripts (*109*). Induction of ATF4 regulates the ISR program, and ATF4 begins a transcription cascade of genes that boost cell health and function, including ATF5 (*110*). If cellular damage is severe, ATF4 induces CHOP expression, and CHOP induces expression of genes involved in the initiation of apoptosis (*111, 112*).

mitochondrial stress signal represents a common node of ISR signalling that can be activated by a wide variety of stressors that are not necessarily mitochondrial in origin (*100*). Accordingly, the tailored transcriptional responses observed with mitochondrial stress cannot be explained solely through DELE1 activity and must be occurring through additional signalling pathways (*77*). Similar to CHOP, no orthologue of DELE1 has been identified in *C. elegans*, positioning DELE1 activity as another key point of divergence between mammalian and *C. elegans* UPR^mt signalling. A summary of the currently proposed mammalian UPR^mt can be found in Figure 1.7.

Specific cellular responses to mitochondrial protein folding stress have also been identified in other organisms. Inactivation of the Lon protease (*113*) or mutation of mtHSP90 (*114*) in *Drosophila melanogaster* leads to an accumulation of aggregated mitochondrial proteins, and a corresponding increase in mitochondrial proteases and chaperones, indicative of an UPR^mt program. More recently, an UPR^mt program has been identified in a species of coral found in the

Caribbean, *Orbicella faveolata*. Of-ATF5, a putative homologue of ATFS-1/ATF5, was identified in *O. faveolata* and together with HSP60 and mtHSP70 was found to be induced in response to thermal stress (*115*). Importantly, Of-ATF5 can rescue an ATFS-1 loss of function (LOF) mediated defect in mitochondrial chaperone induction during mitochondrial protein folding stress in *C. elegans*, supporting the notion that this is a legitimate, conserved UPR^mt response identified in *O. faveolata*. In summary, while there may be divergences in the signalling pathway of the UPR^mt between different organisms, the identification of a UPR^mt pathway in both land and marine invertebrates and mammals suggests that there is conservation in the presence of mitochondrial proteostasis repair pathways throughout evolution.
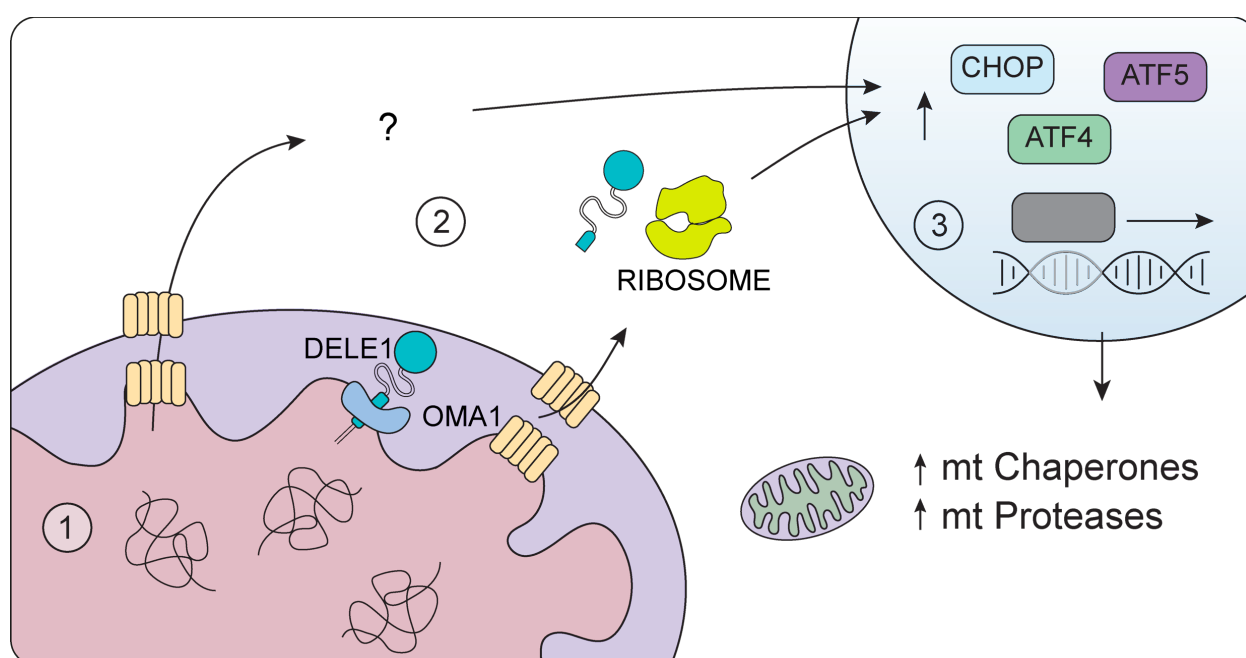
Figure 1.7 **The mammalian UPR^mt pathway.** 1 – Protein aggregates accumulate within the matrix. 2 – DELE1 is cleaved by OMA1 and released to the cytosol, which alters ribosomal activity that together with an unknown mitochondrial signal transmits mitochondrial stress to the nucleus. 3 – Levels of CHOP, ATF4 and ATF5 are increased which activates transcription of mitochondrial protein folding machinery, repairing dysfunctional mitochondria

1.3: Mitochondrial quality control in disease

As demonstrated earlier, if not remedied by PINK1/Parkin mitophagy or the UPR^mt, mitochondrial dysfunction has the capacity to cause systemic and catastrophic disruptions to the cell. While defects in select components of mitochondria have been shown to contribute to the pathogenesis of a variety of diseases, including Type II diabetes (*116*) and select cancers (*117*), defective mitochondrial quality control maintenance manifests strongly through neurodegenerative

phenotypes. Mitochondrial quality control is particularly important for post-mitotic tissue like the neurons in our brain, since if mitochondrial damage is not sufficiently mitigated and apoptosis occurs, neuronal cells cannot replicate to replace the dead cell and instead the tissue degenerates (*118*). Neurons are also highly reliant on ATP to power synaptic transmissions, and have smaller tolerance limits for mitochondrial dysfunction (*119*).

The connection between defects in the PINK1/Parkin mitophagy pathway and the development of Parkinson's disease (PD), a disease characterised by the loss of dopaminergic neurons, is perhaps the clearest example of the link between defective mitochondrial network maintenance and the development of neurodegeneration. Loss of function mutations in both PINK1 and Parkin are causative for familial, early onset PD development and together represent approximately 20% of all familial PD cases (*120*). Cell-based models have robustly demonstrated the defective clearance of dysfunctional mitochondria in the absence of either Parkin or PINK1 (*47, 121*). In addition, PD patient pathologies including increased inflammatory blood markers, excessive ROS production and disruption of cellular energy pools, have all been linked to mitochondrial dysfunction eventuating through inadequate mitochondria quality control (*122-126*). Recently, mice deficient in Parkin were shown to experience widespread inflammation through mtDNA release from severely damaged mitochondria that could not be degraded by PINK1/Parkin mitophagy, reinforcing that many of the pathogenic phenotypes seen in PD can result from inadequate mitochondrial quality control (*124*).

Additional causative mutations for PD development have also recently been linked to disruptions in the PINK1/Parkin mitophagy pathway. Mutations in LRRK2, like PINK1 and Parkin, are causative in familial PD (*127*), and changes in LRRK2 kinase activity have been associated with the development of idiopathic PD (*128*). While the exact function of LRRK2 is unknown, recently it was shown that PD related mutations in LRRK2 conferred a pathogenic increase in kinase activity of LRRK2 (*129*). Increased LRRK2 activity appears to inhibit lysosomal function, preventing the degradation of damaged mitochondria in addition to other autophagic cargo (*130*). Complete abolition of PINK1/Parkin mitophagy does not occur in the cell-based models of LRRK mutations studied, suggesting that inhibition rather than complete abolition of the PINK1/Parkin mitophagy arm may be sufficient to cause neurodegeneration (*129*).

While the role of long-term mitochondrial quality control in the prevention of neurodegeneration is robustly established in relation to PINK1/Parkin mitophagy, our understanding of how the UPR^{mt} pathway contributes to neuronal health is less clear. We do not currently have a comprehensive enough understanding of the signalling components of the mammalian UPR^{mt} pathway to be able to identify components mutated in disease pathologies. However, factors

involved in the UPR^mt transcriptional response have been identified as causative agents for numerous diseases. For example, mutations in the SPG7 gene encoding paraplegin, a subunit of the mAAA+ protease, have been identified as causative factors for the development of spastic paraplegia (*131*), spastic ataxia (*132*) and opthalmoplegia (*131*). More recently mutations in SPG7 have also been associated with late-onset ataxia at a frequency of up to 18.6% in one British cohort (*133*). The mutations identified in the British cohort are loss-of-function mutations that would prevent assembly of the hetereo-oligomeric form of the mAAA+ complex that is also comprised of the AFG3L2 protease subunit. While accumulation of aggregated or misfolded proteins has not been assayed in patient or mouse models of SPG7-/- or AFG3L2-/-, RNAi mediated silencing of SPG-7 in *C. elegans* is a viable method of inducing the UPR^mt pathway (*134*), suggesting aggregation of mitochondrial proteins or an inability to mount a complete UPR^mt program may contribute to the disease pathology characteristic of ataxias and paraplegias.

Loss of function mutations in another mitochondrial protease, HtrA2, have also been identified as causative mutations in a subset of hereditary Parkinson's disease patients (*135*). A progressive movement disorder resembling PD pathology is also seen in HtrA2-/- mouse models, reinforcing the causative nature of HtrA2 mutation (*136, 137*). Interestingly, global ablation of HtrA2 expression in mice leads to an accumulation of unfolded proteins in mitochondria and an induction of CHOP expression specifically in brain tissue (*137*). However, CHOP induction in HtrA2-/- mice was not accompanied by detected increases in HSP60 or ClpP mRNA levels, raising the question of whether the CHOP induction observed with HtrA2-/- is through ISR related upregulation rather than activation of the UPR^mt (*137*).

A confounding factor making it difficult to assess the relative involvement of the UPR^mt in neurodegenerative phenotypes is again, the prevalence of CHOP induction in other stress response pathways and the systemic nature by which mitochondrial dysfunction can trigger other cell stress responses. As discussed in Chapter 1.2.2, severe mitochondrial dysfunction independent of mitochondrial protein folding stress can trigger CHOP induction through both ISR and UPR^er related pathways, where CHOP has been shown to facilitate cell death through induction of apoptosis. Ablation of CHOP expression in the HtrA2-/- model, as well as other models of PD pathology using neurotoxic agents prevents or reduces loss of dopaminergic (DA) neurons supporting the notion that some of the CHOP induction seen in PD models may be due to ISR activation (*137-139*). However, transcriptional analysis of mouse dopaminergic neurons treated with the neurotoxin MPP+, which induces PD like symptoms in mammals through Complex I inhibition, displayed decreases in ER UPR and ISR related transcripts including XBP1, BiP and DNAJB9 (*140*). Together with CHOP, transcripts of ATF3 and CEBP/β were increased in the

MPP+ PD model, and both these genes are induced during acute mitochondrial protein folding stress (*141, 142*).

Both PINK1/Parkin mitophagy and components of the UPR^{mt} appear to be involved in maintaining our neuronal health. A question raised is whether these pathways can act in a compensatory manner and how compensation may affect the presentation of neuronal diseases. Numerous animal models of PD in organisms including *C. elegans*, *Drosophila*, mice and rats have been developed based on PINK1 and Parkin loss of function. However, unlike in human pathology, many of these models require additional mitochondrial stressors to elicit neurodegeneration (a summary of the major PD related animal models of PINK1 and Parkin loss of function can be found in Figure 1.8). For example, Parkin -/- mice are neurotypically normal, but DA neuron loss and motor defects are seen if a Parkin -/- mouse is crossed with a mouse expressing a defective mitochondrial DNA polymerase that introduces mtDNA mutuations (*143*). Furthermore, PINK1 -/- mice only display DA neurodegeneration when an additional stressor such as expression of a misfolding protein in the mitochondrial matrix (*144*) or αSy expression is present (*145, 146*). Ablation of the PINK1/Parkin mitophagy pathway alone may not generate a sufficient basal mitochondrial stress in these models, and an additional quality control pathway such as the UPR^{mt} may be compensating for low levels of mitochondrial damage, before becoming overwhelmed with additional mitochondrial stress. Simultaneous ablation of the UPR^{mt} and PINK1/Parkin mitophagy through deletion of ATFS-1 and PINK1 or Parkin in *C. elegans* is sufficient to cause DA neuron degeneration in the absence of extra mitochondrial stressors, supporting the idea that PINK1/Parkin mitophagy and UPR^{mt} may be compensating for each other in these model systems (*147*).

Indeed, there is robust evidence in both animal and cell-based models to suggest that PINK1/Parkin mitophagy and the UPR^{mt} may cooperatively govern mitochondrial health. Induction of mitochondrial protein folding stress in *Drosophila* leads to increases in UPR^{mt} related factors such as HSP60 and mtHSP70, combined with mitochondrial fragmentation and the formation of punctate LC3B structures indicative of mitophagy activation (*148, 149*). Severe IMS-based protein folding stress has also been shown to activate mitophagy (*150*), suggesting mitophagy may act as a secondary response to the UPR^{mt} by removing mitochondria that the UPR^{mt} pathway has failed to repair. Additionally, selective mitophagy can be stimulated by protein aggregates within mitochondria with an intact membrane potential, suggesting mitophagy may compliment UPR^{mt} activation (*11*). While direct evidence examining mitophagy induction during protein folding stress in *C. elegans* has not been published, the *C. elegans* UPR^{mt} factor ATFS-1 displays the same import dependent mechanism of activation as PINK1 during PINK1/Parkin

mitophagy, so it seems reasonable to conclude that observations of concurrent activation of PINK1/Parkin mitophagy and the UPR^{mt} in other model systems are likely to be recapitulated in *C. elegans*. It is clear from prior literature that both PINK1/Parkin mitophagy and the UPR^{mt} regulate mitochondrial health. However, as each pathway has been studied in isolation to date, how cells balance between degrading or repairing mitochondria, and whether there are signalling mechanisms that facilitate the interplay between these two pathways is unknown.

Animal	Genotype	Phenotypes with ageing	Phenotypes with mitochondrial stress
Human	PINK1 LOF	Early onset DA neurodegeneration, motor defecits [151, 152]	N/A
	Parkin LOF	Early onset DA neurodegeneration, motor defecits [151, 152]	N/A
Mouse	PINK1 -/-	Mitochondrial dysfunction [153]	Motor deficits, DA neuron death (ΔOTC expression)[144] ; DA neuron death (αSy OE)[145]; increased inflammation (exhaustive exercise)[124]
	Parkin -/-	Mitochondrial dysfunction [154]	Mitochondrial dysfunction, motor defecits, DA neuron death (POLG^{D257A})[143] ; increased inflammation (exhaustive exercise)[124]
	PINK1 -/- Parkin -/-	Mitochondrial dysfunction [155]	N/A
Rat	PINK1 -/-	Motor defects, DA neuron death [156, 157]	N/A
	Parkin -/-	Phenotypically normal[156]	N/A
Drosophila	Pink1 -/-	Mitochondrial dysfunction, motor defects, DA neuron death [158]	N/A
	parkin -/-	Mitochondrial dysfunction, motor defects, DA neuron death [159]	N/A
C. elegans	pink-1 -/-	Mitochondrial dysfunction[147]	Phenotypically WT with excessive oxidative stress [147]
	pdr-1 -/-	Mitochondrial dysfunction[147]	Phenotypically WT with excessive oxidative stress [147]
	pink-1 -/- atfs-1 -/-	Mitochondrial dysfunction, DA neuron loss [147]	N/A
	pdr-1 -/- atfs-1 -/-	Mitochondrial dysfunction, DA neuron loss [147]	N/A

Figure 1.8 **Overview of the PD related phenotypes observed in animal models of PINK1 and Parkin loss of function compared to PD pathologies in Humans.** LOF mutations in PINK1 and Parkin are causative for PD development in Humans, leading to early onset DA neuron death presenting as motor skill deficits. Most animal models attempting to replicate these phenotypes present with mitochondrial dysfunction, but do not develop neurodegeneration. In select models, applying an additional mitochondrial stress is sufficient to cause PD like phenotypes (pdr-1 = Parkin; OE = overexpression). LOF =loss of function

1.4: Aims

While we have a robust understanding of the PINK1/Parkin mitophagy pathway and its links to neurodegeneration, our understanding of how the UPR^{mt} pathway functions in mammals and the interplay of the UPR^{mt} with PINK1/Parkin mitophagy is limited. The work in this thesis sought to address these gaps in our understanding of UPR^{mt} related mitochondrial quality control through three main aims.

First, this work sought to further our mechanistic understanding of the UPR^{mt} by clarifying the roles of each CHOP, ATF4 and ATF5 in driving the UPR^{mt} program and protecting mitochondrial proteostasis (Chapter 4). A novel experimental mass spectrometry-based pipeline was developed to allow for proteostatic analysis of the mitochondrial proteome to facilitate mechanistic studies of the UPR^{mt} (Chapter 3). A detailed comparative transcriptomic analysis of the G-TPP-induced UPR^{mt} program was conducted to both define the signalling roles of each CHOP, ATF4 and ATF5, and characterise the global transcriptional changes that are driven by the UPR^{mt} (Chapter 5). Secondly, after clarifying the proteostatic damage mitochondria experience during a protein folding stress, functional analysis of mitochondrial stress and OXPHOS activity were undertaken to define the functional roles of the UPR^{mt} in protecting mitochondrial health (Chapter 5). Lastly, to understand how the UPR^{mt} and PINK1/Parkin mitophagy interact during proteostatic stress, integrated signalling analysis was performed to examine PINK1/Parkin mitophagy and UPR^{mt} activity in the presence/absence of the corresponding pathway (Chapter 6).

Chapter 2

Materials and Methods

2.1: Molecular Biology Techniques

Unless otherwise stated, all DNA and RNA samples were quantified using spectroscopic measurements of sample absorbance at the 260 nm wavelength using a Nanodrop ND-1000 UV-Vis Spectrophotometer (Thermo Fisher Scientific).

2.1.1: Isolation of genomic DNA

Genomic DNA was isolated from mammalian cell pellets using a Quick-gDNA™ MiniPrep Kit (Zymogen) as per manufacturer's instructions and stored at -20 ˚C until use.

2.1.2: Polymerase chain reaction (PCR)

DNA was amplified by Polymerase Chain Reaction (PCR) using MyTaq™ (Bioline) or Phusion High Fidelity™ (New England Biolabs) polymerases as per manufacturer's instructions, with minor modifications (see Table 2.1). PCRs were performed using a T100 Thermocycler (BioRad).

A) PCR conditions using MyTaq™ DNA polymerase

Step	Temperature	Cycle Length	Number of Cycles
Initial denaturation	95 ˚C	30 sec	1
Denaturation	95 ˚C	10 sec	
Annealing	56 ˚C	20 sec	30
Extension	72 ˚C	30 sec	
Final extension	72 ˚C	5 min	1

B) PCR conditions using Phusion™ DNA polymerase

Step	Temperature	Cycle Length	Number of Cycles
Initial denaturation	98 ˚C	30 sec	1
Denaturation	98 ˚C	10 sec	
Annealing	58 ˚C	20 sec	35
Extension	72 ˚C	30 sec	
Final extension	72 ˚C	7 min 30 sec	1

Table 2.1 **PCR conditions for general molecular cloning reactions**

2.1.3: Restriction enzyme digest

Digestion of purified PCR and plasmid DNA products using restriction enzymes was performed by incubating 2 – 5 U of each enzyme in a 25 µL reaction volume containing 1x CutSmart buffer (New England Biolabs) for 16 h at 37 ˚C. Sequencing vectors (pGEM4-Z) and inserts were digested with BamHI-HF (New England Biolabs[®]) and HindIII-HF (New England Biolabs[®]), while CRISPR vectors (pSpCas9(BB-GFP)) were digested with BbsI (New England Biolabs[®]). A summary of the plasmids used in this thesis is found in Appendix I.

2.1.4: Agarose gel electrophoresis

Visualisation of both plasmid and PCR DNA products was performed by agarose gel electrophoresis using a 1% (w/v) agarose (BioRad) gel made with TAE buffer (20 mM Tris, 10 mM acetic acid, 5 mM EDTA; pH 7.6). The nucleic acid stain SYBR Safe™ (Invitrogen™) was added to the gel at a 1:10 000 dilution. Prior to loading onto the gel, a 6x Gel Loading Dye (Purple; New England Biolabs[®]) was added to each sample and Quick-Load® Purple 1 kb Plus DNA Ladder markers (New England Biolabs[®]) were loaded adjacent to the samples to allow for estimation of the approximate DNA fragment size (base pair; bp). Gels were run at 100 V for 25 min after which DNA products were visualised using a ChemiDoc™ XRS+ imager (BioRad) or a PrepOne™ Sapphire (EmbiTec) blue light illuminator.

2.1.5: Ligation assembly of plasmids

Ligation-compatible ends were generated in both the desired plasmid and the DNA fragment insert through digestion with compatible pairs of restriction enzymes (see Chapter 2.1.3). Digested DNA fragments were combined in a 1 : 3 molar ratio of vector : insert in a 10 µL reaction mix containing 1x T4 DNA Ligase Buffer (New England Biolabs) and 400 U of T4 DNA Ligase (New England Biolabs). Reactions were incubated at 16 ˚C for 12 h, after which the assembled plasmids were transformed into competent *E. Coli* cells for downstream PCR screening and Sanger sequencing.

2.1.6: Bacterial Transformation

All bacterial transformations were performed using NEB® 5-α Competent *E. coli* (High Efficiency) cells (New England Biolabs®). In brief, a mixture of 2 µL of purified plasmid DNA and 10 µL of competent cells were incubated on ice for 30 min, and then heat shocked at 42 ˚C for 30 sec. Cells were then placed back on ice for 2 min, prior to the addition of 300 µL SOC Outgrowth Medium (New England Biolabs) and incubation at 37 ˚C with shaking at 200 rotations per minute (rpm) for 2 h. After this 2 h recovery period, cell mixtures were spread onto LB agar pates containing the antibiotic complementary to the conferred antibiotic resistance of the specific plasmid. Plates were then left to dry in aseptic conditions prior to static incubation at 37 ˚C for 16 h, after which plates were removed from incubation and stored at 4 ˚C until use.

2.1.7: Amplification and purification of plasmid DNA

Plasmid DNA was amplified through incubation of transformed *E. coli* cells (see Chapter 2.1.6) in overnight cultures comprised of LB broth and Super Broth (SB; 3.2% (w/v) Bacto-tryptone, 2% (w/v) Bacto-yeast extract, 0.5% (w/v) NaCl; pH 7.0) in a 1 to 1 volume ratio. Cultures were supplemented with antibiotic complimentary to the conferred antibiotic resistance of the plasmid in question. Each culture was incubated for approximately 16 h at 37 °C shaking at 200 rpm. Plasmid DNA was extracted and purified from overnight cultures using a QIAprep® Spin Miniprep Kit (Qiagen) as per manufacturer's instructions and stored at -20 ˚C until use.

2.1.8: Purification of PCR-based DNA products

PCR products were resuspended in Membrane Binding Solution (Promega) at a ratio of 1 part PCR reaction volume : 1 part Membrane Binding Solution (Promega). Mixtures were added to silica spin columns for nucleic acid isolation (Vita Scientific) and incubated at RT for 5 min. Samples were then centrifuged for 30 sec at 16 000 x g. The flow through was discarded, and samples were washed twice through the addition of 500 μL membrane wash buffer (10 mM Tris pH 7.5, 80% (v/v) EtOH) and centrifugation at 16 000 x g for 30 sec, with the flow-through discarded between each wash. A final centrifuge spin at 23 000 x g for 1 min was performed to remove all wash solution from the membrane. Columns were then transferred into sterile microfuge tubes and ~ 20 μL sterile MilliQ water was added to the membrane. Samples were incubated at RT for ~ 5 min, and then DNA was eluted from the column through centrifugation at maximum speed for 30 sec. After quantification, samples were either used immediately in downstream cloning, or stored at - 20 ˚C until further use.

2.1.9: Colony PCR screening

To determine if bacterial colonies incorporated the correctly assembled plasmid during transformation, a PCR screen was performed using DNA from individual colonies and primers specific to the vector and the expected insertion. Approximately 2 μl of this reaction was transferred to 200 μl of Luria-Bertani media (LB; 1% (w/v) Bacto-Tryptone, 0.5% (w/v) Bacto-yeast Extract, 1% (w/v) NaCl; pH 7.0) and supplemented the appropriate selection antibiotic. Reactions were run using a standard MyTaq™ PCR protocol (see Table 2.1 A) with a 10 min initial denaturation period to ensure bacteria in the reaction had sufficient time to lyse and release their DNA into the reaction mix.

Resulting PCR products were run on a 1% (w/v) agarose gel. Colonies that produced a DNA band of the expected size were assumed to contain the correct plasmid insert. Colonies containing the correct plasmid were then sub-cultured in a 1 : 1 mix of LB : SB using standard overnight culture conditions. Plamsids were then purified from the cultures using a standard plasmid DNA purification protocol (see Chapter 2.1.7).

2.1.10: Sanger sequencing

Sequencing of DNA constructs was outsourced to Micromon Genomics (Monash University). Plasmid samples, and plasmids of ligated PCR products in pGEM-4Z vectors for CRISPR edit sequencing were prepared by diluting 300 ng of purified plasmid and 300 nM of an oligonucleotide primer that binds >50 bp from the desired region to be sequenced in sterile MilliQ H_2O to a total reaction volume of 15.5 µL. After Sanger sequencing, sequences were aligned to their predicted sequence or to the NCBI reference genome sequence of the sequenced genome region to calculate CRISPR or TALEN-mediated insertions and deletions (INDELs). For cell lines that were sequenced using the Synthego ICE v2 CRISPR Analysis tool ((synthego.com/products/bioinformatics/crispr-analysis), PCR products of the desired genome region were cleaned up (Chapter 2.1.8) and directly sequenced, instead of subcloned into a pGEM-4Z vector. PCR samples for sanger sequencing analysis were prepared by diluting 10 ng of clean-up PCR product together with 300 nM of a sequencing primer that binds >50 bp from the desired region to be sequenced (that was not the primers used to produce the initial PCR product) in sterile MilliQ H_2O to a total reaction volume of 15.5 µL. After Sanger sequencing, PCR reads were aligned with reads from sequenced PCR products from the unedited parental cell line in the Synthego ICE v2 CRISPR analysis tool.

All cell lines used in this thesis were sequence verified for genomic edits. For CHOP and ATF5 KO, genomic DNA (gDNA) was first isolated and PCR was performed to amplify the targeted regions, which were subsequently cloned into a pGEM-4Z vector for sequencing analysis (Appendix II). For ATF4 KO, PCR products were directly sequenced using sequencing primers that anneal to the amplified regions (Appendix II). The sequencing data for ATF4 was then analysed using Synthego ICE v2 CRISRP Analysis tool.

2.1.11: CRISPR mediated genome editing

CRISPR based gene editing was performed as per *Ran et al.* (2013) with some minor changes (*160*). CRISPR guide sequences were designed using the online program CHOPCHOP (http://chopchop.uib.no/). The sequences CACCG and AAAC were added to the 5' ends of the forward and reverse strands of the guide sequence duplex respectively, and a C was added to the 3' end of the bottom strand.

Annealing of the oligonucleotide sequences and phosphorylation of the 5' ends was performed as per Table 2.2. Oligoduplexes were ligated into BbsI digested pSpCas9(BB-GFP) vector in a 10 µL

ligation reaction using 2 µL of the oligoduplex mixture and 10 ng of digested vector. Resulting plasmids were transformed into competent *E. Coli*, screened by colony PCR and sequenced as per standard protocol to ensure correct insertion of the oligoduplex. CRISPR plasmids were then transfected into the desired cell line as per standard protocol using XtremeGENE™ 9 (Sigma Aldrich; Chapter 2.2.2). After 24 h, transfected cells were sorted into single cells in a 96 well plate by FACS, gating for GFP fluorescence (see Chapter 2.2.6). CRISPR sequences used in this thesis can be found in Appendix II.

Reagent	Volume (µL)	Cycle
F oligonucleotide (100 µM)	1	1. 37 ˚C for 30 min
R oligonucleotide (100 µM)	1	2. 95 ˚C for 5 min
10x T4 ligase buffer	1	3. Ramp down to 25 ˚C (-5 ˚C/min)
T4 Polynucleotide kinase	1	
Sterile MilliQ H_2O	6	

Table 2.2 **Annealing and 5' phosphorylation of CRISPR guide oligonucleotides.** F = forward, R = reverse.

2.1.12: Isolation of total RNA

Cells for total RNA isolation were washed with ice cold phosphate buffered saline (PBS) and frozen at -80 ˚C. Total RNA was isolated using the RNeasy® Plus Mini kit (Qiagen) as per manufacturer's instructions. Concentrations of RNA in each sample were quantified and the samples were stored at -80 ˚C until use.

2.1.13: cDNA library generation

Total RNA samples were thawed on ice and approximately 200 ng of total RNA was aliquoted into a 0.2 mL sterile PCR tube. Complimentary DNA (cDNA) libraries were generated using a High-Capacity cDNA Reverse Transcription Kit (Applied Biosystems™) as per manufacturer's instructions, using Oligo(dT)$_{20}$ primers (Sigma Aldrich) . After synthesis, libraries were frozen at -20 ˚C until use.

2.1.14: qRT-PCR analysis

All steps were performed on ice unless specified otherwise. Prior to quantitative reverse-transcription PCR (qRT-PCR) analysis, cDNA libraries were thawed on ice and diluted through the addition of 60 µL DEPC-treated H_2O to the 20 µL total volume of synthesised cDNA libraries (Chapter 2.1.13). Oligonucleotide primers were diluted to a concentration of 4 µM forward and 4 µM reverse primers in the same solution using DEPC-treated H_2O for each analysed target. Reactions were assembled according to Table 2.3, and the primer sequences used in this work are listed in Table 2.4. qRT-PCR analysis was performed on an RotorGene Q (Qiagen) machine according to the parameters in Table 2.5. Threshold values were set using Rotor-Gene Q Series Software v2.3.5. Cycle threshold (Ct) values were imported into Microsoft Excel, and fold change in mRNA levels were calculated using the $2^{-\Delta\Delta Ct}$ method normalised to GAPDH mRNA levels of each sample (*161*) .

Reagent	Volume (µL)
QuantiTect SYBR® Green (Qiagen) master mix (2x)	5
Primer stock	1
cDNA template	4
Total reaction volume	10

Table 2.3 **qRT-PCR reaction setup**.

Gene	Primer	Primer sequence (5' to 3')
CHOP	Forward	AGCCAAAATCAGAGCTGGAA
	Reverse	TGGATCAGTCTGGAAAAGCA
ATF4	Forward	CAGCAAGGAGGATGCCTTCT
	Reverse	CCAACAGGGCATCCAAGTC
ATF5	Forward	AAGTCGGCGGCTCTGAGGTA
	Reverse	GGACTCTGCCCGTTCCTTCA
GAPDH	Forward	TGACAACTTTGGTATCGTGGAAGG
	Reverse	AGGCAGGGATGATGTTCTGGAGAG

Table 2.4 **qRT-PCR primers used in this work**.

Step	Temperature	Time	Number of cycles
Initial heat activation	95 ˚C	2 min	1
Denaturation	95 ˚C	5 sec	
Combined annealing/extension	60 ˚C	10 sec	40
Melting curve analysis	60 – 95 ˚C, 0.5 ˚C decrease		1

Table 2.5 **qRT-PCR RotorGene Q analysis parameters**.

2.1.15: Next-Generation Sequencing

Next-Generation Sequencing (NGS) was performed in collaboration with Micromon Genomics (Monash University). Total RNA samples were measured using a Qubit™ analyser (Invitrogen™) as per manufacturer's instructions, using 2 µL of each sample, and assayed with the Qubit™ RNA High Sensitivity Assay (Invitrogen™) as per manufacturer's instructions. Each sample was sized and measured for RNA integrity using the Bioanalyzer 2100 (Agilent) and RNA Nano Assay kit (Agilent) as per manufacturer's instructions.

Samples were then processed using an MGI RNA Directional Library Preparation Set V2 (ribodepletion), as per the manufacturer's instructions with some modifications. Modifications were as follows: 500 ng of RNA was used as input, RNA was fragmented at 87 ˚C for 6 min to target an insert size of 200 – 400 bp, adapters were diluted 1/5, and the libraries were amplified with 13 cycles of PCR.

The libraries were then pooled in equimolar concentrations and sequenced using an MGI DNBSEQ-2000RS with reagent chemistry V3.1, aiming for ~ 30 million reads per sample.

2.2: Cell culture techniques and assays

2.2.1: General immortalised cell culture techniques

Unless otherwise state, all cell-based experiments were performed using HeLa cells stably expressing a doxycycline-inducible ΔOTC construct. All HeLa cell lines unless otherwise stated were grown in standard media comprised of Dulbecco's Modified Eagle's Medium (DMEM) supplemented with 10 % (v/v) foetal bovine serum (FBS; Cytiva), 10 mM HEPES pH 7.2 (Gibco™), 1x penicillin/streptomycin solution (Sigma Aldrich), 1x GlutaMAX supplement (Gibco™) and 1x MEM Non-Essential Amino Acids Solution supplement (Gibco™). Cell cultures were maintained in a humidified incubator at 37 ˚C under an atmosphere of 5% CO_2.

Cells were passaged when they reached ~90 – 100% confluency by first removing the culture media through aspiration, and then washing the plate surface in an ample volume of PBS. Trypsin-EDTA (Gibco) at a ratio of 400 µL trypsin-EDTA per T25 flask was added to the culture dish, and cells were incubated at 37 ˚C for approximately 3 min, or until cells were detached into single cell suspensions under a light microscope. Cells were then resuspended in standard culture media at a volume of approximately 3x the volume of trypsin-EDTA used by pipetting, and ¾ of the total volume was removed. Standard culture media was added back to the plate surface, and cultures were returned to a humidified incubator at 37 ˚C under an atmosphere of 5% CO_2.

Cell samples were harvested by washing plates containing cell cultures once with ice cold PBS, and scraping samples into an appropriate volume of ice cold PBS. Plates were washed once with ice cold PBS and the wash and scrape fractions were pooled prior to centrifugation at 10 000 x g for 2 min at 4 ˚C. The supernatant was aspirated from the cell pellet, and pellets were stored at either -20 ˚C if they were to be used for gDNA and SDS-PAGE analysis, or -80 ˚C if they were to be used for mitochondrial isolation or RNA analysis.

2.2.2: Transfection

Cells were seeded in a 6 well plate at a density aiming for ~ 40 % confluency at the time of transfection and left for 24 h to adhere to the cell culture plate surface. After 24 h, media in each plate was aspirated and replaced with fresh standard media. Transfections for were performed with either the Lipofectamine® LTX and Plus™ reagents (Invitrogen) or X-tremeGENE™ 9 (Sigma Aldrich) transfection reagent as per manufactures instructions. For lipofectamine based transfections, 2 µg of plasmid DNA was diluted in 500 µl Opti-MEM™ Reduced Serum Medium (Thermo Fisher Scientific). 3 µL of Plus reagent was added in a 1:1 ratio of µl of Plus™ reagent to µg of DNA transfected, after which the reduced serum medium solution was vortexed for approximately 5 sec to ensure solution homogeneity and left to stand at room temperature. After 5 min at room temperature, 6 µL of Lipofectamine® LTX was added to each solution in a 1:3 volume ratio of µg of DNA to Lipofectamine® LTX after which solutions were again vortexed for approximately 5 sec and left to stand at room temperature for 25 min. After the second incubation step, the transfection solution was added to the corresponding wells in a drop wise manner and the plates were placed back into incubation.

For X-tremeGENE9™ based transfections, 1.6 µg of CRISPR plasmid DNA was diluted in 500 µl of Opti-MEM™ Reduced Serum Medium. 5 µl of X-tremeGENE™ 9 was added and the resulting mixture was vortexed for approximately 5 sec and left to stand at room temperature for 25 min. The transfection solution was then added to the corresponding wells and plates were returned to incubation.

2.2.3: Generation of pseudotyped pantropic retrovirus

HEK293T cells from the National Institute of Health (USA) were seeded in a 6 well plate at a density of 8×10^5 cells/well. After 24 h, cells were transfected using Lipofectamine® LTX transfection reagent (See Chapter 2.2.2). Transfection mixtures contained 1 µg and 0.5 µg of the

viral packaging plasmids Gag-Pol and VSV-G respectively, and 1.5 µg of the desired retroviral plasmid. Media containing the transfection mixture was removed after ~ 16 h and replaced with 1 mL standard media. Cells were placed back into incubation for 36 h, after which media containing retrovirus was collected from each well. An additional 1.5 mL of standard media was then added to each well and plates were placed back into incubation for 36 h, after which the supernatant was again collected. Retrovirus from the collected supernatant was precipitated as per Chapter 2.2.4 prior to immediate use in an infection or storage at -80 ˚C until use.

2.2.4: Virus precipitation

Viral supernatant was filtered through a 0.45 µm polyvinyldene fluoride (PVDF) membrane filter unit (Millex) into a sterile 50 mL conical tube. Viral precipitation solution (40% (w/v) PEG-8000, 1.2 M NaCl in PBS) was added to the filtered viral supernatant at a ratio of 1 part precipitation solution to 3 parts viral supernatant. Tubes were manually inverted for 60 sec to ensure the solution had mixed together and were then incubated at 4 ˚C with gentle rocking or rotation for at least 16 h. Mixtures were then centrifuged at 1 600 x g for 1 h at 4 ˚C. The supernatant was removed carefully, and the pellet was resuspended in the desired volume of fresh standard media (usually 500 µL per 6 well starting volume) by gentle pipetting. Resuspended viral aliquots were then frozen at -80 ˚C for later use in infections, or used immediately.

2.2.5: Retroviral infection

Cells were seeded in 6 well plates at a density aiming for ~50% confluency at the time of infection (~180 K cells/well). After 24 h, media in each well was replaced with 1.5 mL fresh media and a 500 µL retrovirus aliquot. Polybrene (Sigma) to a concentration of 8 µg/mL was added to each well to increase infection efficiency prior to returning plates to incubation. Infections were left to incubate for 48 h, and then the viral media was removed and replaced with 2 mL standard media.

2.2.6: Fluorescence activated cell sorting (FACS)

Cells were sorted into sub-populations or clonal populations according to their fluorescence. In brief, cells were trypsinised as per standard procedures and resuspended in an appropriate amount of standard media. Samples were then centrifuged for 5 min at 800 x g. The supernatant was removed, and cell pellets were resuspended in an appropriate volume of sorting media (10% (v/v)

FBS (Cytiva), 1 mM EDTA in 1x PBS) and passed through a sterile 0.45 μM PVDF filter to generate a single cell suspension. Cell suspensions were then transported on ice to the Monash FlowCore Research Platform facility (Monash University) and sorted into 96 well plates containing 200 μL standard media/well for clonal cell suspensions, or 15 mL tubes containing 2 mL standard media/tube for non-clonal bulk population suspensions. Clonal sorted cells were left to grow into sizeable colonies prior to screening for gene edits. Bulk population suspensions were immediately centrifuged at 800 x g for 5 min, and the supernatant was removed. Cell pellets were then resuspended in an appropriate volume of media and transferred to a tissue culture plate of an appropriate size depending on the number of cells sorted into the bulk population, aiming for a seeding density of ~ 20 – 50% confluency at the time of seeding.

2.2.7: Cryopreservation of immortalised cell lines

Immortalised cells to be cryopreserved were dissociated from their culture dish or flask using trypsin, and then pelleted by centrifugation at 800 x g for 5 min at room temperature (RT). The supernatant was removed and pellets were resuspended by gentle pipetting in 400 μL Bambanker™ (Wako Chemicals) per $4x10^6$ cells. Cells solutions were then moved to cryovials and stored immediately at -80 ˚C.

When thawing cryopreserved cells, ~ 500 μL of standard media warmed to 37 ˚C was added to the frozen sample, and the solution was gently pipetted up and down until the cryoprotectant was fully dissolved. Cell solutions were then centrifuged at 800 x g for 5 min at RT and the supernatant was removed by pipetting. Cell pellets were then resuspended in ~ 800 μL standard media and added to the appropriate sized culture flask where the cell suspension is at ~ 70% attachment confluency. Cell cultures were then placed into a humidified incubator at 37 ˚C under an atmosphere of 5 % CO_2.

2.2.8: Induction of the UPR^{mt} through ΔOTC expression

Cells stably expressing a docycyline-inducible ΔOTC construct were seeded at a density of 700 000 cells into a T25 flask. A sample of the cell culture was collected at this point and frozen as a day 0 sample. After 24 h, media was aspirated from the flask and replaced with 3.5 mL standard media supplemented with 1 μg/mL doxycycline. Every 24 after the initial doxycycline addition, cells were trypsinised and half the culture was collected, and the remaining cells were placed back into the same flask in fresh media supplemented with 1 μg/mL doxycycline. This process was

repeated for 5 days, at the conclusion of which samples were then analysed together by SDS-PAGE.

2.2.9: Induction of the UPR^{mt} through G-TPP treatment

Cells were seeded into the appropriate sized tissue culture plates, aiming for a confluency of ~ 70 – 80% at the time of treatment 24 h after seeding. Prior to treatment, cells were incubated for 1 h in fresh standard media, after which the media was replaced with fresh standard media containing the mtHSP90 inhibitor gamitrinib-triphenylphosphonium (G-TPP) to a final concentration of 9 µM. Acute treatment durations ranged from 4 – 12 hours, depending on the specific experimental conditions.

For treatments involving a recovery period, cells were treated with G-TPP for 12 h. At the conclusion of the G-TPP treatment, the media was removed and plates were washed in a volume of sterile 1x PBS that was approximately double the treatment volume. Three washes were performed, and after the final PBS wash was removed, standard media equal to the treatment volume was added to each plate. After 24 h, 24 h recovery samples were collected, and the media was replaced with fresh standard media on plates to be collected after 48 h recovery.

2.2.10: Induction of mitophagy with Oligomycin and Antimycin A

Cells with and without stable YFP-Parkin expression were seeded into appropriate tissue culture plates 24 h prior to mitophagy induction, aiming for a density of ~90% at the time of treatment. Mitophagy was induced through the simultaneous inhibition of Complex III and Complex V by addition of Antimycin A and Oligomycin at final concentrations of 4 µg/mL and 10 µg/mL respectively. A pan-caspase inhibitor, QVD-OPh, was added at the time of treatment at a final concentration of 10 mM to prevent cell death during mitophagy induction. Treatment durations ranged from 4 – 8 h depending on the experimental conditions.

2.2.11: Induction of hypoxia-based mitophagy

Cells were seeded into appropriate tissue culture plates 24 h prior to mitophagy induction, aiming for a confluency of ~70 – 80% at the time of treatment. Hypoxia based mitophagy was induced through the addition of the iron chelator deferiprone (DFP) in standard media at a final

concentration of 1 mM. The pan-caspase inhibitor QVD-OPh was added at a final concentration of 10 mM at the time of treatment to prevent cell death. Cells were treated with DFP for 24 h prior to collection for analysis.

2.2.12: Induction of starvation-based autophagy

Cells were seeded into appropriate tissue culture plates 24 h prior to starvation, aiming for a confluency of 90 – 100% at the time of treatment. Prior to starvation induction, cells were incubated in fresh standard media for 1 h. After this initial 1 h feed, cells were washed 3x with ample volumes of 1x PBS, after which the PBS was removed and replaced with an appropriate volume of Earle's Balanced Salt Solution (EBSS; Thermo Fisher Scientific). Cells were incubated in EBSS for 8 h prior to collection and analysis.

2.2.13: mtKeima analysis of mitophagy induction

Cells stably expressing YFP-Parkin and mtKeima were seeded in 24 well plates aiming for a confluency of ~ 70 % at the time of treatment, 24 h after seeding. Cells were treated as per standard protocols according to the specified stress induction listed in the corresponding Figure legend. At the conclusion of the treatment, cells were washed once in PBS and dissociated from the culture plate by a short 2 min trypsin incubation at 37 ˚C. Plates were then placed on ice, resuspended in ice cold standard media and cell suspension were transferred to microfuge tubes. Samples were centrifuged at 1 000 x g for 1.5 min at 4 ˚C and the media was removed carefully by aspiration. Cell pellets were placed on ice, resuspended in chilled FACS media (10% (v/v) FBS, 0.1 mM EDTA in PBS) and transferred to 5 mL polystyrene tubes (Falcon). Samples were kept on ice until immediately prior to FACS analysis. Samples were analysed using the FACSDiva software on a LSR Fortessa X-20 cell sorter (BD Biosciences). Lysosomal mtKeima was measured using dual excitation ratiometric pH measurements at 488 (pH 7) and 561 (pH 4) nm lasers with 695 nm and 670 nm detection filters respectively. Additional channels used include GFP (Ex/Em: 488 nm/530 nm). Sample compensation was performed at the time of sample analysis using the FACSDiva software. A minimum of 30 000 events were collected per sample.

Data was processed using FlowJo v10.7.2. Samples were first gated to exclude debris, and then gated for single cell evens using the forward and side scatter measurements. Individual event emission values collected with the 695 nm and 670 nm detection filters for each sample were exported. mtKeima shifts were calculated according to published methods (*162*). In brief,

B695/YG760 ratios were calculated for each event. The mean B695/YG670 ratio was calculated for each sample, and mitophagy rate fold changes were calculated relative to the corresponding DMSO treated sample of each sample set. To calculate the fold change increase, 1.0 fold change was subtracted from each sample. Each experiment was repeated in biological triplicate. GraphPad Prism (v9) was used to calculated statistical significance between datapoints (one-way or two-way ANOVA).

2.2.14: ATP assay

Samples were seeded in opaque white 96 well plates (Corning) according to the parameters for UPR^{mt} induction through G-TPP treatment, with a treatment volume of 80 µL/well. Samples for 12 h G-TPP treatment, 24 h recovery and 48 h recovery were seeded on separate plates, with additional samples seeded to allow for a DMSO treated sample to be analysed at each time point. At the time of analysis, plates were removed from incubation and 80 µL of the ATP detection reagent from the Mitochondrial ToxGlo Assay kit (Promega) was added to each well. Plates were covered from light and incubated with low shaking (400 rpm) for 5 min at RT prior to luminescence analysis on a FLUOstar OPTIMA (BMG LABTECH) plate reader. For galactose-based treatments, media changes into a galactose-based media (10% (v/v) dialysed FBS (Gibco™), 10 mM HEPES pH 7.2 (Gibco™), 1x penicillin/streptomycin solution (Sigma Aldrich), 1x GlutaMAX supplement (Gibco™), 1 mM sodium pyruvate, 25 mM D-(+)-galactose, in glucose-free DMEM (11966025; Gibco™)) occurred as follows:

12 hours treatment: the media was changed to the galactose-based media 12 h prior to G-TPP treatment, and cells were treated in galactose-based media.

24 hours recovery: cells were treated in glucose based media, and switched to galactose media at the 12 h G-TPP or DMSO treatment washout stage.

48 hours recovery: cells were treated in glucose-based media, and treatment media was replaced with glucose-based media at the 12 h G-TPP/DMSO treatment washout time point. After 24 h recovery, the media was replaced with galactose-based media, and samples were analysed 24 h later at the 48 h recovery time point.

Ratios of experimental sample luminescence to DMSO sample luminescence were calculated, and experiments were repeated in biological triplicate. Statistical significance was calculated using GraphPad Prism (v9) (one-way or two-way ANOVA).

2.2.15: Oxygen consumption analysis of isolated mitochondria

Oxygen consumption analysis of isolated mitochondria was performed using a modified Seahorse assay (Agilient). The day before each time point, Seahorse cartridges were rehydrated by adding 200 µL calibrant to each well of the hydration plate in which the sensors were submerged, and leaving the cartridge overnight in a 37 ˚C incubator in a CO_2 free environment.

Cells were seeded and treated in 100 mm TC plates as per standard UPR[mt] induction by G-TPP treatment. At each sample collection point, cells were scraped from each plate in mitochondrial isolation buffer (70 mM sucrose, 210 mM mannitol, 5 mM HEPES, 1 mM EGTA, 0.5% (w/v) BSA, pH 7.2) on ice and pellets were collected in a 15 mL conical tube by centrifugation at 3000x g for 5 min at 4 ˚C. Mitochondria were isolated as per Chapter 2.3.5 with some modifications. Cell pellets were stored on ice instead of frozen prior to homogenisation, homogenisation was performed for 27 strokes, and mitochondrial samples were not frozen after quantification. Isolated mitochondria were diluted in mitochondrial assay solution (MAS: 70 mM sucrose, 220 mM mannitol, 10 mM KH_2PO_4, 5 mM $MgCl_2•6H_2O$, 2 mM HEPES, 1 mM EGTA, 0.1 % (w/v) BSA, pH 7.2) to allow for 25 µL aliquots of mitochondria containing 15 µg mitochondria to be added to each well of the sample plate. At least 4 replicates of each sample were included on each plate. Mitochondrial samples were kept on ice while the Seahorse cartridge plate was loaded with the following reagents (volumes added to each chamber, final concentration once added to the sample): 5 mM ADP (20 µL, 0.5 mM), 25 µg/µL oligomycin (22 µL, 2.5 µg/µL), 10 µM FCCP (24 µL, 1 µM), 40 µM antimycin A (26 µL, 4 µM). Cartridges were returned to incubation at 37 ˚C in a CO_2 free environment until immediately prior to commencement of the assay. To load the sample plate, 25 µL of each diluted mitochondrial sample and 155 µL of substrate (10 mM glutamate and 10 mM malate in MAS buffer) was added to the appropriate well with the sample plate sitting on ice. Plates were rocked back and forth gently to ensure even spread of mitochondria across the plate surface, and then plates were centrifuged at 2 000 x g for 20 min at 4 ˚C. The calibration cycle was started on the Seahorse XFe96 Analyzer (Agilent) and then mitochondrial plates were left on ice until insertion into the analyser. Oxygen consumption analysis cycles were performed sequentially as follows:

1. <u>Basal</u>: 3 min mix, 3 min measurement, 3 min mix, 3 min measurement
2. <u>ADP</u>: Injection (ADP port), 30 sec mix, 3 min measurement
3. <u>Oligomycin</u>: Injection (oligomycin), 30 sec mix, 30 sec wait, 3 min measurement
4. <u>FCCP</u>: Injection (FCCP), 20 sec mix, 3 min measurement
5. <u>Antimycin A</u>: Injection (antimycin A), 30 sec mix, 3 min measurement

This protocol was repeated each day at the time of sample collection (12 h G-TPP (Day 1), 24 h R (Day 2), 48 h R (Day 3)). DMSO treated controls were analysed alongside experimental samples each day. Raw data files were exported from Wave software v2.6 and imported into Microsoft Excel. The average basal oxygen consumption of the initial DMSO treated samples (12 h G-TPP analysis day) was calculated and used to generate normalisation factors with subsequent DMSO treated samples to normalise oxygen consumption measurements across each day of analysis. Normalised oxygen consumption rate values were then used to calculate the basal respiration rates, spare respiratory capacity, and total respiratory capacity of each experimental sample across the G-TPP treatment and recovery time course. All data was then displayed using Graphpad Prism v9.1.

2.2.16: Isolation of primary cortical neurons

Mice (C57BL6/J) were housed at the Monash Animal Research Platform (Monash University) on a 12 h light-dark cycle in temperature-controlled high-barrier facilities with free access to food and water. All experiments were performed in accordance with the National Health and Medical Research Council (NHRMC) Australian Code of Practice for the Care and Use of Animals. All protocols were approved by the Monash University School of Biomedical Sciences Animal Ethics Committee (ethics number: 2020-19202-50731).

Prior to neuron isolation, the desired number of plates were incubated in 0.05 mg/mL poly-D-lysine (Gibco™) overnight in in a humidified incubator at 37 ˚C under an atmosphere of 5 % CO_2. The next morning, the poly-D-lysine solution was aspirated from each plate, and plates were washed 3x in ample amounts of sterile MilliQ H_2O and left to dry. Plates were then sealed with ParaFilm and stored at 4 ˚C until use, for a maximum of 1 week after coating. Once mice reached P0-P2, they were euthanised by decapitation using sharp scissors. Brains were removed and cortical tissue was extracted and placed in a 15 mL concial tube containing dissection media (1 mM sodium pyruvate (Gibco™), 0.1% (w/v) glucose (Sigma), 10 mM HEPES pH 7.2 (Gibco™) in HBSS (Ca^{2+} and Mg^{2+} free) (Gibco™)). Lyophilised papain (Worthington Biochemical) was reconstituted by adding 5 mL sterile EBSS (Gibco™), mixed through inversion, and then left at 37 ˚C until required. Tubes containing brain tissue were left to sit until all tissue reached the bottom of the 15 mL conical tube. Approximately 80 – 90% of the dissection media was removed by pipette and replaced with 10 mL fresh dissection media. This constitutes 1 wash. Samples were washed a total of 3 times in dissection media. After the final wash, dissection media was added to each tube to total ~4.5 mL/tube, and 2.5 mL of the papain/EBSS solution was added to each tube

and each tube was gently inverted 2 times to mix. Samples were then incubated in a 37 ˚C waterbath for 15 min. During this incubation period, DNase (Worthington Biochemical) was reconstituted though adding 500 µL EBSS to the vial and mixing the vial through inversion. At the conclusion of the papain incubation period, 125 µL DNase/EBSS solution was added to each tube, and tubes were gently swirled to mix and left to incubate for a further 5 min at RT. After the DNase incubation, 80 – 90% of the supernatant was removed by pipette, and two washes in 10 mL dissection media/wash were performed. After the final dissection media wash, two more washes were performed using 10 mL plating media (10% (v/v) FBS (Cytiva), 1 mM sodium pyruvate (Gibco™), 1x GlutaMAX (Gibco™), 1x penicillin/streptomycin solution (Sigma), 0.45% (w/v) glucose (Sigma) in Basal Medium Eagle (BME; Gibco™)) per wash. After the final wash, fresh plating media to a total of 2.5 mL plating media/tube was added to each sample. Using the lid of a 100 mM cell culture plate, tissue samples were titruated with a fire-polished glass pasture pipette ~ 10 – 13 times (until most tissue chunks were broken up). The concentration of cells in each sample was then calculated using an appropriate dilution factor in Trypan blue (Sigma) using a haemocytometer. The desired number of cells were seeded onto each plate (3 million per 100 mm dish) in fresh plating media. Plates were left to incubate in a humidified incubator at 37 ˚C under an atmosphere of 5% CO_2 for 1.5 h. All media in each plate was then removed by pipette and replaced with fresh maintenance media (1x GlutaMAX (Gibco™), 1x penicillin/streptomycin solution (Sigma), 1x B-27™ supplement (Gibco™) in Neurobasal™ medium (Gibco™)). Plates were then returned to incubation in a humidified incubator at 37 ˚C under an atmosphere of 5 % CO_2.

At DIV 2, Cytosine β-D-arabinofuranoside (Ara-C; Sigma Aldrich) was added to each plate at a final concentration of 2.5 µM to kill any contaminating mitotic cells that carried over from the isolation procedure. Standard primary cortical neuronal culture techniques were then followed.

2.2.17: General primary cortical neuronal cell culture techniques

Cortical neuronal samples isolated from C57BL6/J P0-P2 pups were cultured on poly-D-lysine coated plates in standard cortical neuronal culture media comprised of a base of Neurobasal™ Medium (Gibco™) supplemented with 1x B-27™ supplement (Gibco™), 1x penicillin/streptomycin (Sigma) and 1x GlutaMAX supplement (Gibco™). Cortical neuron cell cultures were maintained in a humidified incubator at 37 ˚C under an atmosphere of 5 % CO_2. Every 4 days, cortical neuronal cell cultures were fed by removing half the current volume of

media on each plate and replacing that with an equal volume of fresh standard cortical neuronal culture media.

Primary cortical neuronal cell samples were harvested by replacing the culture media with ice cold Dulbecco's phosphate buffered saline (DPBS) without calcium and magnesium (Gibco™), and scraping the cells into the DPBS. Plates were washed once with ice cold DPBS and the wash and scrape fractions were pooled prior to centrifugation at 10 000 x g for 2 min at 4 ˚C. The supernatant was removed by aspiration, and an additional 500 µL of DPBS was added to each tubes, and samples were again centrifugation at 10 000 x g for 2 min at 4 ˚C to wash away any residual standard cortical neuronal culture medium remaining. After the supernatant of the final wash was removed, samples were then stored at either -20 ˚C or -80 ˚C, depending on their downstream use.

2.2.18: Induction of the UPR^{mt} through G-TPP treatment (primary neurons)

At DIV 12 – 14, 1 or 2 days after a half feed, G-TPP was added directly to each plate at the final concentrations specified in the corresponding figure legends. Plates were gently agitated to mix, and then placed back into a humidified incubator at 37 ˚C under an atmosphere of 5 % CO_2 for the specified incubation times prior to sample harvest.

2.3: Protein analysis techniques

Unless otherwise specified, protein amounts were quantified by spectroscopic measurement of sample absorbance at the 280 nm wavelength using a Nanodrop ND-1000 UV-Vis Spectrophotometer (Thermo Fisher Scientific).

2.3.1: Bicinchoninic assay (BCA)

Total protein concentrations of isolated mitochondria for oxygen consumption analysis (Chapter 2.2.15) were quantified using a Pierce™ BCA Protein Assay Kit as per manufacturer's instructions. Assays were analysed using a FLUOstar OPTIMA (BMG LABTECH) plate reader.

2.3.2: Preparation of whole cell samples for SDS-PAGE analysis

Whole-cell samples to be analysed by SDS-PAGE were resuspended in 1x LDS loading dye (Life Technologies) supplemented with 25 mM DTT, vortexed to ensure lysis, and then boiled at 99 ˚C with shaking for 10 min. After they had returned to ~ RT, samples were quantified and aliquoted into separate tubes with standard protein and volume amounts across the sample set. Samples were then either analysed immediately or frozen at -20 ˚C to be thawed out at a later date for SDS-PAGE analysis.

2.3.3: SDS-PAGE and Western blotting techniques

Samples to be analysed by sodium dodecyl sulphate-polyacrylamide gel electrophoresis (SDS-PAGE) were loaded onto NuPAGE™ 4-12% Bis-Tris gels (Invitrogen™). Samples were run in 1x MOPS buffer (Invitrogen™) at 100 V for 10 min, 150 V for 10 min, and then 200 V for 40 min. The running buffer in the cathode chamber was supplemented with 0.25% (v/v) NuPAGE™ Antioxidant (Invitrogen™). After SDS-PAGE, a wet Western transfer method was used to transfer proteins onto a PVDF membrane for immunoblotting. SDS-PAGE gels were removed from their casings and placed into chilled transfer buffer (20% (v/v) MeOH, 25 mM bicine, 25 mM Bis-Tris, 1 mM EDTA) to equilibrate. The PVDF membrane was activated in 100% (v/v) MeOH for approximately 20 sec, rinsed three times in distilled H_2O, and then added to transfer buffer to equilibrate. Transfer stacks were assembled as follows: Whatman® filter paper, SDS-PAGE gel, PVDF membrane and a second piece of Whatman® filter paper. Stacks were placed in cassette holders and inserted into a Criterion™ Blotter (Biorad), along with a frozen ice pack. Chilled transfer buffer was added to the tank and transfers were run at 100 V for 1 h. At the conclusion of the western transfer, the PVDF membrane was removed from the stack and placed in PVDF destain (70% (v/v) MeOH, 20% (v/v) acetic acid) for 2 min while rocking. The membrane was then washed 3 times, with each wash consisting of a 3 min incubation in PBS/0.05% (v/v) Tween 20 with rocking at RT. Membranes were blocked in 5% (w/v) Carnation® Skim Milk in PBS/0.05% (v/v) Tween 20 for 20 min with rocking at RT, washed a further 3 times, and then cut into appropriate sections, placed into primary antibodies and incubated overnight at 4 ˚C with rocking. After primary antibody incubation, membranes were washed a further 3 times and placed into secondary antibody incubation for 1 h at RT with rocking. Blots were washed three more times, with the final wash in PBS instead of PBS/0.05% (v/v) Tween 20. After the final wash, membranes were incubated in Amersham™ ECL™ Primer Western Blotting Reagent (Cytiva) or Super Signal® West Femto Maximum Sensitivity Substrate (Thermo Fisher Scientific) for 5 min prior

to imaging on a ChemiDoc™ XRS+ imager (Biorad). A summary of the primary and secondary antibodies used in this thesis is provided in Table 2.5.

Samples for OPA1 immunoblotting were run on 8% Tris-Glycine NuPage™ gels (Invitrogen™) in chilled 1x Tris-Glycine running buffer (Invitrogen™). Gels were run at 50 V for 5 h, with the gel tank submerged in ice. All Western blotting and immunoblotting procedures after SDS-PAGE were performed as described above.

Antibodies	Company	Species	Catalog #
CHOP	Cell Signaling	Mouse	2895
ATF5	Santa Cruz	Mouse	sc-377168
ATF4	Santa Cruz	Mouse	sc-390063
PINK1	Cell Signaling	Rabbit	6946
p62	Abnova	Mouse	H00008878-M01
Actin	Cell Signaling	Mouse	3700
PGAM5	N/A	Rabbit	In house
LRPPRC	Abcam	Rabbit	ab97505
AARS2	Abcam	Rabbit	ab197367
GRSF1	Sigma	Rabbit	HPA036985
VDAC1	Cell Signaling	Rabbit	4661
TOMM20	Santa Cruz	Mouse	sc-17764
Parkin	Santa Cruz	Mouse	sc-32282
VCP	Santa Cruz	Mouse	sc-133212
OPA1	BD Biosciences	Mouse	612606
ATP5A	Abcam	Mouse	ab14748
NDUFS1	Proteintech	Rabbit	12444-1-AP
NDUFS3	Invitrogen	Mouse	A21343
TUJ1	BioLegend	Mouse	801201
Anti-Mouse IgG, HRP-linked	Cell Signaling	Horse	7076
Anti-Rabbit IgG, HRP-linked	Cell Signalling	Goat	7074

Table 2.5 **Details of the antibodies used in this thesis.**

2.3.4: Colloidal Coomassie staining

SDS-PAGE gels were incubated in fixative (40% (v/v) EtOH, 10% (v/v) acetic acid in MilliQ H_2O) with agitation at RT for 1 h, washed twice with distilled water for 10 min with agitation at RT for 1 h, and then incubated in colloidal stain (0.1% (w/v) Coomassie Brilliant Blue G250, 2% (v/v) ortho-phosphoric acid, 10% (w/v) ammonium sulphate) with agitation overnight. Gels were then washed twice in 1% (v/v) acetic acid for 10 min at RT with agitation, and then imaged on a ChemiDoc™ XRS+ imager (Biorad)

.

2.3.5: Densitometry analysis

The density of bands from Western blot images were calculated using the Image Analysis tool in Image Lab software (Biorad; v6.0). GraphPad Prism (v9.0) software was used to perform statistical analysis, as specified in the corresponding Figure legends.

2.3.6: Mitochondrial isolation

All steps were performed on ice unless specified otherwise. Cell samples with a confluency of >70% in a 100 mm tissue culture plate were collected by standard procedures, pelleted at 1 000 x g for 3 min, and then frozen at -80 ˚C for at least 30 min. Frozen cell pellets were thawed and homogenised in 3 mL per sample of Solution B (20 mM HEPES pH 7.6, 220 mM mannitol, 70 mM sucrose, 1 mM EDTA and 0.5 mM PMSF) using a Dounce Homogeniser with 30 strokes. Homogenates were centrifuged at 800 x g for 5 min at 4 ˚C, and post-nuclear supernatant was moved to a clean tube and centrifuged at 10 000 x g for 10 min at 4 ˚C. The supernatant was removed by gentle aspiration, and mitochondrial pellets were resuspended in 400 μL Solution B and centrifuged at 10 000 x g for 10 min at 4 ˚C. The supernatant was removed by gentle aspiration, and samples were resuspended in 150 – 300 μL of mitochondrial storage buffer (10 mM HEPES pH 7.6, 0.5 M sucrose). Concentration estimates were performed as follows: 15 μL of each sample was centrifuged at 10 000 x g for 10 min at 4 ˚C to pellet the mitochondria. The supernatant was removed by aspiration and each mitochondrial pellet from the 15 μL starting sample was resuspended in 5 μL of 1x SDS loading dye (5% (w/v) SDS, 50 mM Tris-Cl pH 6.8, 100 mM DTT, 10% (v/v) glycerol). Each sample was boiled at 99 ˚C with shaking for 10 min, cooled, and then protein concentration estimates were performed. Resuspended mitochondrial stock samples were split into three individual aliquots and stored at -80 ˚C until use. Aliquots of mitochondria were thawed on ice when required and freeze/thawed a maximum of 3 times.

2.3.7: Isolation of soluble and insoluble mitochondrial protein fractions

All steps were performed on ice unless otherwise noted. Approximately 15 – 80 µg of isolated mitochondria were centrifuged at 10 000 x g for 10 min at 4 ˚C. The supernatant was removed by aspiration, and chilled lysis buffer (0.1% (v/v) TX-100 in PBS) was added to each sample at a ratio of 1 µL lysis buffer : 1 µg mitochondria. Samples were vortexed for ~ 7 sec, incubated on ice for 15 min, and vortexed again for ~7 sec. After lysis, samples were centrifuged at 12 000 x g for 10 min at 4 ˚C. While being careful not to disturb the pellet, 95% of the supernatant volume was removed by pipette and placed into a clean microfuge tube. This fraction is the soluble protein fraction. A volume of lysis buffer equal to 95% of the volume of supernatant removed was added back to each tube containing the insoluble pellet, and the tube was flicked ~ 8 times to wash the sides of the tube. Samples were then centrifuged at 12 000 x g for 10 min at 4 ˚C. The same volume of the soluble protein fraction removed initially (95% of the starting lysis volume) was removed from each tube by pipette, and placed into a clean microfuge tube and labelled as the 'wash' fraction. The wash procedure was repeated once more to make a total of two washes of the insoluble pellet fraction. After the second wash volume was removed, a volume of lysis buffer equal to the 95% removed at the soluble fraction stage was added back to the pellet, representing the 'insoluble' protein fraction. For experiments requiring western blotting analysis, an additional aliquot of isolated mitochondria was processed alongside the fractionated sample described above. This aliquot, corresponding to the total mitochondrial sample, was lysed as described above, but set aside on ice instead of undergoing centrifugation-based fractionation. Samples of neuronal mitochondria were processed in the same manner as described above, but the lysis buffer compositions were altered as described in the corresponding Figure legends. All samples were then kept on ice until used in downstream processing for western blotting or mass spectrometry analysis.

2.3.8: Preparation of whole cell samples for SDS-PAGE analysis

Whole-cell samples to be analysed by SDS-PAGE were resuspended in 1x LDS loading dye (Invitrogen™) supplemented with 25 mM DTT, vortexed to ensure lysis, and then boiled at 99 ˚C with shaking for 10 min. After they had returned to ~ RT, samples were quantified and aliquoted into separate tubes with standard protein and volume amounts across the sample set. Samples were then either analysed immediately or frozen at -20 ˚C to be thawed out at a later date for SDS-PAGE analysis.

2.3.9: Preparation of mitochondrial samples for SDS-PAGE analysis

The specified μg quantities of isolated mitochondria were centrifuged at 10 000 x g for 10 min at 4 ˚C. The supernatant was removed by aspiration, and 1x SDS loading dye was added to each mitochondrial sample at a ratio of 1 μL SDS loading dye : 1 μg mitochondria. Samples were vortexed for ~3 sec to mix, and then boiled at 99 ˚C for 10 min with shaking. After samples had cooled to RT, they were loaded directly onto an SDS-PAGE gel.

2.3.10: Preparation of soluble and insoluble protein fractions for SDS-PAGE analysis

Fractionated total, soluble and insoluble mitochondrial samples for SDS-PAGE analysis were left to stand until their temperature had equilibrated to ~RT. Aliquots of 4x SDS loading dye (20% (w/v) SDS, 200 mM Tris-Cl pH 6.8, 400 mM DTT, 40% (v/v) glycerol) were boiled at 99 ˚C with shaking for 30 sec to thaw. A volume of 4x SDS loading dye was added to each sample to a final concentration of 1x SDS loading dye (5% (w/v) SDS, 50 mM Tris-Cl pH 6.8, 100 mM DTT, 10% (v/v) glycerol, 0.05% (w/v) bromophenol blue). Samples were vortexed to mix and boiled for 10 min at 99 ˚C with shaking. Once samples had cooled completely to RT, each sample was sonicated in a waterbath sonicator for 2 min. Each sample was allowed to cool to RT, vortexed for ~ 3 sec to mix and then samples were loaded onto an SDS-PAGE gel in a ratiometric manner, loading amounts of soluble, insoluble and total mitochondrial protein representative of the same μg quantity of starting material.

2.4: Mass spectrometry techniques

2.4.1: Preparation of mitochondrial fractions for mass spectrometry analysis

Soluble and insoluble fractions from isolated mitochondria were spiked in with 3 ng of recombinant diacylglycerol acyltransferase/mycolyltransferase (Ag85A) from *Mycobacterium tuberculosis* (Abcam; ab124604) per 1 μg of starting mitochondrial sample in a ratiometric manner. After equilibrating to RT, samples were then solubilised by adding an equal volume of 2x SDS-solubilisation buffer (10% (w/v) SDS, 200 mM HEPES pH 8.5) and then vortexing for ~ 5 sec to mix. Each sample was then sonicated in a waterbath sonicator for 10 min, and then vortexed at the conclusion of the sonication. Lysates were reduced and alkylated by adding TCEP and chloroacetamide (CAA) to final concentrations of 10 mM TCEP (Pierce™) and 40 mM CAA

(Sigma), and incubating samples statically at 37 ˚C for 45 min. Lysates were then acidified by adding phosphoric acid to a final concentration of 1.2 %. Binding buffer (100 mM TEAB, 90% (v/v) MeOH, pH 7.1 with phosphoric acid) was added to each sample at a ratio of 1 : 7 sample volume to binding buffer, and samples were vortexed to ensure a homogenous solution. Lysates were then loaded onto S-Trap™ Mini columns (Protifi™) and centrifuged at 6 500 x g for 30 sec, repeated until the total sample was loaded with flow through discarded between each spin. Columns were washed by adding 400 µL binding buffer and centrifuging at 6 500 x g for 30 sec. One wash was performed in the loading orientation, and then one wash was performed with the tube orientation flipped by 180 ˚C, and then the tube orientation was changed to its starting position for a further 2 washes. The lid of each column was then snipped free from the collection tube, and columns were moved to 2 mL LoBind microfuge tubes (Eppendorf). To each sample, 125 µL of digestion buffer (50 mM TEAB) supplemented with sequencing grade Trypsin (Promega) at a concentration of 1 µg trypsin : 50 µg equivalent sample per 125 µL was added directly to the column filter. Samples were centrifuged at 1 000 x g for 30 sec to ensure the digestion buffer penetrated the total filter surface. The digestion buffer flowthrough was then pipetted back onto the top surface of the filter and samples were sealed with parafilm and incubated statically at 37 ˚C for 16 h overnight. To elute the digested peptides, 80 µL of digestion buffer (no trypsin) was added and samples were spun at 3 200 x g for 60 sec, 80 µL of 0.2% (v/v) formic acid (FA) was added and samples were centrifuged at 3 200 x g for 60 sec, and 80 µL of 50% (v/v) acetonitrile (ACN)/0.2% (v/v) FA was added and samples were centrifuged at 6 500 x g for 60 sec. The pooled elutions were then lyophilised and stored at -80 ˚C for downstream analysis.

2.4.2: TMT-labelling

Lyophilised samples were reconstituted in 100 mM TEAB through incubating samples at RT for 15 min, and then sonicating samples in a waterbath sonicator filled with ice slurry for 5 min. Concentration estimates were performed by spectroscopic measurement of sample absorbance at the 280 nm wavelength using a Nanodrop ND-1000 UV-Vis Spectrophotometer (Thermo Fisher Scientific). Aliquots of 10 µg of each sample were diluted to a total volume of 100 µL in 100 mM TEAB. A pooled batch control was generated by dividing 100 µg by the total number of samples in the dataset, and pooling that µg quantity of peptides from each sample into a single tube, and diluting the total volume to 100 µL in 100 mM TEAB (eg. for 100 samples, 1 µg of peptides from each sample are pooled together). Samples were divided into batches of 10 samples (see Appendix IV for batch label layout), and the volume of each TMT label was divided by the number of batch

samples to be labelled (maximum 7 batches per 0.8 mg label). TMT labels (A37725; Thermo Scientific™) were equilibrated to RT and reconstituted in 41 µL ACN per tube by incubation at RT for 5 min with occasional vortexing. The desired volume of each label was added to each sample, samples were vortexed to mix, and the labelling reaction was left to proceed at RT for 1 h. To quench the reaction, 8 µL 5% (v/v) hydroxylamine (Pierce™) was added to each sample and samples were vortexed to mix, and then incubated at RT for 15 min. Batches of samples were then combined together in one tube, and batches were lyophilised and stored at -80 ˚C prior to fractionation.

2.4.3: Reverse-phase high pH-based fractionation

Lyophilised samples were reconstituted in 300 µL of 0.1% (v/v) trifluoroacetic acid (TFA) by incubation at RT for 15 min followed by 5 min sonication in an ice slurry in a waterbath sonicator. Samples were loaded onto High pH Reversed Phase Fractionation columns (Pierce™) and fractionated as per manufacturer's instructions, with a modified elution gradient (Table 2.7). After elution, samples were concantenated in an equidistant manner to generate 6 sample fractions per batch sample (Elution 1 combined with elution 6, elution 2 combined with elution 7, cont.). Concantenanted samples were lyophilised and reconstituted in 50 µL of 2% (v/v) ACN/0.1% (v/v) FA and stored at 4 ˚C prior to mass spectrometry analysis.

Elution step	% ACN	% TEA (0.1%)
Wash	5	95
1	9	91
2	13	87
3	17	83
4	21	79
5	25	75
6	29	71
7	33	67
8	37	63
9	41	59
10	45	55
11	50	50
12	55	45

Table 2.7 **Modified high pH-based fractionation gradient**.

2.4.4: TMT-based mass spectrometry parameters

Using a Dionex UlitMate 3000 RSLCnano system equipped with a Dionex UltiMate 3000 RS autosampler, the samples were loaded via an Acclaim PepMap 100 trap column (100µm×2cm; nanoViper; C18; 5µm; 100Å; Thermo Fisher Scientific) onto an Acclaim PepMap RSLC analytical column (75µm×50cm; nanoViper; C18; 2µM; 100Å; Thermo Fisher Scientific). The peptides were separated by increasing concentrations of 80% (v/v) ACN/0.1% (v/v) FA at a flow of 250 nL/min^{-1} for 158 min and analysed with an Orbitrap Fusion Tribrid mass spectrometer (Thermo Fisher Scientific) operated in data-dependent acquisition mode. Each cycle was set to a fixed cycle time of 2.5 sec consisting of an Orbitrap full ms1 scan at resolution of 120 000, normalised AGC target of 50%, maximum IT of 50 ms, scan range of 380 – 1580 m/z. ms1 precursors were filtered by setting monoisotopic peak determination to peptide, intensity threshold to 5.0e3, charge state to 2 – 6 and dynamic exclusion to 60 s. Precursors were isolated in the quadrupole with a 1.6 m/z isolation window, collected to a normalised AGC target of 40% or maximum injection time (150 ms), and then fragmented with a CID collision energy of 30%. For ms3 scans, spectras were then filtered with a precursor selection range of 400 – 1200 m/z, isobaric tag loss exclusion of TMT and precursor mass exclusion set to 20 m/z low and 5 m/z high. Subsequently, 10 synchronous precursor ions were selected and scans were acquired at resolution of 50 000, normalised AGC target of 100%, maximum IT of 250 ms, and scan range of 120 – 750 m/z.

2.5: Data analysis techniques

2.5.1: Calculation of mitochondrial protein solubility

Raw instrument files were processed using MaxQuant version 1.6.17 with the Andromeda search engine (*163*), searching against the Uniprot human database containing reviewed and canonical isoform variants in FASTA format (2021), with the recombinant Ag85A sequence added as an entry in the human database. All data was analysed using the MaxQuant proteomics data analysis workflow with modifications (*163*). In brief, LC-MS run was set to "Reporter ion MS3" and TMT11-plex labels were set as isobaric labels with a reporter ion mass tolerance of 0.003 Da. Trypsin/P cleavage specificity was used with a maximum of 2 missed cleavages. Oxidation of methionine and N-terminal acetylation were set as variable modifications, and carbamidomethylation of cysteine was set as a fixed modification. A search tolerance of 4.5 ppm was used for ms1 and 20 ppm was used for ms2 matching. False discovery rates (FDR) were

determined through the target-decoy approach and set to 1% for both peptides and proteins. The 'Match between runs' option was enabled with a match time window of 0.7 min. The 'Dependent Peptides' option was enabled, with an FDR of 1% and a mass bin size of 0.0065 Da. Minimum unique and razor peptides was set to 1, and label min. ratio count was set to 2.

Data from the proteinGroups.txt output table was then normalised according to methods described previously (*164*). The internal spiked control (Ag85A) intensities were averaged across each reporter ion channel, and this value was used to generate scaling factors for each channel to normalise reporter ion intensities for each protein to the relative starting intensities in each sample at the time of Ag85A addition. After normalisation, data was imported into Perseus v1.6.15 and 'only identified by site', 'reverse', and 'potential contaminant' identifications were removed (*165*). Cleaned data was exported from Perseus and imported into Microsoft Excel, where data was then filtered according to a database of mitochondrial proteins so as to only include mitochondrial proteins for downstream analysis (*166*). Computationally derived total intensities were then generated for each protein in each sample through addition of the soluble and insoluble sample fraction intensities. A percentage of total protein that was in the insoluble fraction was then calculated using the calculated total intensity.

Calculations used to determine protein solubility (%):

$$Protein\ solubility\ (\%) = \left(\frac{normalised\ insoluble\ sample\ intensity}{normalised\ total\ sample\ intensity}\right) \times 100$$

Aggregation index (AI) analysis was performed by calculating the average percentage of protein that is insoluble across a defined process group of mitochondrial proteins.

Calculation used to determine aggregation indices:

$$Aggregation\ index = \frac{summed\ protein\ solubility\ (\%)}{total\ number\ of\ proteins}$$

All calculations were performed in biological triplicate, and solubility shifts were not calculated for proteins that were only detected in the soluble or insoluble sample fractions.

2.5.2: Transcriptomic data analysis

Bioinformatics analysis of NGS data was performed with the support of the Monash Bioinformatics Platform (Monash University). Analysis of NGS data was performed using the rnasik 1.5.4 pipeline with STAR aligner, using the GRCh38 (*Homo sapiens*) reference genome (*167*). A UPR^{mt} induced change in gene expression was defined as changes that were statistically significant (FDR ≤ 0.05) with increased or decreased expression relative to the WT DMSO control samples of $> \pm 0.2$ fold.

Chapter 3

Development of an experimental system to analyse endogenous mitochondrial proteostasis

3.1: Introduction

To date, a wide variety of experimental systems have been employed to trigger a mitochondrial proteostatic stress to study the UPR^{mt}. The first study to identify the mammalian UPR^{mt} used transient ectopic expression of truncated transcript of ornithine transcarboxylase (OTC), a mitochondrial protein which is basally expressed only in liver tissue (*77*). Truncated OTC (ΔOTC) misfolds when imported into mitochondria, inducing a proteostatic stress and triggering the UPR^{mt} (*77*). Levels of ΔOTC accumulation in mitochondria provide a readout on the protein-quality control capacity of mitochondria and let researchers identify defects in the UPR^{mt} pathway. While other methods of inducing a protein folding stress, including pharmacological inhibition of LONP1 and genetic knockdown of mitochondrial protein folding machineries have also been employed to study the UPR^{mt}, these methods have seen less widespread use due to problems with the pleiotropic effects of the LONP1 inhibitor CDDO (*168-170*), and the risk of unintended beneficial or maladaptive changes to the mitochondrial proteome through constitutive proteostatic stress with stable gene knockout (KO) or knockdowns (KD) (*171*).

Accordingly, the ΔOTC model of UPR^{mt} induction has become the most widely adopted method of studying the mammalian UPR^{mt} pathway. Its use has led to numerous important discoveries in the signalling and machinery of the UPR^{mt} in both mammalian cell culture and *Drosophila Melanogaster* models (*86, 149*). However, the ΔOTC method of UPR^{mt} induction has some limitations. The ΔOTC system requires chronic doxycycline treatment to induce ΔOTC

accumulation, and doxycycline is a well-documented mitochondrial toxin that impairs mitochondrial protein translation (*172*). Doxycycline may generate a compounding stressor and complicate study of UPR^{mt} specific aspects of the stress response. Lastly, analysis of ΔOTC levels also provides limited information on the overall protein-folding capacity of mitochondria during the UPR^{mt} program, as changes in ΔOTC levels may not reflect the behaviour of the endogenous mitochondrial proteome.

This chapter details the initial characterisation of a ΔOTC-driven UPR^{mt} program in a HeLa cell model, including documentation of additional experimental limitations encountered through its use. In response to those limitations, a new method of UPR^{mt} analysis using an acute endogenous protein folding stress has been developed to address limitations of the ΔOTC system and to allow for comprehensive study of endogenous mitochondrial proteostasis and the UPR^{mt} pathway.

3.2: Characterising UPR^{mt} induction during ΔOTC stress

While an acute ΔOTC expression stress has been used to identify UPR^{mt} components, little work has been conducted on the kinetics of UPR^{mt} stress signalling and the interplay between the UPR^{mt} related transcription factors. To examine UPR^{mt} signalling kinetics, WT HeLa cells stably expressing a doxycycline-inducible ΔOTC cassette were treated with 1 μg/mL doxycycline for 5 days to monitor the induction of UPR^{mt} signalling. Samples were collected every 24 h to monitor transcription factor induction and ΔOTC levels as a readout of protein aggregate accumulation and UPR^{mt} mediated removal. Immunoblot analysis of ΔOTC levels showed a continual accumulation of ΔOTC across days 1 – 3 prior to gradual reduction in levels at days 4 - 5, indicating a biphasic response of accumulation, then active removal of mitochondrial protein aggregates in response to a chronic protein-folding stress (Figure 3.1 A, B). A biphasic response may indicate either a delay in activation of the UPR^{mt} until a threshold level of protein folding stress is reached, or a delay in the effects on mitochondrial protein aggregation after upstream UPR^{mt} signals are initiated. To clarify when stress signalling begins during the doxycycline time course, CHOP levels were measured by immunoblot (Figure 3.2 A, B). Expression of CHOP was weakly detected at day 2 and then clearly detected at day 3 which correlated with the peak of ΔOTC accumulation (Figure 3.2 A). CHOP levels remained elevated through to day 5, suggesting the biphasic trends in ΔOTC levels may be due to UPR^{mt} activation after a threshold of protein misfolding is breached (Figure 3.2 A, B).
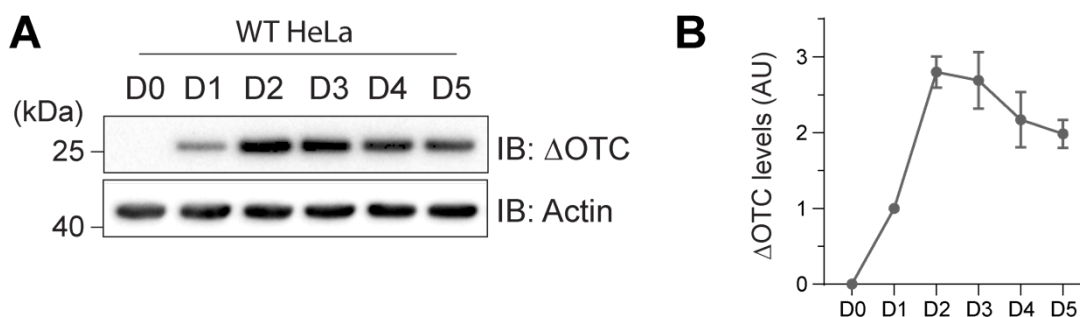
Figure 3.1 **ΔOTC induction in WT HeLa cells. A**, **B**. Cells were treated with 1 μg/mL doxycycline for 5 days (D, day) and ΔOTC accumulation was measured by immunoblot (IB; **A**) and quantified (**B**). Data in **B** was generated from 3 independent experiments.

Given that CHOP can also be activated in response to non-mitochondrial derived cell stress, PINK1 levels were measured by immunoblot as a readout of mitochondrial stress to determine if the CHOP signalling observed was independent of mitochondrial damage (Figure 3.2 A, C). While low levels of PINK1 stabilisation were seen at day 2, strong accumulation began at day 3 and continued to increase throughout the time course (Figure 3.2 A, C). PINK1 accumulation trends mirrored CHOP expression levels, suggesting CHOP signalling is coupled to mitochondrial stress levels.

To confirm if the UPR^{mt} through CHOP is driving the proteostatic repair and ΔOTC clearance observed during day 4 – 5, CHOP KO cells were generated by TALEN gene editing from the parental WT cells expressing the inducible ΔOTC construct (Appendix V). Both WT and CHOP KO cells were subjected to the 5-day time course doxycycline treatment and ΔOTC levels were measured by immunoblot (Figure 3.3 A). In contrast to the biphasic ΔOTC levels observed in
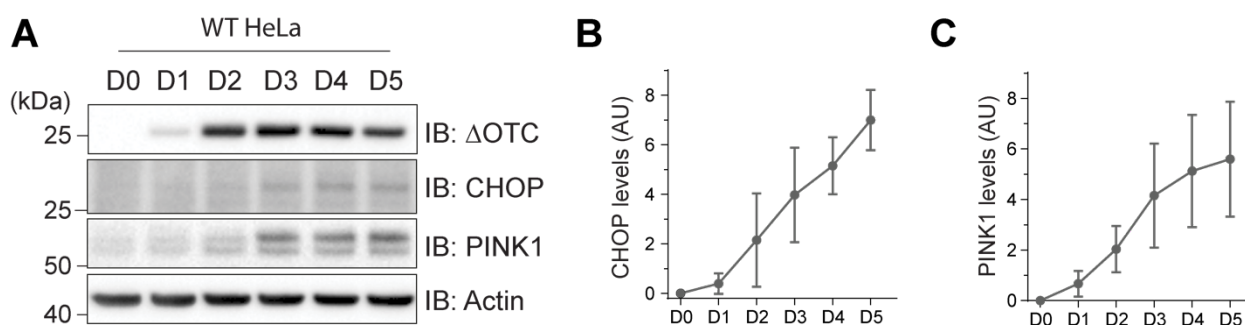
Figure 3.2 **Mitochondrial stress induction through ΔOTC expression in WT HeLa cells.** Cells were treated with 1 μg/mL doxycycline for 5 days (D, day) and levels of CHOP induction and PINK1 accumulation were measured by immunoblot (**A**) and quantified (**B**, CHOP; **C**, PINK1). Data in (B, C) was generated from 3 independent experiments.

WT cells, CHOP KO cells continued to accumulate ΔOTC throughout the time course and showed no evidence of ΔOTC aggregate removal throughout the 5 day period, indicating CHOP plays an important role in ΔOTC clearance (Figure 3.3). However, as the CHOP KO cells are a single clonal line derived from the parental WT line, it cannot be guaranteed that the cell line is expressing the same amount of the ΔOTC construct as the WT population which could perturb results. High expression of ΔOTC may overwhelm the mitochondrial protein import system, affecting the ability of the UPR^{mt} program to import molecules to repair proteostasis. The higher molecular weight (MW) band corresponding to the unimported, unprocessed precursor in the immunoblot of OTC in Figure 3.3A suggests import disruption may be occurring in the CHOP KO cell line. The problem with clonal ΔOTC expression variation would also be further amplified through the creation and integrated analysis of other KO lines (eg ATF4 KO, ATF5 KO).
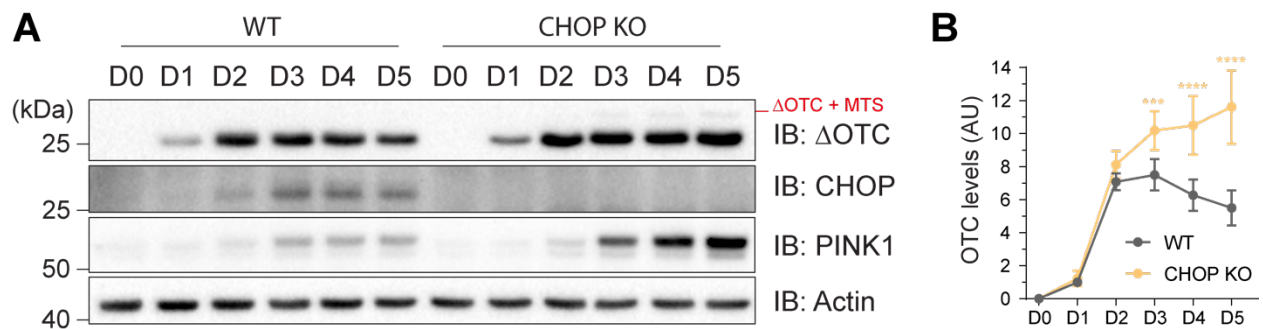
Figure 3.3 **ΔOTC induction in WT and CHOP KO cells**. WT and CHOP KO cells were treated with 1 µg/mL doxycycline for 5 days (D, day) and levels of CHOP, PINK1 and ΔOTC accumulation were measured by immunoblot (**A**). ΔOTC accumulation in WT and CHOP KO cells was quantified relative to WT levels at D1 (**B**). ***$P \leq 0.001$, ****$P \leq 0.0001$ (two-way analysis of variance (ANOVA)). Data in **B** was generated from 3 independent experiments.

In addition to potential expression level issues, there is no capacity in the ΔOTC assay to analyse changes to endogenous mitochondrial proteostasis to validate if ΔOTC changes reflect proteome wide responses. Unlike ΔOTC where total protein levels represent total misfolded protein, total levels of endogenous mitochondrial proteins give no indication of the folding state of the protein, as protein from the spectrum of misfolded to fully functional exist within those total levels. Whether or not there is specific susceptibility of certain mitochondrial proteins to protein-folding stress cannot be answered with the ΔOTC assay. Localised PINK1/Parkin mitophagy has also been shown to occur selectively at ΔOTC aggregates in regions with no loss of membrane potential

(*173*). Mitochondrial stress and PINK1 accumulation observed with ΔOTC expression (Figure 3.3 A) may form through localised import blocks in selected mitochondrial regions with ΔOTC aggregates, rather than through endogenous changes in mitochondrial proteostasis. With consideration of these issues, the decision was made to move away from the ΔOTC system for inducing the UPR^mt.

3.3: Induction of the UPR^mt using G-TPP

A recent study by *Fiesel et al.* (2017) demonstrated that Gamitrinib-triphenylphosphonium (G-TPP), a small molecule inhibitor of mitochondrial HSP90 (TRAP1) can induce an acute and specific mitochondrial protein folding stress that leads to induction of UPR^mt associated genes including CHOP, ATF4 and ATF5 (*102, 142*). Instead of overwhelming protein folding capacity through exogenous expression of a misfolded protein, G-TPP instead reduces the intrinsic protein folding capacity of mitochondria by reducing chaperone activity. Endogenous protein misfolding is the preferred method of inducing mitochondrial proteostatic stress as the composition of the mitochondrial proteome remains intact and isn't affected by overexpression of proteins that do not normally reside in mitochondria. The resulting signalling can then be more confidently presumed to be occurring through proteostatic stress rather than the pleiotropic effects of an overexpressed misfolded protein. To confirm that G-TPP treatment induces signalling indicative of the UPR^mt, WT HeLa cells were treated with G-TPP for up to 10 h. Strong induction of CHOP was detected by immunoblot, increasing as the treatment duration progressed, confirming that G-TPP induces a UPR^mt like signalling response in our HeLa cell system (Figure 3.4).
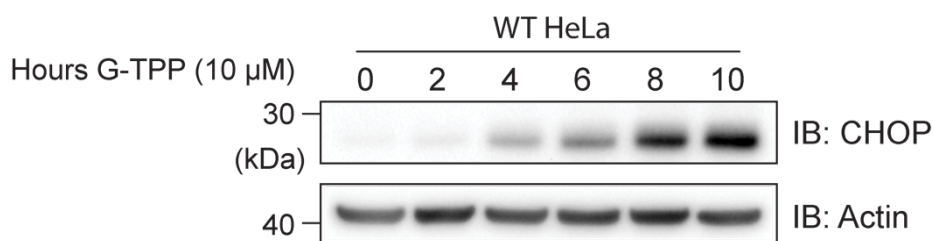
Figure 3.4 **CHOP induction in WT HeLa cells with G-TPP treatment.** Cells were treated with 10 μM G-TPP for the indicated times, and levels of CHOP were analysed by immunoblot.

3.4: Trialling methods of soluble and insoluble protein isolation

While G-TPP treatment can trigger endogenous protein folding stress, no method existed to analyse the output of the UPR^{mt} signalling on mitochondrial proteostasis, as the identity of endogenous misfolded proteins is unknown. To enable analysis of UPR^{mt} mediated changes in endogenous mitochondrial proteostasis, I developed an assay that allows for measurement of the proportion of endogenous mitochondrial protein that exist in a folded/soluble state and a misfolded/insoluble state with G-TPP treatment. Both a western blot compatible and a mass-spectrometry based method were developed to allow for both protein-specific and proteome-scale analysis of endogenous mitochondrial proteostasis.

Isolated mitochondria were used as the starting sample for proteostasis analysis instead of whole-cell samples to ensure all protein quantified would be representative of proteins currently within mitochondria, and not pre-imported cytosolic mitochondrial proteins which are typically unfolded and bound to chaperones (*19, 174*). To analyse protein solubility, both the soluble and insoluble mitochondrial fractions need to be isolated and quantified. Two different previously published methods of separating soluble and insoluble protein were trialled using high-speed centrifugation methods common in protein aggregation studies to pellet insoluble protein, which was coupled with the use of ionic or non-ionic detergent solutions to resolubilise protein aggregates (see summary table in Figure 3.5 A). Both the pellet and soluble fractions were isolated from G-TPP and vehicle (DMSO) treated mitochondria using the two different high-speed isolation methods. Soluble and pellet fractions were run on an SDS poly-acrylamide gel and global changes in pellet protein composition were analysed using colloidal-coomassie staining (Figure 3.5 B). Method #1 using an SDS-based lysis buffer produced poor isolation of aggregated proteins. No difference in the aggregated protein load of mitochondria with and without G-TPP treatment was seen with this method, suggesting the ionic detergent lysis over-solubilised the sample preventing protein aggregate isolation. In contrast, significantly more protein was seen in the insoluble fractions isolated from G-TPP treated mitochondria compared to DMSO treated mitochondria using method #2, suggesting the non-ionic detergent-based lysis allows for extraction of insoluble protein and separation from soluble protein. Soluble and insoluble samples extracted using method #2 were analysed by mass spectrometry using standard preparation and resolublisation techniques including boiling samples, water bath sonication and urea-based denaturation. Chloroform/methanol precipitation was used to remove the NP-40 detergent from the lysates. After resolubilisation of the sample, some flakes of material were observed in solution indicating some proteins were highly resistant to resolublisation after ultra-centrifugation. Accordingly, some material could not be analysed due to this issue. When the protein that was sufficiently

resolubilised was analysed by mass spectrometry, the spectral patterns produced from these samples displayed characteristic features of detergent contamination, including repeating peaks at +44 Da indicative of PEG contamination from the NP-40 detergent, and late sample elution across the LC run, indicating the chloroform/methanol precipitation was insufficient to fully remove the NP-40 detergent from samples. Accordingly, the detergent contamination prevents mass spectrometry analysis of samples isolated using method #2 (Figure 3.5 C) (*175*).

A third method of aggregate isolation was trialled, based on a publication from *Jin et al.* (2013) that used a low concentration, non-ionic, detergent-based lysis and low speed centrifugation to isolate insoluble protein (Figure 3.5 A) (*173*). As high-speed centrifugation can induce artificial protein aggregation (*176*), it was thought the low speed spin of this protocol may result in both easier sample solubilisation and more biologically relevant protein aggregate isolation. Unfortunately, trials of fraction isolation using method #3 still produced visible pellet flakes seen in method #2 that visibly did not fully resolubilise with standard boiling and sonication. To promote sample solubilisation, a 5% (w/v) SDS resolubilisation solution coupled with a short water bath-based sonication was trialled, and these changes led to successful resolubilisation of the visible protein pellets. Fraction samples from G-TPP treated and DMSO treated mitochondria were isolated using method #3 and relative protein concentrations in each fraction were analysed using colloidal-coomassie staining (Figure 3.5 D). Unlike the trials of methods #1 and #2, no protein bands were present in the well-area at the top of the gel, indicating that the new resolubilisation method effectively resolubilised the isolated protein aggregates (Figure 3.5 B, D). A clear increase in insoluble protein can be seen in the G-TPP treated pellet fraction of Figure 3.5 D, demonstrating the low-speed centrifugation method can differentially isolate misfolding protein with a proteostatic stressor while avoiding introducing centrifugation-based aggregation artifacts (*176*). Given that detergent carry-through in samples is problematic for mass spectrometry analysis, and since 5% (w/v) SDS is a considerably higher concentration of a stronger detergent than the 0.4% (v/v) NP-40, which was not successfully removed in earlier attempts with chloroform/methanol precipitations, a commercial detergent extraction kit for mass spectrometry sample preparation from Protifi™ was used to test the mass spectrometry analysis of samples isolated using method #3. Mass spectrometry samples prepared using S-Trap™ columns from Protifi™ showed no indication of detergent carry-over and produced clean samples that eluted gradually across the LC-MS run time as expected (Figure 3.5 E). Taken together, the mass spectrometry and colloidal-staining data (Figure 3.5 D, E) confirmed that isolation method #3 could successfully isolate insoluble protein from mitochondria and produce samples that can be

analysed by mass spectrometry. With validation of these critical technical components, an analytical pipeline was then developed to enable analyses of mitochondrial proteome solubility.
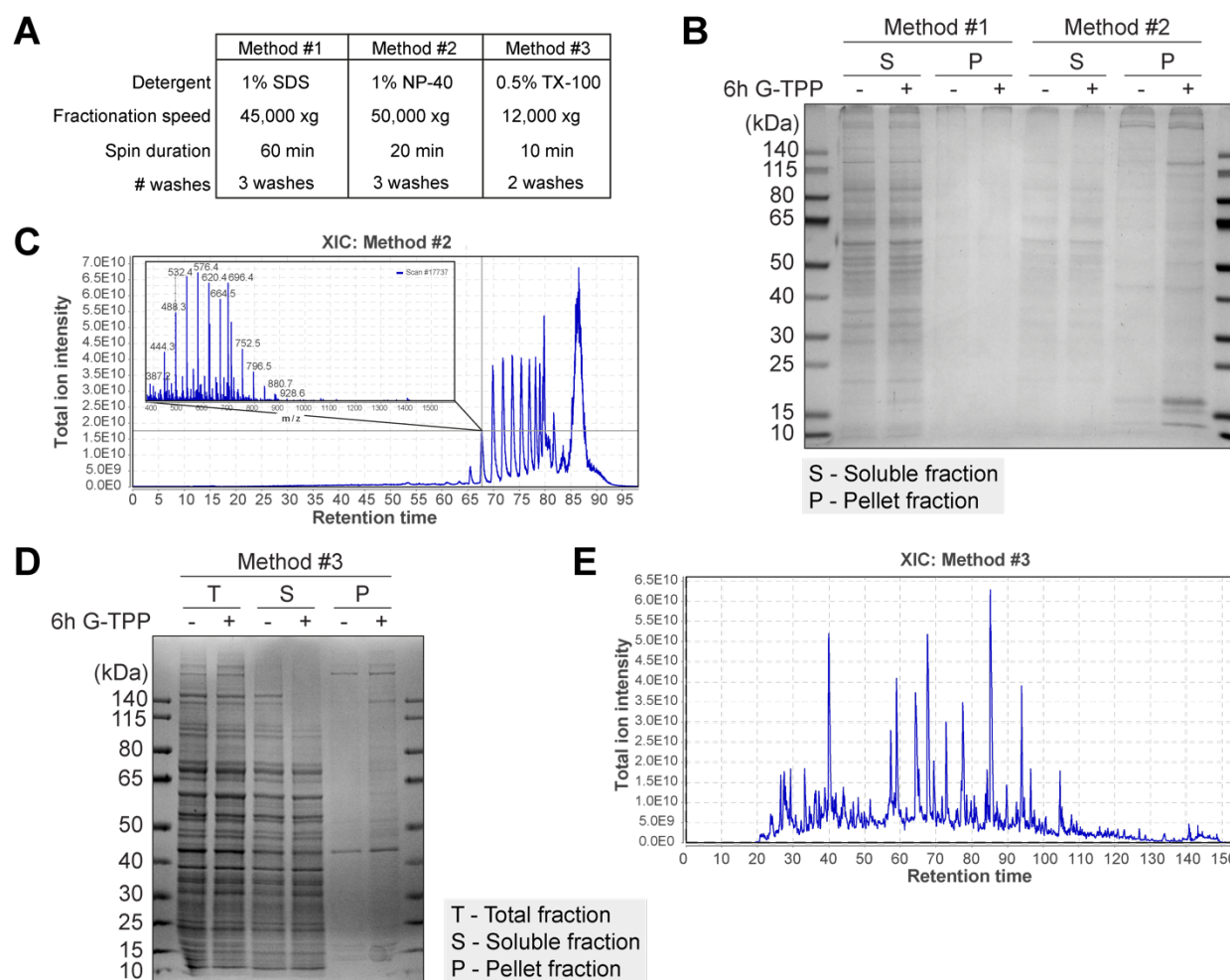
Figure 3.5 **Trialling alternative methods of isolating soluble and insoluble mitochondrial protein fractions.** A summary of key parameters of the different fractionation methods trialled in this work has been provided in **A**. Method #1 (*142*), method #2 (*177*), and method #3 (*173*) were sourced from previously published literature. Isolated mitochondrial samples from WT cells treated with DMSO or G-TPP as indicated were fractionated using methods #1 - #3 from **A** and isolated proteins were analysed by SDS-PAGE and colloidal-coomassie staining (**B, D**). The extracted ion chromatogram (XIC) representative of the total ion current chromatogram from the mass spectrometry analysis of the aggregated protein fraction prepared using method #2 has been provided in **C**, and method #3 has been provided in **E**. A representative ion trace with the characteristic repeating +44 Da units of PEG contamination through detergent carry through that was found throughout the sample has been provided in the inset of **C**. Chromatogram traces were generated using MZmine2 (*178*).

3.5: Developing an analysis pipeline to analyse endogenous mitochondrial proteostasis

Identifying proteins that increase in the insoluble fraction after G-TPP treatment provides important information about the cohort of proteins that may be more susceptible to proteostatic stress. However, it is difficult to draw functional conclusions from identity-based data alone. This is because a large amount of insoluble protein could either represent aggregation of that protein, or it could instead result from an increase in the total amount of the protein. In the latter case, increased levels of aggregation resulting from higher total levels may not change the amount of soluble, functional protein in mitochondria, meaning the aggregation observed may not strongly affect mitochondrial function. Conversely, a small enrichment in an insoluble protein fraction of a lowly abundant protein may represent the loss of a majority of the soluble functional protein of that gene in mitochondria, which could have important impacts on mitochondrial function.

To analyse the functional impact of protein aggregation, changes were made to the initial sample isolation and mass spectrometry protocol used in Chapter 3.4 to allow for calculation of the solubility of each mitochondrial protein detected by mass spectrometry, relative to the total amount of that protein present in the starting mitochondrial sample.

In brief, a bacterial-origin protein with no homology to the human proteome, Ag85A (*Mycobacterium tuberculosis*), was spiked in at a standard amount to each soluble and insoluble protein fraction prior to resolublisation in a 5% (w/v) SDS solution. By spiking in a protein standard at this stage, the relative amounts of each protein can be preserved throughout downstream sample preparation and analysis. Protein levels in the mass spectrometry samples can be normalised back to their relative starting intensities using Ag85A quantification after standardised amounts are loaded on a mass spectrometer, thereby preventing over-inflation of protein intensities in samples with a small amount of precipitated protein. The sample intensities of both the soluble and insoluble fractions can then be combined to generate a computationally derived total fraction intensity. A benefit of the low-speed centrifugation method that allows for this analysis is the 'dirty' sample isolation relative to a high-speed centrifugation methods with more washes. Through the impure separation from the low-speed centrifugation protocol, nearly all mitochondrial proteins are present in both the soluble and insoluble samples, simply varying in their relative amounts depending on their propensity to aggregate in that sample (Figure 3.6 B), meaning accurate solubility shifts can be calculated for nearly all mitochondrial proteins. A summary of the mass spectrometry workflow developed for this work is provided in Figure 3.6.
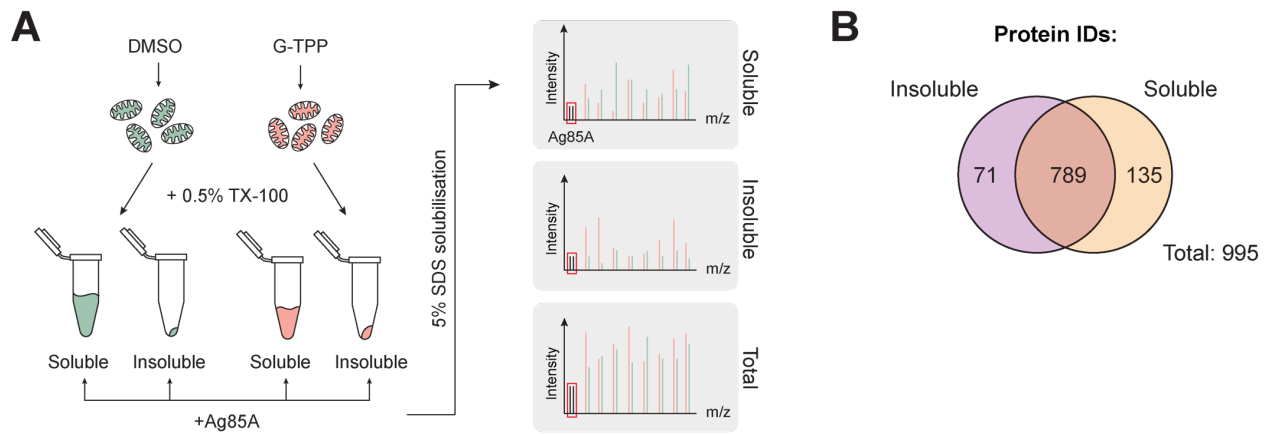
Figure 3.6 **Overview of protein solubility procedure and analysis pipeline. A**. Schematic of the mass spectrometry analysis procedure developed in Chapter 3. **B**. Venn diagram of protein IDs that were identified in either the soluble, insoluble, or both soluble and insoluble fractions in mass spectrometry analysis of fractionated samples from G-TPP and DMSO treated mitochondria.

3.6: Investigating the protein solubility signature in WT cells with a functional UPR^mt during an acute G-TPP treatment

Mitochondrial protein solubility in WT HeLa cells undergoing vehicle (DMSO) or G-TPP treatment for 12 h were analysed using the endogenous protein solubility assay developed in this chapter. A total of 995 mitochondrial proteins were analysed, and solubility shifts were able to be calculated for 789 mitochondrial proteins (Figure 3.6 B). Global heat map analysis of changes in mitochondrial protein solubility with G-TPP treatment showed specific increases in the aggregation of select clusters of mitochondrial proteins, suggesting some mitochondrial proteins may be more susceptible to proteostatic stress, or not well protected by the UPR^mt (Figure 3.7 B). Gene ontology (GO) analysis of proteins with >20% increase in aggregation following G-TPP treatment (257 proteins) produced distinct clusters of proteins associated with transcription and translation, OXPHOS, and metabolism related proteins, confirming that proteins from select biological classes show a higher propensity to aggregate with G-TPP treatment (Figure 3.7 A). As anticipated from prior literature, increased total levels of mitochondrial proteases and chaperones were detected, indicative of UPR^mt activation (Figure 3.7 D). Surprisingly, some clusters of highly aggregation prone proteins such as the translational machinery of mitochondria appeared to increase in total levels during G-TPP treatment (Figure 3.7 D). While increased expression of the translation machinery seems counterintuitive, particularly if the protein is aggregating shortly after import as the decreased levels of soluble protein suggests, the increased protein levels could indicate a block in the basal turnover of mitochondrial ribosomes through proteases becoming

preoccupied with breaking down new protein aggregates. Lower levels of soluble LONP1 and the ClpP complex were present in G-TPP treated samples, even though total levels of those proteases increased, suggesting some of the increases in total protein levels detected may be explained through blocks in basal degradation usually performed by these proteases (Figure 3.7 D). Western blot analysis of fractionated mitochondria undergoing G-TPP treatment was performed to validate both the total protein trends and the aggregation trends calculated in the mass spectrometry samples. A custom 5% SDS loading dye was used to mirror the mass spectrometry sample resolubilisation conditions. In agreement with the mass spectrometry data, proteins such as LRPPRC and MRPS27 increased in total levels by western blot, while VDAC1 showed no change in total level (Figure 3.7 C). As G-TPP inhibits a specific mitochondrial chaperone (mtHSP90), a question raised is whether the aggregation trends observed above comprise the aggregation of mtHSP90 clients. While TRAP1 clients are not comprehensively well defined, a published IP-MS based dataset using HEK293T cells expressing a mutant TRAP1 gene to capture client proteins was compared to the aggregation data in Figure 3.7 (*179*). In total, 10 mtHSP90 client proteins were detected, which saw minimum and maximum aggregation % shifts with G-TPP treatment of -0.52% and 54.24% respectively. A median aggregation of 3.33% was seen in the detected HSP90 client proteins. In contrast, another published IP-MS dataset of mitochondrial HSP60/HSP10 client proteins were compared to the data in Figure 3.7 (*180*). This second dataset contained more starting candidate proteins than the HSP90 dataset, with 200 HSP60/HSP10 client proteins identified in the data in this thesis. Those 200 clients saw a minimum aggregation % shift of -0.31%, a maximum aggregation shift of 69.24%, and a median aggregation shift of 26.84%. Although G-TPP specifically targets the HSP90 chaperone, this analysis demonstrates that other chaperone systems actually experience more proteostasis disruption than the HSP90 client system. A flow on collapse of the proteostasis capacity of mitochondria appears to be occurring, confirming that the analysis hasn't been restricted to HSP90 clients and is instead representative of the aggregation that occurs with widespread stress to the mitochondrial protein folding system. Overall, the analysis of WT cells with and without G-TPP treatment has validated the capability of the solubility assay to accurately analyse stress-induced changes in mitochondrial proteostasis. Additionally, the solubility analysis revealed a selective collapse of specific clusters of proteins involved in OXPHOS and translation during mitochondrial protein-folding stress in cells with a functional UPR^{mt} program. A more detailed analysis of changes to the mitochondrial proteome during proteostatic stress is performed in the following chapters.
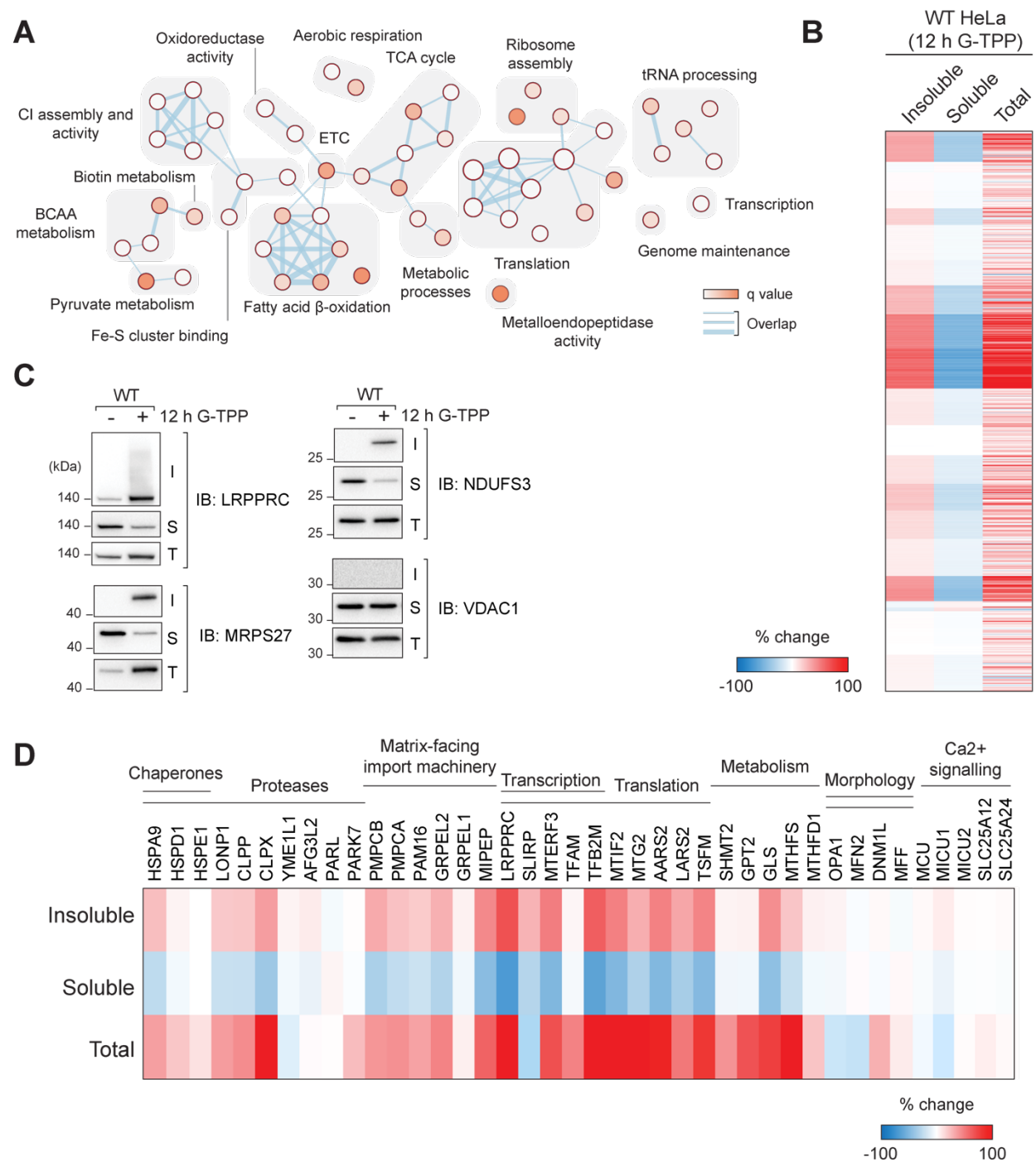
Figure 3.7 **Analysis of mitochondrial protein solubility in WT cells treated with G-TPP**. **A.** Gene ontology analysis of proteins that shift towards the aggregated fraction in G-TPP treated WT cells. **B**. Heat map of the percentage (%) change in composition of the soluble, insoluble and total mitochondrial protein fractions in WT cells undergoing G-TPP treatment, compared to WT vehicle (DMSO) treated cells. **C**. Immunoblot validation of the aggregation patterns identified through mass spectrometry analysis for LRPPRC, MRPS27, NDUFS3 and VDAC1. I – insoluble, S – soluble, T – total. **D**. Heat map representation of select proteins from (**B**). Data in **A**, **B**, **D** was generated from 3 independent experiments.

3.7: Discussion

3.7.1: Use of a G-TPP induced proteostatic stress compared to ΔOTC-based stress induction

Mitochondria are thought to activate stress signalling responses according to the initiating stress stimulus. For example, a cytosolic stress response encompassing increased levels of cytosolic chaperones and increased proteasomal activity is activated in response to mitochondrial protein import block (*181*). Mouse models of mitochondrial DNA dysfunction display CHOP, ATF4 and ATF5 transcription factor induction, similar to what is observed during the UPR^mt, but traditional UPR^mt proteases and chaperones including ClpP and YME1L1 are not induced (*182, 183*). Instead, mitochondrial one-carbon metabolism related proteins are strongly upregulated, indicating that mtDNA depletion stress induces specific cellular pathways to boost mtDNA synthesis and repair (*182*). It is therefore important when studying the intricacies of mitochondrial stress response pathways to ensure that a targeted mechanism of stress induction is used to prevent accidental study of alternative co-activated mitochondrial stress response pathways.

The ΔOTC system has been successfully used to identify components of the UPR^mt pathway, but when studying intricacies of the UPR^mt signalling response, the use of ΔOTC can pose some risks. Intrinsic to the method of selective ΔOTC expression is the treatment of cells with doxycycline over a prolonged 5 day period. Doxycycline is a well-documented, potent inhibitor of mitochondrial translation (*172*). Treatment as short as 24 – 48 hours at the concentration required to induce ΔOTC expression can cause mitochondrial fragmentation, a selective reduction in mtDNA encoded OXPHOS subunits, and a decrease in basal mitochondrial respiration (*172, 184*). Accordingly, doxycycline treatment may induce deleterious mitochondrial phenotypes before a ΔOTC induced UPR^mt response can be triggered. While doxycycline itself has been used to trigger mitochondrial stress responses (*101*), it is unclear whether decreased mitochondrial translation triggers a UPR^mt specific program. Treatment of cells with chloramphenicol, another inhibitor of mitochondrial translation, produces a stress response signature of CHOP, ATF4 and ATF5 expression, but UPR^mt-related mRNA transcripts including mtHSP70, ClpP and HSP10 instead decrease from basal levels during treatment, suggesting activation of a non-UPR^mt related stress response (*185*). Accordingly, a 5-day treatment of cells with the translation inhibitor doxycycline is highly undesirable when we are intending to study misfolded protein stress-response related signalling pathways of the UPR^mt as we cannot be sure we are studying a UPR^mt specific response.

In contrast, G-TPP selectively targets the mitochondrial HSP90 protein chaperone. No off-target effects of G-TPP have been documented to date during characterisation of G-TPP, suggesting G-TPP is a targeted method of inducing mitochondrial protein folding stress compared to ΔOTC expression (*186*). Stress-response induction also occurs in a much more acute manner with G-TPP treatment, as evidenced from the short duration of G-TPP treatment in which a period of hours is required to induce CHOP expression (Figure 3.4), relative to the CHOP expression detected after 5 days of ΔOTC expression (Figure 3.2 A). While a stronger, more acute stress can risk overwhelming mitochondrial health and cross activating other mitochondrial or cellular stress response pathways, previous literature using G-TPP based UPR^{mt} models has demonstrated that activation of the integrated stress response can be avoided with G-TPP treatment (*102*). A concentration and treatment duration for the work in this thesis was optimised to ensure it was a strong enough stress to allow for study of the UPR^{mt} repair, but not so severe as to excessively overwhelm WT repair programs and cross-induce other cellular stress responses (data included in Chapter 5).

3.7.2: Considerations of protein solubility in proteomic analysis of mitochondrial stress conditions

Traditionally, mass spectrometry sample preparation methods have been developed with the goal of documenting the soluble and functional cellular proteome to be able to generate functional conclusions from changes to protein levels. An added difficulty is introduced when studying cellular stress conditions that can cause protein damage and misfolding, as these proteins can be missed in proteomic analyses if considerations aren't taken during the sample preparation stage to ensure these proteins are fully resolubilised and therefore are not lost from the sample.

Proteomic analysis of G-TPP treated mitochondria has previously been performed by *Münch et al.* (2016) using traditional sample preparation methods. Strong trends of decreases in protein levels of mitochondrial translation related and ribosomal related proteins were seen during G-TPP treatment, including decreases in LRPPRC and the MRP subunits (*102*). Decreased mitochondrial transcription and translation was also observed in these G-TPP treated samples, leading the authors to conclude that an active decrease in the levels of transcription and translation machinery leads to a shutdown of mitochondrial protein production during an acute protein folding stress (*102*). In contrast, the solubility analysis of G-TPP treated mitochondria presented in this chapter indicates that transcription and translation proteins are generally increased in levels during a G-TPP treatment, but the majority of these proteins are in an insoluble state (Figure 3.7 A, C, D). Changes

in total protein levels detected by *Münch et al.* (2016) mirrored the trends of decreased soluble protein levels in the analysis in Figure 3.7, suggesting the insoluble protein portion of the mitochondrial proteome may not have been detected in their analyses. While a decrease in soluble, functional protein levels will result in the same observed outcome as an overall decrease in total protein levels that are not misfolded, the biological explanation behind the observed decrease in translation would change. Instead of an active reduction in levels of transcription and translation proteins changing mitochondrial translation, the data in this chapter suggests an inherent susceptibility to proteostatic stress leads to a collapse of the transcription and translation machinery, which would also lead to decreased translation rates. Similar problems in data interpretation can occur even if efficient solubilisation of a partially aggregated sample is performed, but protein solubility is not taken into account. For example, if only total levels of the mitochondrial ribosome were analysed in Figure 3.7, the conclusion reached would be that increased mitochondrial translation may occur from an increase in mitochondrial ribosome levels, when instead the increase in total levels does not represent increases in soluble and functional protein. Discrepancies between mRNA induction and detected protein levels have also been noted during mitochondrial stress by *Quirós et al.*, (2017) who observed lower levels of MRP and OXPHOS proteins in their proteomic analysis than their transcriptomic analysis suggested (*101*). As both translation and OXPHOS related proteins were two of the most highly aggregation-prone sub-groups identified in the mass-spectrometry analysis in this chapter, the specific discrepancy in mRNA and detected protein levels in this data could suggest insoluble protein was lost in previously published analyses (*101, 102*). With consideration of solubility, more robust functional conclusions can be developed from proteomic data analysis, improving the ability of proteomic data to inform biological questions.

3.7.3: UPR^{mt} solubility signatures during G-TPP treatment

While multiple studies have looked at global changes in protein expression in response to UPR^{mt} activation, few studies have examined how mitochondrial stressors can affect mitochondrial proteostasis. In the data presented in this chapter, a strong bias to aggregation of proteins involved in specific biological pathways including OXPHOS and pyruvate metabolism were identified, while the solubility trends of other proteins groups such as calcium signalling and dynamics related proteins were largely unaffected (Figure 3.7 A, D). Comparison of HSP90 and HSP60/HSP10 client datasets further showed that these trends were not produced through a HSP90 client aggregation bias (Chapter 3.6). As the UPR^{mt} is thought to protect mitochondrial proteostasis,

strong aggregation of selected subsets of proteins raises a question of whether the timeframe of stress induction we are studying is too severe for the UPR^{mt} to properly protect and repair mitochondrial proteostasis, or whether certain protein groups are so aggregation-prone that the UPR^{mt} simply cannot prevent a degree of proteostatic collapse.

In a previous study involving genetic KO of CLPB, a mitochondrial disaggregase, compositional analysis of protein pellets isolated from mitochondria of cells lacking CLPB identified proteins involved in Complex I assembly as preferentially aggregated (*187*). Additionally, knockdown of the protease LONP1 produced a heat-misfolding stress induced protein aggregation signature in mitochondria that includes select transcription and translation related proteins, including TUFM and LRPRPC, and proteins involved in pyruvate metabolism such as HADHA and PYC (*188*). While the stress stimuli in these studies differ in their chronic, constitutive nature compared to the acute stress induction used in this chapter, the overlap in protein aggregation signatures with this work suggests there may be a metastable portion of the mitochondrial proteome comprising OXPHOS, select metabolism, and transcription/translational machinery that is particularly sensitive to protein folding stress. Overlap of previous studies with the aggregation prone proteins detected in this chapter's data also suggests the apparent lack of protection from the UPR^{mt} of these protein sub-groups may be from their intrinsic propensity for aggregation, and there may in fact be a degree of protection from the UPR^{mt} that could be revealed by examining cells with a block in the UPR^{mt} pathway (explored further in Chapter 4).

Unexpectedly, total protein levels of proteins not currently thought to be involved in the UPR^{mt} program were seen to increase in Figure 3.7, including mitochondrial ribosomal and mtDNA related proteins. From the data presented in this chapter, the decrease in the availability of protein chaperones and proteases could interrupt basal turnover of mitochondrial proteins and lead to a degree of accumulation. However, kinetic studies of mitochondrial ribosomal subunit replacement have demonstrated that over a 12 h period, the maximal rate of mitochondrial ribosome subunit turnover was ~25% (*189*), whereas some mitochondrial ribosomal proteins doubled in total levels across the 12 h treatment time used in Figure 3.7 D. Such a large discrepancy in the total amount of protein relative to the expected turnover rate suggests active upregulation in the expression and import of these proteins. Critical components of the mitochondrial protein import machinery, such as the MPP protease and the PAM motor complex showed strong aggregation in our data which would suggest disruptions to efficient protein import by 12 h of treatment (Figure 3.7 D). Import deficiencies have also been identified in other models of mitochondrial protein folding stress (*76, 190*). Accordingly, increased protein levels in context of damage to the import machinery suggests there may be early boosts in protein expression and import into mitochondria prior to collapse of

the import machinery at the time point analysed in this data. Indeed, a recent study by *Poveda-Huertes et al.* (2021) identified increased levels of protein import early during a mitochondrial protein folding stress, followed by a subsequent import block, supporting the hypothesis that ribosomal and mtDNA related proteins may be increased in import in the early stages of a G-TPP induced protein folding stress prior to a block in import. If some mitochondrial ribosome and mtDNA proteins can be resolubilised following UPR^mt induction, boosted protein levels, even if initially aggregated, may represent a quick and efficient way for mtDNA encoded protein production to resume and restore following resolution of a protein folding stress, and may represent a previously unidentified feature of the UPR^mt program.

In summary, the solubility assay developed in this chapter to measure endogenous mitochondrial proteostasis has allowed us to characterise for the first time the mitochondrial proteostasis signature that develops with G-TPP treatment in cells with a functional UPR^mt program. By using this analysis pipeline, how different signalling and effector components of the UPR^mt directly affect mitochondrial proteostasis can now be examined.

Chapter 4

Characterising the roles of CHOP, ATF4 and ATF5 in protecting and restoring mitochondrial proteostasis

4.1: Introduction

Transcription factors are the major drivers of the UPR^{mt}. In *C. elegans*, ATFS-1 and DVE-1 are the main UPR^{mt} transcription factors whereas in humas there are three main transcription factors that are thought to drive the UPR^{mt}: CHOP, ATF4 and ATF5. While each human transcription factor has been independently linked to regulating the mammalian UPR^{mt} program, whether CHOP, ATF4 and ATF5 act independently during UPR^{mt} signalling or in concert to cooperatively regulate mitochondrial health is currently unclear. Previous studies have focussed on each transcription factor in isolation without considering the influence of the other transcriptional pathways, preventing proper analysis of the relative importance and contribution of CHOP, ATF4 and ATF5 to the UPR^{mt} program. Additionally, it is unclear whether there is a master regulator transcription factor which exerts primary regulatory control over the UPR^{mt} program, as is seen in other cellular stress response pathways such as the ISR (*100*). Such limited understanding of the complex signalling dynamics of the UPR^{mt} have hampered our ability to conceptualise the UPR^{mt} program, leading to contradictory interpretations where the UPR^{mt} is sometimes considered as a distinct signalling entity, and at other times grouped with other better characterised stress related programs (*101, 191, 192*).

Typically, the UPR^{mt} has been studied in the context of damage mitigation during an acute protein folding stress. However, bioenergetically it is not favourable for cells to harbour dysfunctional mitochondria if those mitochondria are not eventually repaired to a fully functional state. How the

UPR^{mt} program regulates the full recovery of mitochondria following a proteostatic stress, and how each transcription factor contributes to that recovery is currently unknown. A further missing piece in the puzzle of the UPR^{mt} program has been understanding exactly how the UPR^{mt} protects and repairs mitochondrial proteostasis. Studies of the UPR^{mt} have typically assessed transcription of chaperones and proteases as readouts of proteostatic stress and repair but have not directly confirmed the activity and the effect these readouts have on mitochondrial health, meaning the UPR^{mt} has been mainly studied in a correlative manner. Due to limitations in the experimental protocols available, in-depth characterisation of the proteostatic and functional damage mitochondria encounter during a protein folding stress, and how the UPR^{mt} protects and repairs that damage has not yet been explored.

In this chapter, integrated signalling dynamics of each transcription factor are examined during UPR^{mt} induction to clarify the signalling hierarchy and dynamics of CHOP, ATF4 and ATF5 expression. Next, the newly developed experimental pipeline for protein solubility analysis (see Chapter 3) is used to examine how each transcription factor regulates mitochondrial proteostasis during an acute stress phase (12 h G-TPP treatment), and at two time points in the recovery period (24 h and 48 h recovery) to comprehensively characterise the roles of transcription factors in driving mitochondrial protection and repair.

4.2: Characterising the signalling hierarchy of CHOP, ATF4 and ATF5 during the UPR^{mt} program

A genetic epistasis approach was adopted to analyse the signalling hierarchy of the UPR^{mt}. Separate clonal HeLa cell lines that are genetic KOs for CHOP, ATF4 and ATF5 were generated using either CRISPR/Cas9 or TALEN technology (see Appendix III and V for details). If expression of any two transcription factors becomes ablated in a single transcription factor KO cell line, this would indicate a position downstream in a signalling hierarchy and a temporal reliance on initial transcription factor expression for activation of that signalling node. Expression of CHOP, ATF4 and ATF5 was examined by immunoblot during a G-TPP treatment time course in both WT cells and in each KO cell line (Figure 4.1). Surprisingly, the expression of remaining transcription factors was not fully ablated in any single transcription factor KO cell line (Figure 4.1 A – B). While ATF5 expression was reduced in both the CHOP KO and ATF4 KO lines at the 8 h and 12 h time points, suggesting a minor contribution of CHOP and ATF4-driven transcriptional programs in driving ATF5 expression, a robust induction of ATF5 was still detected which confirms that ATF5 expression can be induced independently of CHOP and ATF4 (Figure

4.1 A – B). In contrast, CHOP KO and ATF5 KO resulted in higher ATF4 levels relative to WT controls. At the 12h G-TPP treatment time point, ATF5 KO, and to a lesser degree ATF4 KO, resulted in stronger CHOP induction, indicating that compensatory upregulation of different transcription factor signalling pathways is occurring in the absence of a single signalling arm of the UPR^{mt} (Figure 4.1 A – B).

As the UPR^{mt} has been associated with alterations in global translation, and as each transcription factor has been associated with preferential translation of existing transcripts during a translational shutdown (*100*), mRNA levels of each transcription factor were examined across a 4 – 12 h treatment time course to confirm whether the observations in protein expression in Figure 4.1 A-B were related to signalled transcriptional changes in expression of each transcription factor (Figure 4.1 C). Induction of CHOP mRNA was observed in ATF4 and ATF5 KOs, while increased expression of ATF4 mRNA was seen in CHOP and ATF5 KOs (Figure 4.1 C), confirming the protein level changes observed in Figure 4.1 A - B correlate with transcription driven changes in mRNA expression. Surprisingly, ATF5 mRNA levels did not significantly differ across transcription factor KO relative to WT expression after G-TPP treatment. Instead, ATF5 mRNA levels initially reduced with G-TPP treatment in all cell lines, followed by an increase in mRNA expression at the 8 and 12 h time points (Figure 4.1 C). While ATF5 mRNA expression in WT cells reached above the baseline (DMSO) level of ATF5 expression at the 12 h time point, expression in CHOP KO and ATF4 KO cells did not reach above their baseline expression levels during the time course analysed (Figure 4.1 C). This indicates that the reduced ATF5 protein expression seen in Figure 4.1 A - B is at least partially due to reduced signalling in the absence of CHOP or ATF4. Interestingly, the reduction in mRNA and corresponding increase in ATF5 protein suggests ATF5 activation during the UPR^{mt} may be triggered primarily by translational or post-translational changes promoting either protein production of existing transcripts or stabilisation of the protein instead of through increased transcript production. While there are some apparent interactions between each transcription factor driven pathway that alter levels of residual transcription factors, collectively the sustained expression of the remaining transcription factors in each KO cell line confirms that CHOP, ATF4 and ATF5 are independently expressed during the UPR^{mt}. Neither CHOP, ATF4 nor ATF5 act as master regulating transcription factors in the context of mammalian UPR^{mt} signalling.
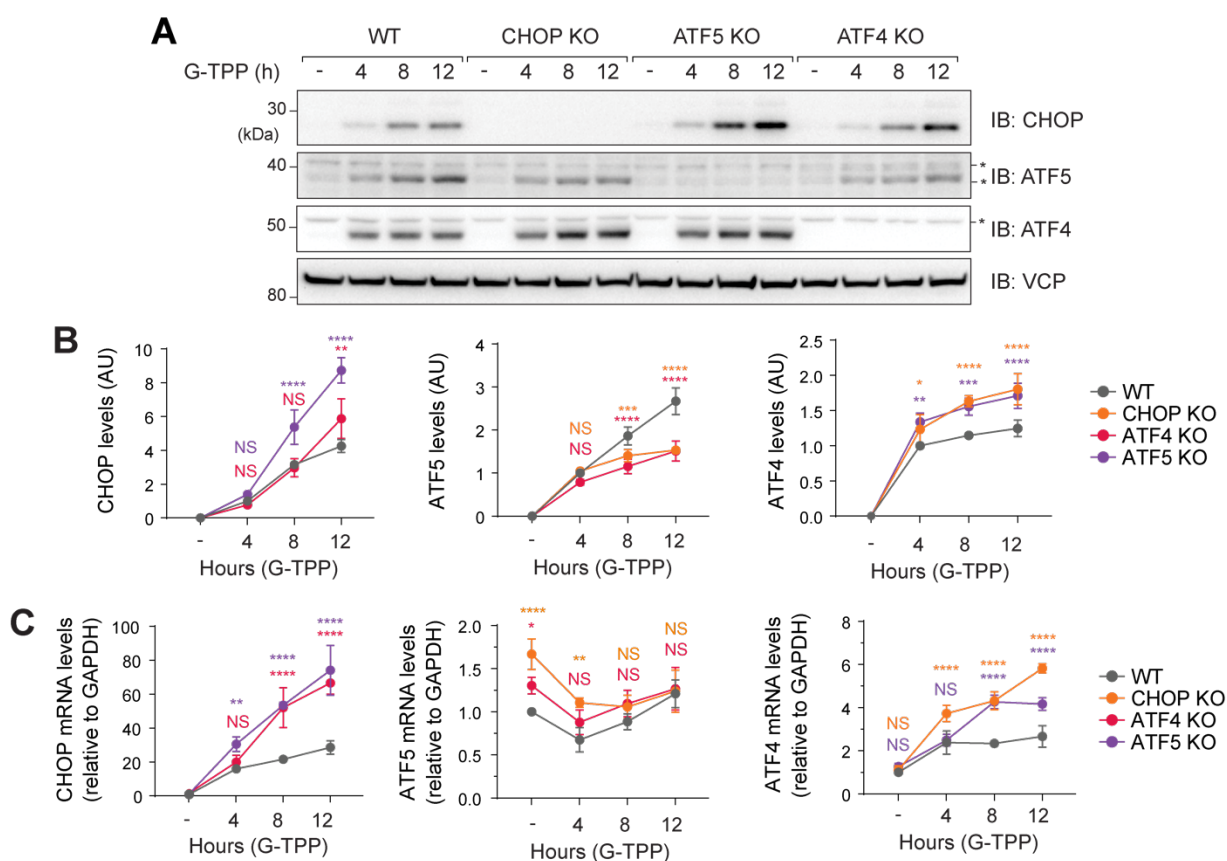
Figure 4.1 **CHOP, ATF4 and ATF5 are independently expressed during the UPR^{mt}**. **A**, **B**. WT, CHOP KO, ATF4 KO and ATF5 KO cells were treated with 9 µM G-TPP for 0 – 12 hours (h), and CHOP, ATF4 and ATF5 levels were analysed by immunoblot (IB; **A**) and quantified relative to WT protein levels at 4 h (**B**). **C**. RNA was isolated from WT, CHOP KO, ATF4 KO and ATF5 KO cells after treatment with 9 µM G-TPP for the indicated times. Expression of CHOP, ATF4 and ATF5 mRNA levels were quantified by qRT-PCR and normalised to GAPDH mRNA expression in each sample. Transcription factor expression was then calculated relative to untreated WT expression (-). – samples in **A** – **C** were treated with DMSO (vehicle) for 4 h. ****P≤0.0001, ***P≤0.001, **P≤0.01, *P≤0.05, NS P>0.05 (two-way ANOVA). Data in **B**, **C** was generated from three independent experiments.

4.3: Characterising the roles of CHOP, ATF4 and ATF5-driven transcriptional programs in protecting mitochondrial proteostasis

Each transcription factor is independently induced during a UPR^{mt} stress, but it remains unclear how their expression directly influences mitochondrial repair. The proteomics-based approach developed in Chapter 3 was utilised to determine the contribution of CHOP, ATF4 and ATF5 signalling pathways in protecting and repairing mitochondrial proteostasis both during and after a protein folding stress. Mitochondria were isolated from WT, CHOP KO, ATF4 KO, ATF5 KO and CHOP/ATF4/ATF5 triple KO (TKO) cells in biological triplicate after either: 1) 12 h DMSO treatment to calculate basal proteostasis, 2) 12 h G-TPP treatment to analyse acute proteostatic

protection, 3) 24 h or 4) 48 h recovery period after washout of a 12 h G-TPP treatment to analyse proteostasis repair. A TKO cell line missing all three transcription factors was included to determine if each transcription factor drove additive proteostatic protection (Appendix III, V). Soluble and insoluble protein fractions from a 0.5% (v/v) TX-100 solution were isolated from each mitochondrial sample followed by analysis using TMT-based multiplex proteomics. To produce a readout of the proteostasis of each individual protein, protein solubility across each sample was calculated relative to total protein levels. Basal solubility of each protein from DMSO treated cells was then used as a benchmark to calculate the temporal changes in proteostasis during the initial stress insult and the recovery period of each sample set. The approach allows for comparative analysis of proteostasis trends across the mitochondrial proteome in the presence and absence of each UPR^{mt} signalling arm. An overview summary of the experimental workflow has been provided in Figure 4.2.

Principle component analysis (PCA) of global protein solubility trends confirmed that no individual sample across the time course set was a clear outlier in solubility trends since all replicates in each biological condition clustered together confirming robustness of the experiment (Appendix V). Similar clustering of the 12 h samples of each cell line were observed, indicating some similarity in protein solubility patterns at 12 h in all cell lines (Appendix V). A separate PCA analysis was performed on each sample set for each cell line to more closely examine the relationships between each time point of each sample set (Figure 4.3 A). In each transcription factor KO cell line, the final 48 h recovery time point remained in a distinct quadrant from the DMSO treated samples, whereas the 48 h recovery time point returned to similar positioning of the DMSO treated samples in WT samples (Figure 4.3 A). Similar positioning of the 48 h and DMSO treated samples in WT demonstrates restoration to basal proteostasis trends by the 48 h recovery time point in WT cells that was not observed in transcription factor KO cell lines. To confirm the computational analysis did not introduce any artificial variation into the sample, protein solubility trends across the experimental time course were analysed by immunoblot for five different proteins (LRPPRC, AARS2, SHMT2, NDUFS1 and VDAC1) selected from the proteomic proteostasis data set based on their different solubility trends ranging from high insolubility (e.g. LRPPRC) to low insolubility (e.g. VDAC1) (Figure 4.3 B). The solubility trend of each of LRPPRC, AARS2, SHMT2, NDUFS1, and VDAC1 as analysed by immunoblotting agreed with the mass spectrometry data, confirming the accuracy of the solubility calculations and the overall proteomic workflow.
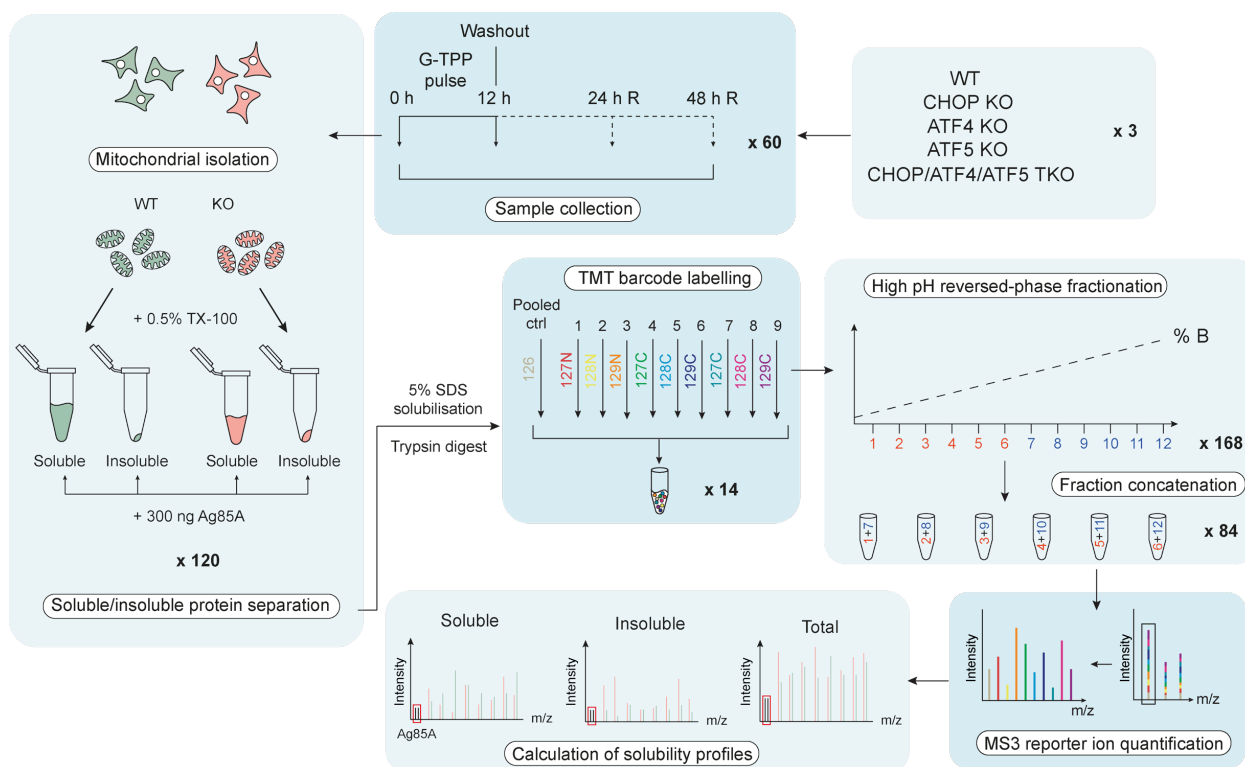
Figure 4.2 **Overview of the solubility analysis workflow used to analyse temporal proteostasis dynamics.** WT, CHOP KO, ATF4 KO, ATF5 KO and TKO cells were treated with DMSO or 9 μM G-TPP for 12 h (12 h), followed by removal of the treatment and subsequent sample collection at 24 h and 48 h of recovery (24 h R, 48 h R). Mitochondria were then isolated from each sample and separated into 0.5% (v/v) TX-100/PBS soluble and insoluble protein fractions. Recombinant Ag85A protein from *Mycobacterium tuberculosis* was spiked into each sample at a standard amount, and samples were then resolubilised in 5% (w/v) SDS prior to tryptic digest and TMT-labelling. Each TMT batch was fractionated by reversed-phase high pH fractionation and concatenated into 6 fractions per batch prior to mass spectrometry analysis. Solubility profiles for each mitochondrial protein in each sample were then calculated using computational estimations of the total protein levels in each starting mitochondrial sample prior to fractionation. Batch labelling layouts are listed in Appendix III, and analysis pipelines are described in Chapter 2.5.

Next, the average solubility of each protein from each sample was calculated and plotted to generate a comparative aggregation index (AI) calculation. DMSO treated sample solubility remained similarly clustered for each cell line, indicating that basal loss of transcription factors did not affect baseline protein solubility (Figure 4.3 C). A clear peak in the AI was seen in WT cells at the 12 h G-TPP time point, demonstrating that maximal aggregation occurs during the acute treatment period. Protein solubility in WT cells then begins to improve during the initial recovery period (24 h R), eventually resulting in a return to a baseline AI at the 48 h recovery point (48 h R), which correlates with the PCA trend in Figure 4.3 A. In contrast, each transcription factor KO cell line had a higher peak AI at 12 h G-TPP treatment, indicating increased aggregation load (~1.6 fold more than WT), with the loss of any single transcription factor during an acute
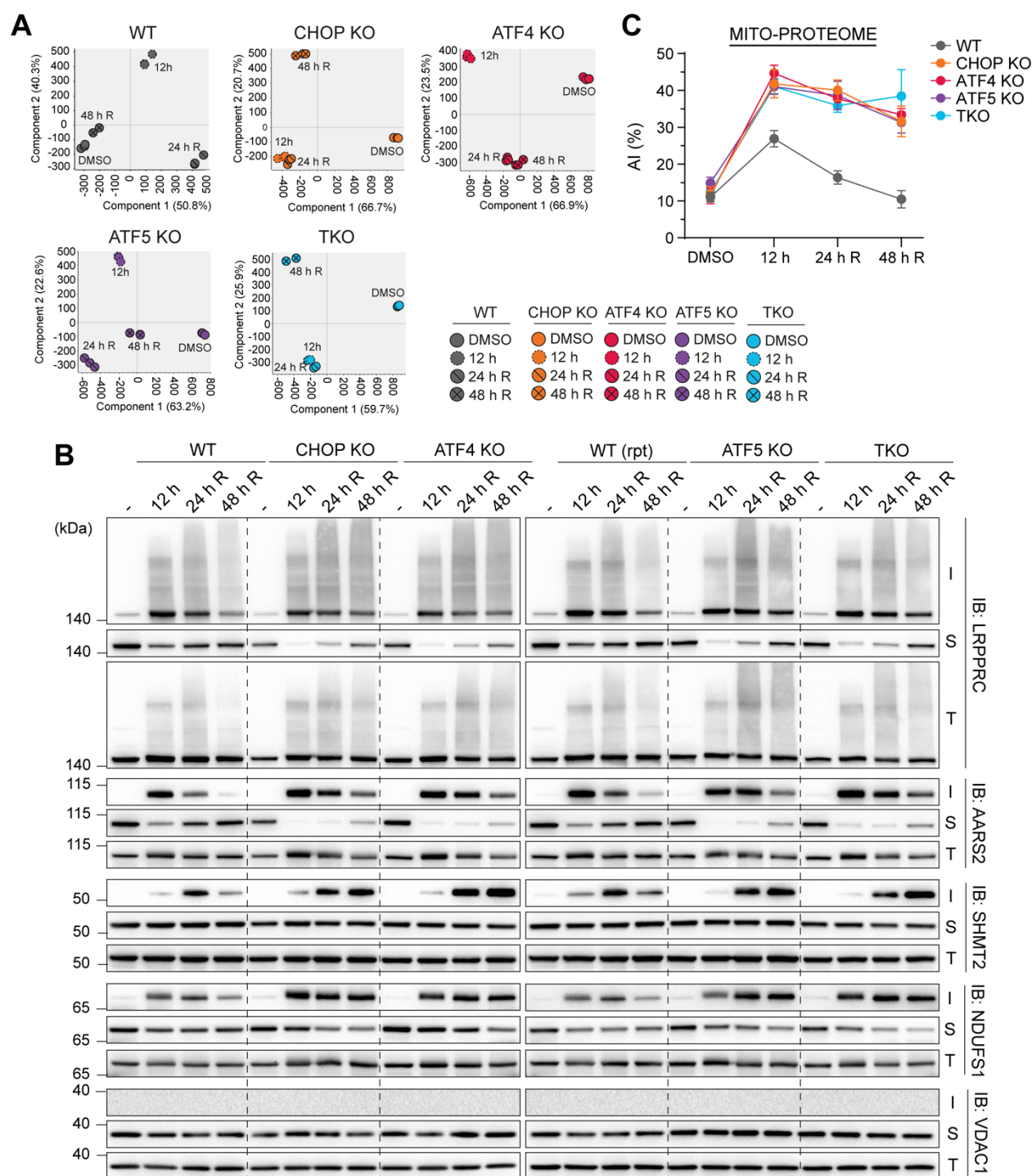
Figure 4.3 **Decreased solubility of the mito-proteome during the UPR^mt occurs with transcription factor removal. A**. Principal component analysis (PCA) were performed using the protein-specific solubility profiles of each WT, CHOP KO, ATF4 KO, ATF5 KO and TKO sample set generated from the data produced in Figure 4.2. PCA plots were generated using Perseus v1.6.15. **B.** An aggregation index (AI) representing the average percentage (%) insolubility of each protein across the mito-proteome was calculated for each sample and plotted, with error bars representing S.D.. **C**. WT, CHOP KO, ATF4 KO, ATF5 KO and TKO cells were treated with DMSO (-) or G-TPP (12 h) for 12 h. Samples were collected at 12 h (- and 12 h), 24 h after G-TPP treatment was removed (24 h R) and 48 h after treatment removal (48 h R). Mitochondria were isolated from each sample and 0.5% (v/v) TX-100 soluble and insoluble fractions were collecting using the protocol outline in Figure 4.2. Levels of LRPPRC, AARS2, SHMT2, NDUFS1 (cont.)

and VDAC1 in the insoluble (I), soluble (S) and total (T) fractions of each sample were then analysed by immunoblotting (IB). WT samples from the same biological experiment were run in duplicate on each SDS-PAGE gel (denoted by rpt). Kilodalton – kDa. Statistical analysis of AI levels relative to WT 12 h G-TPP AI are included in Table 4.1 (see 'Mito-proteome). Data in **A**, **B** was generated from three independent experiments.

protein-folding stress. While some reduction in the AI was evident in each transcription factor KO cell line during the recovery period, AI levels in each KO cell line remained high, above the peak AI of WT samples (12 h; Figure 4.3 C), across the entire recovery period analysed. The results show significant defects in mitochondrial proteostasis remain with the loss of any transcription factor even after a 48 h recovery period in which WT cells have almost completely recovered. Interestingly, the mitochondrial proteome (mito-proteome) AI calculations demonstrated similar maximal aggregation loads and recovery trends with each single transcription factor KO relative to TKO cells lacking all three transcription factors. The similar AI trends between each KO cell line indicates that each transcription factor is regulating a non-redundant program of mitochondrial protection and repair that is critically required for UPR^{mt} mediated proteostasis protection.

4.4: UPR^{mt} signalling differentially effects mitochondrial process-based protein subgroups

Each transcription factor KO line had a similar overall proteostasis defect (Figure 4.3 C). However, there could be specific differences in the activity of each transcription factor-controlled program on a specific mitochondrial process or at an individual protein level. To tease apart the intricacies of proteostasis protection driven by each transcription factor, mitochondrial proteins were first grouped by their insolubility % to determine if loss of an individual transcription factor specifically decreases solubility of those proteins and prevents proteostasis recovery of specific clusters of mitochondrial proteins. Similar numbers of mildly aggregating proteins across the 15 – 30% AI range, and the 30 – 50% AI range, were seen in WT cells and all transcription factor KO cell lines at the acute 12 h treatment time point (Figure 4.4 A). However, transcription factor KO cell lines had much higher numbers of strongly aggregating proteins in the >50% AI range at 12 h G-TPP treatment relative to WT (Figure 4.4 A), pointing towards a potential subset of mitochondrial proteins that are more susceptible to aggregation with loss of a UPR^{mt} arm. In addition, the small subset of strongly aggregating proteins seen in the >50% AI range in WT cells reduced in aggregation and fell out of that category by the 24 h recovery time point (Figure 4.4 A). This result

shows that proteostasis repair of severely aggregating proteins occurs in WT cells. In contrast, the number of proteins in the >50% AI range remained stable at 24 h recovery in each transcription factor KO cell line (Figure 4.4 A), with only a small decrease by the 48 h recovery time point.

Protein aggregation was also visualised using a heat map clustering (Figure 4.4 B). The heat map analysis displayed clusters of proteins with a high AI in each transcription factor KO cell line which persisted across the acute and recovery time course (Figure 4.4 B). While aggregation was elevated in WT cells at 12 h, recovery of these protein clusters was evident supporting the notion that there may be differential susceptibility of components of the mito-proteome to protein folding stress and UPR^{mt} induction. Interestingly, the heat map analysis also showed widespread increases in protein aggregation across the mito-proteome during both acute G-TPP treatment and recovery in each transcription factor KO cell line (Figure 4.4 B). Enhanced aggregation of specific clusters of mitochondrial proteins appeared to be coupled with mild but widely distributed increases in protein aggregation across the mito-proteome in UPR^{mt} disrupted cell lines (Figure 4.4 B).

A GO analysis using combined GO Biological Process and Molecular Function datasets was performed on proteins with >50% aggregation at the 48 h time period from all cell lines to determine if the aggregation-prone and recovery-resistant protein clusters belonged to specific mitochondrial processes (Figure 4.4 C). Interestingly, GO clustering produced large nodes of transcription/translation related processes and OXPHOS-related processes, indicating specific susceptibility to protein misfolding with loss of any arm of the UPR^{mt} in these mitochondrial protein groups (Figure 4.4 C). Smaller nodes of metabolism and mtDNA related processes were also detected, suggesting high levels of proteostatic stress damage multiple functional pathways of mitochondria during UPR^{mt} dysfunction. To determine whether the GO trends observed in Figure 4.4C were similar across the transcription factor KO cell lines, as appears to be the case in the heat map analysis from Figure 4.4 B, a separate GO analysis was performed on proteins showing >50% aggregation at 48 h recovery in each transcription factor KO cell line (Figure 4.4 D). Consistent with the combined GO analysis in Figure 4.4 C, each independent analysis of the KO lines produced clusters associated with mitochondrial transcription/translation machineries and OXPHOS related machineries (Figure 4.4 D) highlighting these processes groups as the most heavily reliant on every arm of the UPR^{mt} to maintain their proteostasis during stress.
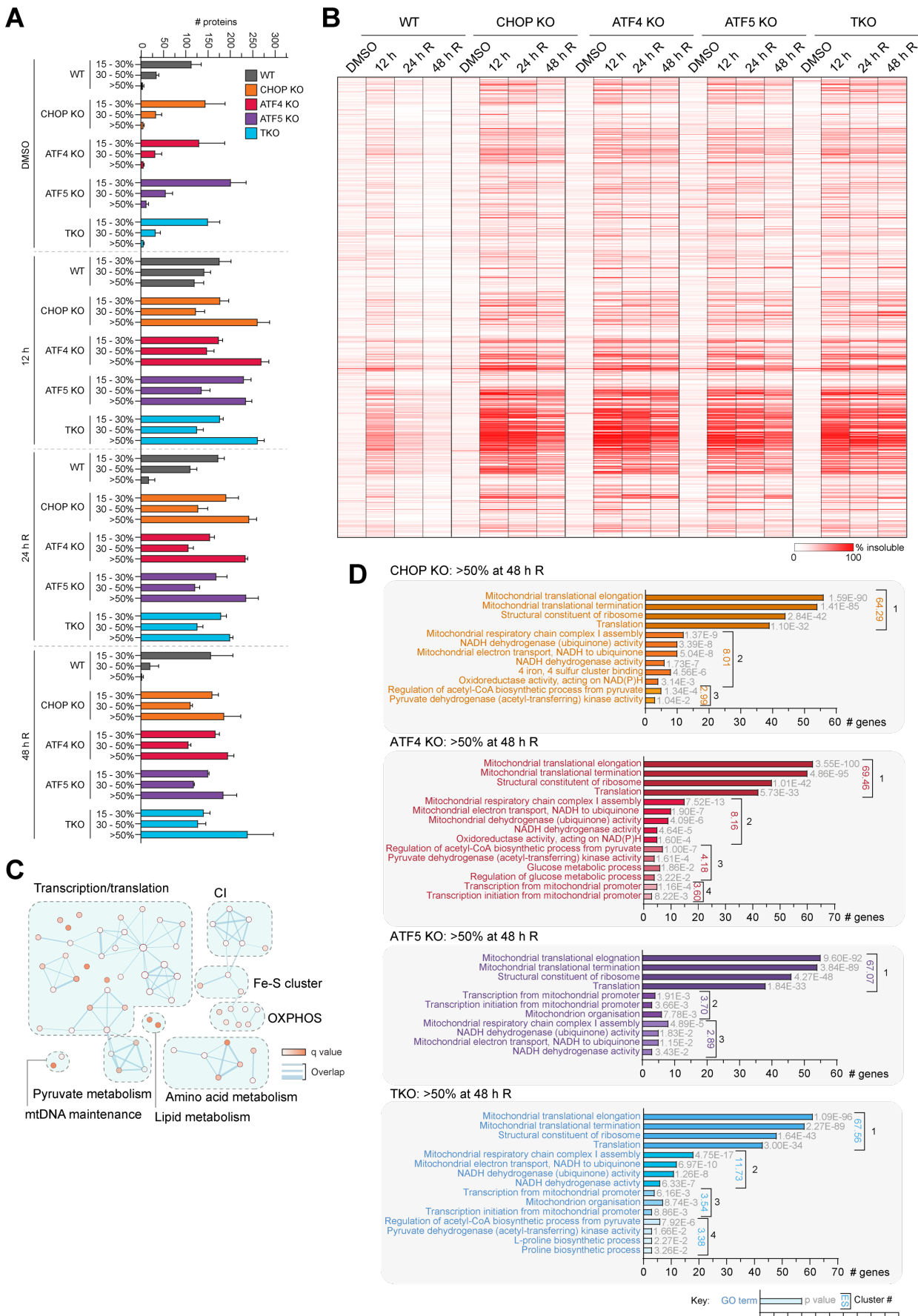
Figure 4.4 **Clusters of mitochondrial proteins relating to transcription/translation and metabolism processes demonstrate resistance to repair with defective UPR^{mt}.** (cont.)

A. Proteins were grouped by their aggregation % and grouped into three separate classifications of mild (15 – 30%), moderate (30 – 50%) or severe (>50%) aggregation. The total number of proteins falling into each grouping were normalised to the total number of proteins detected in each sample and plotted, with error bars representing S.D. **B.** Heat map representation of the AI of each mitochondrial protein detected in each sample. Samples were clustered according to mitochondrial process grouping classification (*166*). **C.** Gene ontology (GO) analysis on proteins with >50% aggregation at the 48 h R time point across all cell lines. **D.** GO analysis was performed using the subset of proteins with >50% aggregation at the 48 h R time point in each sample set. GO analysis in **C**, **D** was performed using the 'Biological Process' and 'Molecular Function' categories in the DAVID v6.8 platform (*193, 194*). Data in **A** – **D** was generated from three independent experiments.

Next, since mitochondrial process annotation in global GO analysis data sets are often not sufficiently detailed to provide information on smaller but essential mitochondrial processes, a published curated mitochondrial process grouping list produced by the Filipovska lab was used to cluster mitochondrial proteins based on their main process activity in mitochondria (*166*). A representative AI value for each process group at each time point was calculated for all cell lines to provide an in-depth characterisation of solubility trends and assess whether there is transcription factor specificity in mitochondrial processes (Figure 4.5, Table 4.1). Of the 29 process groups analysed, only 7 process groups (*Apoptosis, Glycolysis, Mitochondrial carrier, Mitochondrial dynamics, Pentose phosphate pathway, ROS defence, Transmembrane transport*) did not display a significant increase in AI at 12 h G-TPP treatment in WT cells, showing that many mitochondrial processes were acutely affected by mtHSP90 inhibition, even with a functional UPR^{mt} program. Of those 7 unaffected process groups in WT cells, all displayed a significant increase in aggregation in each transcription factor KO cell line (Figure 4.5, Table 4.1). Therefore, UPR^{mt}-mediated protection is occurring for proteins in these process groups in WT cells, but at a level that is sufficient to maintain basal proteostasis. Similar AI changes to WT in transcription factor KO were only seen in 3 of the remaining 27 processes (*Cardiolipin biosynthesis, Import and sorting, Mitophagy*), suggesting these process groups are not targets affected by UPR^{mt} mediated protection. All remaining process groups examined displayed significantly increased aggregation with loss of any transcription factor, demonstrating that the UPR^{mt} program has wide-reaching roles in protecting proteostasis across the mitochondrial proteome (Figure 4.5, Table 4.1). During the recovery period, only three process groups returned to baseline levels of proteostasis in any transcription factor KO cell line (*Apoptosis, Calcium signalling and transport, Glycolysis*) (Figure 4.5, Table 1). The UPR^{mt} is therefore critical not only for providing active protection during a proteostatic stress, but also to mediate the restoration of mitochondrial proteostasis in proteins spanning most biological processes in mitochondria.

Interestingly, very little transcription factor specificity was seen in the protection of any mitochondrial process group during either the acute stress (12 h G-TPP treatment) or the initial 24 h recovery period. CHOP and ATF5 displayed higher aggregation at 24 h recovery in the *Heme biosynthesis* category, and ATF5 KO displayed higher aggregation in the *Cardiolipin biosynthesis* category. However, all samples returned to similar AI levels relative to the remaining transcription factor KO cell lines by the 48 h recovery time point, making it unlikely that these relatively minor transcription factor-specific changes will have significant biological impact (Figure 4.5, Table 4.1). TKO cells showed similar levels of acute aggregation to single transcription factor KO cell lines across all processes, reinforcing the trends observed in the global AI calculations (Figure 4.3 C), although AI levels trended slightly higher in TKOs relative to single transcription factor KOs at 48 h recovery across most mitochondrial process groups, with the exception of *Apoptosis, Calcium Signalling and Transport, Metabolism of Lipids and Lipoproteins, and Mitochondrial carrier* process groups. It is possible that individual transcription factors play slightly redundant roles in the recovery of mitochondrial proteostasis. However, differences in aggregation at 48 h R between single transcription factor KO and TKO cells were small, and all KO cells still displayed high levels of defective aggregation relative to WT at that time point, raising the question of whether the slight increase in aggregation at 48 h R in TKO cells will be of biological significance compared to single transcription factor KO cells (Figure 4.5, Table 4.1). Overall, mitochondrial process based proteostasis analysis has comprehensively demonstrated that each transcription factor is critically and non-redundantly required for widespread protection across the mito-proteome.
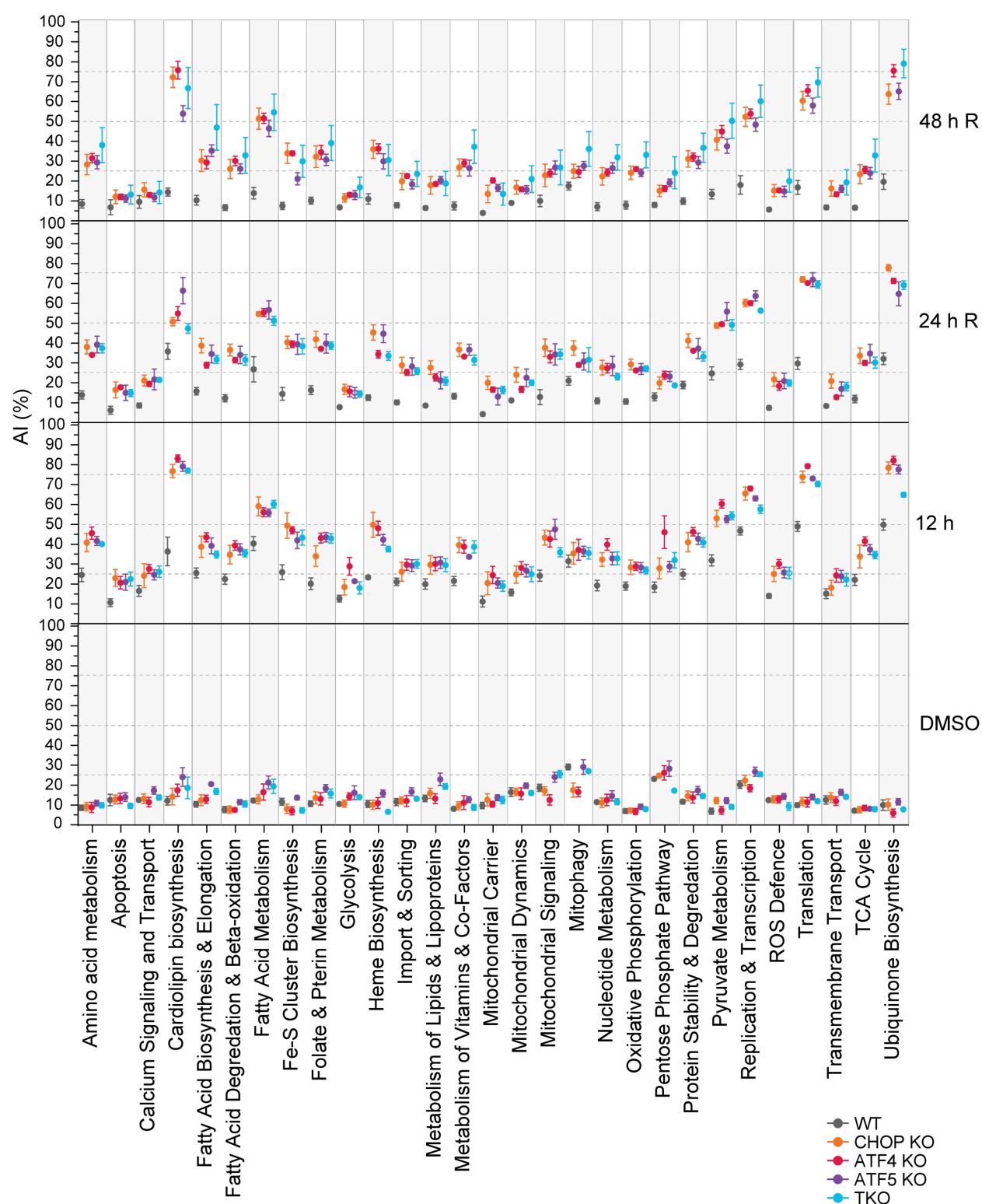
Figure 4.5 **Mitochondrial process groups display varied AI trends.** Aggregation index (AI) values representing the average subunit aggregation of all proteins comprising a mitochondrial process group were calculated and displayed, with error bars representing S.D.. Statistical analysis of AI levels relative to WT levels at each time point are included in Table 4.1. Data was generated from three independent experiments

	DMSO				12 h				24 h recovery				48 h recovery			
	CHOP KO	ATF4 KO	ATF5 KO	TKO	CHOP KO	ATF4 KO	ATF5 KO	TKO	CHOP KO	ATF4 KO	ATF5 KO	TKO	CHOP KO	ATF4 KO	ATF5 KO	TKO
Amino acid metabolism	NS	NS	NS	NS	****	****	****	****	****	****	****	****	****	****	****	****
Apoptosis	NS	NS	NS	NS	****	***	***	****	****	****	***	***	NS	NS	NS	NS
Calcium Signaling and Transport	NS	NS	NS	***	**	****	**	***	****	****	****	****	NS	NS	NS	NS
Cardiolipin biosynthesis	NS	**	****	**	****	****	****	****	****	****	****	****	****	****	****	****
Fatty Acid Biosynthesis & Elongation	NS	NS	****	NS	****	****	****	***	****	****	****	****	****	****	****	****
Fatty Acid Degredation & Beta-oxidation	NS	NS	NS	***	****	****	****	****	****	****	****	****	****	****	****	****
Fatty Acid Metabolism	NS	*	****	***	****	****	****	****	****	****	****	****	****	****	****	****
Fe-S Cluster Biosynthesis	NS	*	NS	*	****	****	****	****	****	****	****	****	****	****	***	****
Folate & Pterin Metabolism	NS	NS	****	*	****	****	****	****	****	****	****	****	****	****	****	****
Glycolysis	NS	NS	**	NS	*	****	**	*	***	**	**	**	NS	NS	NS	**
Heme Biosynthesis	NS	NS	**	NS	****	****	****	****	****	****	****	****	****	****	****	****
Import & Sorting	NS	NS	*	NS	NS	**	**	***	**	****	****	****	***	***	**	**
Metabolism of Lipids & Lipoproteins	NS	NS	****	**	***	***	****	***	****	****	****	****	**	***	****	***
Metabolism of Vitamins & Co-Factors	NS	NS	*	NS	****	****	****	****	****	****	****	****	****	****	****	**
Mitochondrial Carrier	NS	NS	NS	NS	***	****	***	**	****	*	***	****	**	****	*	****
Mitochondrial Dynamics	NS	NS	NS	NS	***	****	****	***	****	****	****	***	*	NS	NS	**
Mitochondrial Signaling	NS	**	**	***	****	****	****	****	****	****	****	****	****	****	****	****
Mitophagy	****	****	NS	NS	NS	*	NS	NS	****	**	****	****	*	NS	**	****
Nucleotide Metabolism	NS	NS	NS	NS	****	****	****	****	****	****	****	****	****	****	****	****
Oxidative Phosphorylation	NS	NS	NS	NS	***	***	***	**	****	****	****	****	****	****	****	****
Pentose Phosphate Pathway	NS	NS	*	**	***	****	***	****	**	****	****	*	NS	*	**	****
Protein Stability & Degredation	NS	NS	**	NS	****	****	****	****	****	****	****	****	****	****	****	****
Pyruvate Metabolism	**	NS	**	*	****	****	****	****	****	****	****	****	****	****	****	****
Replication & Transcription	NS	NS	**	*	****	****	****	****	****	****	****	****	****	****	****	****
ROS Defence	NS	NS	NS	NS	****	****	****	****	****	****	****	****	**	**	*	****
Translation	NS	NS	NS	NS	****	****	****	****	****	****	****	****	****	****	****	****
Transmembrane Transport	NS	NS	NS	NS	NS	***	**	**	NS	NS	***	****	**	NS	*	***
TCA Cycle	NS	NS	NS	NS	****	****	****	****	****	****	****	****	****	****	****	****
Ubiquinone Biosynthesis	NS	NS	NS	NS	****	****	****	****	****	****	****	****	****	****	****	****
Mito-proteome	NS	NS	*	NS	**	***	**	**	***	**	**	***	**	***	***	*

Table 4.1 **Statistical analysis of AI trends across mitochondrial proteome and process groupings.** Samples were analysed relative to WT AI levels at each time point. ****P≤0.0001, ***P≤0.001, **P≤0.01, *P≤0.05, NS P>0.05 (two-way ANOVA). Data was generated from three independent experiments.

4.5: Transcription factor-dependent rate of recovery from proteostatic stress

Trends in AI levels clearly indicated that removal of any individual transcription factor results in excessive accumulation of insoluble protein during G-TPP treatment, and that these levels of insoluble protein tend to persist even once the protein-folding stress is removed (see Chapter 4.4). However, higher starting aggregation loads after 12 h G-TPP treatment in transcription factor KOs can confound interpretation of the elevated proteostasis loads seen in the recovery period since a return to baseline in these cells would require repair at an elevated rate to that seen in WT cells over the same time frame. Instead of analysing static protein solubility, analysing the rate of protein resolubilisation can provide an indication of how the actions of each transcription factor are regulating mitochondrial repair.

Relative rates of proteostasis recovery were first determined by calculating the overall percentage reduction in insolubility per 24 h period after G-TPP washout. As protein resolubilisation appears to plateau at 24 - 48 h R as mito-proteome proteostasis reaches baseline in WT cells (Figure 4.3 C), only data from the 24 h recovery period was used in calculating WT recovery rates, while the 24 – 48 h R period was included in transcription factor KO calculations as they do not reach baseline proteostasis (Figure 4.3 C).

Resolubilisation of the mito-proteome occurred at a slower rate with the loss of any individual transcription factor (Figure 4.6 A, Table 4.2). TKO cells missing all three transcription factors trended towards a slower rate of recovery than single transcription factor KO cells with a mean rate decrease in recovery at an additive order of magnitude relative to single KO cells (mean range single KO: 4.88–5.64% recovery; mean TKO: 1.30% recovery). However, TKO resolublisation rates were not of a statistically significant difference when compared to single transcription factor KO rates due to the variability in resolubilisation rates seen in TKO cells (Figure 4.6 A, Table 4.2), making it difficult to confidently conclude whether each transcription factor plays a partially redundant role in facilitating proteostasis recovery.

Rate analysis was then further separated into mitochondrial process-based group calculations to determine whether the rate of recovery was specifically defective in any particular mitochondrial process group across the transcription factor KO cell lines (Figure 4.6 B, Table 4.2). Multiple process groups appeared to be resolubilising at a similar rate in KO lines relative to WT controls including *Apoptosis, Calcium Signalling and Transport, Folate & Pterin metabolism, Glycolysis, Mitochondrial dynamics, Mitochondrial signalling, Pentose Phosphate Pathway, Protein stability and degradation, Pyruvate Metabolism, and ROS defence* (see process group labels marked with

a red # sign in Figure 4.6 B). A similar resolublisation rate to WT indicates that UPR^{mt} transcription factors play a more important role during an acute proteostatic stress when protecting these mitochondrial processes. Accordingly, defective protection in the acute stress period appears to be the primary reason why resolubilisation defects were observed in the recovery period for these process groups.

Major defects in recovery rate upon transcription factor KO were seen in the *Fatty Acid Metabolism, Import & Sorting, Oxidative Phosphorylation, Replication & Transcription, Translation, and Ubiquinone biosynthesis* process groups (Figure 4.6 B, Table 4.2). In each of these process groups, single transcription factor KO lines clustered together showing similarly defective recovery rates relative to the WT control. In *Oxidative Phosphorylation*, *Replication and Transcription*, *Translation* and *Ubiquinone Biosynthesis* process groups, TKO cells showed a further reduced recovery rate compared to single transcription factor KOs indicating that there is partial redundancy in proteostatic recovery driven by each transcription factor for these groups which is exacerbated by the simultaneous loss of CHOP, ATF4 and ATF5. The remaining process groups demonstrated trends of reduced recovery rate upon transcription factor KO. However, the trends were typically not of statistical significance relative to WT samples demonstrating only mild defects in the recovery of these groups with loss of an individual transcription factor (Figure 4.6 B, Table 4.2). Throughout the process groups which showed mild recovery defects, the TKO cell line showed a trend of increased recovery delay compared to the single transcription factor KO cells (see *Nucleotide Metabolism* and *TCA cycle* in Figure 4.6 B as examples). Collectively, no single transcription factor KO cell line demonstrated a specific defect in recovery rate for a mitochondrial process relative to the other transcription factors, which reinforces earlier conclusions that removal of each transcription factor has similar phenotypic effects on mitochondrial proteostasis.

Overall there was an ~50% or more reduction in the recovery rate of the KO lines (Figure 4.6 A), supporting the conclusion that CHOP, ATF4 and ATF5 play important roles mediating the recovery of mitochondrial proteostasis after an acute stress. A longer recovery time was also considered as it may help better tease apart different trends in recovery rates across mitochondrial processes, while the additional data may also allow for more robust calculations of changes in rate. A longer recovery period up to 4 days was examined by immunoblot analysis of the solubility of three highly aggregation prone proteins, LRPPRC, AARS2 and GRSF1, in WT, ATF4 KO and TKO cells to explore whether transcription factor KO cells display persistent aggregation with an extended recovery period (Figure 4.6 C). Persistent aggregation was seen at 3 days recovery in both ATF4 KO and TKO cells, further supporting the rate defects with transcription factor KO

observed in earlier data (Figure 4.6 A – C). More substantial recovery was observed at 4 days of recovery (Figure 4.6 C). However, since HeLa cells are mitotic and still undergoing cell division during this period, it is difficult to account for the possibility of dilution via mitochondrial biogenesis and cell division in aiding the recovery of damaged mitochondria in KO lines at these later time points.
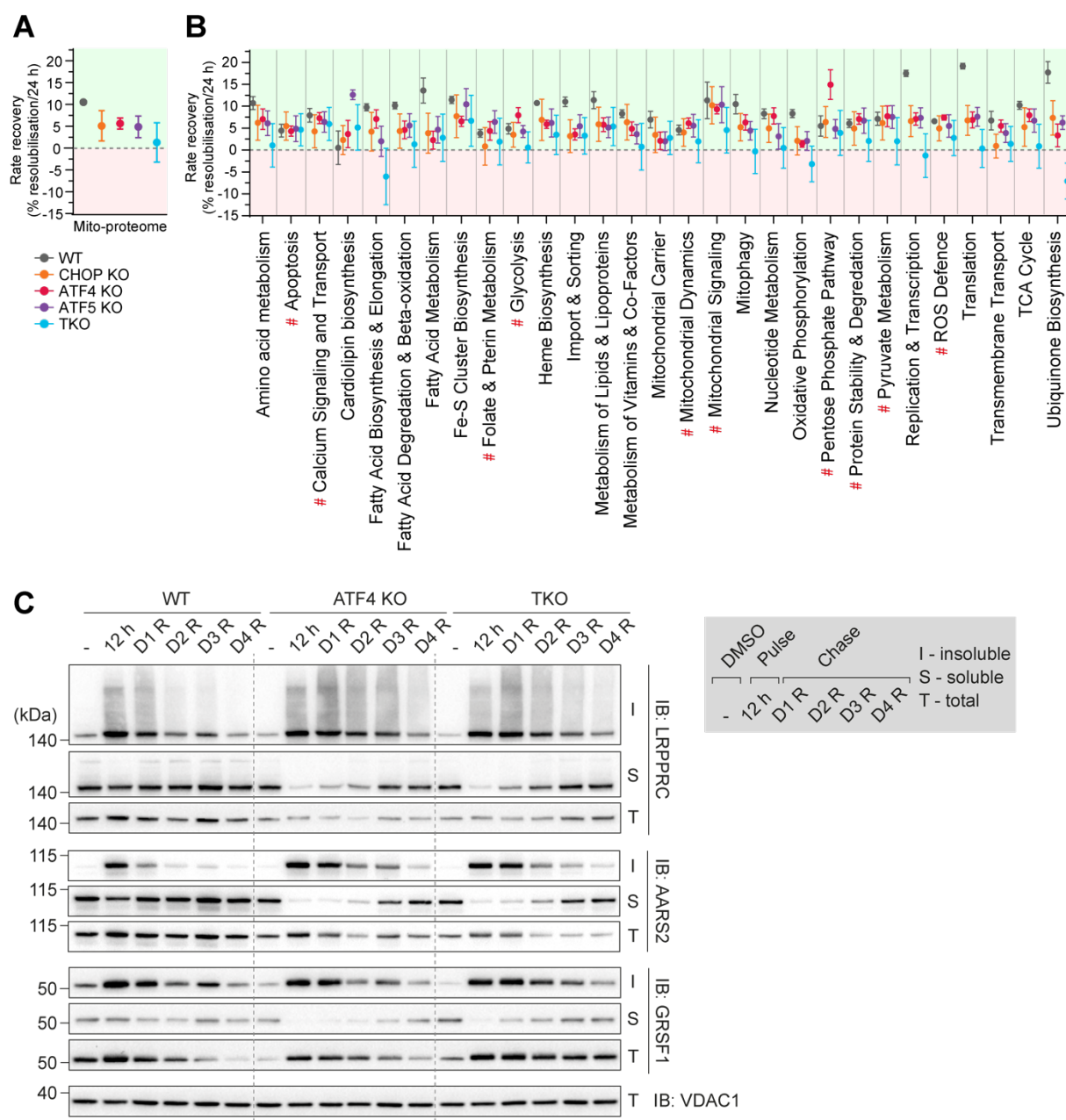
Figure 4.6 **Transcription factor removal leads to defective rates of proteostasis recovery.** The reduction in aggregation % between the 12 h and 24 h R time points were (continued) calculated for WT, CHOP KO, ATF4 KO, ATF5 KO and TKO samples using AI % across the mito-proteome (**A.**), and for the AI % across mitochondrial process groups (**B.**). **C.** WT, ATF4 KO and TKO cells were treated with DMSO (-) or G-TPP (12 h) for 12 h. Samples were collected at 12 h (cont.) (- and 12 h) and every 24 h after G-TPP washout for 4 days (D1 R – D4 R). Mitochondria were isolated from each sample and 0.5% (v/v) TX-100 soluble and insoluble fractions were collecting using the protocol outline in Figure 4.2. Levels of LRPPRC, AARS2, GRSF1 and VDAC1 (cont.)

in the insoluble (I), soluble (S) and total (T) fractions of each sample were then analysed by immunoblotting (IB). Kilodalton – kDa. Statistical analysis of rate changes relative to WT recovery rates are included in Table 4.2. Data in **A**, **B** was generated from three independent experiments.

	Relative to WT				Relative to TKO		
	CHOP KO	ATF4 KO	ATF5 KO	TKO	CHOP KO	ATF4 KO	ATF5 KO
Amino acid metabolism	NS	NS	NS	**	NS	NS	NS
Apoptosis	NS	NS	NS	NS	NS	NS	NS
Calcium Signaling and Transport	NS	NS	NS	NS	NS	NS	NS
Cardiolipin biosynthesis	NS	NS	**	NS	NS	NS	*
Fatty Acid Biosynthesis & Elongation	NS	NS	*	***	**	**	*
Fatty Acid Degredation & Beta-oxidation	NS	NS	NS	**	NS	NS	NS
Fatty Acid Metabolism	*	**	*	**	NS	NS	NS
Fe-S Cluster Biosynthesis	NS	NS	NS	NS	NS	NS	NS
Folate & Pterin Metabolism	NS	NS	NS	NS	NS	NS	NS
Glycolysis	NS	NS	NS	*	NS	**	NS
Heme Biosynthesis	NS	NS	NS	*	NS	NS	NS
Import & Sorting	**	**	*	**	NS	NS	NS
Metabolism of Lipids & Lipoproteins	NS	*	*	*	NS	NS	NS
Metabolism of Vitamins & Co-Factors	NS	NS	NS	*	NS	NS	NS
Mitochondrial Carrier	NS	NS	NS	NS	NS	NS	NS
Mitochondrial Dynamics	NS	NS	NS	NS	NS	NS	NS
Mitochondrial Signaling	NS	NS	NS	NS	NS	NS	NS
Mitophagy	NS	NS	*	**	NS	*	NS
Nucleotide Metabolism	NS	NS	NS	**	NS	*	NS
Oxidative Phosphorylation	*	**	*	***	*	NS	*
Pentose Phosphate Pathway	NS	**	NS	NS	NS	**	NS
Protein Stability & Degredation	NS	NS	NS	NS	NS	NS	NS
Pyruvate Metabolism	NS	NS	NS	NS	NS	NS	NS
Replication & Transcription	**	**	**	****	**	**	**
ROS Defence	NS	NS	NS	NS	NS	*	NS
Translation	***	***	***	****	*	*	**
Transmembrane Transport	*	NS	NS	*	NS	NS	NS
TCA Cycle	NS	NS	NS	**	NS	*	NS
Ubiquinone Biosynthesis	**	***	**	****	***	**	***
Mito-proteome	*	NS	*	**	NS	NS	NS

Table 4.2 **Statistical analysis of rate recovery trends across mitochondrial proteome and process groupings.** Samples were analysed relative to WT rate recovery per 24 h ('Relative to WT' column) or TKO rate recovery per 24 h ('Relative to TKO' column). ****P≤0.0001, ***P≤0.001, **P≤0.01, *P≤0.05, NS P>0.05 (one-way ANOVA). Data was generated from three independent experiments.

4.6: Analysis of OXPHOS stability during G-TPP treatment and recovery

A contradiction was observed between the global GO analysis performed in Chapter 4.3, which detected OXPHOS related proteins as a cluster of highly aggregated and recovery-resistant proteins, and the mitochondrial process-based analysis in Chapter 4.4 that did not display *Oxidative Phosphorylation* as a highly aggregated process category. To explore these contradictions in aggregation trends, OXPHOS subunits and assembly factors were separated and the average aggregation across biological triplicate samples of each OXPHOS subunit for each cell line were plotted and compared across the treatment time course (Figure 4.7). While changes in the median aggregation of both WT and transcription factor KO samples was low (<20% across all samples), the spread of sample aggregation increased to an aggregation % of >50% in all samples at the 12 h G-TPP time point and remained elevated in each transcription factor KO cell line during the recovery period unlike the WT control (Figure 4.7). These observations indicate that specific subunits of the OXPHOS machinery are displaying trends of strong aggregation that are not representative of the behaviours of the rest of the OXPHOS machinery. Given that the OXPHOS machinery comprises 5 distinct protein complexes, the average aggregation of each protein that comprises each OXPHOS complex (complex I – V) was plotted in WT samples across the treatment time course to determine which components of the OXPHOS machinery are comprising the upper tail spread of proteins that are intrinsically more susceptible to damage during proteostatic stress (Figure 4.8 A). While some subunits of each OXPHOS complex increased in aggregation with acute G-TPP treatment, the upper tail of each violin plot was primarily comprised of complex I (CI) subunits (Figure 4.8 A). Strikingly, even at the 48 h recovery time point, where globally WT samples have recovered to back to baseline (see Figure 4.3 C), a number of CI subunits did not fully return to baseline levels of solubility even with a functional UPR^{mt} (Figure 4.8 A). CI comprises multiple distinct modules which span both the IMM and matrix space of mitochondria (*195*). To determine if a particular module of CI was more prone to aggregation, CI plots were analysed by CI modules (Figure 4.8 B). A clear preference for aggregation of Q-module subunits, and to a lesser extent N-module subunits, was seen at 12 h G-TPP treatment. Subunits of the Q-module and select N-module subunits also primarily comprised the upper tail of the CI plots at the 48 h recovery time point, highlighting that these modules are both highly susceptible to acute proteostatic stress and also encounter difficulties in returning to baseline proteostasis during the recovery period analysed. Studies by *Vincow et al.* (2013) and *Keeney et al.* (2006) have shown that particular subunits of CI are turned over by Parkin-based
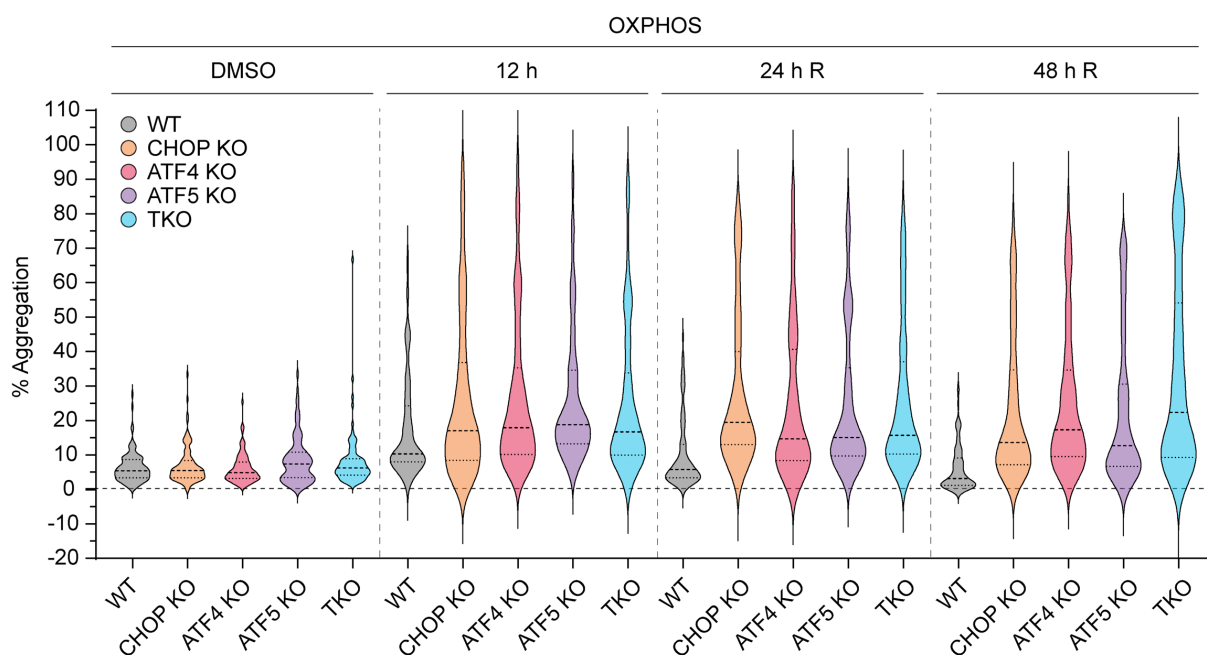
Figure 4.7 **Temporal OXPHOS solubility trends during G-TPP treatment and subsequent recovery.** The average solubility across biological triplicate samples of each core OXPHOS subunit comprising CI – CV and associated assembly factors in WT, CHOP KO, ATF4 KO, ATF5 KO and TKO samples are displayed by violin plot. Median subunit aggregation is represented by thick dashed lines, while thin dashed lines represent S.D..

mitophagy and the autophagy machinery (*196, 197*). These autophagy-regulated subunits were mapped onto CI subunit plots in WT cells to assess how they correlate to CI subunit aggregation trends (Figure 4.8 C). While no clear pattern in starting solubility is seen in DMSO treated samples, the upper tail of 12 h G-TPP and both 24 and 48 h recovery samples comprised primarily of the subunits previously shown to be regulated by both Parkin and autophagy. An increased severity of OXPHOS aggregation was observed in transcription factor KO lines (Figure 4.7). In addition, a wider spread in subunit aggregation levels (>70%) across all OXPHOS subunits was seen at 12 h G-TPP, and this spread was mostly maintained in all transcription factor KO lines across the recovery period but not in WT controls. A more detailed analysis of CI-V subunit aggregation patterns was therefore performed for each transcription factor KO cell line to determine if CI subunits comprised the aggregation prone clusters as was observed in WT , or whether aggregation of additional OXPHOS complexes occurs with UPR^{mt} removal (Figure 4.9). In contrast to the CI specific aggregation trends observed in WT, enhanced aggregation was seen in subunits from each OXPHOS complex in transcription factor KO cell lines (Figure 4.9). However, some subunits remained in the basal aggregation range for each complex and therefore were not affected by loss of UPR^{mt} (Figure 4.9).
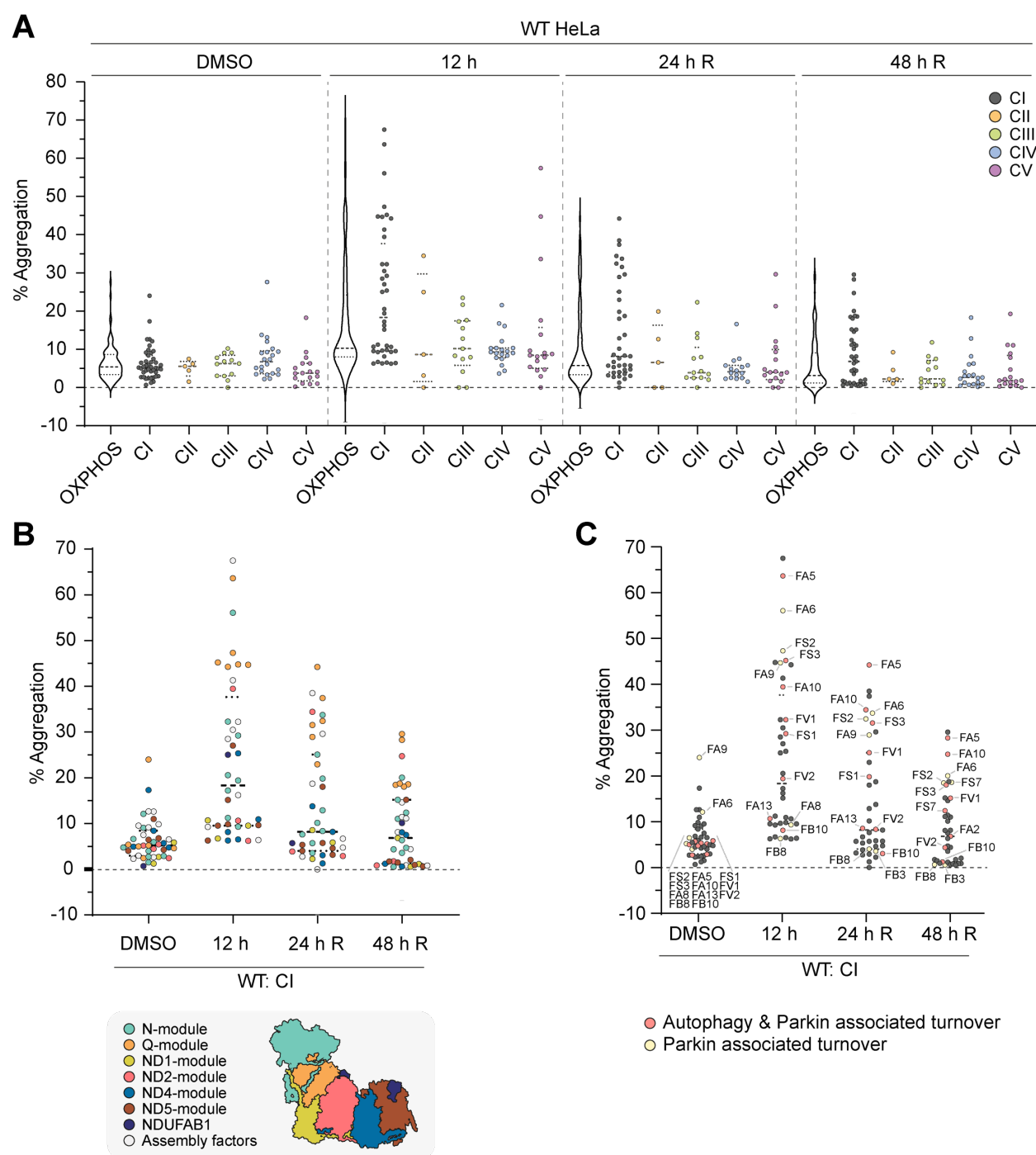
Figure 4.8 **Matrix-facing modules of CI are specifically sensitive to proteostasis stress. A.** The average protein subunit solubility across biological triplicate samples of each OXPHOS complex protein in WT cells were calculated and displayed by violin plot. Each dot represents an individual protein subunit of the corresponding OXPHOS complex (CI – CV). Grouped OXPHOS complex data displayed in Figure 4.7 has been included alongside separate complex graphs at each time point in **A.** for comparative purposes. **B.** Individual subunits comprising CI from **A** have been classified by CI module component. **C.** Individual CI subunits previously shown to be regulated by Parkin and autophagy associated processes have been labelled on CI plots extracted from **A** (*196, 197*). Median subunit aggregation is represented by thick dashed lines, while thin dashed lines represent S.D..

The least affected complexes of the OXPHOS machinery upon transcription factor KO as assessed by median aggregation were CIV and CV, while the most highly aggregated and recovery-resistant complexes in KO lines were CI, followed by CII (Figure 4.9). The violin plots for CI subunits displayed a large upper tail of aggregated subunits which persisted across the recovery time course in UPR^{mt} deficient cells (Figure 4.9 A). The CI module location for each subunit was plotted for KO lines to determine if the upper tail of CI subunit aggregation comprised similar modules to WT (Figure 4.10). Instead of a bias towards Q- and N- module subunits as observed in WT samples, removal of any transcription factor resulted in a more wide-spread collapse of CI module proteostasis, with subunits from ND5, ND1, and ND2 modules migrating to the upper plot tail in addition to N- and Q- module subunits (Figure 4.10).

Taken together, the aggregation trends within the multiple distinct components of the OXPHOS machinery demonstrate that the UPR^{mt} protects and repairs components of each OXPHOS complex. However, the extent of proteostatic damage varies across each complex with CI standing out as the most sensitive complex to proteostatic damage and the most reliant on the UPR^{mt}.
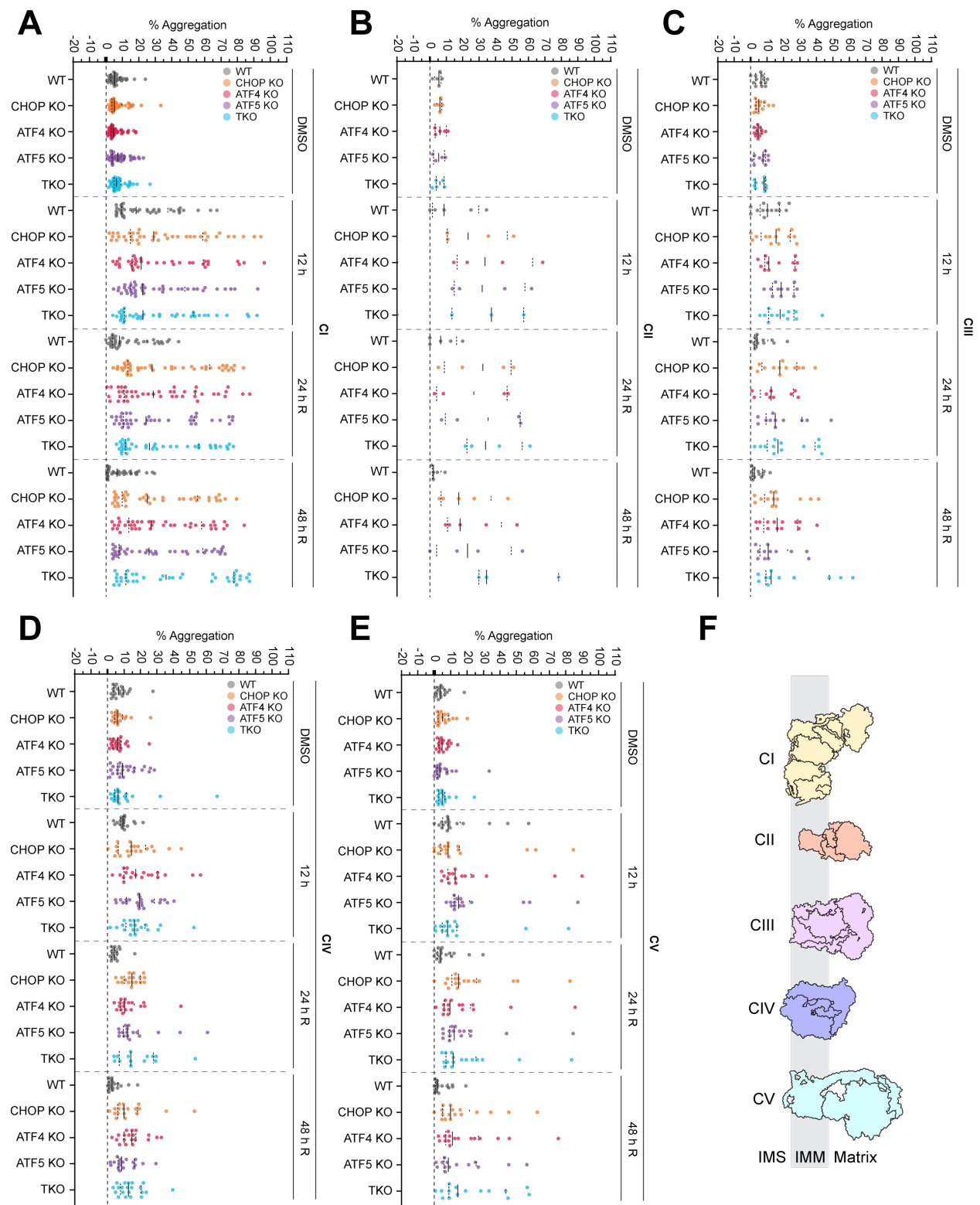
Figure 4.9 **Temporal OXPHOS subunit trends in transcription factor KO cells separated by OXPHOS complex. A – E**. The average protein subunit solubility for each OXPHOS complex protein was calculated and then displayed by violin plot for CHOP KO, ATF4 KO, ATF5 KO and TKO cells according to OXPHOS complex (**A** – CI; **B** – CII, **C** – CIII, **D** – CIV, **E** – CV). **F**. Schematic representation of OXPHOS complex module localisation. WT data from Figure 4.9 has been included alongside **A** – **E** for comparative purposes. Each plot point represents an individual protein. Median subunit aggregation is represented by continuous black line, while thin dashed lines represent S.D..
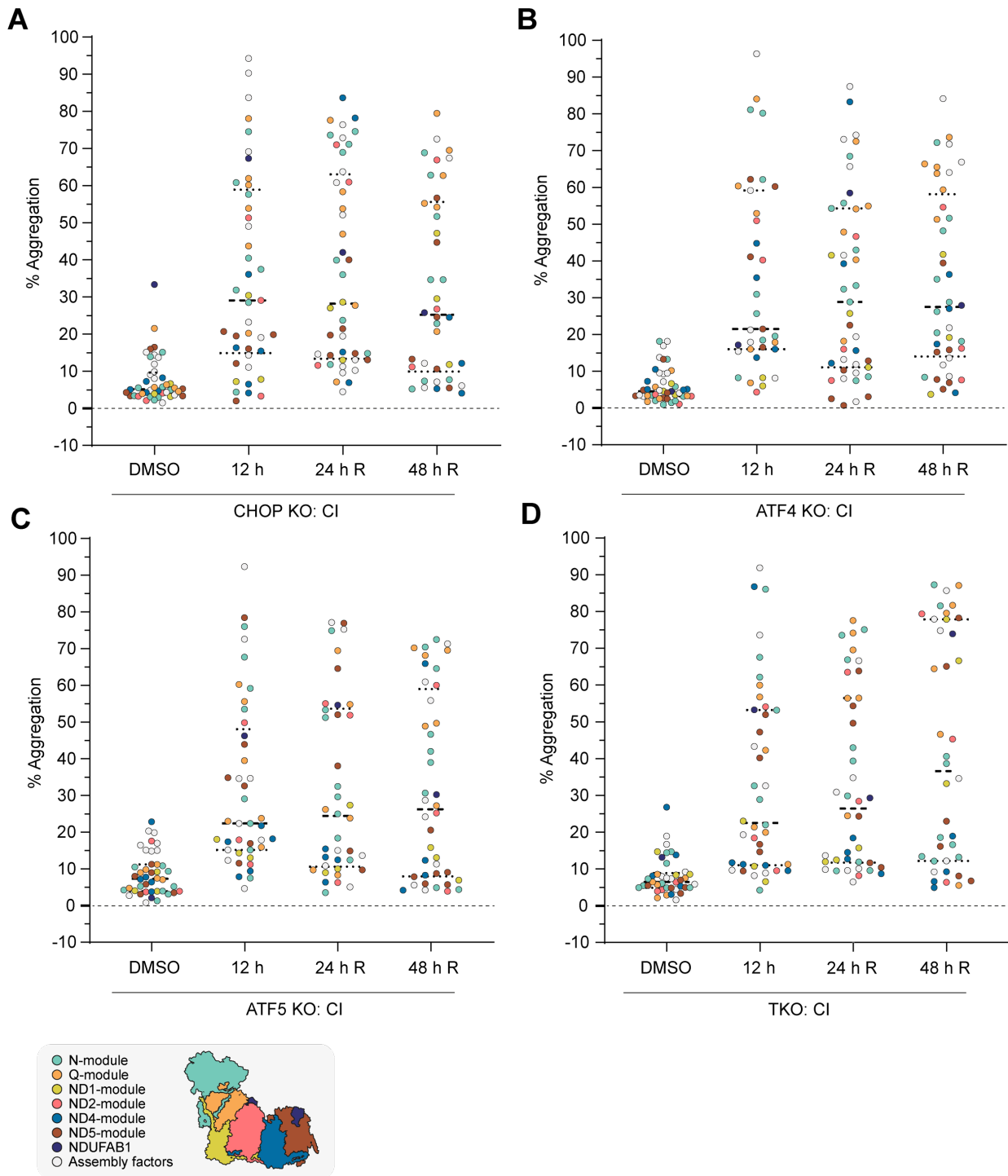
Figure 4.10 **Temporal Complex I aggregation trends in transcription factor KO cells reveal widespread collapse of CI proteostasis. A – D**. CI subunit aggregation values were extracted from Figure 4.10 and classified by CI module localisation in CHOP KO (**A**), ATF4 KO (**B**), ATF5 KO (**C**) and TKO (**D**) samples. Each plot point represents an individual protein. Median subunit aggregation is represented by continuous black line, while thin dashed lines represent S.D.. Data in **A – D** was generated from three independent experiments.

4.7: Analysis of mitochondrial ribosome aggregation during G-TPP treatment and recovery

Blunted mitochondrial transcription through decreased protein expression of transcription machinery has been associated with UPR^{mt} signalling and was previously proposed as a mechanism to prevent additional mitochondrial translation that may overwhelm proteostasis during stress (*102*). However, mitochondrial process and mito-proteome GO analysis of proteins resistant to proteostasis repair repeatedly identified transcription and translation machineries as being highly sensitive components to proteostatic stress (Figure 4.4 C, D; Figure 4.5). Sensitisation to aggregation and misfolding of the transcription/translation machinery during stress may represent an alternative model for regulating protein production. Given this, a more detailed analysis was conducted on the central player of mitochondrial translation, the mitochondrial ribosome (mitoribosome).

The average aggregation of mitoribosome subunits was plotted and compared across time points and cell lines (Figure 4.11). Unlike the OXPHOS machinery, almost the entire mitoribosome structure displayed increased aggregation in both WT and transcription factor KO cells following 12 h G-TPP treatment (Figure 4.11). Aggregation was substantially enhanced in all transcription factor KO lines with an additional median increase of ~35% aggregation over WT. While some recovery was observed by 48 h in WT cells, the baseline solubility of the entire mitoribosome was still not fully restored by 48 h even with a functional UPR^{mt} program (Figure 4.11). Almost no recovery was apparent at the 24 h recovery time point in any transcription factor KO cell line, and only minor recovery was observed at the 48 h time point demonstrating that recovery of the mitoribosome is severely blunted with removal of any arm of the UPR^{mt} (Figure 4.11) Interestingly, no recovery at all was observed in TKO cells according to median subunit aggregation pointing toward potential additive roles of CHOP, ATF4 and ATF5 in repairing the mitoribosome (Figure 4.11). However, the severity of aggregation observed at the 48 h recovery in single transcription factor KO lines raises questions into whether any additional aggregation from a high starting level will lead to different biological phenotypes in TKOs, or if the aggregation is already sufficiently high in a single transcription factor KO that further aggregation in TKOs is unlikely to compound any functional phenotypes (Figure 4.11).
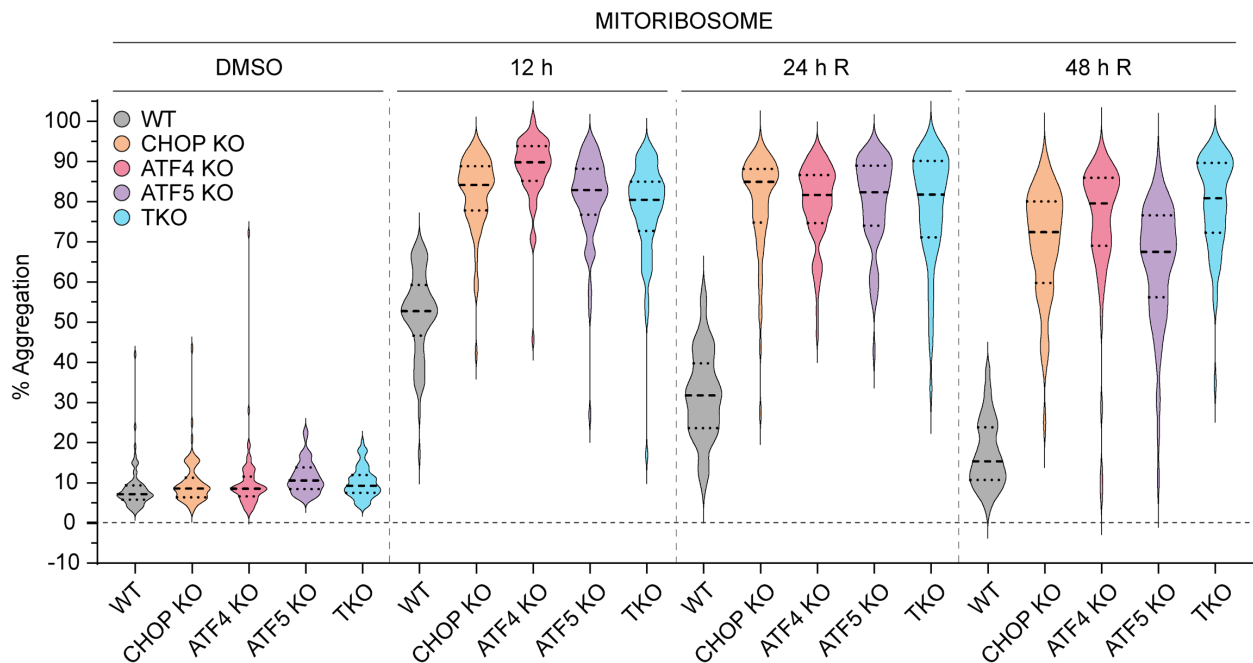
Figure 4.11 **Temporal mitoribosome solubility trends during G-TPP treatment and recovery.** The average solubility of each protein component comprising the mitochondrial ribosome (mitoribosome) in WT, CHOP KO, ATF4 KO, ATF5 KO and TKO samples are displayed by violin plot. Median subunit aggregation is represented by thick dashed lines, while thin dashed lines represent S.D.. Data was generated from three independent experiments.

Assembly of the mitoribosome involves the attachment of separate 39s and 28s subunit components during translation initiation (*198*). The mitoribosome data was further broken down into 39s and 28s aggregation trends to examine whether there are differences in the aggregation propensity of either ribosome subunit (Figure 4.12). In each cell line, including WT cells, the 28s subunit displayed a higher median aggregation and slower recovery relative to the 39s subunit. However, 28s subunit proteins appeared to have an increased baseline propensity for aggregation in the DMSO samples of each cell line (Figure 4.12), suggesting the experimental differences in aggregation may be due to intrinsic biophysical properties of the 28s subunit, and therefore the susceptibility of each subunit to proteostatic damage with and without the UPR^{mt} are likely to be similar. The 39s subunit is known to anchor to the IMM to promote insertion of newly translated proteins into the membrane, suggesting perhaps the portion of the 39s subunit tethered to the IMM may be more soluble in these experimental conditions (*199*). Collectively, the data in this section demonstrates that the entire mitoribosome appears to be inherently sensitive to proteostatic stress, raising the possibility that this could be a mechanism by which mitoribosome translation is regulated during stress.
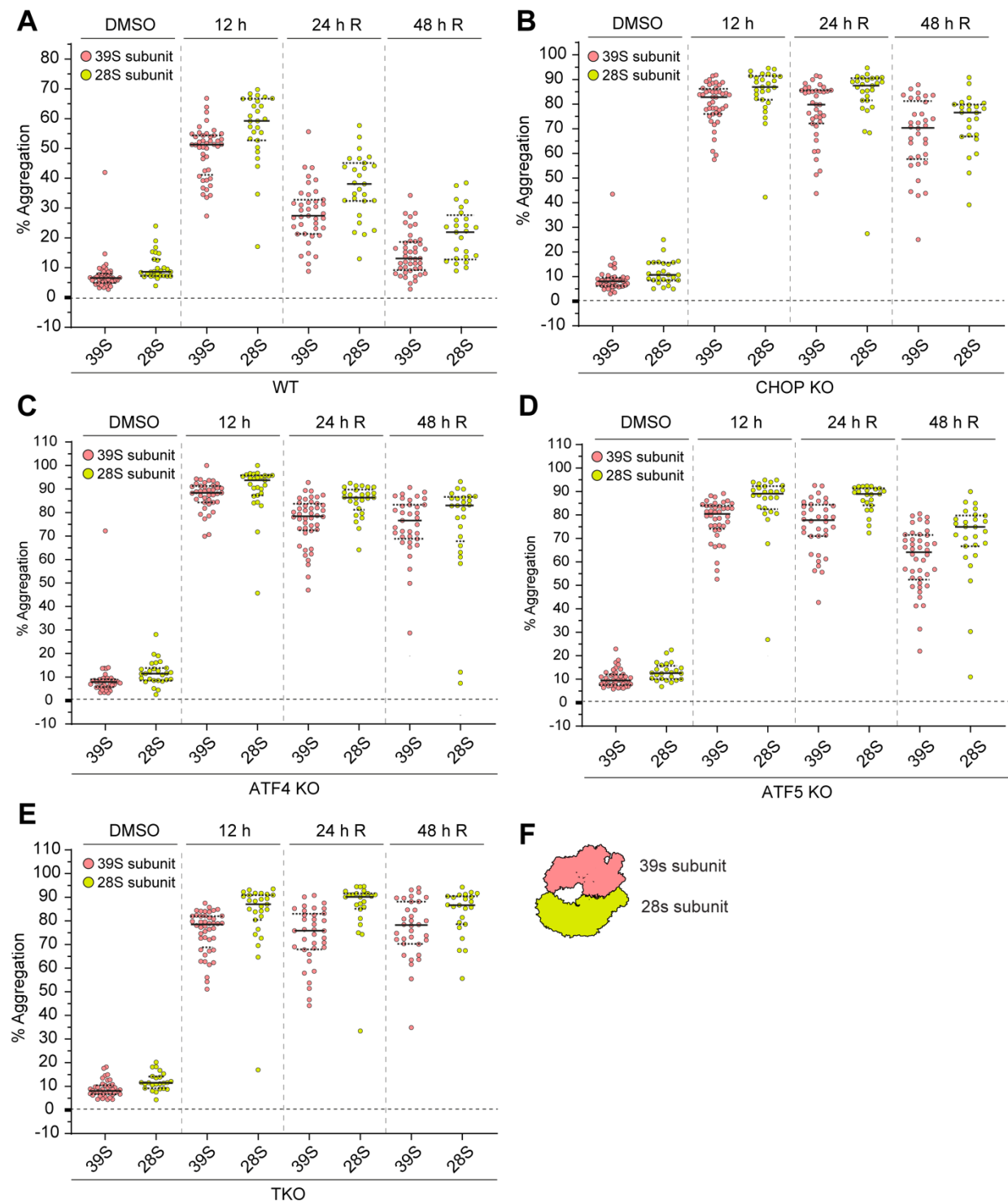
Figure 4.12 **28S and 39S subunits display similar aggregation trends in both WT and transcription factor KO cells.** The average protein subunit aggregation across biological triplicate samples for each protein comprising the 28S and 39S components of the mitochondrial ribosome were calculated and displayed by violin plot for WT (**A**), CHOP KO (**B**), ATF4 KO (**C**), ATF5 KO (**D**), TKO (**E**) samples. **F**. Schematic representation of mitoribosome subunit assembly. Each plot point in **A** – **E** represents an individual protein. Median subunit aggregation is represented by continuous black line, while thin dashed lines represent S.D.

4.8: Solubility profiles of metabolism related process components

Metabolism related mitochondrial process graphs displayed modest increases in metabolism factor aggregation across WT cells (Figure 4.5), which was mildly exacerbated upon transcription factor KO (compare *Amino Acid Metabolism* to *Translation* groupings in Figure 4.5). Disruption to individual proteins of metabolic pathways within mitochondria could have severe downstream effects on metabolic functions, as exemplified through mitochondrial and neuropathic diseases associated with mutations in genes involved in amino-acid synthesis, TCA cycle, lipogenesis, and 1-C metabolism (*200-203*). Additionally, a growing body of evidence indicates that mitochondrial metabolites are important signalling molecules, meaning even minor disruptions to metabolic pathways in mitochondria may have important indirect downstream effects on cellular signalling (*204*).

To gauge the extent of proteostatic disruption of each metabolic pathway that may have been masked by the grouped metabolism process analysis, the aggregation trends of individual protein components of key mitochondrial metabolic pathways were examined by heat map analysis (Figure 4.13). Overall, while mild to medium increases in aggregation (aggregation range 4.95 – 50.46 %) were seen across all groupings, only select proteins from the metabolic pathways examined showed strong increases in aggregation at 12 h G-TPP treatment in WT samples (Figure 4.13). GLS, involved in the glutamate metabolism steps of non-essential amino acid synthesis (*205*), BCKDHA/BCKDHB involved in branched chain amino acid (BCAA) metabolism (*206, 207*), and multiple components of the Pyruvate dehydrogenase complex showed medium to high levels of aggregation (aggregation range 50.11 – 62.50 %) at 12 h G-TPP treatment (Figure 4.13). Only one component of the Pyruvate dehydrogenase complex, PDK4, remained aggregated at 48 h recovery in WT, demonstrating that most metabolic perturbations from the mild aggregation observed at 12 h in WT may be transient disruptions to mitochondrial function. In contrast, severe aggregation (aggregation range 62.21 – 92.75 %) was observed in components of most metabolic pathways analysed in each transcription factor KO cell line (Figure 4.13), showing that proteostatic disruptions may have widespread effects on metabolic function in cells with defective UPR^mt. Aggregation persisted in components of each affected metabolic pathway in transcription factor KO cells, meaning proteostasis issues in metabolic pathways may persist in the recovery period unlike WT cells which can recover via a functional UPR^mt. The only metabolic pathway examined that showed minimal proteostatic disruption in both WT and transcription factor KO cells was *Nucleotide synthesis* (Figure 4.13). Taken together, the detailed analysis of metabolic pathways illustrates that the metabolic machinery in mitochondria are a key components of mitochondrial function that are protected by all arms of the UPR^mt.
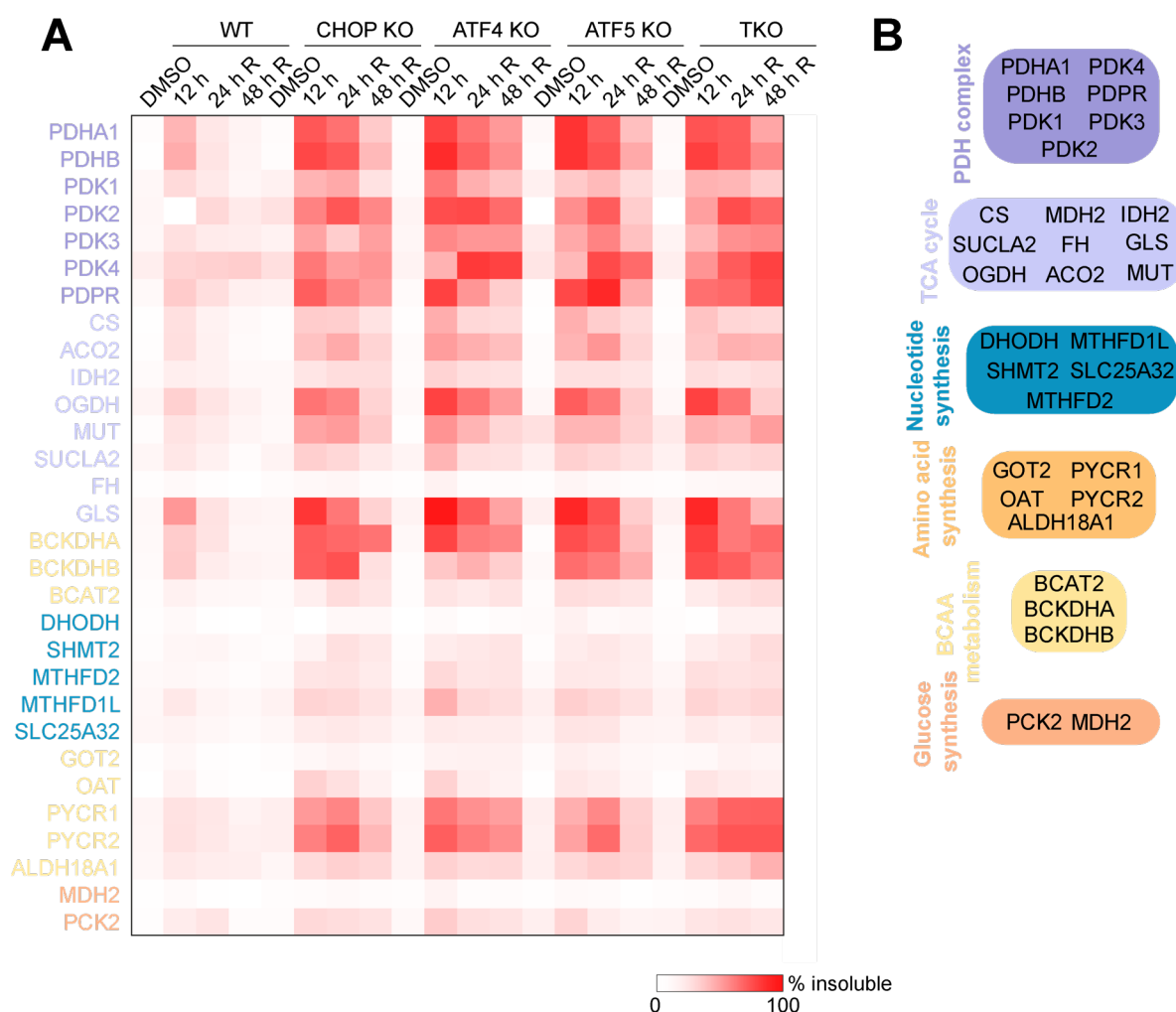
Figure 4.13 **Transcription factor KO leads to elevated and persistent protein aggregation across multiple metabolic pathways.** Proteins comprising key mitochondrial metabolic pathways (**B**) were displayed by heat map analysis of aggregation % in WT, CHOP KO, ATF4 KO, ATF5 KO and TKO samples (**A**). Data in **A**, **B** was generated from three independent experiments.

4.9: Rewiring of mitochondrial proteostasis following UPR^mt-mediated recovery

Intriguingly, while WT cells overall appeared to return to baseline proteostasis at the 48 h recovery time point, analysis of OXPHOS and mitoribosome complexes at 48 h recovery indicated that some proteins did not return to baseline proteostasis (see Figures 4.4 C-D, 4.5, 4.7, 4.8, 4.9, 4.11). To balance out the increased aggregation of select proteins, other proteins may be developing improved proteostatic profiles with recovery from a temporary proteostatic stress. To explore the potential of a rewired mitochondrial proteome after recovery from a proteostatic stress, proteins from each sample were grouped according to whether their solubility increased or decreased compared to baseline solubility levels (DMSO). Remarkably, in WT cells, ~32% of the analysed

proteome demonstrated improved solubility at 48 h recovery after G-TPP treatment, while ~ 23% of the analysed mito-proteome had reduced solubility after 48 h recovery when improvements and decreases are classified as >5% deviations from baseline (Figure 4.14 A). Clustered GO analysis was performed on the proteins that improved and decreased in solubility in WT cells to inform what mitochondrial processes are affected by proteostatic rewiring (Figure 4.14 B). Ion and protein transport, and ROS-defence related proteins demonstrated improved solubility, in addition to morphology related processes (Figure 4.14 B). Numerous transcription related protein clusters also demonstrated decreased solubility after the recovery period. A dichotomous solubility profile change was observed in OXPHOS-related processes, which produced clusters of proteins of both improved and decreased protein solubility at the 48 h recovery time point (Figure 4.14 B). Collectively, temporal proteostasis analysis demonstrates that while proteostasis overall returns to baseline DMSO treated levels in WT cells after 48 h recovery, select groups of proteins actually have improved proteostasis profiles following recovery from a protein folding stress.
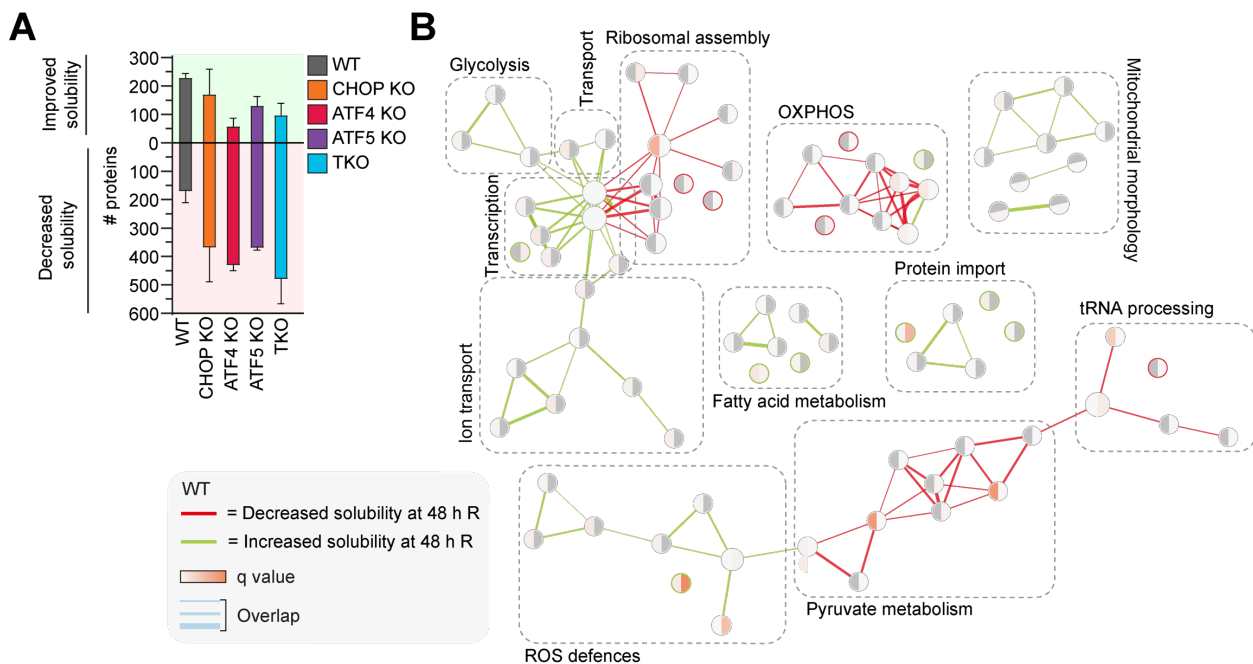
Figure 4.14 **Recovery from G-TPP stress alters the proteostasis profile of mitochondria. A.** The number of mitochondrial proteins that showed an increase or decrease in aggregation relative to their starting DMSO levels of </> 5% aggregation were counted and graphed. **B.** GO analysis was performed on proteins showing > 5% increase or decrease in aggregation in WT samples. GO analysis in **B** was performed using the 'Biological Process' and 'Molecular Function' categories in the DAVID v6.8 platform (*193, 194*). Data in **A**, **B** was generated from three independent experiments.

4.10: Discussion

4.10.1: CHOP, ATF4 and ATF5 are signalled independently during the mammalian UPR^mt

Challenges in detecting the mammalian UPR^mt signalling pathway have been compounded by the roles of CHOP, ATF4 and ATF5 in other cell stress response pathways. Although specific UPR^mt programs have been observed in a variety of organisms (*77, 115, 208-210*), and mitochondrial stress responses are commonly tailored according to the initiating stimulus (*101, 181, 182, 185, 211*), potential signatures of the UPR^mt in the literature are commonly grouped together with the better-characterised, generalised ISR-related signalling pathways. This occurs due to our lack of knowledge and understanding of the UPR^mt which prevents precise identification of its signalling signatures. In addition, the contribution of each identified transcription factor to the UPR^mt is unclear, as to date they have each been studied in isolation (*77, 95, 101*). Whether CHOP, ATF4 and ATF5 drive independent programs, or function in a linear pathway with one transcription factor acting as the master regulator of the pathway was unknown prior to this work.

Genetic epistasis studies performed in this chapter revealed that CHOP, ATF4 and ATF5 are independently induced during a mitochondrial protein folding stress (Figure 4.1), providing an important point of divergence in their induction dynamics from ISR-mediated induction in which ATF4 is the master regulator (*100*). Different induction patterns to what is seen during the ISR suggest that an additional signalling mechanism is induced upstream of transcription factor induction to tailor the stress response to protect and repair mitochondrial proteostasis. DELE1 release from stressed mitochondria has been identified as a signalling mechanism that transmits mitochondrial stress signals to the nucleus (*104, 105*). Recent studies showed that DELE1 interacts with the kinase HRI and activates its kinase activity, leading to phosphorylation of the eIF2α subunit of the cytosolic ribosome which stalls translation and allows for translation of select stress-response transcripts, as occurs during the ISR (*104, 105*). Ablation of DELE1 expression is sufficient to block UPR^mt signalling (*104, 105*). However, both the data in this thesis and previously published data have confirmed that canonical ISR signatures are not robustly detected during mitochondrial protein folding stress (*77, 102, 141*). Ribosome phosphorylation by both HRI and other kinases are a common activation point in the ISR program (*212*), meaning ribosome-mediated changes in translation aren't sufficient to explain the unique signalling patterns of the UPR^mt that are divergent from the canonical ISR response. Additional stress signals from mitochondria must be acting together with DELE1 to drive the tailored transcript specificity of the UPR^mt program. Parallel signalling lineages have been identified in *C. elegans*, where the

chromatin-remodelling factors *dve-1*, *hda-1* and *ube-5* have been shown to regulate full UPR^{mt} induction independently of *atfs-1* signalling activity (*80, 213*). Chromatin remodelling in *C. elegans* is thought to promote *atfs-1* mediated transcription of UPR^{mt} related genes by increasing the accessibility of these gene regions to transcription machinery (*80*). Direct experimental evidence supporting these hypotheses have not yet been published, however, *dve-1*, *hda-1* and *ubl-5* all have corresponding homologues in humans (SATB1/2, HDAC1/2 and UBL5 respectively) which have been shown to influence chromatin organisation in other cellular contexts (*99, 214-216*). Recent studies have also begun to untangle the important role mitochondrial metabolites play in regulating signalling, including modulation of histone acetylation through Acetyl-CoA production (*204*). Whether a separate chromatin remodelling program, perhaps triggered through metabolic changes during mitochondrial stress, acts alongside DELE1 signalling to mediate the specificity of the UPR^{mt} response in mammals remains to be explored.

4.10.2: The UPR^{mt} comprises a bimodal program of proteostasis protection and repair

Previous studies and the data in this chapter have demonstrated activation of a UPR^{mt} signalling program when components of the mitochondrial protein folding machinery are compromised, be that through drug treatment or genetic manipulation of mitochondrial protein folding machinery (*77, 169, 171*). Unfortunately, analysis of how mitochondrial proteins and mitochondrial function are affected by protein folding stressors and how the UPR^{mt} modulates functional mitochondrial repair have not accompanied these previous studies since adequate experimental systems to study mitochondrial function in such depth were not available. Without understanding the extent and degree of mitochondrial damage and dysfunction experienced during these stressors, it is difficult to conceptualise the importance of the UPR^{mt} program in regulating mitochondrial health. In addition, previous studies have focussed on analysing how the UPR^{mt} functions in an acute stress setting (*76, 77, 95, 102*). While acute protection is important, the UPR^{mt} program is generally considered a repair pathway, and arguably the most important outcome of the UPR^{mt} is how effectively mitochondrial health can return to baseline after encountering a biological stress to prevent mitochondrial degradation. As a result of these previous limitations, only one aspect of the UPR^{mt} program, the acute stress signalling of the UPR^{mt} has been studied to date.

In this chapter, the newly developed proteostasis analysis approach developed in Chapter 3 was used to develop a comprehensive profile of the temporal changes in mitochondrial proteostasis that occur at each stage of the UPR^{mt} program: basal proteostasis, proteostasis damage during an

acute stressor, and proteostasis changes across the repair period after the stressor is removed. The analyses revealed that the UPR^{mt} can be separated into two main stages with distinct proteostatic trends across the 'acute' stress stage, and the 'recovery and repair' stage. Mild aggregation across most protein process groups in the mito-proteome is seen in WT cells with a functional UPR^{mt} during an acute G-TPP treatment that is consistent with a mild level of mitochondrial damage (Figure 4.5). In the recovery phase, aggregation quickly begins to subside, and WT cells return to baseline proteostasis by 48 h recovery, demonstrating successful repair of the mild mitochondrial damage. Examination of CHOP, ATF4, ATF5 KO and TKO cells with a dysfunctional UPR^{mt} revealed that the UPR^{mt} plays direct roles in facilitating both acute stress and recovery and repair phases. During the acute stress phase, the UPR^{mt} is responsible for mitigating severe proteostatic damage across the mito-proteome and keeping the accumulation of aggregated protein to a minimum (Figures 4.3 C, 4.5). Disruption of any single transcription factor of the UPR^{mt} leads to significantly elevated levels of aggregated protein by 12 h G-TPP treatment across the mito-proteome, and direct comparison of UPR^{mt} disrupted and WT cells illustrates the important protective role the UPR^{mt} is playing during the acute stress phase (Figure 4.3 C). The elevated level of aggregated protein fail to subside in the recovery phase, and when taking into account the elevated starting aggregation loads at the beginning of the recovery phase, cells with a defective UPR^{mt} program also show a reduced rate of recovery which implies the UPR^{mt} program is also facilitating repair of mitochondrial proteostasis (Figure 4.6). Some process groups with defective protein aggregation at the acute stage did not have defective recovery rates (e.g. *Folate & pterin metabolism* and *Pyruvate metabolism*), suggesting there may be different roles of the UPR^{mt} in repairing mitochondria vs. protecting mitochondria from acute stress depending on the mitochondrial process. Collectively, the data in this chapter illustrates that when analysing the UPR^{mt} pathway, both phases of the UPR^{mt} program must be studied in order to properly analyse UPR^{mt} activity and its effect on mitochondrial health. A schematic of the proposed UPR^{mt} model developed from the data in this chapter is displayed in Figure 4.15.

An interesting variable that has not been accounted for in the data analysis performed in this chapter is the effect that cell division may have on mitochondrial repair. Elevated levels of mitochondrial biogenesis are seen during cell division which may serve to dilute the pool of aggregated protein and help improve overall proteostasis (*217*). Highly mitotic cell populations could have an adapted UPR^{mt} program that focuses more on protection during an acute proteostasis stress rather than facilitating recovery and repair if mitochondrial biogenesis can contribute to the restoration of difficult-to-recover mitochondrial proteins. UPR^{mt} mediated repair in post-mitotic cells such as neurons that cannot rely on dilution through cell-division associated mitochondrial

biogenesis may instead be more highly reliant on the UPR^{mt} for mitochondrial repair. Future studies involving comparative analysis of UPR^{mt} signalling across different tissues or cell types could help broaden our understanding of the physiological roles of the UPR^{mt}.
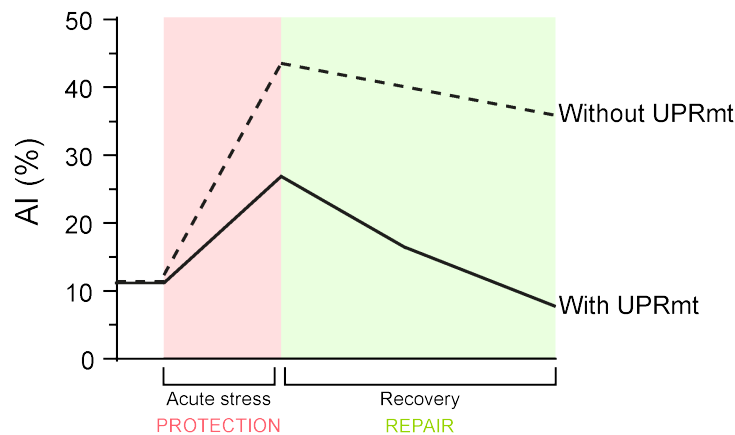
Figure 4.15 **Proposed model of bimodal UPR^{mt} activity.** Temporal proteostasis analysis in Chapter 4 indicates the UPR^{mt} functions in a bimodal manner, encompassing an initial protection stage during an acute stress where the UPR^{mt} acts to mitigate the accumulation of proteostasis damage, and a subsequent recovery stage after the acute stressor has been removed where the UPR^{mt} repairs mitochondrial proteostasis. Comparative analysis of temporal proteostasis trends between WT and transcription factor KO cells with a defective UPR^{mt} program has revealed that the in the acute phase, cells with a defective UPR^{mt} accumulate more misfolded protein through defective proteostasis protection. In the recovery phase, cells with a defective UPR^{mt} recover at a slower rate and fail to reach baseline, demonstrating a failure in active repair driven by the UPR^{mt} program.

4.10.3: CHOP, ATF4 and ATF5 non-redundantly regulate protection and repair of mitochondrial proteostasis through the UPR^{mt}

Following the genetic epistasis studies in this chapter which clarified that each transcription factor is induced independently of the others (Figure 4.1), the next logical line of enquiry leading from this data was to examine how important each signalling arm is to maintaining mitochondrial health through the UPR^{mt}. Temporal proteostasis profiles in KO cell lines of CHOP, ATF4, ATF5, and combined KO of CHOP/ATF4/ATF5 (TKO) were generated and compared to the WT temporal proteostasis profile to calculate the extent of proteostasis protection afforded by each transcription factor. Remarkably, each transcription factor KO cell line, including the TKO line, led to similarly exacerbated proteostatic damage to mitochondria upon G-TPP treatment. Every parameter assessed, including mito-proteome aggregation, KO specific GO analysis, mitochondrial process focused analysis, and rate recovery analysis produced defects of a similar magnitude in both the acute and recovery phases in every single transcription factor KO and TKO cell line. The similarity

in the protein aggregation phenotypes observed with loss of any individual transcription factor demonstrates that each transcription factor is equally important in driving the UPR^{mt} and protecting mitochondrial proteostasis. A lack of clear additive aggregation damage in any analysed metrics in the TKO cells relative to single KO cells suggests each transcription factor driven arm of the UPR^{mt} is critically required for UPR^{mt} function and no signalling arm can compensate for loss of a single signalling node. Therefore, removal of a single signalling node is sufficient to produce maximal levels of protein aggregation.

The similarity in aggregation loads across single KO and TKO cells extended to almost all mitochondrial process-specific metrics assessed. All mitochondrial process groups displayed similar aggregation trends and broadly similar recovery rates across each single and TKO cell line. It is noted that the rate of recovery of selected mitochondrial processes did appear to be further defective in TKOs relative to single KOs (see Chapter 4.5) suggesting there may be some redundancy in select UPR^{mt}-related signalling pathways relating to proteostatic recovery. However, in each process group with additive TKO defects, single KO cells were still defective relative to WT recovery rates meaning it can be confidently concluded that each transcription factor still plays significant, non-redundant roles in facilitating proteostatic recovery in these cases. The stark, broad phenotypic similarities at a process-based analysis level indicate that each transcription factor is driving the expression of proteins or pathways that have broad effects across the mitochondrial proteome. The near-identical phenotypes across transcription factor KO cell lines could also occur through each transcription factor affecting the same biological processes, but in unique ways.

Transcription/translation machineries and specific components of multiple metabolic pathways showed significant aggregation above WT levels in all transcription factor KO lines (Figure 4.11, 4.13). Aggregation of select subunits from each OXPHOS complex, and further aggregation of additional CI module subunits not seen in WT cells was also observed with the loss of any single transcription factor (Figure 4.9, 4.10). Since CI formation is shown to be sensitive to loss of individual subunits (*218*), the severity of CI aggregation points toward significant defects in OXPHOS activity that are made worse with UPR^{mt} disruption. Examination of the functional consequences of the process-based proteostasis defects identified in this chapter and detailed examination of the transcriptional programs driven by CHOP, ATF4 and ATF5 that lead to their non-redundant activities will be conducted in Chapter 5.

4.10.4: Sensitivity to proteostatic stress varies across the mito-proteome

Analysis of process-specific trends in mitochondrial proteostasis across the UPR^{mt} program revealed that specific groups of mitochondrial proteins are highly sensitive to a matrix-based proteostatic stress. The groups include the OXPHOS and transcription/translation machineries, which had elevated aggregation and a resistance to repair in WT cells that was further exacerbated with a defective UPR^{mt} (Figures 4.5, 4.7 – 4.11).

Aggregation sensitivity was also varied within the OXPHOS process group. Analysis of individual OXPHOS complexes in WT cells revealed that CI, in particular the Q- and N- modules, specifically aggregated during the acute stress phase, and were also resistant to recovery across the repair period (Figure 4.8). Both the Q- and N- modules comprise the matrix arm of CI (*195*). During oxidative respiration, NADH is oxidised at the N- module, and electrons are then transported through the Q- module and transferred to ubiquinone (*195*). Both oxidation and electron transfer create hostile environments for protein stability, and damaged subunits from both the N- and Q- module of CI have been shown to undergo exchange with functional subunits within the fully assembled CI module (*219-221*). Proteostatic stress may be preventing CI module cycling through disrupted supply of replacement subunits, or damaged CI subunits may be accumulating within mitochondria as chaperones and proteases are overwhelmed with aggregated proteins during acute G-TPP treatment. Interestingly, elevated levels of aggregated CI subunits remained even after 48 h recovery in WT cells once baseline mito-proteome proteostasis was achieved (Figure 4.8). Several of these subunits have been previously shown to be turned over by autophagy-related processes, including Parkin-based mitophagy (*196, 197*). Whether simultaneous PINK1/Parkin mitophagy activity is required alongside the UPR^{mt} to further restore proteostasis is an interesting question for future research particularly given the links of CI dysfunction in Parkinson's disease.

In contrast to the varied aggregation sensitivity observed across OXPHOS proteins, the mitoribosome displayed consistent, severe aggregation and a resistance to repair in WT cells in most of the proteins in its structure (Figure 4.11). Aggregation of the mitoribosome, was further elevated in transcription factor KO lines which indicates the UPR^{mt} does regulate the protection and repair of these protein groups, but some proteostasis damage still occurs with a functional UPR^{mt} (Figure 4.11). As was briefly explored in Chapter 3, aggregation of the transcription/translation machinery presents an interesting potential biological mechanism for regulating mitochondrial protein production during proteostatic stress. An inherent biophysical sensitivity of the transcriptional/translational machinery aggregation could be an adaptive

mechanism within mitochondria to ensure that protein is only produced if the protein folding environment is in an optimal state, thereby coupling mitochondrial translation rates to protein folding capacity. Interestingly, while elevated aggregation with transcription factor KO was a common trend across mitochondrial process groups in the acute phase, a significant defect of a large magnitude in the repair rate of transcription/translation proteins was observed in transcription factor KOs that was not seen to the same degree in other process groups (Figure 4.6 B). This data suggests that each transcription factor driven arm of the UPR^{mt} plays a critical role in actively facilitating repair of the transcription and translation machinery. Dynamics of the transcription and translation machinery, in particular the mitochondrial ribosome, are an interesting component of the proteostasis analysis as their high level of sensitivity to protostatic stress could position them as a robust readout of the general protein folding environment within mitochondria. Assessing early time points of acute stress (<12 h G-TPP) or using lower concentrations of G-TPP to induce a weaker proteostasis stress would be interesting avenues of further research to determine if the mitoribosome could function as an early readout of even mild protein folding stress and dysfunction within mitochondria.

4.10.5: Does mitochondrial proteostasis damage leave an imprint on the mitochondrial proteome?

An intriguing result found in the aggregation analysis of WT cells, which had largely reached baseline levels of proteostasis by 48 h recovery (Figure 4.3 C), was an increase in solubility profile of several proteins including those associated with ROS defences and glycolysis (Figure 4.14). Altered but 'recovered' proteostasis poses an interesting potential for mitochondrial proteomic memory of damage following an acute stress. Improved baseline solubility may make these proteins more resistant to experiencing the same severity of aggregation with another proteostatic stressor, in essence, improving mitochondrial fitness in case the stress returns. Whether these solubility changes result from localised, temporary changes within the mitochondrial environment or long-term epigenetic changes is an interesting avenue of future investigation, since long term changes could imply treatment with a mild proteostatic stressor may be a mechanism of improving long term mitochondrial health. However, any improvement in the solubility of mitochondrial proteins would be negated by insufficient repair of a portion of the mitochondrial proteome from the first stress-cycle, as was observed in OXPHOS proteins in this data (Figure 4.8). The persistence of some proteostatic damage within WT mitochondria with a functional UPR^{mt} raises questions regarding the ability of the UPR^{mt} program to function in isolation. UPR^{mt} repair-

resistant CI subunits correlate with those previously shown to be regulated by autophagy and Parkin-based mitophagy (*196, 197*). As the temporal studies in this chapter were undertaken in HeLa cells lacking Parkin expression to study the UPR^mt in isolation of PINK1/Parkin mitophagy activity, an important point to clarify in future research is whether these 'repair resistant' portions of the WT mito-proteome would be removed and restored by PINK1/Parkin mitophagy. Clarifying the relationship between the UPR^mt and PINK1/Parkin mitophagy is important to inform whether the UPR^mt program can improve mitochondrial resistance to proteostatic stress in the long term, provided it is accompanied by PINK1/Parkin mitophagy. Additionally, investigating the combined role of PINK1/Parkin mitophagy and the UPR^mt in restoring proteostasis is important to inform our understanding of mitophagy dysfunction observed in neurodegenerative disease. If PINK1/Parkin mitophagy activity is required alongside the UPR^mt to restore proteostasis following stress, then disruption to PINK1/Parkin mitophagy could lead to neuronal dysfunction through insufficient repair of the mito-proteome from a proteostatic stress rather than solely through a failure to remove severely damaged mitochondria. A preliminary analysis of the interplay between PINK1/Parkin mitophagy and the UPR^mt is explored in Chapter 6.

In summary, work in this chapter has allowed us for the first time to visualise how the functional mito-proteome collapses in response to a proteostatic stress. Temporal analysis of proteostatic trends in CHOP KO, ATF4 KO, ATF5 KO and TKO cells has allowed us to identify the proportions of the mito-proteome which are protected and repaired by the UPR^mt, which include the OXPHOS machinery and the mitochondrial transcription/translation machinery. The proteostasis analysis in this chapter has also confirmed that each CHOP, ATF4 and ATF5 driven arm of the UPR^mt are critically required to protect and repair mitochondrial proteostasis.

Chapter 5

Functional consequences of disrupted mitochondrial proteostasis

5.1: Introduction

Proper proteostasis is widely acknowledged as essential to maintaining mitochondrial homeostasis, which is reinforced by the disease phenotypes observed with disruption to components of the mitochondrial translation machinery such as DARS2 and MRPL3 (*222, 223*). However, due to the previous limitations in techniques available to comprehensively analyse mitochondrial proteostasis (see Chapter 4.1), there has been little direct study of the specific consequences to mitochondrial function when misfolded protein accumulates in mitochondria. Whether temporary increases in misfolded protein are sufficient to result in deleterious consequences for mitochondrial function is an important question to answer and can help to clarify how the UPR^{mt} protects mitochondrial health. In addition, determining whether the additional aggregation seen with UPR^{mt} disruption causes further damage to mitochondrial function will help improve our understanding of the cellular consequences of a faulty UPR^{mt} program.

Proteostatic trends across the mito-proteome with removal of CHOP, ATF4 or ATF5 showed remarkable similarity between each cell line. Similar aggregation trends were observed across both the acute stress phase and the recovery phase of the mitochondrial repair program. No additive aggregation was observed in TKO cells, illustrating that each signalling arm of the UPR^{mt} is essential for mitochondrial repair. From these observations it was concluded that each transcription factor must non-redundantly drive the expression of genes critical for UPR^{mt} induction. The identity of these genes and the unique genetic signatures of each transcription factor-related program are currently unknown.

In this chapter, a variety of assays will be employed to assess mitochondrial health and function in the presence or absence of CHOP, ATF4 and ATF5 during an acute protein folding stress and following a recovery period. In addition, a detailed investigation of the transcriptional program triggered by each transcription factor will be performed through comparative transcriptomic analysis of WT, single transcription factor KO and TKO cell lines in the initial signalling phase of the UPR^mt.

5.2: Increased aggregated protein load causes mitochondrial dysfunction

Multiple stress-related mitochondrial signalling programs are triggered through protein cleavage events. Optic Atrophy-1 (OPA1) is a GTPase located within the IMM which drives fusion of the IMM (*224*). Mitochondrial stress leads to increased fission which is facilitated by cleavage of OPA1 into shorter, inactive isoforms (*225*). To examine whether OPA1 cleavage could serve as a readout of mitochondrial stress during the UPR^mt, OPA1 isoforms were analysed by immunoblot in WT and transcription factor KO cells during an acute 12 h vehicle (DMSO) or G-TPP treatment (Figure 5.1 A). Substantial cleavage of full-length OPA1 was observed following G-TPP treatment in both WT and transcription factor KO cells (Figure 5.1 A). OPA-1 cleavage occurred within 2 h G-TPP treatment, suggesting mitochondria are sensitive to small changes in protein aggregation which would likely produce a fragmented network when analysed by microscopy (Figure 5.1 B). However, due to the almost complete cleavage of the long OPA1 isoforms in WT cells, OPA1 is unsuitable for use as a comparative assay to measure mitochondrial stress in WT and KO lines using G-TPP treatment.

PGAM5 is a mitochondrial serine/threonine phosphatase that primarily exists in its full length, uncleaved form (PGAM5-L) when mitochondria area healthy. During mitochondrial stress, PGAM5 is cleaved into a shorter isoform (PGAM5-S) by the proteases PARL and OMA1 (*226, 227*). Accordingly, calculating the ratio of PGAM5-L to PGAM5-S within mitochondria could be used a readout of mitochondrial stress. Ratios of PGAM5-L to PGAM5-S were analysed by immunoblot of isolated mitochondria in WT and transcription factor KO cells during the acute stress and recovery phases of the UPR^mt. Mild cleavage of PGAM5-L was seen in WT cells at 12 h of G-TPP treatment (Figure 5.2), followed by restoration of the PGAM5-L/PGAM5-S ratio during the recovery period (Figure 5.2). Restoration of PGAM5-L/PGAM5-S ratios in WT cells by 48 h R correlates with the restoration of proteostasis observed in Figure 4.3 C of Chapter 4.3.
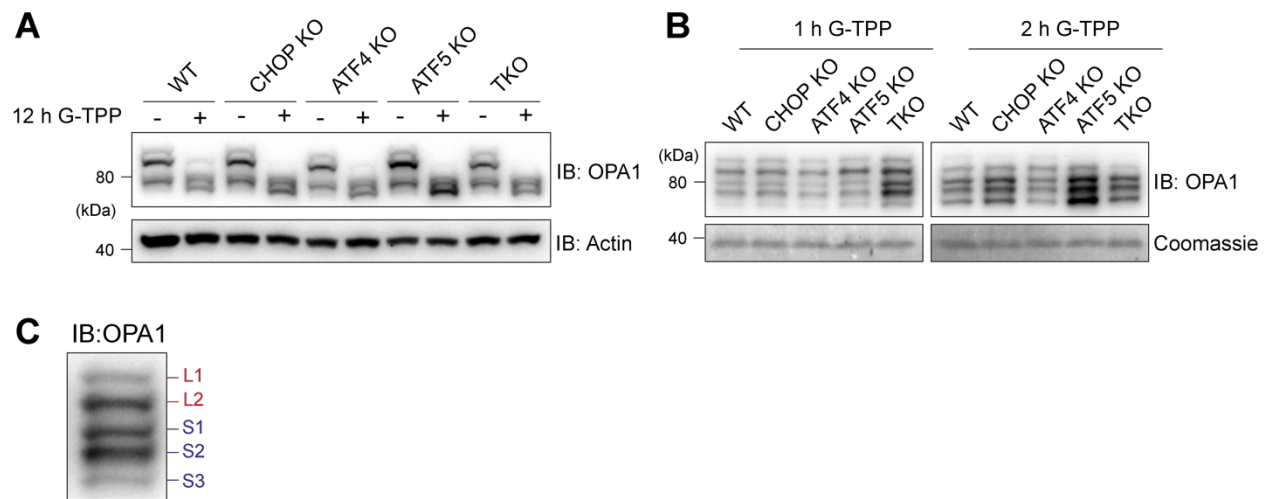
Figure 5.1 **OPA1 is cleaved in response to mitochondrial proteostasis stress**. **A**, **B**. WT, CHOP KO, ATF4 KO, ATF5 KO and TKO cells were treated with either DMSO or 9 μM G-TPP for 12 h (**A**) or 1 - 2 h (**B**) and analysed by immunoblot (IB). **C**. Schematic of the long forms (L) and shorter cleavage forms (S) of OPA1.

Relative to the WT control, significantly elevated levels of PGAM5-L cleavage were observed in each single KO cell line and TKO cells following 12 h G-TPP treatment (Figure 5.2). This demonstrates that there is significantly more mitochondrial stress in cells lacking a functional UPR^{mt} (Figure 5.2). The elevated stress in KO cells correlates with the increased protein aggregation loads observed in Figure 4.3 C. However, in contrast to the persistent protein aggregation observed in transcription factor KO lines (Figure 4.3 C), PGAM5-L/PGAM5-S ratios showed significant levels of recovery at the 24 h and 48 h R time points in all KO cells (Figure 5.2). This data indicates that some CHOP/ATF5/ATF5 independent recovery in mitochondrial stress is occurring during the recovery period following G-TPP treatment.

Overall, mitochondrial stress trends as measured by PGAM5 cleavage have confirmed that damaged proteostasis leads to increased mitochondrial stress, and that the CHOP, ATF4 and ATF5 driven UPR^{mt} is required to protect mitochondria from this stress during an acute proteostatic challenge. The cleavage trends in this data have also demonstrated that some CHOP/ATF4/ATF5 independent recovery in mitochondrial stress does occur at 24 and 48 h R, and this recovery is independent of changes to the total misfolded protein load.
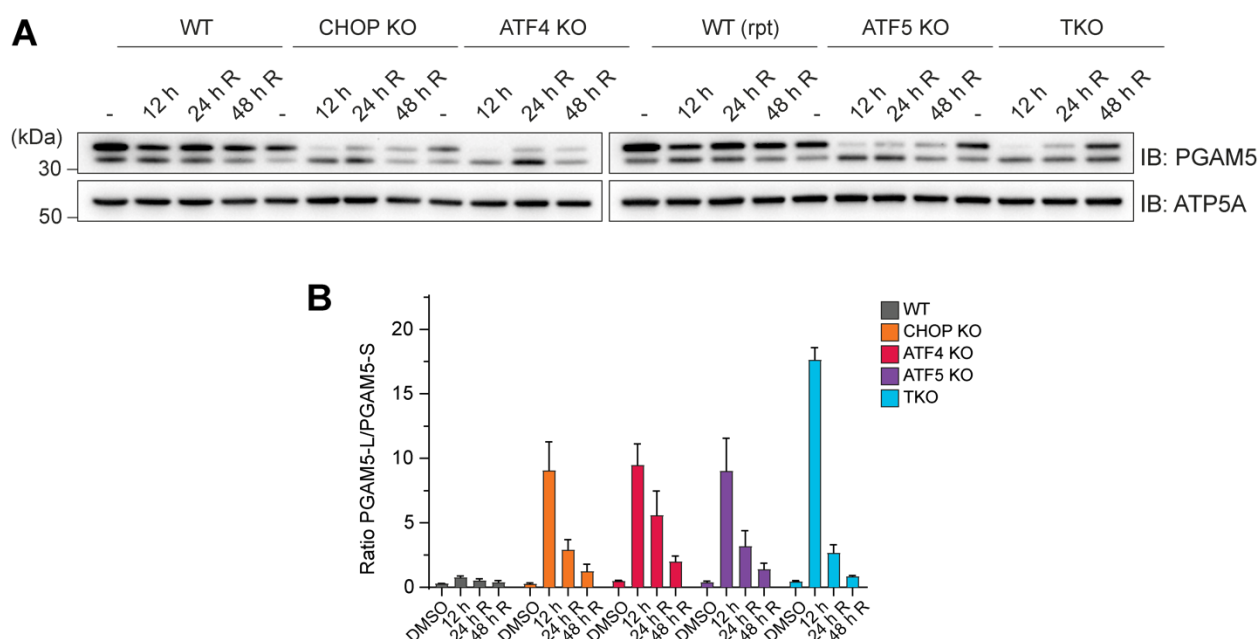
Figure 5.2 **PGAM5 is cleaved in response to mitochondrial proteostasis stress**. **A**, **B**. Mitochondria were isolated from WT, CHOP KO, ATF4 KO, ATF5 KO and TKO cells treated with either DMSO or 9 µM G-TPP for 12 h and PGAM5-S/PGAM5-L levels were analysed by immunoblot (IB; **A**) and quantified (**B**). Data in **B** was generated from three independent experiments.

5.3: The UPR^{mt} is required to protect and restore OXHPOS function

As established in Chapter 4, aggregation of the OXPHOS machinery was observed in WT cells during G-TPP treatment, particularly in the N- and Q- modules of CI (Figure 4.8). Exacerbated aggregation of all OXPHOS complexes (CI – CV) was observed in all single transcription factor KO cells and TKO cells, and there was little observed recovery of OXPHOS proteostasis in these cells (Figures 4.5, 4.9). However, it was unclear whether the magnitude of OXPHOS machinery aggregation observed in WT and transcription factor KO cells was sufficient to disrupt OXPHOS function. To examine whether the OXPHOS aggregation trends in WT and transcription factor KO cells correlated with a loss of OXPHOS activity, cellular ATP levels of cells in galactose-based media were quantified using a luminescence-based assay. Incubating cells in a galactose-based media lacking glucose shifts ATP production to relying on the OXPHOS machinery instead of glycolysis, meaning cellular ATP levels can function as a readout of OXPHOS activity. A significant decrease in ATP was seen in WT cells at 12 h G-TPP treatment relative to DMSO controls, indicating a strong defect in OXPHOS function which correlates with the CI aggregation patterns observed in WT cells (Figure 5.3 A). While some recovery in ATP levels was seen at 24 h R in WT cells, ATP levels only began to show strong signs of restoration at 48 h recovery, but they still did not reach DMSO treated levels (Figure 5.3 A). Some residual aggregation of CI

subunits remains in WT cells at 48 h R, suggesting these low levels of aggregation may be sufficient to cause OXPHOS dysfunction (Figure 4.8 A). In contrast to the significant decrease in ATP levels observed in WT cells at 12 h, an almost complete abolition of ATP levels was observed in all transcription factor KO cells at 12h G-TPP, indicating that increased OXPHOS aggregation with UPR^mt disruption causes substantial damage to OXPHOS function (Figure 5.3 A). No restoration in ATP levels was observed at 24 h R in any transcription factor KO cell line, and very minimal recovery of ATP levels was observed at 48 h R (Figure 5.3 A). Overall, ATP measurements confirm that each transcription factor driven arm the UPR^mt is essential to protect and repair OXPHOS function during and after a protein folding stress (Figure 5.3 A).
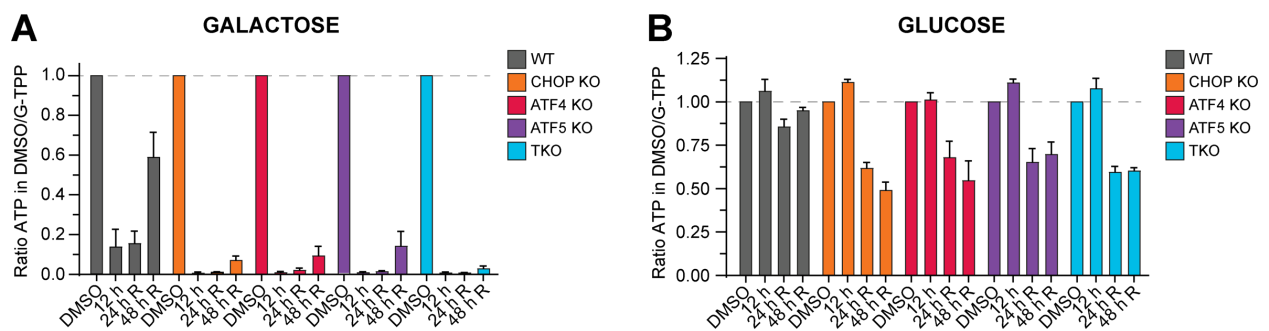
Figure 5.3 **CHOP, ATF4 and ATF5 are required to maintain OXPHOS derived ATP pools during G-TPP treatment and recovery**. **A**, **B**. WT, CHOP KO, ATF4 KO, ATF5 KO and TKO cells were treated with DMSO or G-TPP (12 h) for 12 h, prior to G-TPP washout and either a 24 h (24 h R) or 48 h (48 h R) recovery period. Cells were either grown in glucose based standard media (**A**), or were switched to a galactose based media 24 h prior to sample analysis (**B**). ATP levels were then measured by luminescence and quantified relative to DMSO ATP levels in glucose (**A**) or galactose (**B**) based media. Data in **A**, **B** were generated from three independent experiments.

Metabolic shifts towards glycolysis have been observed in *C. elegans* undergoing a proteostasis stress (*228*). As cells are critically reliant on ATP to power a plethora of biological processes, including processes such as protease activity that is presumably required for restoration of proteostasis in WT cells, the low amounts of ATP produced by the OXPHOS machinery during G-TPP treatment indicates that other metabolic pathways are likely contributing to ATP generation. To determine if glycolysis may be activated in mammalian cells during the UPR^mt, cellular ATP levels were measured during the G-TPP treatment and recovery time course in WT and transcription factor KO cells in a glucose-based media where both OXPHOS and glycolysis can contribute to ATP production. Remarkably, no decrease in ATP was observed in either WT or transcription factor KO cells during 12 h G-TPP treatment (Figure 5.3 B). When compared to the ATP trends observed in galactose media (Figure 5.3 A), the maintenance of ATP levels observed at 12 h G-TPP in Figure 5.3 B suggests the predominant metabolic pathway of ATP generation

during an acute G-TPP treatment is glycolysis. ATP levels were maintained across the recovery period in a glucose-based media in WT samples, indicating glycolysis is sufficient to maintain cellular ATP stores in cells with an operational UPR^{mt} until the OXPHOS machinery can be fully repaired and functionally restored (Figure 5.3 B). Surprisingly, a significant drop in ATP levels down to ~50% of DMSO treated controls was observed in all transcription factor KO cells during the recovery period (Figure 5.3 B). This drop could represent a failure to upregulate glycolysis in the recovery period when UPR^{mt} signalling is disrupted. Failure to upregulate glycolysis would be consistent with the reported role for the UPR^{mt} in upregulating glycolysis in *C. elegans* (*76, 81*). Alternatively, the increased levels of aggregated protein in cells with a dysfunctional UPR^{mt} may be resulting in elevated ATP consumption that glycolysis cannot keep up with. Further investigation into the glycolytic activity of transcription factor KO cells during the recovery period after a G-TPP treatment would be required to clarify what is causing the decrease in cellular ATP levels. Irrespective of the molecular cause of this drop in ATP, decreased total ATP levels mean cells with a dysfunctional UPR^{mt} likely experience additional disruptions and dysfunction in other cellular pathways that are reliant on ATP.

While the cellular ATP trends observed did mirror the proteostasis trends in Chapter 4.6, the levels of cellular ATP can be influenced by processes that consume ATP including ATP-dependent proteolysis. An analysis of the respiratory capacity of the OXPHOS machinery in isolated mitochondria was performed in collaboration with Dr. Runa Lindbolm (Lazarou Lab) to determine whether the ATP levels observed in Figure 5.3 A are representative of OXPHOS function. Mitochondria were isolated from WT, CHOP KO, ATF4 KO, ATF5 KO and TKO cells during the acute G-TPP treatment and recovery time course. Isolated mitochondrial samples were placed into media containing the CI substrates, glutamate and malate, and measurements of oxygen consumption were collected at 5 different stages: 1) during basal respiration, 2) after stimulation of respiration through the addition of ADP, 3) after blocking ATP production through inhibiting CV with oligomycin, 4) after decoupling mitochondria through the addition of FCCP, and 5) after further ablating the electron transport chain through the addition of Antimycin A to inhibit CIII. Basal respiratory rates, spare respiratory capacity and the total respiratory capacity of mitochondria were calculated for each WT, single transcription factor KO and TKO sample during 12 h DMSO, 12 h G-TPP, at 24 h R and 48 h R time points to calculate the extent of OXPHOS damage and subsequent repair with and without the UPR^{mt}.

No difference in basal respiratory rates were detected between DMSO treated samples of WT, single transcription factor KO and TKO cells (Figure 5.4 A – E, G). Similar basal respiratory rates were expected given that CHOP, ATF4 and ATF5 are stress induced transcription factors and so

would presumably have little impact on basal respiratory capacity in unstressed cells (Figure 4.1). Basal respiration rates were maintained across the acute treatment and recovery time course in WT cells (Figure 5.4 A – E, G). In contrast, basal respiration rates dropped significantly during G-TPP treatment in transcription factor KO cells and showed no evidence of a return to baseline levels across the recovery period, demonstrating an almost complete shut down in OXPHOS activity with UPR^mt disruption (Figure 5.4 B – E, G). Basal respiration rates were maintained at all G-TPP treatment and recovery treatment time points in WT cells (Figure 5.4 A, G). However, a decrease in the spare respiratory capacity of WT mitochondria was seen after 12 h G-TPP treatment, meaning mitochondria in WT cells were functioning close to their maximal capacity to maintain the basal respiration rate (Figure 5.4 A, H). The steep drop in maximal respiratory capacity of WT cells at 12 h G-TPP treatment (Figure 5.4 A, I) further confirmed acute damage to the respiratory chain at 12 h G-TPP treatment as was expected from the protein aggregation and cellular ATP trends (Figures 5.3, Chapter 4.6). During the recovery period, total respiratory capacity in WT cells showed signs of quick repair, with significant levels of restoration by 24 h R that approached baseline levels by 48 h R (Figure 5.4 A, I). Repair of the spare respiratory capacity was not as pronounced, with a decreased spare respiratory capacity of WT mitochondria persisting following 48 h recovery (Figure 5.4 A, H). A minor increase in basal respiration was observed in WT cells after 48 h recovery (Figure 5.4 G). After recovery from a protein folding stress, WT mitochondria appeared to be undergoing higher levels of OXPHOS mediated respiration than prior to the stress, which in turn leads to a smaller spare respiratory capacity (Figure 5.4 A, G - I). Collectively the respiration analysis confirmed that WT cells undergo significant OXPHOS damage during an acute protein folding stress, and robust restoration to both basal and total respiratory capacity by 48 h of recovery, albeit with a reduced spare respiratory capacity.

Although a functional UPR^mt program was insufficient to prevent OXPHOS damage, the damage inflicted was much less severe than that observed in cells with a defective UPR^mt. Mitochondria from transcription factor KO cells displayed almost no spare respiratory capacity and a significantly reduced maximal respiratory capacity following 12 h G-TPP treatment (Figures 5.4 B – E, H, I). These trends show the OXPHOS machinery in each transcription factor KO cell line is both severely damaged after 12 h G-TPP treatment and operating at maximal capacity, which is still insufficient to maintain basal respiration rates (Figure 5.4 B – E, G). Negligible recovery in spare respiratory capacity, maximal respiratory capacity or basal respiration levels was observed in all transcription factor KO cells across the recovery period, demonstrating that each transcription factor driven UPR^mt program is essential for OXPHOS protection and repair (Figure 5.4 B – E, G - I).
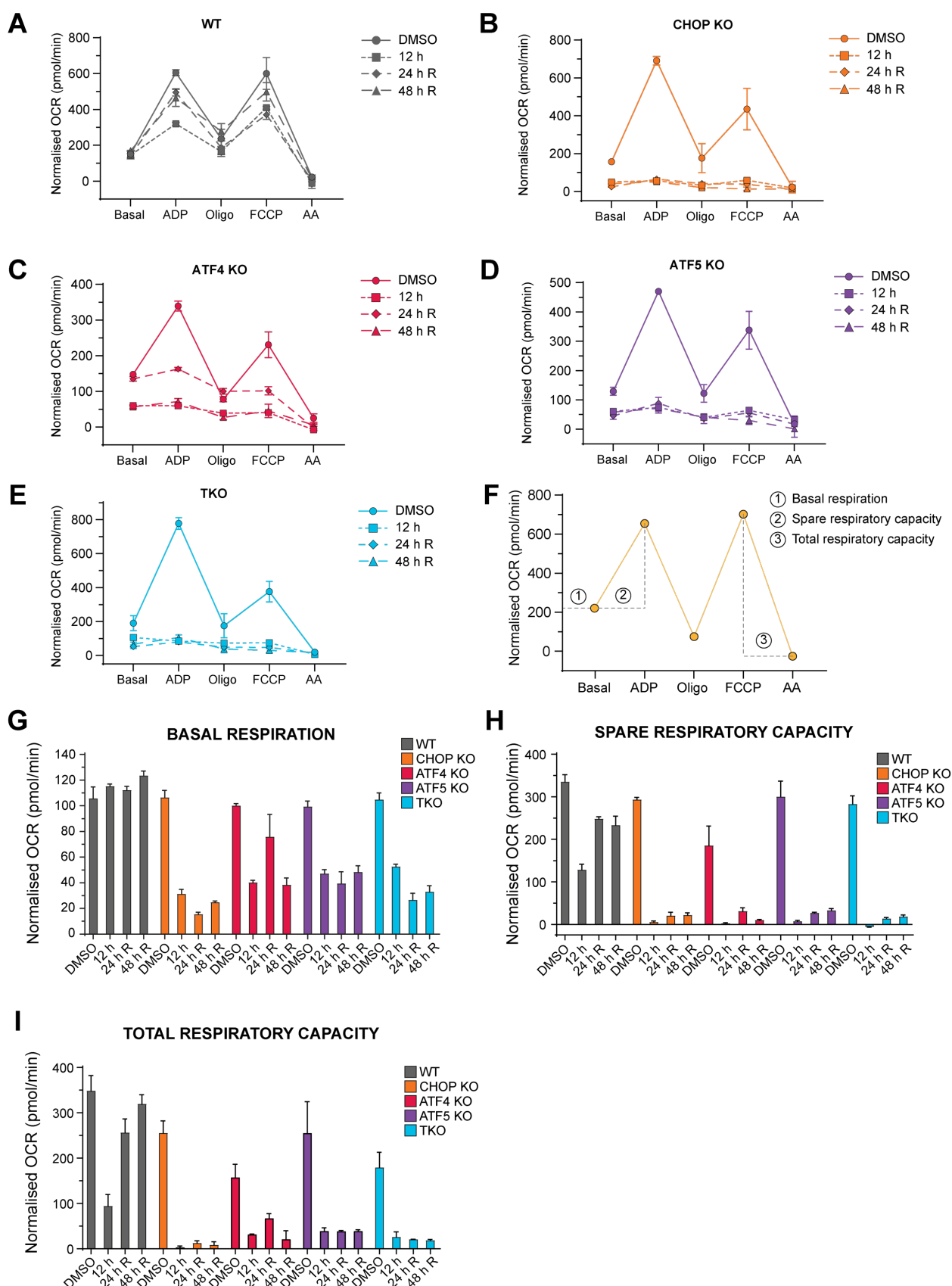
Figure 5.4 **CHOP, ATF4 and ATF5 are required to protect and restore the respiratory capacity of the OXPHOS machinery during G-TPP treatment and recovery**. **A – E.** Mitochondria were isolated from WT (**A**), CHOP KO (**B**), ATF4 KO (**C**), ATF5 KO (**D**) and TKO (**E**) cells treated with DMSO (DMSO) or G-TPP (12 h) for 12 h, prior to G-TPP washout (cont.)

and either a 24 h (24 h R) or 48 h (48 h R) recovery period. Equal quantities of mitochondria were then placed into a solution containing glutamate and malate and the basal respiration rate was calculated, in addition to the respiration rate after each sequential addition of ADP, oligomycin (Oligo), FCCP, and antimycin (AA). Each time point was analysed on the day of collection. Untreated WT, CHOP KO, ATF4 KO, ATF5 KO and TKO mitochondrial samples were analysed alongside the experimental samples (DMSO, 12 h, 24 h R, 48 h R) at each time point, and a correction scale value was calculated for each sample set at each time point to correct for minor variations in Seahorse machine performance each day. Normalised OCR refers to the corrected OCR measurements. **F.** Schematic of the measurements performed on the data in Figure 5.4 to generate the quantitative measurements in **G – I**. **G – I**, Normalised OCR values from Figure 5.4 were used to calculate the basal respiration rates (**G**), spare respiratory capacity (**H**) and total respiratory capacity (**I**) of the OXPHOS machinery at the indicated time course collection points. Data in **A – E, G – I** was generated from three independent experiments.

5.4: CHOP, ATF4 and ATF5 control unique transcriptional signatures during the UPR^{mt}

As established in Chapter 4, CHOP, ATF4 and ATF5 are required for proper UPR^{mt} function. Removal of any single transcription factor or simultaneous removal of all three transcription factors produces near identical trends of elevated proteostasis damage. Such similar phenotypes suggest that CHOP, ATF4 and ATF5 could interact and form a complex to drive the same transcriptional signalling program. Alternatively, they may each drive an independent transcriptional program which is essential for proper UPR^{mt} activity. A transcriptomic analysis of the UPR^{mt} signalling program was performed with WT cells and then compared to transcription factor KO cells to map out the transcriptional signatures of each transcription factor. The analysis was performed at the acute 12 h G-TPP treatment time point since peak transcription factor levels were observed at that time point (Figure 6.1). Briefly, total RNA was isolated from WT cells treated with DMSO or G-TPP for 12 h, and isolated mRNA was sequenced via Next-Generation sequencing (NGS) and quantified. Levels of mRNA were compared between DMSO and G-TPP treated samples, and genes showing >+/- 0.2 log$_2$ fold expression changes with G-TPP treatment were classified as the WT UPR^{mt} driven transcriptional program. Next, mRNA levels were quantified in CHOP KO, ATF4 KO, ATF5 KO and TKO samples after 12 h G-TPP treatment, and expression levels of each gene identified in the WT UPR^{mt} program were assessed in each transcription factor KO line. Genes showing >-0.2 log$_2$ fold expression change in a transcription factor KO sample relative to the expression seen in 12 h G-TPP treated WT samples were classified as a gene whose expression was driven by the transcription factor in question. Using this analytical approach, the genetic footprint of the transcription factor dependent UPR^{mt} program was mapped.

Overall, 16,919 genes were identified and quantified in WT samples and 4,611 genes had altered expression following G-TPP treatment that was indicative of UPR^{mt} program activity. Of these 4,611 genes, 48.1% were seen to decrease in expression, while 51.9% of genes increased in expression (Figure 5.5 B). Although the split between increased/decreased expression was similar in gene number, the magnitude of expression changes was much higher in the subset of genes that were upregulated with UPR^{mt} induction (Figure 5.5 A). Clustered GO analysis of genes with decreased expression revealed clusters of genes associated with cell division, histone methylation, mRNA processing and TCA cycle metabolism (Figure 5.5 C '*Downregulated*'). In contrast,
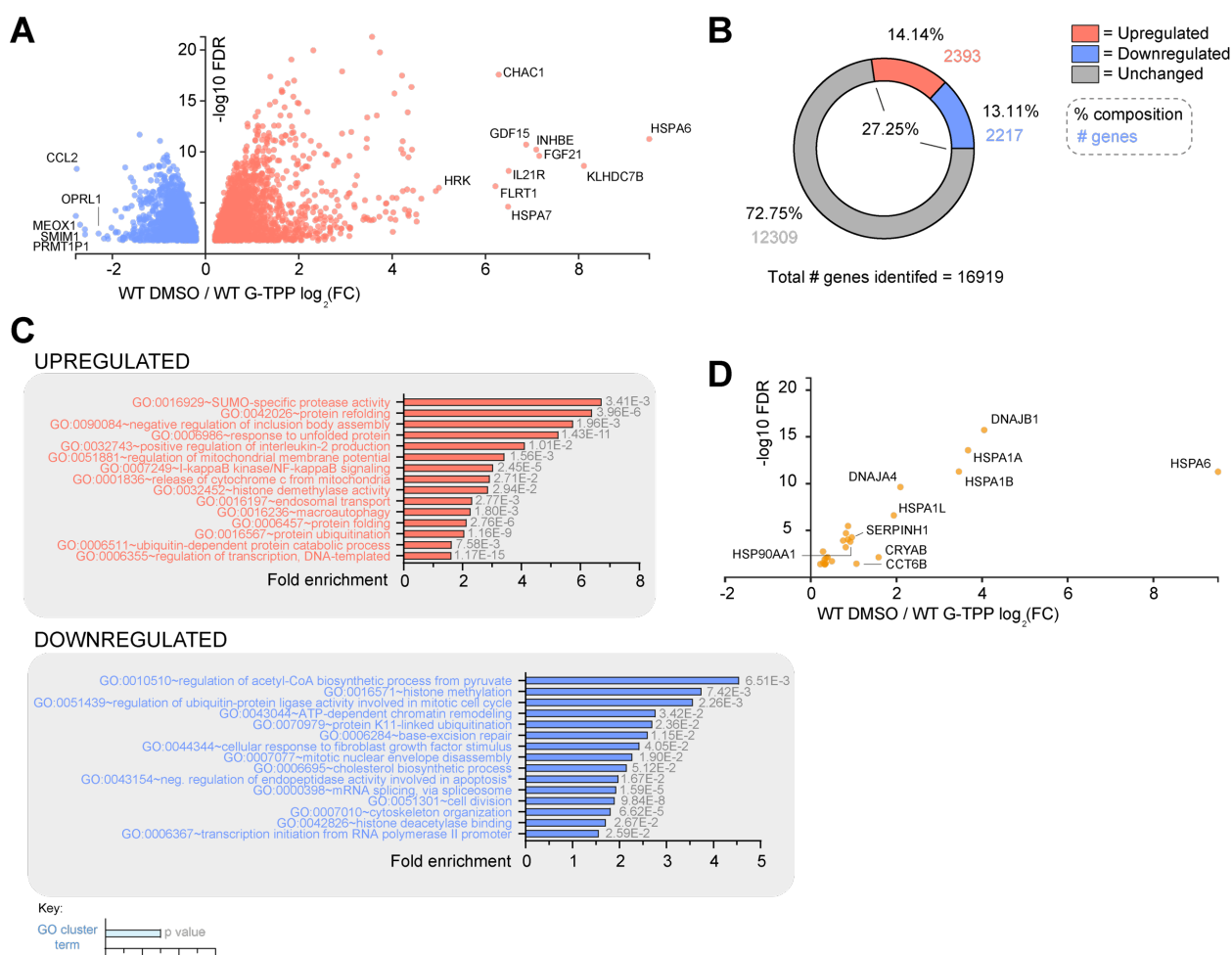
Figure 5.5 **G-TPP treatment induces widespread remodelling of the transcriptome**. WT cells were treated with DMSO or 9 µM G-TPP for 12 h. mRNA levels were quantified and expression changes in G-TPP treated samples were calculated relative to DMSO treated samples. **A**. Genes showing significant changes in expression of +/- 0.2 log2 fold are displayed by volcano plot. The 10 genes showing the highest increase in expression or top 5 genes showing the largest decrease in expression are labelled. **B**. The percentage composition of the analysed transcriptome showing upregulated, downregulated, or no expression changes were quantified and displayed by pie chart. **C**. Clustered GO analysis was performed on the upregulated and downregulated portions of the significantly altered transcriptome. Representative GO groups for each cluster have been labelled together with the enrichment p value of that representative GO process. **D**. Cytosolic chaperones showing +/- 0.2 log2 fold expression changes with G-TPP treatment were analysed by volcano plot. The 10 genes showing the highest fold increase in expression with G-TPP treatment (cont.)

have been labelled. Data in **A** – **D** were generated from three independent experiments. GO analysis in **C** was performed using the combined Biological Processes and Molecular Function categories in the DAVID v6.8 platform (*193, 194*).

upregulated genes included clusters involving protein folding, immune related signalling pathways, histone demethylation, autophagy and proteosome mediated degradation (Figure 5.5 C, '*Upregulated*'). Induction of numerous components of the cytosolic chaperone machinery was also observed (Figure 5.5 D). Ontology analysis collectively demonstrates that widespread reprogramming of multiple cellular processes occurs through the UPR^{mt} program. Interestingly, most clusters of UPR^{mt} regulated genes involved processes not directly related to mitochondrial function (Figure 5.5 C). To ensure that the transcriptional signatures observed were not a result of generalised mitochondrial dysfunction triggering other cellular stress pathways, transcriptional signatures were analysed in DELE1 KO HeLa cells undergoing a 12 h treatment with DMSO or G-TPP. DELE1 functions as an essential signalling molecule of the UPR^{mt} by mediating transmission of stress within mitochondria to the nucleus (*104, 105*). Analysis of the DELE1 transcriptome can therefore reveal how much of the WT UPR^{mt} program is generated specifically through mitochondrial-derived stress signalling, and how much is generated through generalised cellular stress signalling triggered by mitochondrial dysfunction. In contrast to the large signalling program observed in WT cells (4,611 genes), only 124 genes were seen to significantly change in expression with G-TPP treatment in DELE1 KO cells (Figure 5.6). The almost complete abolition of the signalling program observed in WT cells with DELE1 KO confirms that the broader cellular pathways are being signalled directly in response to localised mitochondrial stress, and do not represent off-target, indirect activation of other stress response pathways.
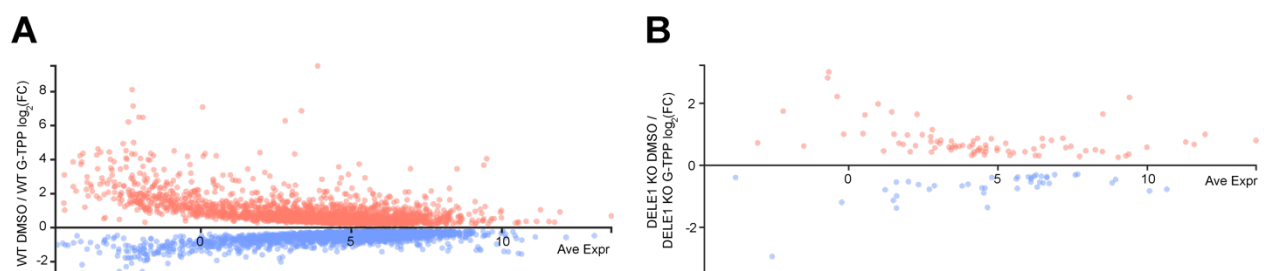
Figure 5.6 **DELE1 KO abolishes the transcriptional signature seen in WT cells during G-TPP treatment**. **A**, **B**. WT (**A**) and DELE1 KO (**B**) cells were treated with DMSO or 9 μM G-TPP for 12 h. mRNA levels were quantified and expression changes in G-TPP treated samples were calculated relative to DMSO treated samples. Genes showing +/- 0.2 log2 fold change in expression with G-TPP treatment were graphed according to their average mRNA expression. Data in A, B was generated from three independent experiments.

Next, WT UPR^{mt} expression signatures were compared to each 12 h G-TPP treated transcription factor KO line. Of the 4,611 genes defined earlier as the WT UPR^{mt} program, approximately 55.7% of those genes were determined to be regulated by CHOP, ATF4 or ATF5 expression (Figure 5.7 A). Interestingly, just under half of the UPR^{mt} transcriptional program is not under control of the transcription factors studied, indicating that there are unidentified UPR^{mt} related transcription factors driving a significant portion of the identified UPR^{mt} program (Figure 5.7 A). A mosaic pattern of transcription factor-controlled gene expression was observed for the 2,568 genes consisting of the CHOP/ATF4/ATF5 UPR^{mt} program. That is, some genes required a single transcription factor, others required two transcription factors, whereas another set of genes were signalled redundantly and required simultaneous loss of CHOP, ATF4 and ATF5 (Figure 5.7 B). However, the most common occurrence was genes which simultaneously required all three of CHOP/ATF4/ATF5, comprising 34.6% of the transcription factor mediated UPR^{mt} transcriptome (Figure 5.7 B). GO analysis of genes requiring all three of CHOP/ATF4/ATF5 revealed involvement in cell cycle regulation, cytoskeletal organisation and Wnt signalling pathways (Figure 5.7 C). The second largest category of transcription factor mediated UPR^{mt} genes was genes requiring ATF4 alone for expression which comprised 20.8% of the transcription factor regulated UPR^{mt} transcriptome (Figure 5.7 B). GO analysis revealed that ATF4 regulates genes involved in tRNA expression, mtDNA metabolism, histone dephosphorylation and oxidative stress signalling (Figure 5.7 C). Genes regulated by CHOP or ATF5 alone, or combinations of CHOP/ATF4, CHOP/ATF5 and ATF4/ATF5 represented smaller gene categories (~6 % each), but unique gene ontology categories were identified in these gene groupings (Figure 5.7 B). In particular, GO analysis of ATF4/ATF5 gene sets produced RNA methylation and autophagy categories, while analysis of CHOP/ATF5 regulated genes indicated involvement in the MAPK signalling cascade (Figure 5.7 C). CHOP and ATF5 independently regulate much smaller sets of genes compared to ATF4 (~6 – 7% of the transcription factor regulated UPR^{mt} transcriptome), and GO analysis revealed unique categories including mRNA polyadenylation and O-glycan processing for ATF5 and CHOP dependent genes respectively (Figure 5.7 C). A small set of genes appear to be redundantly signalled across CHOP, ATF4 and ATF5 as they were only reduced in expression in TKO cells (Figure 5.7 B). Redundantly signalled genes involved one-carbon metabolism and K-11 ubiquitination related groupings, which were unique to this gene subset (Figure 5.7 C). Overall, while there were functionally unique aspects of each individual transcription factor signalling program, significant overlap was also observed. The common functional processes included cell division (seen in CHOP/ATF4/ATF5, CHOP/ATF5, CHOP/ATF4, ATF5 groupings), ubiquitin mediated proteolysis (seen in CHOP/ATF4/ATF5, CHOP/ATF5, CHOP/ATF4, ATF4 and redundantly signalled groupings) (Figure 5.7 C).
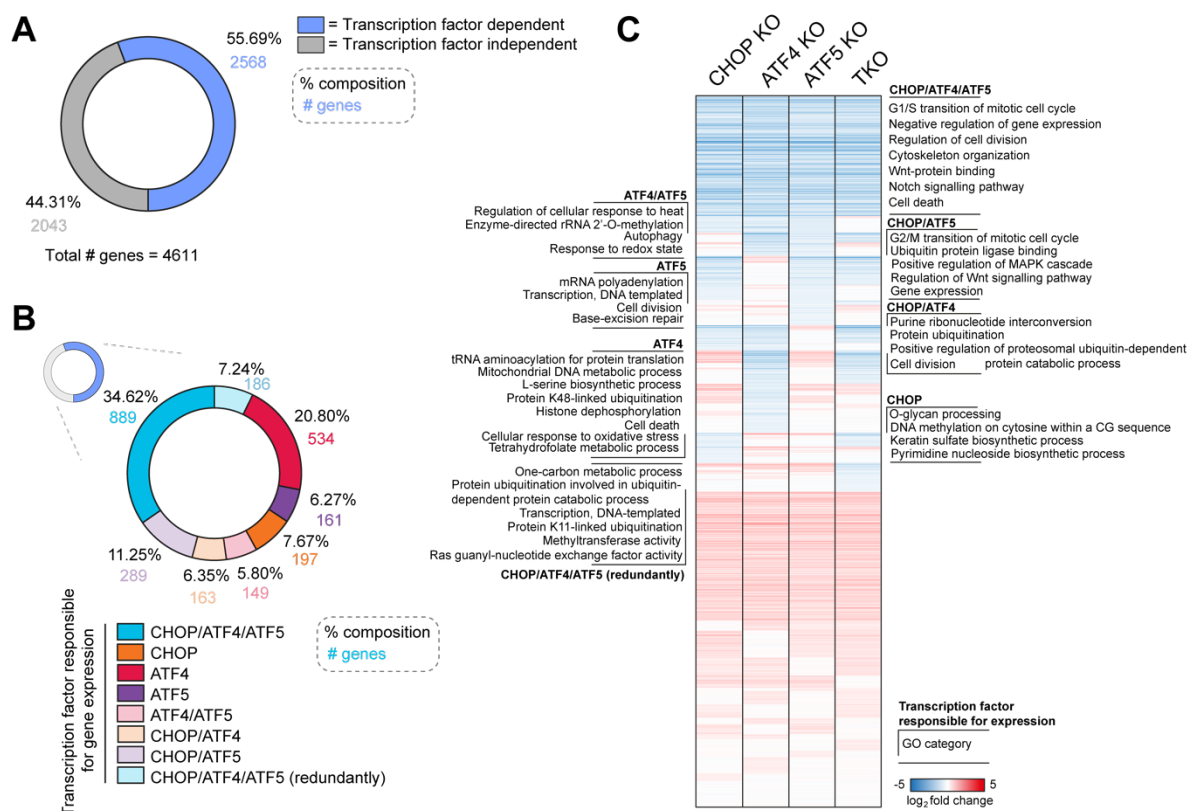
Figure 5.7 **CHOP, ATF4 and ATF5 exert a mosaic, interconnected pattern of regulation across the UPR^mt induced transcriptome**. CHOP, ATF4 KO, ATF5 KO and TKO cells were treated with 9 μM G-TPP for 12 h. mRNA levels were analysed and quantified relative to WT 12 h G-TPP mRNA levels (see Figure 5.6). Genes showing > -0.2 fold decrease in expression relative to WT 12 h G-TPP levels were classified as being under the regulatory control of the transcription factor in question. **A**. The proportion of the WT UPR^mt transcriptome determined to be under the regulatory control of either CHOP, ATF4 or ATF5, or independently expressed, was calculated and displayed by pie chart. **B**. The portion of the UPR^mt transcriptome determined to be under the regulatory control of one or more transcription factors was further separated into groupings according to transcription factors required for expression pattern. The relative proportional composition of these groups were then calculated and displayed by pie chart. **C**. Gene ontology (GO) analysis was performed on genes in each transcription factor dependent grouping. Select GO categories were labelled alongside gene clusters of the WT UPR^mt transcriptome displayed by heat map. GO in **C** was performed using the combined Biological Process and Molecular Function categories in the DAVID v6.8 platform (*193, 194*). Data in **A** – **C** was generated from three independent experiments.

Due to the presence of multiple signalling pathways in the broader GO analysis, a more detailed KEGG pathway analysis was performed to investigate the signalling pathways which are altered during UPR^mt induction. Multiple signalling pathways were identified in KEGG analysis of the WT UPR^mt transcriptome, including the Hippo, Wnt, FoxO and MAPK signalling pathways

(Figure 5.8 A). Closer analysis of the Wnt signalling pathway revealed patterns of both upregulated and downregulated UPR^{mt} mediated gene expression. Upregulated gene expression was focused in the canonical and Ca^{2+} mediated Wnt signalling arms, while core components of the planar cell polarity (PCP) mediated signalling pathway were downregulated with UPR^{mt} induction (Figure 5.8 B). Downregulation of multiple inhibitory factors of the canonical Wnt signalling pathway was also observed. The signalling trends collectively indicate an upregulation in the expression of genes actioning the canonical and Ca^{2+} regulated Wnt signalling pathways, with supressed expression of PCP pathway effectors. Of the 37 Wnt signalling genes altered with UPR^{mt} induction, 17 were under the regulatory control of CHOP/ATF4/ATF5 (Figure 5.8 B). Multiple core components of both the Ca^{2+} driven and PCP mediated Wnt signalling pathway, and some accessory proteins of the canonical Wnt signalling pathway required all three of CHOP, ATF4 and ATF5 for their expression (Figure 5.8 B). CHOP and ATF5 were together required for the expression of the accessory canonical pathway signalling components LRG4, DKK and CTBP1, while ATF4 alone was required for expression of the effector molecule c-Jun (Figure 5.8 B). The regulatory patterns of transcription factor mediated control across the three distinct Wnt signalling pathways suggests a similar magnitude of suppression of Wnt signalling with removal of either CHOP, ATF4 or ATF5.

Collectively, gene ontology analysis of the genetic footprint of each transcription factor demonstrated that CHOP, ATF4 and ATF5 independently regulate subsets of genes that comprise ~ 3.5 – 11.6% of the UPR^{mt} mediated transcriptome. A large portion of the UPR^{mt} transcriptome requires integrated signalling of two or more different transcription factor driven nodes, totalling ~32.3% of the UPR^{mt} mediated transcriptome. Extensive remodelling of numerous cellular pathways from cell cycle regulation to proteasomal activity occur with UPR^{mt} induction, and many of these pathways are influenced by the CHOP/ATF4/ATF5 regulated component of the UPR^{mt}. Which of these pathways regulated by CHOP/ATF4/ATF5 that when disrupted through transcription factor KO lead to the similar levels of proteostatic damage observed in Chapter 4 remains to be confirmed through future studies.
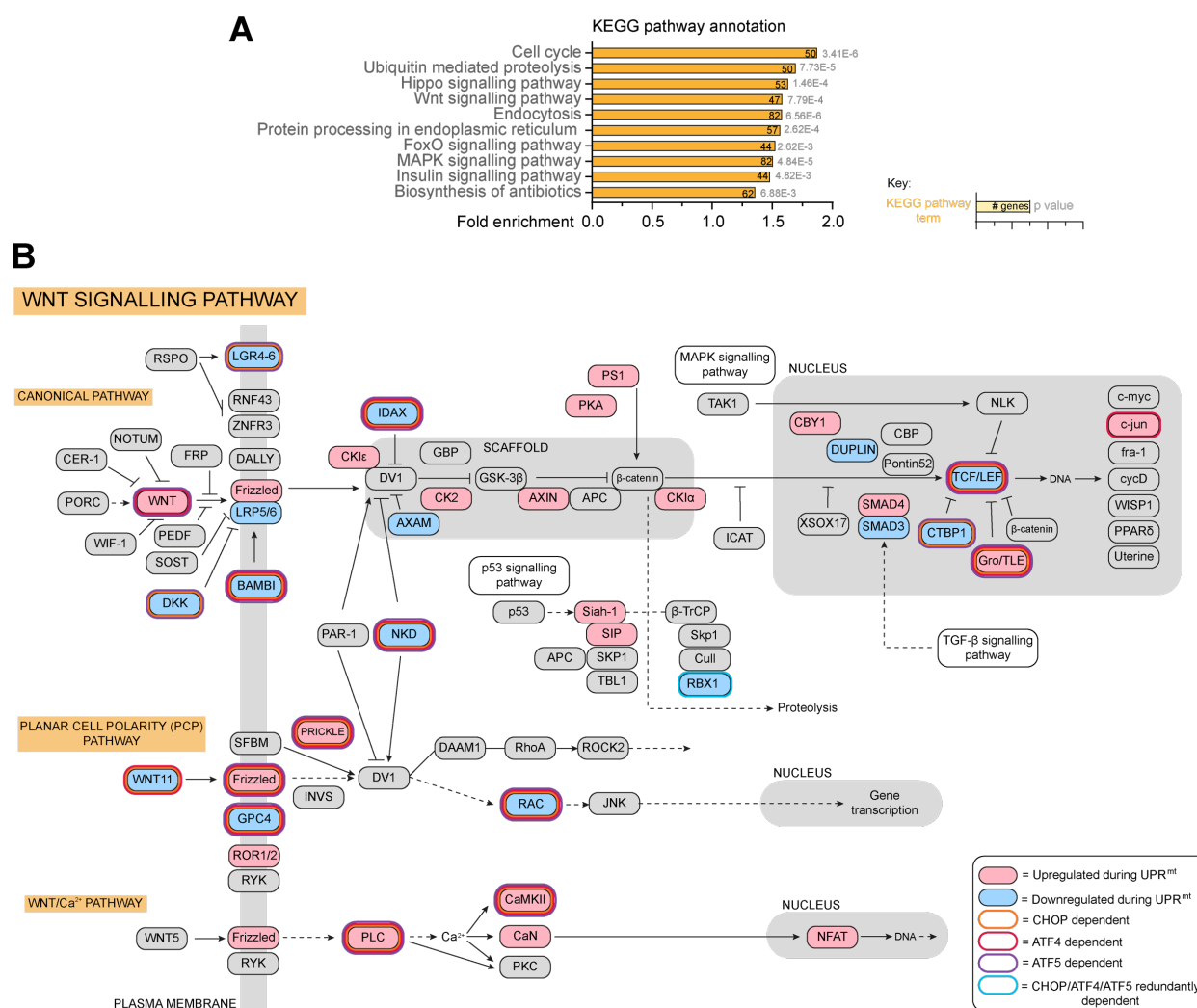
Figure 5.8 **KEGG analysis shows induction of Wnt signalling nodes during the WT UPR^mt program**. **A**, **B**. KEGG pathway analysis was performed on genes comprising the UPR^mt program in Figure 5.6. **A**. The 10 most highly enriched KEGG pathway categories have been graphed according to their fold enrichment. **B**. Components of the different Wnt signalling pathway activation mechanisms have been displayed. Expression changes during the UPR^mt and transcription factor mediated control of these changes annotated alongside each gene.

5.5: CHOP, ATF4 and ATF5 regulate portions of the nuclear encoded mitochondrial genome

Somewhat surprisingly for a signalling program triggered from isolated mitochondrial stress, GO analysis of the WT UPR^mt transcriptome produced few signatures directly involving mitochondrial pathways (Figure 5.7). As genes that encode mitochondrial proteins collectively represent a small proportion of the cellular genome, broad GO and KEGG pathway analysis can hinder detection of changes in mitochondrial pathways when there are also alterations to wider cellular signalling

pathways, as is seen in this dataset (Figure 5.7). A closer examination of mitochondrial related changes during the UPR^{mt} was performed using the mitochondrial processes annotation database used in Chapter 4 (*166*). Overall, of the 1,321 mitochondrial genes identified, 367 genes were found to be altered in expression by the UPR^{mt} program in WT cells (Figure 5.9 A, B). Approximately 56.1% of these genes were determined to be under the regulatory control of CHOP, ATF4 and ATF5 when analysed using the same analytical methods used in Chapter 5.4 (Figure 5.10 A). Similar portions of transcription factor driven control are seen in both the total UPR^{mt} program and mitochondrial specific UPR^{mt} changes (Figures 5.7 A, 5.10 A). Proportionally more mitochondrial genes were found to be decreased in expression (54.8% of the UPR^{mt} program) relative to genes decreased in expression across the total UPR^{mt} program (48.1% of the UPR^{mt} program), suggesting the UPR^{mt} program slightly biases to decreasing production of mitochondrial-destined proteins (Figure 5.9 B). Enrichment analysis of UPR^{mt} regulated mitochondrial process subgroups indicated that *Apoptosis*, *Fatty acid metabolism*, *Mitochondrial signalling*, *Protein stability and degradation*, and *Transmembrane transport* related process groups saw preferential signalling changes during the UPR^{mt} compared to other mitochondrial processes (Figure 5.9 C). Enrichment changes with UPR^{mt} induction were plotted for each mitochondrial protein, and proteins were then separated by their process group annotation to allow for visualisation of process-based enrichment profiles. The percentage of altered genes showing increased expression was then quantified and plotted to identify the mitochondrial process groups showing the most elevated or depleted expression during the UPR^{mt} (Figure 5.9 D). Select process groups including *Metabolism of vitamins and cofactors*, *Mitophagy*, and *Folate & pterin metabolism* showed a trend toward increased expression during the UPR^{mt} suggesting preferential activation of these processes during mitochondrial stress (Figure 5.9 C, D). In contrast, process groups including *Fatty acid degradation & β-oxidation*, *OXPHOS*, and *Replication & transcription* showed a strong trend for UPR^{mt} mediated decreases in expression, indicating an active shutdown of these processes at a transcriptional level. Dysfunctional OXPHOS machinery can produce excessive ROS, and as established in Chapter 5.3 there are already significant functional defects in OXPHOS activity at 12 h G-TPP treatment. Transcription and translation of mtDNA will also elevate the protein folding load of mitochondria with an overwhelmed protein folding machinery, suggesting both the OXPHOS and transcription expression trends are responses aimed at mitigating further mitochondrial damage.
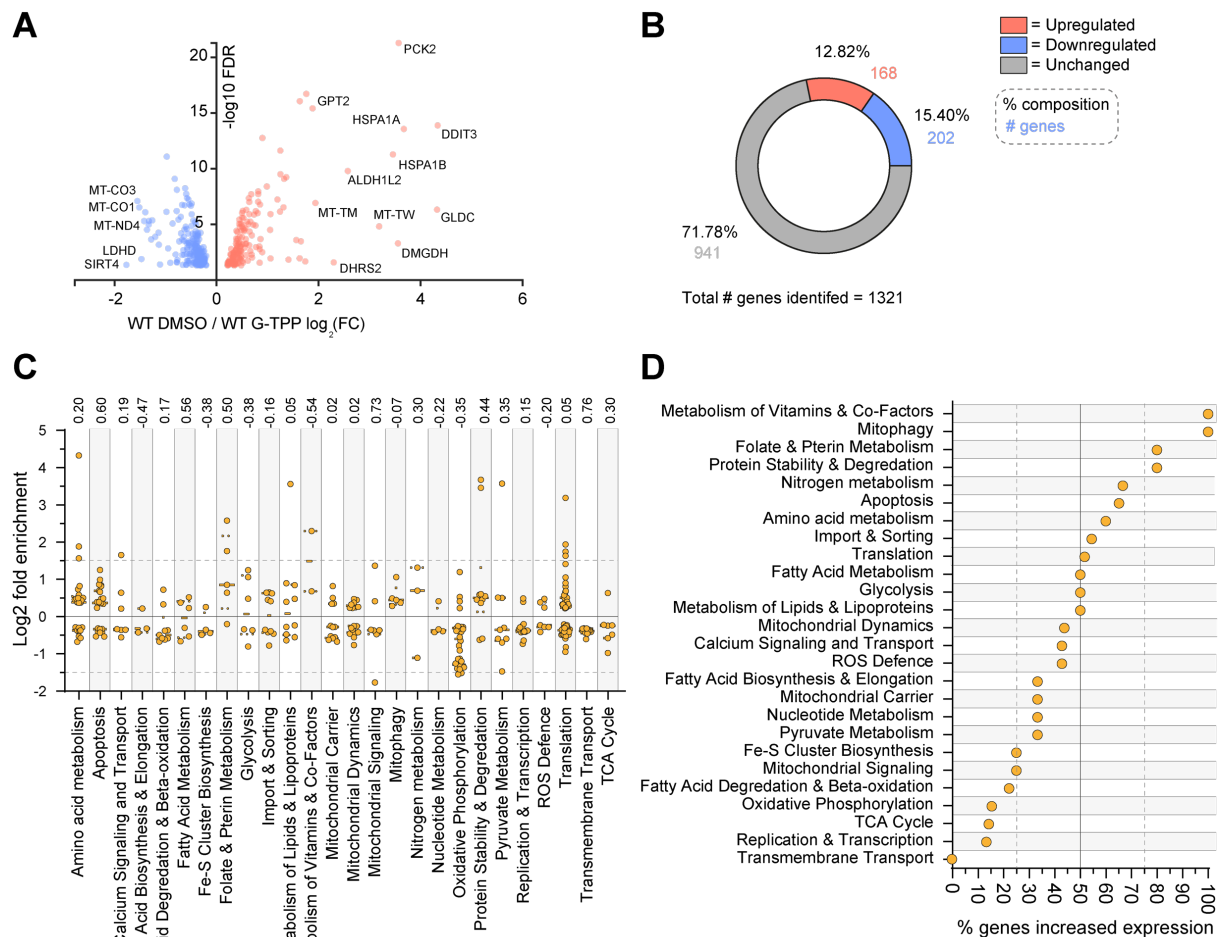
Figure 5.9 **G-TPP treatment induces remodelling of the mtDNA and nuclear encoded mitochondrial transcriptome**. **A – D**. The WT UPR^{mt} program as defined in Figure 5.6 was further filtered to show mitochondrial related genes. **A**. Mitochondrial components of the UPR^{mt} program have been visualised by volcano plot, and the 10 most highly enriched genes and 5 most highly depleted genes have been labelled. **B**. The proportion of the mitochondrial related genome showing increased, decreased or unchanged expression changes were quantified and displayed by pie chart. **C**. Mitochondrial genes in the UPR^{mt} transcriptome were grouped according to mitochondrial process, and individual genes with their log$_2$ fold expression changes with G-TPP treatment are displayed by violin plot. Enrichment values of the bias towards detection of each mitochondrial process group in the UPR^{mt}-signalled dataset has been displayed above the graph axis (< 0 = depleted, > 0 = enriched). **D**. The percentage of UPR^{mt} genes in each mitochondrial process group showing increased expression with G-TPP treatment were plotted and displayed by dot plot. Data in **A – D** was generated from three independent experiments.

While similar portions of the total UPR^{mt} and mitochondrial related UPR^{mt} genes were determined to be under the transcriptional control of CHOP, ATF4, and ATF5, the footprint of each transcription factor differed in the mitochondrial related gene subset. Dual CHOP/ATF5 dependent gene regulation played a larger role in regulation of the mitochondrial UPR^{mt} program, controlling expression of ~17% of transcription factor mediated genes (Figure 5.10 B). Smaller degrees of

regulatory control were noted for CHOP/ATF4 and ATF4/ATF5 regulated gene combinations, comprising ~4.4 % and 3.4 % of genes respectively (Figure 5.10 B). Individual transcription factor driven control and CHOP/ATF4/ATF5 combined control of mitochondrial genes were seen to occur at similar proportions relative to the proportional regulation of these groups observed across the total UPR^{mt} program (Figure 5.10 B). More functional overlap was seen in the mitochondrial processes regulated by different combinations of transcription factors compared to the overlap observed at the cellular level, however, some unique signalling nodes were still observed. These included *ROS defence*, *Glycolysis*, *Pyruvate metabolism*, and *Transmembrane transport* nodes in the CHOP/ATF4/ATF5 dependent gene category, while *Folate & pterin metabolism* and *Nitrogen metabolism* nodes were unique to gene sets independently regulated by ATF4 (Figure 5.10 D). Common process categories spanning multiple gene groupings included *OXPHOS* (seen in CHOP/ATF4/ATF5, CHOP/ATF5 and ATF5 categories), *Translation* (seen in CHOP/ATF4/ATF5, CHOP/ATF5, ATF5, ATF5 and redundantly signalled categories) and *Fatty acid* related categories (seen in CHOP/ATF5, CHOP, and ATF4 categories) (Figure 5.10 D). Interestingly, a majority of the transcription factor regulated mitochondrial genes involved further depletion of genes already significantly reduced in expression in WT cells (~64.6% of transcription factor regulated mitochondrial genes) (Figure 5.10 C). These expression trends suggest a portion of the WT UPR^{mt} genes with decreased expression may actually represent an attempt by cells to maintain expression of these genes in the face of broader disruptions to transcriptional signalling. Indeed, a similar albeit slightly smaller portion of the cellular UPR^{mt} program also involved a further depletion in expression with transcription factor KO relative to WT expression (~58.3% of the transcription factor regulated cellular UPR^{mt} program), indicating this may be a large portion of the UPR^{mt} signalling response that occurs across a wide variety of cellular processes, not just mitochondrial genes.

Expression trends of mitochondrial genes during the UPR^{mt} have demonstrated that the mitochondrial genome is remodelled in a way that preferences the selective shutdown of certain mitochondrial processes, such as OXPHOS, while boosting other processes like Folate metabolism. CHOP, ATF4 and ATF5 coordinate expression of over half of these UPR^{mt} changes and also appear to be critical for preventing excessive shutdown in expression levels of a subset of the mitochondrial genome. While the functional effects of the transcription factor dependent mitochondrial gene expression patterns remain to be determined, it can be concluded from this data that loss of CHOP, ATF4 or ATF5 significantly alters the UPR^{mt} program.
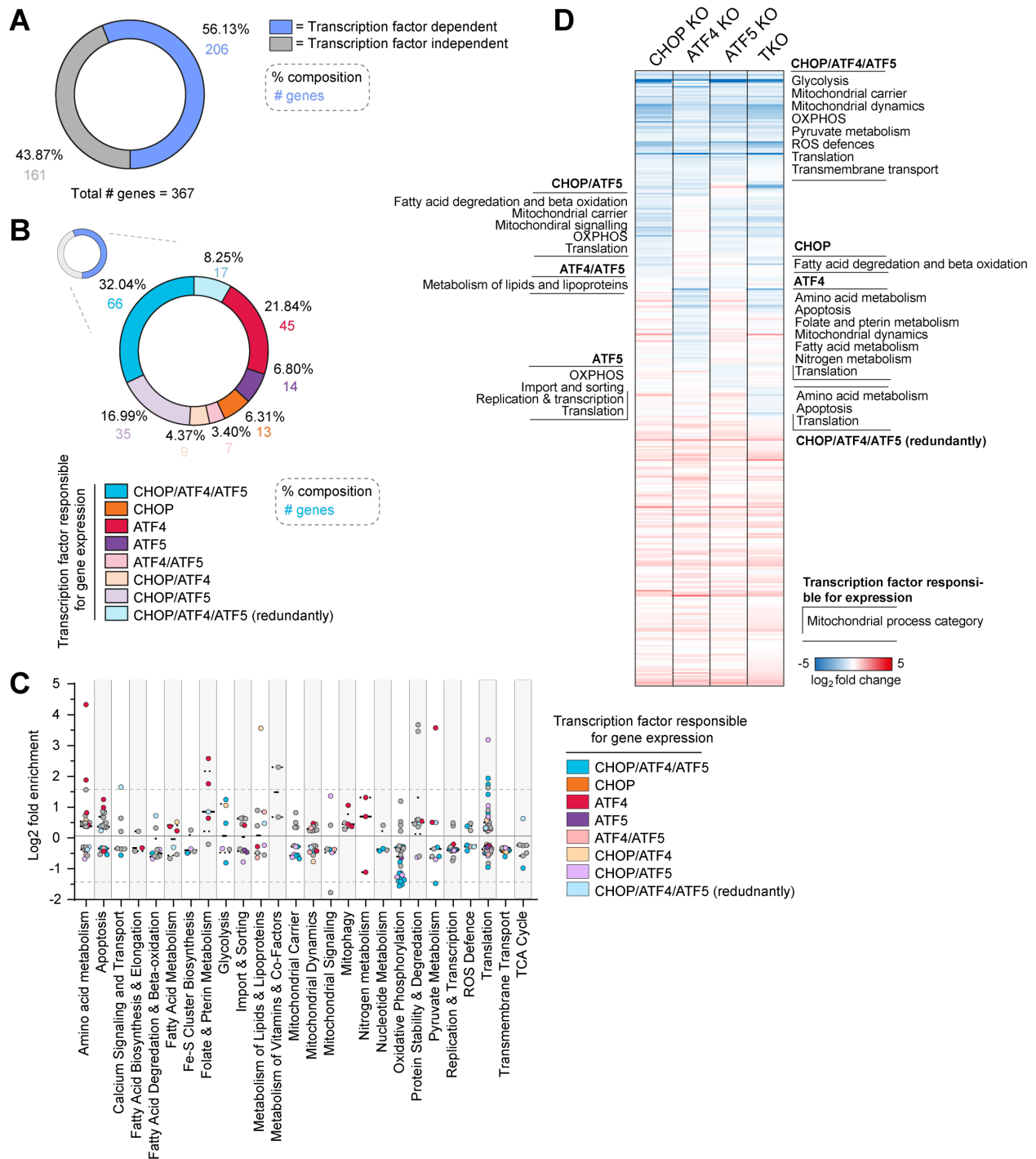
Figure 5.10 **CHOP, ATF4 and ATF5 exert a mosaic, interconnected pattern of regulation across the mitochondrial-related UPR^{mt} induced transcriptome**. **A** – **D**. Mitochondrial gene expression in the WT UPR^{mt} program defined in Figure 5.10 was compared to the gene expression in CHOP KO, ATF4 KO, ATF5 KO or TKO cells. Genes showing > -0.2 fold decrease in expression relative to WT 12 h G-TPP levels were classified as being under the regulatory control of the transcription factor in question. **A**. The proportion of the mitochondrial UPR^{mt} transcriptome determined to be under the regulatory control of CHOP, ATF4 or ATF5, or independently expressed, was calculated and displayed by pie chart. **B**. The proportion of the mitochondrial UPR^{mt} transcriptome determined to be under the regulatory control of one or more transcription factors was further separated into grouping according to the transcription factors required for expression. The relative proportional composition of these groups was then calculated and displayed by pie chart. **C**. WT mitochondrial UPR^{mt} genes from Figure 5.10 C were labelled (cont.)

according to the transcription factor combinations required for expression. **D**. Mitochondrial process groups in transcription factor dependent gene clusters with 2 or more genes belonging to that process group were labelled alongside transcription factor regulated clusters of the mitochondrial WT UPR^{mt} program displayed by heat map. Data in **A** – **D** was generated from three independent experiments.

5.6: The UPR^{mt} facilitates differential expression of mtDNA encoded genes

While mitochondria are comprised of large numbers of nuclear encoded genes, components of the mitochondrial proteome are encoded and transcribed from mtDNA (*16*). An interesting trend in mtDNA expression was observed when examining the mitochondrial-specific UPR^{mt} transcriptome changes. Increased levels of ribosomal RNA (rRNA) encoded by mtDNA were seen with G-TPP treatment in WT cells, while OXPHOS encoded mtDNA transcripts were decreased in levels relative to their expression in DMSO treated samples (Figure 5.11). Differential expression of mtDNA transcripts is unexpected as mtDNA is a circular structure that is typically transcribed in its entirety, and then cleaved into individual transcripts (*16*). As the rRNA encoded by mtDNA forms structural components of the mitochondrial ribosome (*17*), the most logical explanation for these expression patterns is that an accumulation of aggregated ribosomes is leading to an accumulation of rRNA in those ribosomes. To see if similar trends of increased rRNA expression were seen in transcription factor KO lines, which showed even higher levels of ribosome aggregation relative to WT (Chapter 4, Figure 4.11), mtDNA expression profiles were generated for CHOP KO, ATF4 KO, ATF5 KO and TKO cells. Expression trends in ATF4 KO cells demonstrated elevated levels of rRNA transcripts and depleted levels of OXPHOS transcripts relative to WT cells, indicating the elevation in rRNA seen in WT cells may indeed be due to mitoribosome aggregation (Figure 5.12 B, E). However, levels of both rRNA and OXPHOS transcripts were reduced in CHOP, ATF5 and TKO cells which does not match mitoribosome aggregation trends in those samples (Figure 4.11), suggesting the elevated rRNA levels could possibly represent an upregulation driven by CHOP and ATF5 (Figure 5.12 A, C, D, E). As the transcripts measurements performed in this work do not take into account differences in total mtDNA levels across cells, it cannot be concluded from this data whether these measurements represent an abolition of the differential expression in the absence of CHOP or ATF5, or a depletion in overall mtDNA levels in these cells. While it is unclear mechanistically how differential expression of rRNA and OXPHOS encoded mtDNA transcripts could occur based off our established understanding of mtDNA transcription and turnover, multiple nuclear transcription

A WT

B

	WT DMSO (CPM)	WT G-TPP (CPM)
MT-ATP6	1180.25	473.69
MT-ATP8	332.14	137.33
MT-CO1	3442.20	1214.27
MT-CO2	2278.24	869.33
MT-CO3	3733.62	1285.36
MT-CYB	1015.65	426.64
MT-ND1	1401.31	563.26
MT-ND2	1484.75	702.13
MT-ND3	938.39	354.80
MT-ND4	2569.92	970.67
MT-ND4L	615.82	281.79
MT-ND5	435.88	190.42
MT-ND6	56.66	48.36
MT-RNR1	3010.22	6139.83
MT-RNR2	13944.96	22186.97

Log_2 fold change

0.2 - 0.5		-0.2 - -0.5	
0.5 - 1		-0.5 - -1	
1 - 2		-1 - -2	
> 2		> -2	
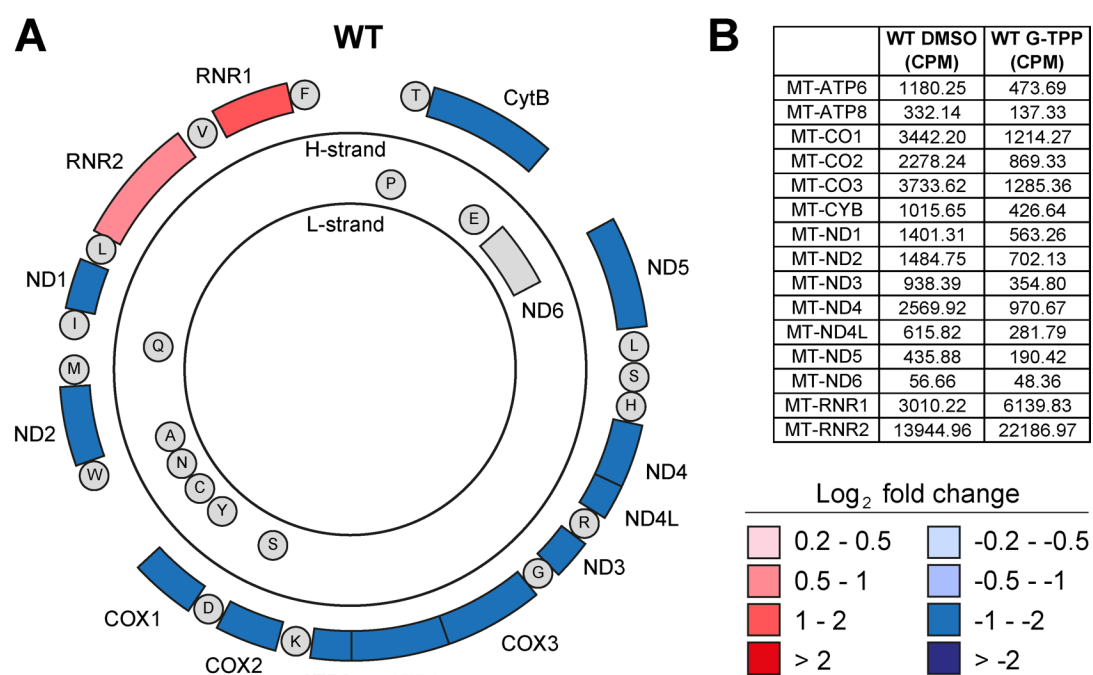
Figure 5.11 **Elevated levels of ribosome and translation related mtDNA encoded genes is seen during G-TPP treatment in the WT UPR^mt program**. **A**. mtDNA encoded genes showing significant +/- 0.2 fold expression changes with G-TPP treatment in WT samples were displayed according to their fold change in expression and location in the mtDNA genome. **B**. Gene expression in counts per million reads (CPM) is displayed by table. Data in **A**, **B** was generated from three independent experiments.

factors have been observed to localise to mitochondrial DNA in different cellular contexts (*229-235*). Whether recruitment of a normally nuclear-localised transcription factor to mitochondria under the regulatory control of CHOP and ATF5 could be altering mtDNA transcription dynamics remains to be established. While still mechanistically unclear, the proteostatic-stress driven alterations to mitochondrial rRNA levels represent a novel genetic component of the UPR^mt pathway.
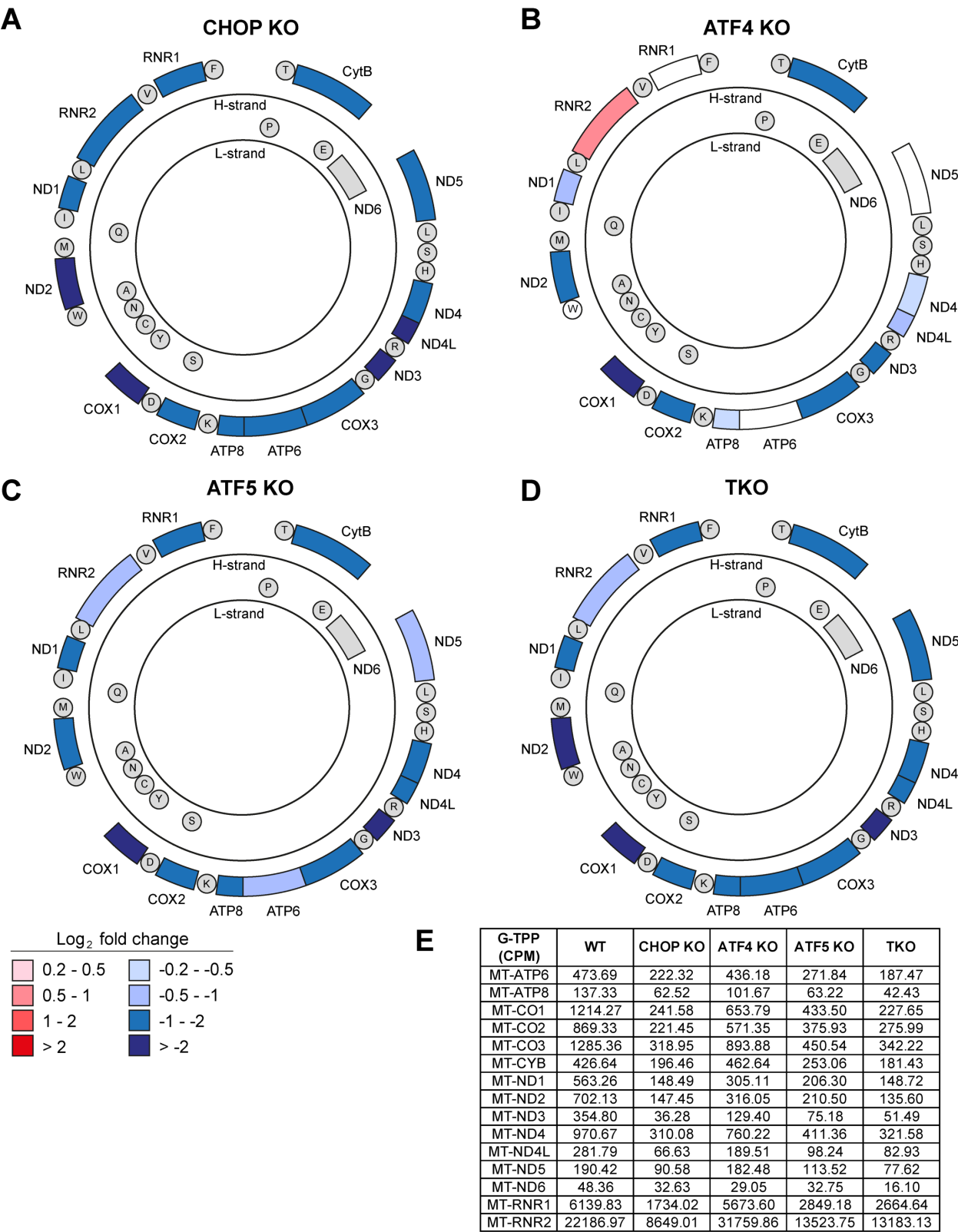
Figure 5.12 **mtDNA expression profiles in CHOP, ATF4, ATF5 and TKO cells**. **A** – **D**. Expression profiles in CHOP KO (**A**), ATF4 KO (**B**), ATF5 KO (**C**) and TKO (**D**) samples of mtDNA genes significantly upregulated or downregulated in the WT UPR^mt program were calculated relative to gene expression in WT 12 h G-TPP samples and displayed according to location in the mtDNA genome. **E.** Gene expression in counts per million reads (CPM) is displayed by table. Data in **A** – **E** was generated from three independent experiments.

G-TPP (CPM)	WT	CHOP KO	ATF4 KO	ATF5 KO	TKO
MT-ATP6	473.69	222.32	436.18	271.84	187.47
MT-ATP8	137.33	62.52	101.67	63.22	42.43
MT-CO1	1214.27	241.58	653.79	433.50	227.65
MT-CO2	869.33	221.45	571.35	375.93	275.99
MT-CO3	1285.36	318.95	893.88	450.54	342.22
MT-CYB	426.64	196.46	462.64	253.06	181.43
MT-ND1	563.26	148.49	305.11	206.30	148.72
MT-ND2	702.13	147.45	316.05	210.50	135.60
MT-ND3	354.80	36.28	129.40	75.18	51.49
MT-ND4	970.67	310.08	760.22	411.36	321.58
MT-ND4L	281.79	66.63	189.51	98.24	82.93
MT-ND5	190.42	90.58	182.48	113.52	77.62
MT-ND6	48.36	32.63	29.05	32.75	16.10
MT-RNR1	6139.83	1734.02	5673.60	2849.18	2664.64
MT-RNR2	22186.97	8649.01	31759.86	13523.75	13183.13

5.7: Which factors are driving the other 45% of the UPR^{mt} transcriptome?

To date, the only transcription factors which have been robustly associated with UPR^{mt} induction in mammalian cells are CHOP, ATF4 and ATF5. An unexpected finding of the G-TPP induced transcriptome analysis was that only ~55% of the UPR^{mt} transcriptome is regulated by these three transcription factors (Figure 5.7 A). What drives the expression of ~45% of the UPR^{mt} program is currently unknown. To identify what other transcriptional programs may be signalling outside the CHOP/ATF4/ATF5 axis of the UPR^{mt}, an analysis of common transcriptional promoter elements and associated gene expression changes in this gene subset was performed using the RegNetwork database (*236, 237*). A large number of enriched transcription factor signalling nodes were detected in the CHOP/ATF4/ATF5 independent UPR^{mt} genes (Figure 5.13). The most highly enriched transcription factors in the CHOP/ATF4/ATF5 independent UPR^{mt} genome were Smad nuclear interacting protein (SNIP1) and Mothers against decapentaplegic homologue 3 (SMAD3). Multiple interconnected transcription factor signalling networks were also produced in this analysis, including the MYC/MAX/MXI1 network and JUN/FOS network which produces the AP-1 signalling complex (*238*). Numerous additional ATF proteins were also identified, including ATF6, ATF7, ATF3, ATF2 and ATF1 in addition to ATF4 and ATF5. ATF proteins are known to bind to the same DNA binding element with additional regulation introduced through heterodynamic binding to other transcription factors (*239*). Some overlap in the ATF signalling programs produced though this analysis may account for the additional identification of ATF5 and ATF4 programs which were removed through comparison to the ATF4 and ATF5 KO cells. However, further identification of the ATF family suggests additional ATF transcription factors are in fact activated, and more specific analysis of ATF transcription factor activity will be required to identify these transcription factors. Overall, analysis of the common transcriptional elements of these genes has generated 4 interconnected signalling networks in addition to 16 other independent transcription factors which may be contributing to UPR^{mt} signalling (Figure 5.13). This list can be used as a starting position to guide future research in mapping the unknown signalling elements of the uncharacterised portion of UPR^{mt} program,
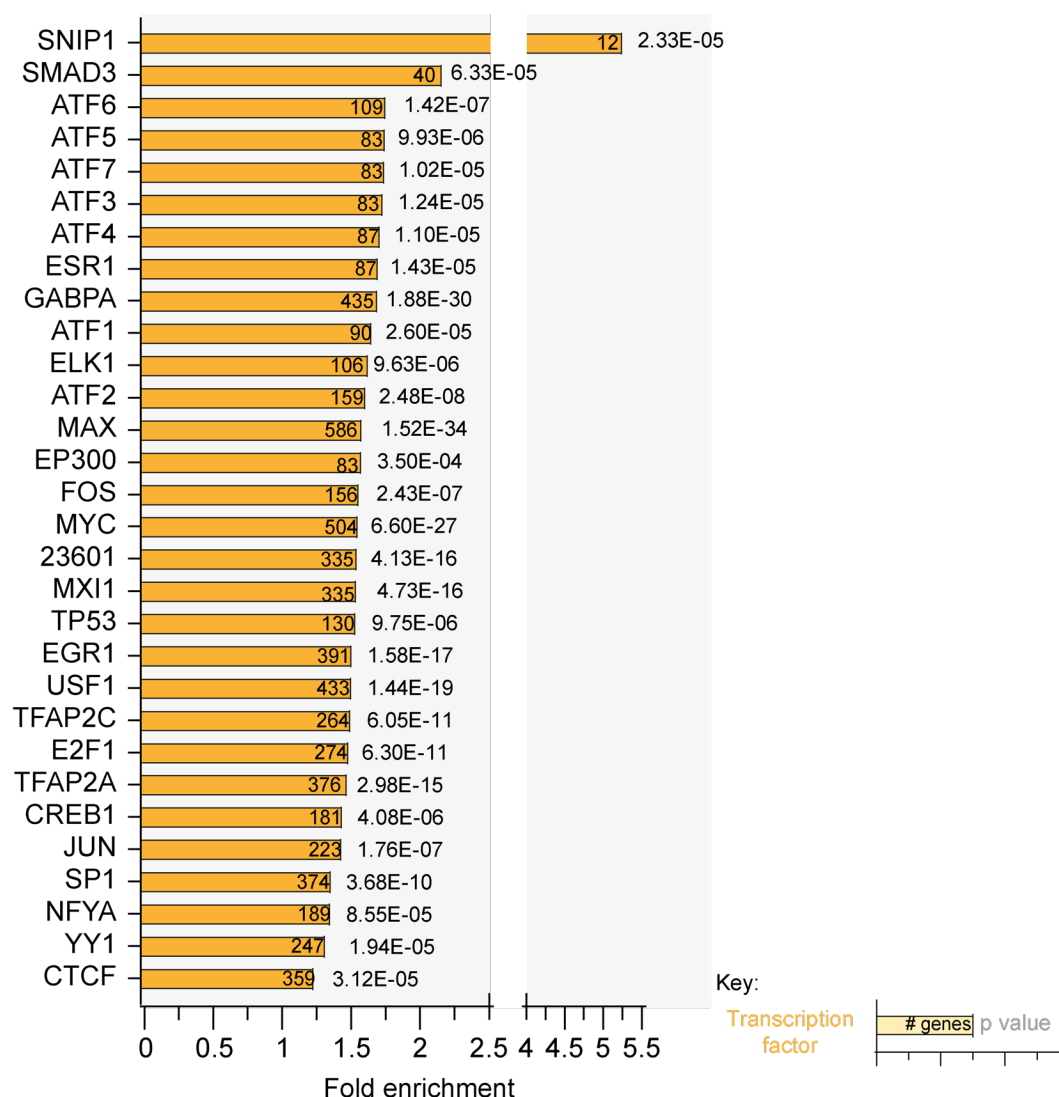
Figure 5.13 **Multiple uncharacterised transcription factor signatures are identified in the portion of the UPR^mt program not regulated by CHOP, ATF4 or ATF5**. Genes showing significant expression changes in WT 12 h G-TPP treated samples which were classified as the G-TPP induced UPR^mt program that were not deemed to be under the regulatory control of CHOP, ATF4 or ATF5 were analysed against the RegNetwork database to detect common transcriptional signatures seen in promoter regions and gene expression in this gene cluster. Transcription factors showing enriched transcriptional signatures in the uncharacterised component of the UPR^mt genome were graphed according to fold enrichment. Data was generated from three independent experiments.

5.8: Discussion

5.8.1: Understanding the functional outcomes of the UPR^mt

Due to limitations in the techniques available to analyse mitochondrial proteostasis prior to this thesis, previous studies examining the UPR^mt have focused on measuring UPR^mt signalling rather than how the UPR^mt program directly affects mitochondrial function. Through coupling analysis of mitochondrial proteostasis to PGAM5 cleavage patterns, it was found that mitochondrial proteostasis disruption causes mitochondrial stress (Chapter 5.2). Proteostasis analysis also allowed the identification of the OXPHOS machinery as a component of mitochondria that is particularly sensitive to protein folding stress (see Chapter 4). In Chapter 5 of this thesis, detailed analysis of cellular ATP levels and mitochondrial respiration complemented the proteostasis analysis and demonstrated that aggregation of the OXPHOS machinery proteins leads to functional defects in the respiratory chain. While CHOP, ATF4 and ATF5 driven UPR^mt programs were required to protect mitochondria from stress affecting PGAM5 cleavage during acute 12 h G-TPP treatment, they are dispensable in recovery from the stress that mediates PGAM5 cleavage. In contrast, each transcription factor driven UPR^mt arm plays an essential role in protecting OXPHOS function during an acute stress and in repairing OXPHOS dysfunction during recovery from the stress. This is evidenced by the finding that KO of CHOP, ATF4 or ATF5 alone is sufficient to produce severe OXPHOS dysfunction that was similar in magnitude to that seen in TKO cells (Figures 5.3, 5.4).

Aggregation trends of OXPHOS proteins in transcription factor KO cells mirrored the functional defects observed in mitochondrial respiration and ATP (Chapter 5.3), which suggests that aggregated protein alone is sufficient to cause OXPHOS dysfunction. However, transcriptomic analysis of CHOP, ATF4 and ATF5 dependent regulation of the UPR^mt transcriptome revealed each transcription factor also regulates the expression of multiple OXPHOS components (Figure 5.11). Therefore, in protecting OXPHOS, the UPR^mt program appears to play both an active role in influencing the expression of OXPHOS proteins, and a passive role in preventing the excessive aggregation of mitochondrial proteins, including those that assemble the OXPHOS machinery. The OXPHOS machinery is an essential component of mitochondrial function, and while direct mutations in OXPHOS components are causative of mitochondrial disease, declining OXPHOS function has been noted in a variety of other disease pathologies (*240-245*). The results of this chapter demonstrate that defects in the UPR^mt lead to prolonged OXPHOS dysfunction even after the stress is removed, raising the possibility that OXPHOS dysfunction observed in some disease states could be a consequence of interrupted UPR^mt activity/signalling. Further specific analysis

of UPR^{mt} activity in disease models and a more comprehensive understanding of the genetic components of the UPR^{mt} program will be required to better understand how the UPR^{mt} may be contributing to mitochondrial dysfunction in disease.

5.8.2: Mitochondrial stress stimuli can affect the resulting transcriptional program

Although the UPR^{mt} is well characterised in *C. elegans*, the lack of conservation of the signalling program has made it difficult to relate previous findings from studies performed with *C. elegans* to the mammalian UPR^{mt} program. Our sparse understanding of the genetic signature of the UPR^{mt} in mammals, combined with the role of each mammalian transcription factor in other stress response pathways makes it difficult to identify clear UPR^{mt} signatures. In the absence of a defined UPR^{mt} signature, incidental detection of UPR^{mt} program activation is unlikely to occur in studies that are not specifically seeking to analyse the UPR^{mt}. It is therefore important to generate a template of UPR^{mt} activation signals that can be used by others to assess whether their experimental system is resulting in UPR^{mt} activation.

Among the clusters of genes showing upregulated expression with G-TPP treatment were genes involved in immune responses, in particular genes involved in the NF-KB pathway (Figure 5.5 C). Induction of immune response related genes in a UPR^{mt} dependent manner has been observed in *C. elegans* during *Pseudomonas aeruginosa* exposure and when treated with *spg-7* or *cco-1* RNAi to disrupt mitochondrial protein turnover and OXPHOS (*228, 246, 247*). Although RNAi can lead to off target effects, immune responses in each of these studies were clarified to be dependent on ATFS-1 signalling, confirming they are bona fide components of the UPR^{mt}. In contrast, transcriptomic analysis of mammalian cells treated with mitochondrial stressors that decrease mitochondrial translation (doxycycline, actinonin), damage the mitochondrial membrane potential (FCCP) or block protein import (MitoBloCK-6) did not produce similar immune related transcriptional signatures (*101*). However, these mitochondrial stressors have not been characterised to induce proteostasis disruption in mammals, as none directly target the protein folding machinery of mitochondria. The presence of a strong transcriptional immune related signature using G-TPP which was similar to observations made in *C. elegans* suggests that activation of an immune response is a genuine component of the UPR^{mt} that is specific to protein folding stress.

As expected from a stress response triggered by misfolded protein, a large cluster of genes associated with protein refolding related processes was upregulated during the UPR^{mt} (Figure 5.5 C). Protein refolding genes have been identified in numerous other studies in both mammalian systems and *C. elegans*. Mitochondrial chaperone and protease induction has been observed in mammalian cells either treated with G-TPP, paraquat (which generates ROS), or through expression of ΔOTC, as well as *C. elegans* using *cco-1* and *tim-23* RNAi, or with paraquat treatment (*77, 95, 102, 142, 228*). The common node of protein folding machinery expression across several studies and systems confirms that increased expression of proteostasis promoting machineries is a canonical node of the UPR^{mt}. While paraquat doesn't directly alter the proteostatic capacity of mitochondria, the increased ROS generated with treatment appears to lead to protein damage and misfolding to generate a robust UPR^{mt} across different species (*248*). Interestingly, doxycycline, actinonin, FCCP and import disruptions in mammalian cells do not stimulate the expression of the mitochondrial protein folding machinery (*101*).

Another important element of the UPR^{mt} program which has recently been characterised in an organismal context in the *C. elegans* system is the transmission of the mitochondrial stress response across tissues via Wnt signaling (*249-251*). It is difficult to study the Wnt signalling pathway in a mammalian context due to the lack of mammalian animal models of UPR^{mt} induction. Wnt signalling pathway induction has not been previously identified in mammalian systems and is not commonly detected in *C. elegans* studies either. Ontology analysis of the WT UPR^{mt} program with G-TPP treatment did not generate a Wnt signature node (Figure 5.5 C). However, KEGG pathway analysis, which is more biased to identification of signalling pathway patterns, identified Wnt signalling in the G-TPP induced WT UPR^{mt} program (Figure 5.8 A). Potentially, due to the large size of the UPR^{mt} transcriptional program and the relatively small number of genes involved in Wnt signalling, a clear signature may have been missed in previous studies through a failure of ontology analysis to isolate Wnt signalling. The Wnt signature identified in Chapter 5.4 demonstrates a pattern of elevated expression that would facilitate Wnt signalling activation, which is also in part driven by the expression of CHOP, ATF4 and ATF5. Wnt signalling appears to be an evolutionarily conserved element of the mammalian UPR^{mt} program that requires a more tailored gene analysis to detect (Figure 5.8). How Wnt signalling may function in a mammalian context remains to be explored.

A unique signalling node identified in the UPR^{mt} transcriptome which has not been previously linked to UPR^{mt} mediated signalling was the specific upregulation of autophagy related machinery (Figure 5.5 C). While PINK1/Parkin mitophagy has been observed to activate in response to ΔOTC stress in mammalian cells, it has been considered consequential rather than through a distinct

regulatory induction (*11, 173*). No literature has identified autophagy upregulation as a component of the UPR^mt program in any system, making the identification of specific autophagy dependent processes a novel finding of this work. In addition to an upregulation of autophagy, a strong upregulation in the expression of the proteasomal machinery and ubiquitination machinery specific to degradative modifications were observed in WT cells (Figure 5.5 C). Proteasomal degradation is again another regulatory process that has not been clearly identified as a UPR^mt mediated response in mammalian systems or in *C. elegans*. However, boosted activity of the proteasomal machinery has been identified as an active response to the accumulation of mistargeted mitochondrial proteins in the cytosol of *Saccharomyces cerevisiae (181)*. An increase in the activity of the proteasomal system has also been observed in *C. elegans* in an ATFS-1 dependent manner during UPR^mt induction, but no discrete transcriptional signature has been identified in the *C. elegans* system (*252*). Mitochondrial HSP70 plays dual roles within mitochondria, forming part of the PAM complex required to power protein import into the matrix while also facilitating protein folding in its chaperone context (*253*). If a proteostatic stress occupies more mtHSP70 towards facilitating protein folding, it stands to reason that this could interrupt mitochondrial protein import. Numerous components of the mitochondrial import machinery were seen to specifically aggregate with G-TPP treatment supporting the idea that protein import may be disrupted during proteostatic stress (Chapter 4, Figure 4.5). Accordingly, a specific upregulation of the proteasomal machinery through the UPR^mt may help prevent an accumulation of unfolded precursor proteins in the cytosol from becoming toxic to the cell.

Collectively, the G-TPP induced transcriptome shares more similarities with the *C. elegans* UPR^mt transcriptome than other studies in mammalian systems that have utilised different mitochondrial stressors. While the transcriptional responses using other mitochondrial stressors also require DELE1 for signalling, a different transcriptional signature that does not induce chaperone and protease expression has been identified across multiple studies performed by different research groups (*101, 104, 105*). Simply disrupting the mitochondrial membrane potential or protein import within mitochondria appears to be insufficient to trigger the UPR^mt in mammalian systems. These differences in signalling output, while utilising similar signalling machinery, highlight the importance of isolating the source of mitochondrial stress and taking into consideration the stress source when identifying and characterising mitochondrial stress response programs.

5.8.3: CHOP, ATF4 and ATF5 differentially regulate a subset of the UPR^{mt}

Since CHOP, ATF4 and ATF5 have each independently been implicated as critical drivers of the UPR^{mt}, it was unclear prior to this thesis how each transcription factor fits into the equation of the UPR^{mt} program. While the requirement of DELE1 for their induction has been well established, how they participated in downstream signalling was unclear. The studies in Chapter 4 illustrated that each transcription factor is independently induced during the UPR^{mt} and is equally important in protecting and repairing mitochondrial proteostasis. The comparative transcriptomic analysis performed in this chapter has mapped which parts of the UPR^{mt} program are driven by CHOP, ATF4 and ATF5. The transcriptional footprint of each transcription factor produced a complex pattern with unique and overlapping signatures indicating highly interactive regulation of the UPR^{mt} transcriptome (Figure 5.7). Genes of the UPR^{mt} program regulated by these transcription factors required the activity of one, two or three different transcription factors for expression (Figure 5.7). Due to the complex nature of the interactions identified in these signalling networks, it is difficult to speculate on which components of these signalling footprints are required for protection of mitochondrial proteostasis. However, the only specific chaperones found to be regulated by the CHOP/ATF4/ATF5 axis were HSPA6 and HSPA7 which are strongly upregulated in the WT UPR^{mt} program and downregulated with KO of each transcription factor (Figure 5.5 D). These are cytosolic chaperones, and while the UPR^{mt} increases expression of mitochondrial chaperones and proteases (Figure 5.9), none of the mitochondrial proteases or chaperones appear to be specifically regulated by CHOP, ATF4 or ATF5. It is possible that a dysfunctional cytosolic misfolded protein response in the absence of the cytosolic chaperones HSPA6 and HSPA7 is impairing the UPR^{mt} program via aggregation of pre-imported mitochondrial precursors. The unimported precursors might include mitochondrial proteases and chaperones. Alternatively, a yet to be identified cellular process critical to UPR^{mt} activity may lie in the transcriptome co-regulated by CHOP, ATF4 and ATF5. An interesting observation which was noted in Chapter 5.5 (Figure 5.10 C) was that loss of either CHOP, ATF4 and ATF5 biased towards a further reduction in expression of mitochondrial genes that were decreased in expression during WT UPR^{mt} induction. If CHOP, ATF4 and ATF5 are required to maintain certain levels of mitochondrial gene expression, the defects observed in proteostasis repair with transcription factor KO could perhaps occur through a failure to produce enough mitochondrial transcripts to facilitate mitochondrial biogenesis or the replacement of damaged components. While the mechanisms behind how each transcription factor functions as an essential component of the UPR^{mt} are still unclear, the transcriptomic analysis performed in this chapter has shown that these transcription factors constitute individual signalling programs with multiple cooperative elements.

Interestingly, the essential nature of each of CHOP, ATF4 or ATF5 for UPR^{mt} activity implies a rigid requirement for the full operational capacity of the UPR^{mt} program to activate mitochondrial repair. Requiring multiple simultaneous transcription factor programs to be activated for UPR^{mt} activity could act as a checkpoint of cellular function to prevent aberrant attempts to repair mitochondria in dysfunctional cells. If mitochondrial damage is severe enough to be impacting cellular health, full coordinated activation of multiple signalling pathways may be interrupted, preventing UPR^{mt} activation and preventing attempted repair of severely damaged mitochondria that instead need to be efficiently removed through mitophagy to repair cellular health. The presence of a stress-based signalling checkpoint could contribute to the earlier observations that severe mitochondrial stressors such as CCCP which completely ablate mitochondrial membrane potential do not appear to activate the UPR^{mt} (*101, 104, 105*).

5.8.4: Is DELE1 the only stress signal?

Previously published literature has identified DELE1 as a critical signalling molecule of the UPR^{mt} in mammalian systems (*104, 105*). Transcriptomic analysis performed on DELE1 KO cells in this chapter has further confirmed that DELE1 is intrinsically required for UPR^{mt} induction (Figure 5.6). A similar reliance on ATFS-1 signalling is seen in *C. elegans*, as removal of only ATFS-1 is sufficient to supress the UPR^{mt} program, however, ATFS-1 is not the sole UPR^{mt} stress signal required for UPR^{mt} activity (*80*). As discussed further in Chapter 4.10.1, the current model proposed for DELE1 activity is insufficient to lead to a specialised mitochondrial stress program. In Chapter 4.10.1 it was speculated that a mitochondrial derived signal may be influencing UPR^{mt} gene expression at an epigenetic level as is seen in the *C. elegans* system (*80*). The transcriptomics data produced in this Chapter has provided further support for this idea. Analysis of the G-TPP induced UPR^{mt} transcriptome showed a marked upregulation in the expression of histone acetylation and histone demethylase related genes, in addition to a decrease in the expression of histone deacetylase and histone methylase genes (Figure 5.5 C). Together, the transcriptomic data suggests there is activation of a program involving histone acetylation and demethylation during the UPR^{mt}. A recent study by the Auwerx laboratory has demonstrated that KO of the histone acetyltransferase P300 blunts the expression of several UPR^{mt} related genes, further supporting the concept of an essential chromatin modifying arm of the UPR^{mt} (*247*). Histone acetylation is typically associated with relaxing chromatin structure while histone methylation can condense chromatin structure and silences it to gene expression (*254, 255*). Acetylation of histones in UPR^{mt} specific regions may allow for tailored transcription of mitochondrial genes. Different histone

modification patterns are observed in the *C. elegans* UPR^{mt}, which critically relies on the generation of specific histone methylation marks and the removal of acetylation modifications (*80*). In *C. elegans*, the epigenetic modulation of UPR^{mt} activity has been demonstrated to involve silencing of specific chromatin regions through methylation marks, opening up other chromatin regions for transcription (*80*). While the methods of chromatin modification may differ, the end outcome of altered transcriptional patterns through epigenetic modification is common between the two different modification patterns. Collectively, evidence in this thesis and mounting evidence in the literature indicates that chromatin modification may be a point of commonality in *C. elegans* and mammalian UPR^{mt} programs.

An open question remains regarding what could be triggering a histone modification arm of the UPR^{mt} in both mammalian cells and the more well-established *C. elegans* system. One of the most highly abundant molecules produced by mitochondria is ATP, and ATP is required for chromatin remodelling in addition to nuclear transport of cytosolic proteins into the nucleus (*256, 257*). Further, previous studies have demonstrated that ATP levels differ in concentration across different cellular compartments (*258, 259*). Cellular ATP levels were seen to be stable and present in similar quantities in WT cells with or without an acute G-TPP treatment (Figure 5.3). The increased protein misfolding within both the mitochondria and the cytosol with G-TPP treatment would presumably increase the localised requirement of ATP in those compartments through the additional activity of ATP dependent proteases, chaperones and the ubiquitin-proteasomal system. Whether these increased localised requirements of ATP in addition to unchanged total levels of ATP leads to a localised depletion of ATP in the nucleus is potential area of future investigation. Localised depletion of ATP may influence epigenetic signalling transcriptional processes, providing an additional mitochondrial derived stress signal to the nucleus to help tailor the transcriptional program. A large node of ATP-dependent chromatin remodelling factors were decreased in expression in the WT UPR^{mt} program, further supporting this hypothesis that modulating the ATP dependent epigenetic response may help activate this aspect of the UPR^{mt} (Figure 5.5 C). Mitochondrial derived Acetyl-CoA has also been shown to function as a substrate source for histone acetylation (*260, 261*). The clear preference for acetylation-based histone modifications in the transcriptomics data produces a potential signalling relay whereby mitochondria can alter levels of a mitochondrial derived substrate and influence nuclear signalling. Future studies examining the metabolome changes driven by mitochondrial derived proteostasis stress would be incredibly informative in shedding light on what factors could be influencing a mitochondrial derived epigenetic UPR^{mt} program.

5.8.5: Regulation of ribosomal activity is an active signalling component of the UPR^{mt}

Examination of the mitochondrial-specific changes of the UPR^{mt} transcriptome revealed that mitochondrial rRNA transcripts increase in abundance during proteostatic stress while OXPHOS related mtDNA transcripts see a decrease in expression (Chapter 5.6). As discussed in Chapter 5.6, these differential expression changes could represent either a decrease in turnover of the rRNA transcripts through mitoribosome aggregation, or a selected upregulation in expression of rRNA. Together with the changes observed in mtDNA expression, an interesting node of rRNA methylation proteins was identified to be induced during the UPR^{mt} through clustered analysis of ATF4/ATF5 regulated genes (Figure 5.7 C). Closer examination of rRNA methylation proteins in the WT UPR^{mt} transcriptome revealed that 5 mitochondrial rRNA methylation enzymes were upregulated with UPR^{mt} induction: MTO1, MRM2, NSUN4, METTL15P1 and METTL15 (Figure 5.14). These enzymes were under a mosaic pattern of transcription factor mediated control, indicating the elevated expression of rRNA methylation genes is an active signalling component of the UPR^{mt} driven by the CHOP/ATF4/ATF5 transcription factor program (Figure 5.14). Methylation of different parts of rRNA has been shown to have different specific effects on ribosomal activity, but a common feature amongst the effects of rRNA methylation is an improvement in the stability of the mitochondrial ribosome structure and an improvement in translation capacity and efficiency of the mitochondrial ribosome (*262-267*). While rRNA components of the mitochondrial ribosome were altered in expression, structural mitochondrial ribosome transcripts were mostly unaltered in transcript expression during the UPR^{mt} (data not shown). Taken together, elevated expression of ribosome methylation proteins, along with a potential elevation in expression or decrease in turnover of mitochondrial rRNA without significantly elevating overall levels of structural mitochondrial ribosome transcripts, suggests a component of the UPR^{mt} signalling program involves boosting and repairing the function of the pre-existing mitochondrial ribosome. Studies into the turnover and reformation of mitochondrial ribosome structures after G-TPP treatment would be required to clarify the functional effect of the rRNA trends observed in this data. It is notable that the mitochondrial ribosome was identified as one of the most highly aggregation sensitive structures to protein folding stress (Chapter 4). An interesting area of investigation would be to assess whether these rRNA and rRNA methylation enzyme expression changes could boost mitochondrial ribosome stability in the long-term following G-TPP treatment to help protect mitochondria from future proteostasis stress.

Figure 5.14 **Mitochondrial rRNA methylation proteins are upregulated during the UPR^{mt} in a CHOP/ATF4/ATF5 dependent manner**. Heat map representation of the log$_2$ fold changes in expression of each gene with G-TPP treatment relative to DMSO (WT), or log$_2$ fold change in expression relative to WT G-TPP treated expression levels (CHOP KO, ATF4 KO, ATF5 KO, TKO).

5.8.6: Potential new transcriptional drivers of the UPR^{mt}

Prior to the work in this thesis, the three main transcription factors which had been independently implicated in driving the UPR^{mt} program were CHOP, ATF4 and ATF5. While the comparative transcriptomic analysis performed in this chapter has allowed us for the first time to understand how each of these three transcription factors integrate into the UPR^{mt} program, it also revealed that ~44% of the UPR^{mt} transcriptome is currently undefined (Figure 5.7 A). By comparing the common gene expression and transcriptional elements of the remaining genes that are not regulated by CHOP, ATF4 and ATF5, a candidate list of potential transcription factors involved in the UPR^{mt} was generated (Chapter 5.7). In addition to 16 individual transcription factors, four interconnected signalling networks were identified.

1) SNIP1/SMAD3

The most highly enriched transcription factor in the analysis conducted in Chapter 5.7 was Smad nuclear interacting protein (SNIP1). In addition to SNIP1, the analysis also revealed SMAD3 as a candidate transcription factor. SNIP1 and SMAD pathway activity has been linked to the suppression of inflammatory cytokine production (*268, 269*). No direct physical interaction between SNIP1 and SMAD3 has been identified in literature, with SNIP1 only showing direct basal interactions with SMAD1 and SMAD2 (*269*). However, the identification of these two highly related protein families could indicate an uncharacterised UPR^{mt} mediated interaction between these genes in potentially driving immune-related aspects of the UPR^{mt}.

2) ATFs

Previous studies have suggested the involvement of additional ATF proteins in UPR^{mt} signalling. Upregulation of ATF3 in particular has been repeatedly identified in response to both G-TPP treatment and a wide variety of proteostasis independent mitochondrial stressors (*101, 142*). ATF3 has also been known to modulate multiple aspects of metabolism and be signalled in response to stress (*270, 271*). Interestingly, ATF3 is also regulated by SUMOylation which was an upregulated node identified in the ontology analysis of Figure 5.5 (*272, 273*). A role of SUMOylation in the mammalian UPR^{mt} has not yet been characterised, although SUMOylation has been identified as a key element of signalling regulation in *C. elegans* through modification of ATFS-1 and DVE-1 (*82*). Other ATF proteins have not been previously identified in UPR^{mt} signalling responses in mammalian cells. However, ATF7 was shown to be activated in response to CI dysfunction in *C. elegans* and to boost autophagy induction (*274*). As CI dysfunction is observed with G-TPP treatment and elevated autophagy regulation was identified by ontology analysis (Figure 5.5 C), ATF7 may be driving components of the UPR^{mt}.

3) MYC/MAX/MAD

The identification of MYC and MAX are particularly interesting signalling components in the context of the UPR^{mt}. MYC and MAX together form a heterodimer which recruits chromatin remodelling factors, in particular acetylation factors, to DNA segments (*275*). These proteins typically function together with MAD, whereby MAD competes to form a heterodimer with MAX which instead recruits deacetylase proteins to repress transcription (*276*). The selective upregulation of the histone acetylation portion of this signalling network further supports the earlier idea discussed in Chapter 5.8.4 that histone acetylation based regulation of transcription may form a component of the UPR^{mt} signal.

4) JUN/FOS

Previous studies by the Hoogenraad laboratory identified an AP-1 element preceding the CHOP gene which they further demonstrated was required for UPR^{mt} mediated CHOP induction (*141*). The AP-1 site is the consensus binding sequence of the large FOS and JUN family of proteins, which together regulate a wide variety of cellular processes (*277*). It is difficult to extrapolate the signalling programs that may be activated amongst the transcriptomic data due to the prolific nature of AP-1 sites across the genome (*278*). However, JUN was identified to be significantly

upregulated in expression upon G-TPP treatment (data not shown). Additionally, FOS and JUN signalling has been shown to interact with SMAD based signalling programs that have also been identified in this data (Figure 5.13) (*279, 280*). Based on the elevated JUN expression, together with the AP-1 consensus sequence confirmed to be important for CHOP expression, it is reasonable to conclude that FOS and JUN mediated signalling may be playing a role in UPR^mt signalling.

5) EP300, NFY, YY1

While the remaining transcription factors identified in the analysis in Chapter 5.7 do not comprise well established networks, there is still strong evidence for multiple independent transcription factors which could suggest a role in UPR^mt signalling. Specifically, EP300 has been shown to influence UPR^mt related genes in response to doxycycline treatment as discussed earlier (Chapter 5.8.4) (*247*). While it is not well established that doxycycline treatment specifically activates a protein aggregation stimulus (see Chapter 5.8.2), a role in inducing the expression of mitochondrial proteins during mitochondrial stress supports a potential role in UPR^mt signalling.

The Nuclear Transcription Factor-Y (NFY) is comprised of three subunits, with both the B and C (NFYB, NFYC) subunits upregulated in expression during G-TPP treatment (data not shown) (*281*). While NF-Y has primarily been associated with driving cell cycle regulation and apoptosis during development, expression of NF-Y has also been identified in post-mitotic neuronal cells (*282*). Studies involving the post-mitotic deletion of a critical component of the NF-Y complex in mice demonstrated a progressive neurodegenerative phenotype together with an accumulation of ubiquitin and p62 foci in neurons (*283*). Although these phenotypes don't immediately suggest a role in UPR^mt signalling, mitochondrial dysfunction is strongly associated with neurodegenerative disease. It remains to be established whether UPR^mt dysfunction can lead to neurodegeneration. However, defects in the mitochondrial quality control pathway mediated by PINK1/Parkin mitophagy are linked to Parkinson's disease pathogenesis (*152*). The neuronal defects identified with NY-A deletion in mice may be through dysfunction in mitochondrial quality control machinery.

Of the transcription factors identified, the transcription factor most tightly related to mitochondrial health is Yin Yang 1 (YY1). Mitochondrial gene expression governed by PGC1α expression was shown to be driven through YY1 activity, and knockdown of YY1 decreased steady state levels of mitochondrial gene transcripts (*284*). Knockdown of YY1 in mice also leads to decreased mitochondrial transcripts with phenotypes indicative of a mitochondrial myopathy (*285*). Low

levels of oxidative stress are shown to activate YY1 expression whereby YY1 then facilitates an antioxidant response through driving Nrf2 activity (*286*). In contrast, highly elevated levels of oxidative stress do not lead to YY1 activation (*286*). Whether YY1 activation may represent a stress-level dependent crossroad between repair pathway activation and non-UPRmt mediated pathway activation is an interesting concept for future analysis.

The promotor-network analysis undertaken in Chapter 5.7 is a powerful analytical tool in helping identify potential signalling pathways active in a large dataset. As mRNA levels of transcription factors do not necessarily denote activation (see Chapter 4.2, Figure 4.1), identifying common promoter elements in a gene set is a more informative method of understanding the underlying signalling processes. With the dataset generated in Chapter 5.7, a more targeted investigative approach can be adopted to facilitate identification of the remaining UPRmt transcription factors in future studies.

Chapter 6

Untangling the molecular connections between PINK1/Parkin mitophagy and the UPR^{mt}

6.1: Introduction

Previous work in this thesis has illustrated the importance of the UPR^{mt} in both protecting mitochondria during a protein folding stress and in facilitating functional recovery of mitochondria. Previous work by the Youle laboratory demonstrated that another quality control pathway, PINK1/Parkin mitophagy, is activated alongside the UPR^{mt} in response to protein folding stress within mitochondria (*11, 173*). Although mitophagy and the UPR^{mt} are co-activated, our current understanding of mitochondrial quality control extends only to how PINK1/Parkin mitophagy or the UPR^{mt} pathway operate in isolation. How the two pathways strike a balance between mitochondrial repair and mitochondrial degradation to maintain a healthy mitochondrial network, and whether elements of their signalling interact to coordinate this relationship is unknown. While UPR^{mt} dysfunction has not yet been implicated in disease development, PINK1/Parkin mitophagy mutations are determinants for a subset of Parkinson's Disease (PD) patients (*152*). Understanding how the UPR^{mt} interacts with PINK1/Parkin mitophagy and contributes to the maintenance of a healthy mitochondrial population will help inform our understanding of how UPR^{mt} dysfunction may contribute to disease development. The presence of a co-activated repair program opens also up a unique opportunity of potentially upregulating UPR^{mt} activity to compensate for pathogenic defects in the PINK1/Parkin mitophagy arm of the mitochondrial quality control machinery. For such a treatment to be feasible, we must first understand how these pathways collectively fit into the equation of mitochondrial quality control.

In this Chapter, transcription factor signalling dynamics of the WT UPR^{mt} program are investigated in the presence/absence of PINK1/Parkin mitophagy. The corresponding interaction is then analysed through assessing mitophagy dynamics with and without transcription factor driven UPR^{mt} activity. Lastly, preliminary investigations into UPR^{mt} pathway in a primary neuronal cell model are detailed.

6.2: PINK1/Parkin mitophagy does not influence UPR^{mt} signalling

As HeLa cells do not express Parkin, the preceding work in this thesis investigating UPR^{mt}-mediated protection and repair of mitochondria has been performed in the absence of PINK1/Parkin mitophagy (*287, 288*). To examine how PINK1/Parkin mitophagy may influence UPR^{mt} signalling, a HeLa cell line with exogenously expressed YFP-tagged Parkin was generated. Cells with and without YFP-Parkin expression were then treated with vehicle (DMSO) or G-TPP for 4, 8 and 12 h. The expression levels of CHOP, ATF4 and ATF5 were assessed by immunoblot to determine if PINK1/Parkin mitophagy activity attenuates or boosts UPR^{mt} activation (Figure 6.1 A). No differences in CHOP, ATF4 or ATF5 protein levels were observed in cells with or without YFP-Parkin expression (Figure 6.1 A). While PINK1/Parkin mitophagy does not appear to influence initial UPR^{mt} signalling, removal of damaged mitochondria may facilitate a faster shut-down of the repair phase of the UPR^{mt} program. Transcription factor levels in the recovery phase (24 - 48 h R) of the UPR^{mt} were assessed by immunoblot in the presence or absence of YFP-Parkin (Figure 6.1 B). No difference in the shutdown of CHOP, ATF4 or ATF5 expression was observed in cells with and without PINK1/Parkin mitophagy activity (Figure 6.1 B). From the acute stress and stress-recovery transcription factor level trends, it can be concluded that UPR^{mt} signalling involving transcription factor induction operates independently of PINK1/Parkin mitophagy.
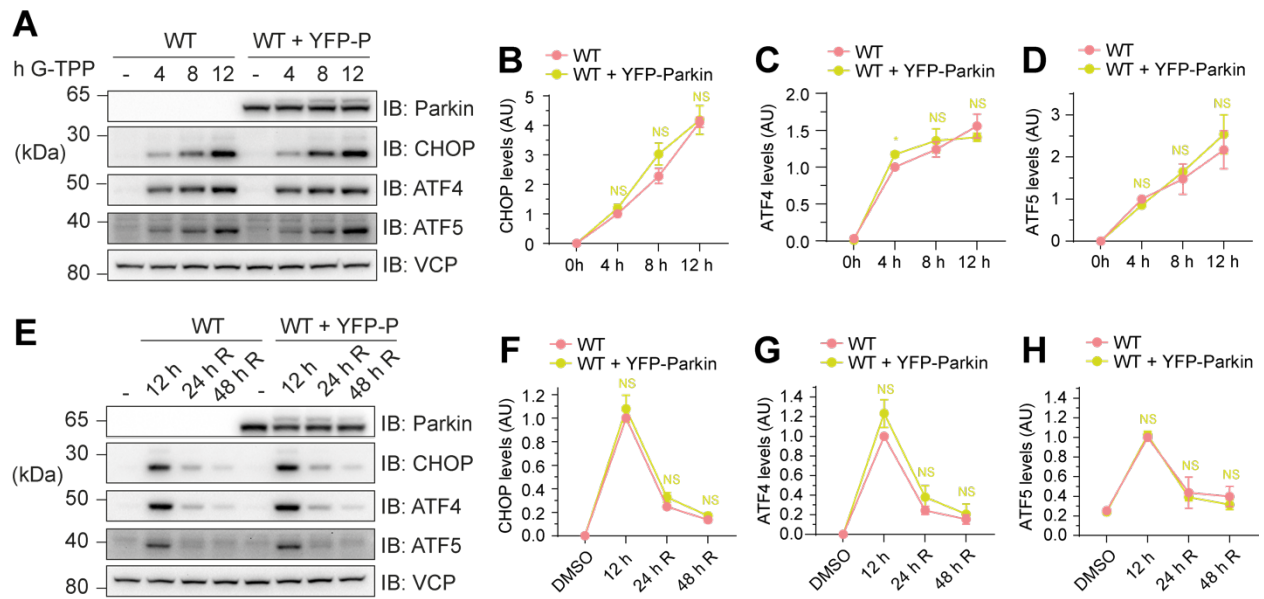
Figure 6.1 **PINK1/Parkin mitophagy does not influence UPR^mt signalling during acute stress or recovery**. **A** – **D**. WT cells stably expressing YFP-Parkin (YFP-P) were treated with DMSO (-) or G-TPP for the indicated times. Levels of CHOP, ATF4 and ATF5 were analysed by immunoblot (**A**) and quantified (**B** – CHOP, **C** – ATF4, **D** – ATF5). **E** – **H**. WT cells stably expressing YFP-P were treated with DMSO (-) or G-TPP (12 h) for 12 h prior to G-TPP washout and subsequent recovery for 24 h or 48 h (24 h R and 48 h R respectively). Transcription factor expression was analysed by immunoblot (**E**) and quantified (**F** – CHOP, **G** – ATF4, **H** – ATF5). Transcription factor expression was quantified relative to WT 4 h G-TPP treated samples (**B** – **D**) or WT 12 h G-TPP treated samples (**F** – **H**). *P≤0.05, NS P>0.05 (two-way ANOVA). Data in **B** – **D**, **F** – **H** was generated from three independent experiments.

6.3: CHOP, ATF4 and ATF5 influence PINK1/Parkin mitophagy activation in the repair phase of the UPR^mt

Although UPR^mt signalling operates independently of PINK1/Parkin mitophagy, the UPR^mt program, or specific transcriptional arms of the UPR^mt, may regulate mitophagy activity. To assess mitophagy activity in the presence and absence of the UPR^mt program, WT, CHOP KO, ATF4 KO, ATF5 KO and TKO cell lines expressing YFP-Parkin and mitochondrially targeted Keima (mtKeima) were generated (Figure 6.2 B). mtKeima is a fluorescent protein which shows different sensitivity to two excitation wavelengths depending on the pH of the surroundings (*289*). By comparing emission spectra of cells analysed by flow cytometry using each excitation wavelength, a quantitative ratio of mitochondria in the cytosol (~ pH 7.8) compared to the lysosome (~ pH 4) can be calculated that represents mitophagy flux. WT, single transcription factor KO and TKO cells expressing both YFP-Parkin and mtKeima were treated with DMSO or G-TPP and collected at 4, 8 and 12 h G-TPP treatment, and after 24 h and 48 h recovery (24 h R and 48 h R respectively). Samples were analysed by flow cytometry and mitophagic flux was calculated for each sample to

allow for comparative analysis of mitophagy rates during acute stress and during the repair phase after stress removal. During the acute stress period (4 – 12 h), small but significant elevations in mitophagy activity were observed in each transcription factor KO cell line relative to WT samples (Figure 6.2 A). No difference in mitophagy levels was observed between any single or TKO cell line, which is consistent with the elevated but similar protein aggregate loads observed in Chapter 4 (Figure 4.3 C). Surprisingly, mitophagy rates during the repair phase of the UPR^{mt} displayed very different dynamics to those observed during acute stress. While WT cell proteostasis loads decreased by ~ 50% by 24 h recovery (Figure 4.3 C), mitophagy in WT cells instead remained elevated at 24 h R and only returned close to baseline after 48 h recovery (Figure 6.2 A). A strong increase in mitophagy levels was seen in every single transcription factor KO cell line at 24 h R with an increase of ~4.5x the WT cell mitophagy rate (Figure 6.2 A). Mitophagy levels in ATF4 KO cells continued to increase at 48 h R, while CHOP KO and ATF5 KO cells saw a minor drop in mitophagy levels at 48 h R. Mitophagy rates in the repair phase of the UPR^{mt} in each WT and transcription factor KO cell line do not follow the proteostasis trends observed in Chapter 4 (Figure 4.3 C). Interestingly, TKO cells did not recapitulate the mitophagy trends observed in single transcription factor KO cells. While TKO cells displayed some elevation in mitophagy levels at 24 h R, it was a much smaller increase compared to the single transcription factor KO lines (~2.5x WT) (Figure 6.2 A). TKO cells displayed similar levels of protein aggregation to single transcription factor KO cells during both the acute stress and the recovery phase, even trending to
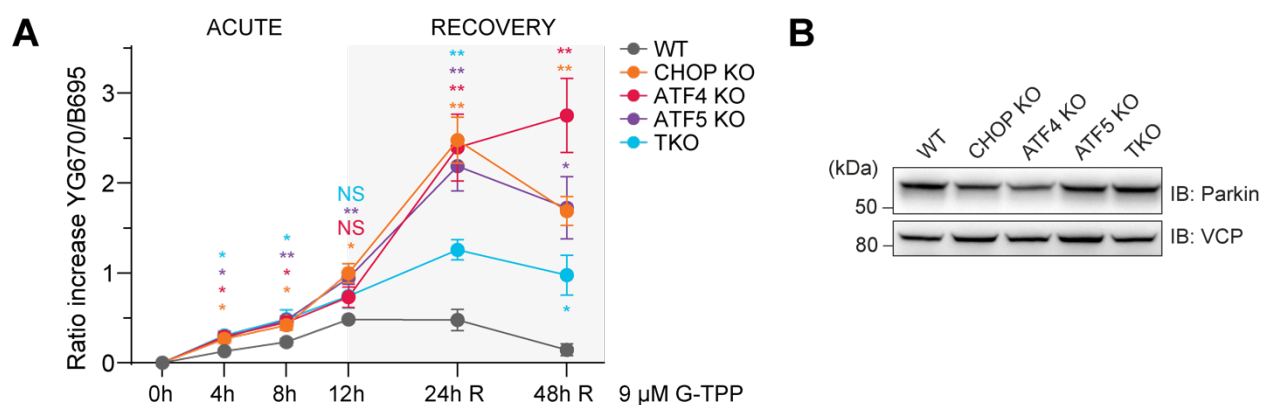
Figure 6.2 **CHOP, ATF4 and ATF5 expression influences mitophagy rates during recovery from G-TPP induced stress**. **A**, **B**. WT, CHOP KO, ATF4 KO, ATF5 KO and TKO cells stably expressing YFP-Parkin (**B**) and mtKeima were treated with G-TPP and samples were analysed during the indicated acute treatment time course, and at 24 h and 48 h after 12 h G-TPP treatment and washout (24 h R and 48 h R respectively). Emission ratio values indicative of mitophagic flux for each cell were calculated per previously published methods (*162*) and averaged across each biological repeat for each sample. Ratio increase values were calculated by subtracting the DMSO (0 h) treated ratio from G-TPP treatment or recovery ratios. **P≤0.01, *P≤0.05, NS P>0.05. Data in **A** was generated from three independent experiments.

higher levels of overall protein aggregation at 48 h R (Figure 4.3 C). In Chapter 5, mitochondrial functional assays also indicated TKO cells experienced slightly higher levels of functional defects relative to single transcription factor KO cells (Figures 5.2, 5.3) Accordingly, although mitophagy in TKO cells was still elevated over WT levels across the time course, it was anticipated that TKO cells would display similar or higher mitophagy rates to single transcription factor KO cell lines. Instead, TKO cells demonstrated mitophagy rates only slightly elevated above WT levels (Figure 6.2 A). The combined removal of CHOP, ATF4 and ATF5 UPR^{mt} signalling arms in TKO cells appears to produce a defect in PINK1/Parkin mitophagy during the repair phase of the UPR^{mt}.

6.4: TKO cells display a G-TPP-specific PINK1/Parkin mitophagy defect

PINK1/Parkin mitophagy is a complex pathway involving the recruitment of autophagy initiation factors which drive the sequestration of damaged mitochondria within a double membrane vesicle termed an autophagosome (*290*). After sequestration, damaged mitochondria are delivered to the lysosome where the autophagosome and its contents are degraded (*291*). Following degradation, lysosomes undergo a process of recycling and reformation, allowing further rounds of autophagy to occur (*292*). For autophagy to proceed, many different integrated steps need to successfully occur in a stepwise manner. Defects in any step of the autophagy pathway can lead to slower autophagy rates or, depending on the source of the defect, a complete block in autophagy (*71, 72*).

Defects in multiple different areas of the PINK1/Parkin mitophagy pathway could be responsible for the flux-defect observed in the TKO cells. To investigate the fidelity of the PINK1/Parkin mitophagy pathway in TKO cells, a stepwise approach was taken to examine key points in the autophagy pathway. The most upstream element of PINK1/Parkin mitophagy involves the stabilisation of PINK1 on the outer mitochondrial membrane of damaged mitochondria (*48*). PINK1 levels were quantified by immunoblot of isolated mitochondria in cells lacking Parkin expression to prevent mitophagy associated degradation of PINK1 which would affect quantitation analyses. Cells were treated for 12 h with DMSO or G-TPP, as well as a 24 h and 48 h recovery following G-TPP removal (24 h R and 48 h R respectively) (Figure 6.3 A). PINK1 detection by immunoblot at ~62 kDa represents uncleaved full-length PINK1 localised on the OMM where it is protected from proteolytic cleavage by PARL (*50, 293, 294*). At 12 h G-TPP treatment, clear stabilisation of PINK1 is seen in WT cells (Figure 6.3). A strong reduction in WT PINK1 levels is then observed at 24 h R and 48 h R (Figure 6.3). PINK1 levels in WT cells remained slightly elevated above baseline DMSO levels after 48 h R, suggesting some residual mitochondrial stress

at this time point (Figure 6.3). In contrast, each single transcription factor KO cell line and TKO cells displayed significantly elevated levels of PINK1 after 12 h G-TPP treatment relative to the WT control, correlating with the elevated mitophagy rates seen with UPR^{mt} disruption at 12 h G-TPP (Figures 6.2 A, 6.3) and elevated proteostatic stress (Figure 4.3 C). A strong reduction in PINK1 levels was observed in CHOP KO, ATF5 KO and TKO cells at 24 h and 48 h recovery, while ATF4 KO cells showed a more minor drop in PINK1 levels at 24 h R, and then a slight uptick in PINK1 levels at 48 h R, correlating with the increased mitophagy observed between 24 h R and 48 h R in ATF4 KO cells (Figures 6.2 A, 6.3). Overall, no clear defect between single transcription factor KOs and TKO cells in PINK1 levels was observed, suggesting the mitophagy defect in TKO cells lies downstream of this initiation stage.

As PINK1/Parkin mitophagy uses unique initiation machinery compared to other autophagy processes, defects in PINK1/Parkin mitophagy can be specific to the pathway. Alternatively, the defect could be via a generalised defect of the autophagy system that is appearing in PINK1/Parkin mitophagy analysis (*290*). Clarifying whether a defect is specific to PINK1/Parkin mitophagy can be undertaken by analysing mitophagy rates in alternative mitophagy pathways that act independently of the PINK1/Parkin machinery.
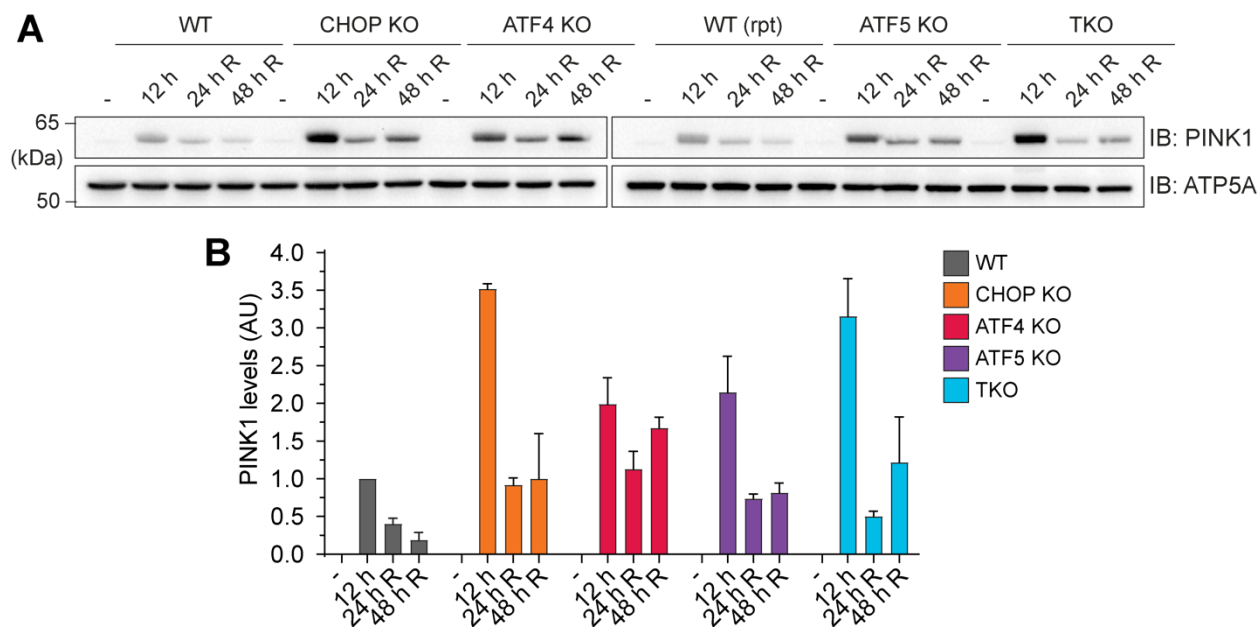
Figure 6.3 **Elevated levels of stabilised PINK1 are seen in UPR^{mt} deficient cells during G-TPP treatment and recovery**. **A**, **B**. Mitochondria were isolated from WT, CHOP KO, ATF4 KO, ATF5 KO and TKO cells treated with DMSO (-) or G-TPP (12 h) for 12 h, followed by a subsequent G-TPP washout and either 24 h or 48 h recovery (24 h R and 48 h R respectively). Levels of stabilised PINK1 were analysed by immunoblot (**A**) and quantified (**B**). PINK1 levels were quantified relative to WT 12 h G-TPP levels. Data in **B** was generated from three independent experiments.

Deferiprone (DFP) is an iron chelator which sequesters iron within mitochondria and triggers PINK1/Parkin-independent mitophagy (*295, 296*). WT, CHOP KO, ATF4 KO, ATF5 KO and TKO cells expressing YFP-Parkin and mtKeima were treated with DFP for 24 h prior to flow cytometry analysis to assess whether defective mitophagy in TKO cells is also observed in a PINK1/Parkin independent mitophagy pathway. No significant defect in DFP-induced mitophagy was detected in any single transcription factor KO or TKO cells, confirming generalised mitophagy is not defective in TKO cells (Figure 6.4 A).

While mitophagy from the DFP and PINK1 stabilisation assays appears functional, there could be a TKO-specific defect in activation of PINK1/Parkin mitophagy in response to a proteostatic stress. WT, single KO and TKO cells expressing YFP-Parkin and mtKeima were treated with Oligomycin (CV inhibitor) and Antimycin A (CIII inhibitor; OA) for 8 h to assess proteostasis damage independent PINK1/Parkin mitophagy. Minor defects in OA induced PINK1/Parkin mitophagy were observed in all single transcription factor cells and TKO cells (Figure 6.4 B). Although this indicates a deficiency in mitophagy in all transcription factor KO cell lines, the defects observed in PINK1/Parkin mitophagy with OA treatment do not match the elevated mitophagy seen with transcription factor KO during G-TPP treatment and recovery, and they do not match the mitophagy defect of G-TPP treated TKO cells (Figure 6.2 A). Due to the severity of OA induced mitochondrial stress compared to G-TPP treatment, each transcription factor KO cell line may possess unrelated defects in reaching maximal PINK1/Parkin mitophagy rates, but these defects do not appear to be impacting mitophagy activation at the levels observed during G-TPP treatment (*142*). The mitophagy defect in TKO cells therefore appears to be specific to proteostatic stress induced by G-TPP treatment.

Due to the prolonged time course of G-TPP treatment and recovery, the autophagy defect in TKO cells may lie further downstream at the lysosomal degradation or lysosome reformation stage of the mitophagy process which isn't apparent during the shorter treatment times used for DFP and OA induced mitophagy. A common mechanism of assessing lysosomal function during autophagy is to monitor the degradation of specific substrates in response to an autophagy trigger (*297*). To rule out a defect in the lysosomal machinery, the degradation of the substrate sequestome-1 (p62) through starvation-induced autophagy was assessed in each WT, single transcription factor KO and TKO cell line (Figure 6.4 C, D) (*297*). Cells were placed into standard media, or into media depleted of amino acids (EBSS) to induce a starvation state. After 8 h, the levels of p62 in each cell line in standard media and starvation media were assessed by immunoblot, and the percentage of p62 remaining after 8 h starvation period was calculated for each cell line (Figure 6.4 C, D). A
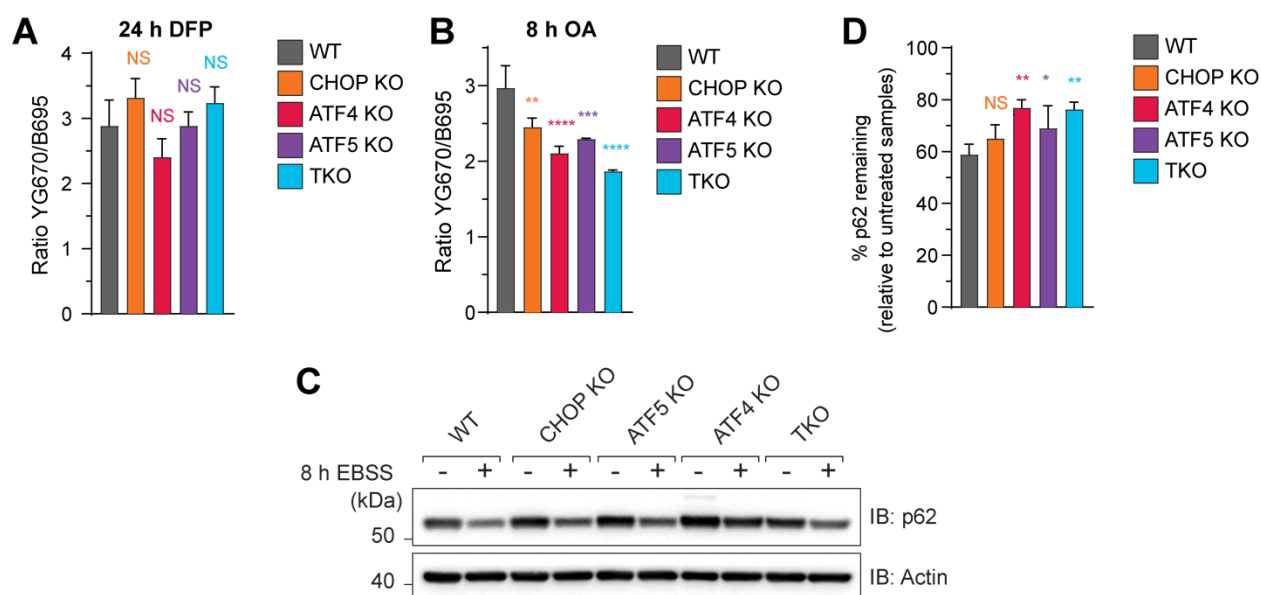
Figure 6.4 **TKO cells demonstrated a mitophagy defect that is specific to G-TPP induced mitophagy**. **A**, **B**. WT, CHOP KO, ATF4 KO, ATF5 KO and TKO cells stably expressing YFP-Parkin (see Figure 6.2 B) and mtKeima were treated with oligomycin and antimycin A (OA) for 8 h (**A**) or deferiprone (DFP) for 24 h (**B**) prior to FACS analysis. Emission ratios for each cell indicative of mitophagy rate were calculated per previously published methods and averaged across each biological repeat for each sample (*162*). Ratio increase values were calculated by subtracting DMSO treated control ratios from OA or DFP treated samples. **C**. WT, CHOP KO, ATF4 KO, ATF5 KO and TKO cells were placed into standard media (-) or Earle's Balanced Salt Solution (EBSS) to induce starvation autophagy for 8 h. p62 levels were analysed by immunoblot (**C**) and quantified (**D**). ****$P \leq 0.0001$, ***$P \leq 0.001$, **$P \leq 0.01$, *$P \leq 0.05$, NS $P > 0.05$ (one-way ANOVA). Data in **A**, **B**, **D** was generated from three independent experiments.

higher percentage of p62 remaining is indicative of a defect in autophagy-mediated degradation (*71*). Minor defects in p62 turnover were detected in each single transcription factor KO and TKO cell line, suggesting a minor defect at the autophagosome-lysosome fusion/degradation stage of the autophagy pathway with removal of each transcription factor (Figure 6.4 C, D). However, the magnitude of p62 degradation defects were similar between single transcription factor KO cells relative to TKO cells (Figure 6.4 C, D). Accordingly, the autophagy defect generating the p62 accumulation with UPR[mt] disruption still does not sufficiently explain the G-TPP induced mitophagy defect that was seen only in TKO cells.

Collectively, analysis of proteostasis-independent PINK1/Parkin mitophagy, PINK1/Parkin independent mitophagy, and autophagosome formation/lysosomal degredation has ruled out any clear, obvious mechanistic defects in the autophagy pathway as the cause of the mitophagy defect in the TKO cells. The cause of the G-TPP induced mitophagy defect in TKO cells remains to be determined.

6.5: Insight into CHOP, ATF4 and ATF5 mediated regulation of the autophagy machinery through transcriptional signatures

Although the G-TPP induced UPR^mt transcriptome analysis was performed at 12 h G-TPP treatment while the defect observed in TKO cells occurred in the recovery phase (Figure 6.2 A), the transcriptome analysis in Chapter 5 identified autophagy related processes as upregulated in expression by the UPR^mt (Chapter 5, Figure 5.5 C). In case the transcriptome analysis at 12 h G-TPP could point towards the origin of the TKO PINK1/Parkin mitophagy defect in the recovery phase of the UPR^mt, a detailed examination of autophagy-related transcriptomic trends and transcript changes at each stage of the autophagosome formation process was performed. The curated autophagy-related process database created by the Cecconi laboratory was used to identify autophagy-related genes altered in expression with UPR^mt induction (*298*). A proportionally larger than average number of autophagy related genes were altered through UPR^mt induction compared to the total genome changes observed in Figure 5.5 B of Chapter 5 (Figure 6.5 B). CHOP, ATF4 and ATF5 regulated the expression of ~47% of the autophagy related UPR^mt program (Figure 6.5 C). Genes requiring all CHOP, ATF4 and ATF5 for expression remained the largest subgroup of the transcription factor mediated UPR^mt program, representing genes involved in basal autophagy-candidate proteins, mTORC1 related genes, and RAB proteins required for autophagosome formation (Figure 6.5 E). Multiple areas of functional overlap were observed in the genes regulated by each transcription factor grouping. mTORC-related genes were observed in every gene grouping except for redundantly signalled genes (Figure 6.5 E). Genes relating to lysosomal function were observed in CHOP/ATF5, CHOP and ATF4 categories, while genes relating to the positive regulation of autophagy related processes were detected in CHOP/ATF4/ATF5, ATF4/ATF5 and ATF4 groupings (Figure 6.5 E). In fact, only three unique autophagy-related process groupings were identified across the analysis. Genes relating to the negative regulation of autophagy were exclusively seen in the CHOP/ATF5 grouping, while basal autophagy candidate proteins were only detected in the CHOP/ATF4/ATF5 combined regulatory group. The only process grouping identified in the small cluster of redundantly signalled genes that decreased in expression in TKO cells were mitophagy-associated genes (Figure 6.5 E). Two of these genes, UBE2L3 and VCP have been previously associated with driving membrane-potential damage driven PINK1/Parkin mitophagy, and will be discussed in more detail in Chapter 6.7 (*299-303*).

It is important to note that the mitophagy defect in TKO cells was only observed in the repair phase of the UPR^mt program. During the acute stress stage, TKO cells demonstrated similarly elevated
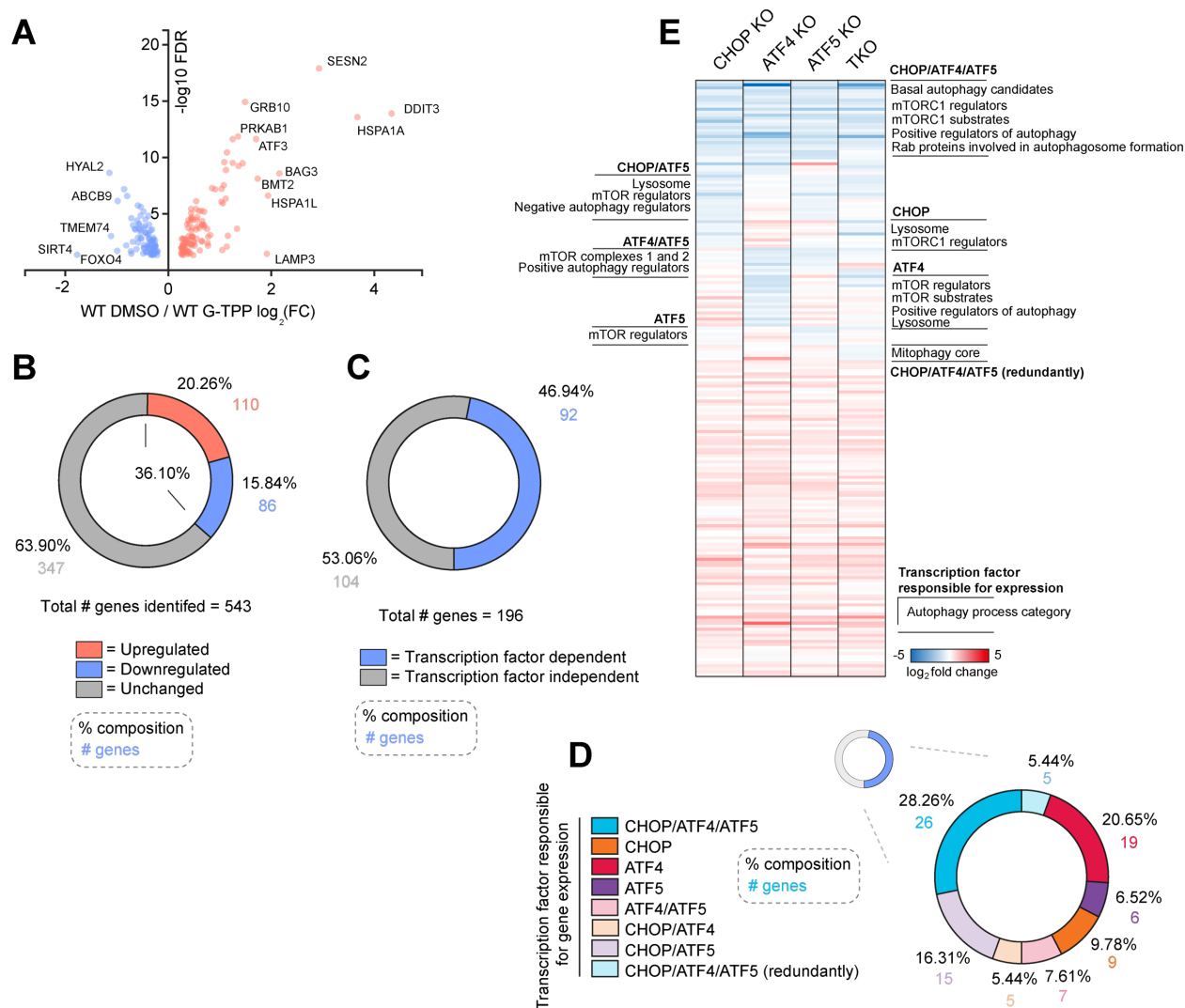
Figure 6.5 **G-TPP treatment induces a remodelling of autophagy-related gene expression which is partially under the control of CHOP, ATF4 and ATF5**. **A**, **B**. The WT UPR^mt program defined in Figure 5.6 (Chapter 5.4) was further filtered to show autophagy related genes. **A**. Autophagy related components of the UPR^mt program have been visualised by volcano plot and the 10 most highly enriched genes and 5 most highly depleted genes have been labelled. **B**. The proportion of the autophagy related genes identified which were enriched or depleted with UPR^mt activation in WT cells was quantified and is displayed by pie chart. **C** - **E**. Autophagy-related gene expression in the WT UPR^mt program defined in **B**. was compared to the gene expression in CHOP KO, ATF4 KO, ATF5 KO and TKO cells. Genes showing >-0.2 $\log_2$ fold decrease in expression relative to WT 12 h G-TPP levels were classified as being under the regulatory control of the transcription factor in question. **C**. The proportion of the autophagy-related UPR^mt transcriptome determined to be under the regulatory control of CHOP, ATF4 or ATF5, or independently expressed, was calculated and displayed by pie chart. **D**. The proportion of the autophagy related UPR^mt transcriptome determined to be under the control of one or more transcription factors was further separated into grouping according to the transcription factors required for expression. The relative proportional composition of these groups was then calculated and displayed by pie chart. **E**. Autophagy-related process groups in transcription factor dependent gene clusters with 2 or more genes belonging to that process group were labelled alongside transcription factor regulated clusters of the autophagy-related WT UPR^mt program displayed by heat map. Data in **A** – **E** was generated from three independent experiments.

mitophagy rates as each single transcription factor KO cell line (Figure 6.2 A). Prolonged mitophagy requires continual replenishment of autophagy factors since they are continually degraded along with their cargoes. Cumulative transcriptional depletion of multiple autophagy genes whose expression is driven by individual or dual transcription factor groupings could therefore lead to decreased autophagy flux in TKO cells. Several genes were identified across different autophagy processes that displayed cumulative loss in specific single or double transcription factor KO combinations, and in TKO cells. All autophagy genes whose expression was decreased in TKO cells were isolated and displayed by heat map (Figure 6.6). A few of the genes with depleted expression in TKO cells were structural genes related to autophagosome formation, but these were not specific to TKO cells (Figure 6.6). The primary gene clusters observed to be depleted in TKO cells related to the lysosome, the positive regulation of autophagy induction, and the select mitophagy-associated genes referenced earlier (Figure 6.6). Overall, it is difficult to determine mechanistically what may be driving the autophagy defect in TKO cells based on the transcriptomic data since a unique loss of key autophagy genes was not observed in TKO cells. More detailed analysis of the autophagy pathway, autophagy protein levels and transcript levels during the recovery phase of the UPR^{mt} program will be required to identify how each transcription factor is contributing to boosting PINK1/Parkin mitophagy in future studies.
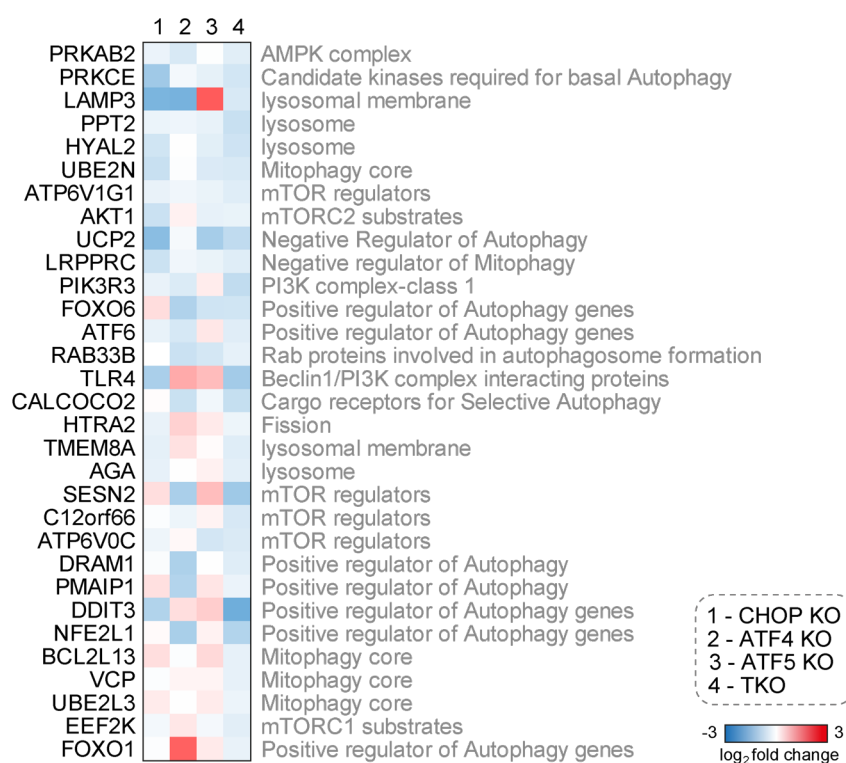
Figure 6.6 **Additive loss in expression of select autophagy related components is seen in TKO cells**. Autophagy components of the UPR^{mt} program which display loss in expression relative to WT 12 h G-TPP expression in TKO cells but not every single transcription factor KO cell (cont.)

line are displayed by heat map. Autophagy related processes for each gene have been displayed next to their position in the heat map. Data was generated from three independent experiments.

6.6: Establishing UPR^{mt} analysis in a primary neuronal system

Mitochondria are essential for cellular health and when mitochondrial quality control breaks down it predominately manifests as a neurological disease (*304*). For example, mutations in the genes encoding either PINK1 or Parkin causes Parkinson's disease which involves the death of dopaminergic neurons in the brain (*305, 306*). Neurons are post-mitotic cells that cannot be replenished, with a slow turnover of cellular components relative to other cells seen in our body (*307, 308*). During an acute proteostatic stress, neurons cannot dilute misfolded mitochondrial protein through mitochondrial biogenesis driven by cell division, meaning neurons may rely more heavily on the UPR^{mt} to maintain mitochondrial health. A large amount of energy is required to sustain neuronal function which places an increased demand on mitochondria (*309, 310*). Mitochondrial quality control machinery is therefore of critical importance in neurons to protect against mitochondrial-dysfunction triggered apoptosis (*311*). Direct study of the UPR^{mt} in mammalian neurons has not been performed to date, in part due to limitations in the experimental systems available. Accordingly, how the UPR^{mt} pathway facilities mitochondrial protection and repair in neurons, and whether there are neuron specific signalling dynamics between PINK1/Parkin mitophagy and the UPR^{mt} remains to be determined.

To set-up a pipeline to investigate neuronal UPR^{mt} signalling, primary cortical neurons were isolated from WT C57BL6/J post-natal mice. At DIV 14, neurons were treated with an acute time course of G-TPP prior to immunoblot analysis of CHOP, ATF4 and ATF5 expression (Figure 6.7). Initial experiments using the same concentration of G-TPP used in HeLa cells resulted in cell death within ~ 2 h (data not shown). Given this, concentration titrations were performed on the nanomolar scale to identify a suitable G-TPP concentration. Primary cortical neurons displayed clear CHOP and ATF4 induction which increased with treatment duration using 100 nM G-TPP (Figure 6.7). Minor ATF5 induction appears evident at 100 nM G-TPP, but to a lesser degree than was observed for CHOP and ATF4 (Figure 6.7). Surprisingly, a shut-down of UPR^{mt} signalling occurred at G-TPP concentrations above 100 nM. Signalling shutdown at higher G-TPP concentrations indicates the UPR^{mt} is tightly regulated and shuts down with excessive proteostatic stress.

The emergence of G-TPP as a method of triggering an endogenous proteostasis stress and the development of an experimental assay to analyse mitochondrial proteostasis were critical elements
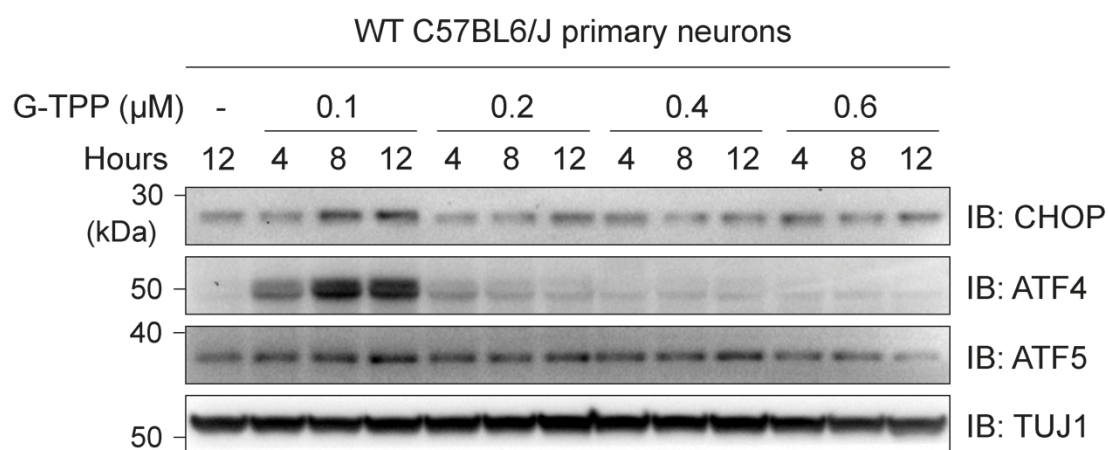
Figure 6.7 **G-TPP treatment triggers CHOP, ATF4 and ATF5 expression in cortical neuronal cells in a dose dependent manner**. Primary cortical neuronal cells were isolated from WT C57BL6/J P1 mice. At DIV 14, cells were treated with G-TPP for the indicated times at the indicated concentrations prior to sample collection. Levels of CHOP, ATF4 and ATF5 were analysed by immunoblot.

that facilitated in-depth investigation into the UPR^mt in this thesis. To confirm whether the solubility assay developed in Chapter 3 can be transferred to primary neuronal mitochondrial samples, mitochondria were isolated from WT C57BL6/J cortical neurons treated with 100 nM G-TPP for 8 h. The standard solubility assay protocol using 0.5% (v/v) TX-100/PBS lysis of mitochondria was performed (see Chapter 3), and the solubility of three mitochondrial proteins which displayed strong aggregation in HeLa cells were assessed by immunoblot (Figure 6.8 A). A very small reduction in the levels of soluble LRPPRC, AARS2 and GRSF1 were observed in the G-TPP treated mitochondrial samples, but no difference was observed in the insoluble fractions between the treatment conditions (Figure 6.8 A). The solubility of VDAC1, an outer membrane protein that is unaffected in solubility by G-TPP treatment in HeLa cells (Figure 4.3 B) was also analysed to ensure successful lysis of the mitochondrial samples had occurred. A significant level of VDAC1 was present in the insoluble protein fraction of these samples, indicating that the lysis conditions used were unsuitable to properly solubilise neuronal mitochondria into insoluble and soluble protein fractions (Figure 6.8 A). The inability of 0.5% (v/v) TX-100 to properly solubilise mitochondria suggests the lipid content of neuronal mitochondria is different to HeLa cells. Lysis in higher percentages of TX-100 was trialled to determine whether increased detergent concentration would enhance lysis while still allowing for isolation of insoluble protein. A titration of TX-100 concentrations up to 2% (v/v) TX-100/PBS were tested and the levels of VDAC1 were analysed in the insoluble fraction by immunoblot (Figure 6.8 B). Decreased levels of VDAC1 in the insoluble fraction were observed with increasing TX-100 concentrations, confirming that

membrane solubilisation was the issue as opposed to a lack of aggregation at the low concentrations of G-TPP used (Figure 6.8 B). As some VDAC1 was still precipitating into the insoluble fraction, a trial fractionation was performed in 5% (v/v) TX-100/PBS, and the levels of LRPPRC, GRSF1, AARS2 and VDAC1 were analysed by immunoblot (Figure 6.8 C). Almost no VDAC1 was observed in the insoluble fraction using 5% (v/v) TX-100/PBS lysis, confirming proper solubilisation of the mitochondrial membranes had occurred. An increase in insoluble fraction levels of LRPPRC, AARS2 and GRSF1 was observed with G-TPP treatment using the 5% (v/v) TX-100 lysis, confirming that G-TPP treatment in primary cortical neuronal cells causes mitochondrial protein aggregation similar to the trends observed in HeLa cells (Figure 6.8 C).
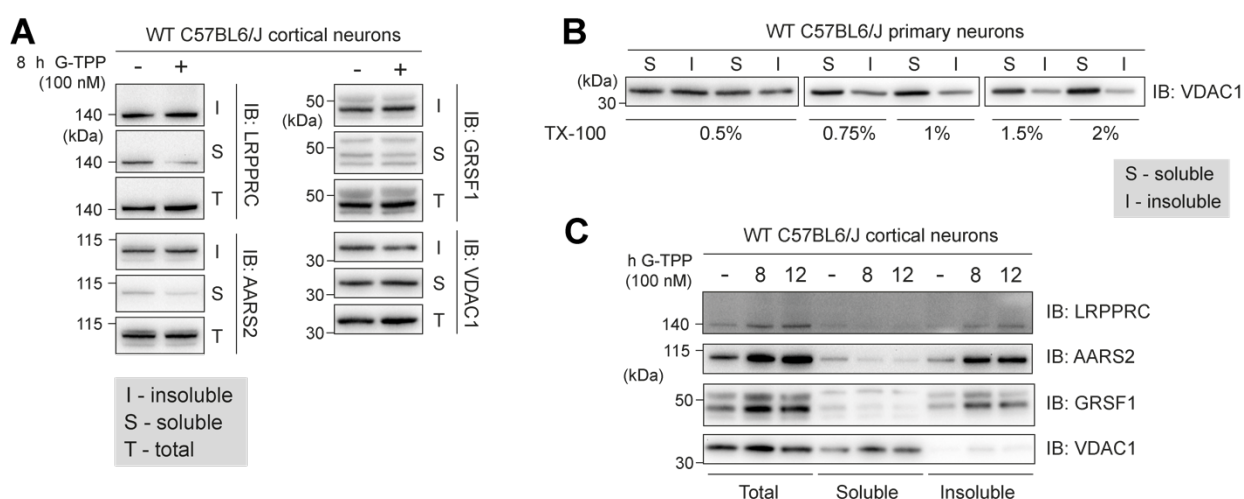
Figure 6.9 **G-TPP treatment causes changes in mitochondrial protein proteostasis in cortical neuronal cells**. **A**. Primary cortical neuronal cells were isolated from WT C57BL6/J P1 mice and treated with 100 nM G-TPP for 8 h prior to sample collection. Mitochondria were isolated from each sample prior to solubility fractionation (See Figure 3.6 A) using a 0.5% (v/v) TX-100/PBS based lysis. Expression of LRPRPC, AARS2, GRSF1 and VDAC1 in each fraction were analysed by immunoblot. **B**. Primary cortical neuronal cells were isolated from WT C57BL6/J P1 mice and treated with 100 nM G-TPP for 12 h prior to sample collection. Mitochondria were isolated from each sample prior to solubility fractionation using lysis buffers comprised of the indicated percentages of TX-100 in PBS. Levels of VDAC1 in each soluble and insoluble fraction of each lysate were analysed by immunoblot. **C**. Primary cortical neuronal cells were isolated from WT C57BL6/J P1 mice and treated with 100 nM G-TPP for the indicated times prior to sample collection. Mitochondria were isolated from each sample prior to solubility fractionation using a 5% (v/v) TX-100/PBS based lysis buffer. Expression of LRPPRC, AARS2, GRSF1 and VDAC1 in each fraction were analysed by immunoblot.

Confirmation of both transcription factor induction and mitochondrial protein aggregation shows that the neuronal-specific UPR^{mt} program is able to be detected and can now be analysed in future studies. With this experimental system established, the role of the UPR^{mt} and its contribution to maintaining mitochondrial health in neurons can now be defined. Neurons from WT, CHOP KO, Parkin KO, and Parkin/CHOP DKO mice which were generated over the course of this PhD will be valuable tools for future analyses.

6.7: Discussion

6.7.1: Insights into UPR^{mt} signalling through PINK1/Parkin mitophagy activity

The dominant mitochondrial quality control system that has been studied and implicated in disease pathology to date is PINK1/Parkin mitophagy. Although both PINK1/Parkin mitophagy and the UPR^{mt} have been observed to respond to the same stimuli, whether there is cooperation in the signalling of their pathways has remained unclear (*11, 173*). The signalling analyses in this chapter indicate that there is indeed signalling communication between the two pathways, but that communication is unidirectional. No changes in the induction of CHOP, ATF4 or ATF5 were observed in the presence or absence of mitophagy in either the acute stress period or the repair period following stress removal (Figures 6.1, 6.2). A lack of influence of mitophagy on the UPR^{mt} is somewhat unexpected, as PINK1/Parkin mitophagy was previously shown to be specifically recruited to aggregates of ΔOTC in HeLa cells (*11, 173*). Accordingly, PINK1/Parkin mitophagy would presumably reduce some of the protein aggregate stress load in mitochondria through the mitophagy activity that was confirmed to be occurring (Figure 6.2 A). If protein aggregation levels are propagating the UPR^{mt} signal, a mitophagy mediated reduction in protein aggregates might be expected to decrease transcription factor expression and UPR^{mt} activity. Instead, no changes in transcription factor levels were observed with PINK1/Parkin mitophagy degrading mitochondria (Figure 6.1).

As discussed in Chapter 3, ΔOTC is an exogenously expressed mitochondrial protein. It remains to be confirmed whether Parkin is recruited to endogenous protein aggregates within mitochondria. Further, it remains to be established whether G-TPP triggered PINK1/Parkin mitophagy could be degrading dysfunctional mitochondrial segments that do not necessarily contain protein aggregates. Clarifying the nature of mitochondria degraded by PINK1/Parkin mitophagy during proteostasis stress is critical to understand the signalling triggers of the UPR^{mt} program. DELE1 cleavage by OMA1 has been shown to signal mitochondrial stress through the release of cleaved

DELE1 from mitochondria, but how misfolded protein begins this process is unknown (*104, 105*). If PINK1/Parkin mitophagy degrades protein aggregates, the data in this Chapter would indicate a functional change triggered by proteostasis stress is signalling the UPR^mt, as aggregate removal is not affecting UPR^mt signalling in this scenario. On the other hand, if PINK1/Parkin mitophagy is not directly degrading protein aggregates but is instead degrading dysfunctional mitochondrial segments, the data in this chapter would suggest protein aggregates are directly initiating and propagating UPR^mt signalling. Future analysis of mitochondrial proteostasis in the presence and absence of PINK1/Parkin mitophagy, and microscopy analysis of the cargo delivered to lysosomes by PINK1/Parkin mitophagy will provide valuable insight into the mitochondrial derived signalling of the UPR^mt.

6.7.2: UPR^mt regulates PINK1/Parkin mitophagy activity

While PINK1/Parkin mitophagy did not influence UPR^mt signalling, UPR^mt signalling did influence PINK1/Parkin mitophagy activity. Mild elevation of mitophagy levels were observed during acute stress with UPR^mt disruption relative to WT controls (Figure 6.2 A). Mitophagy was sustained up to the 24 h R time point in WT cells, while a strong increase in mitophagy over 12 h G-TPP levels was observed during the repair phase of the UPR^mt in transcription factor KO cells (Figure 6.2 A). The elevated or sustained mitophagy levels observed in the recovery phase do not mirror the proteostasis trends of each cell line observed in Chapter 4 (Figure 4.3 C). However, the elevation of mitophagy levels with removal of a single transcription factor correlates with a response that is dependent on the severity of the protein aggregation occurring since single transcription factor KO cells had higher protein aggregation loads relative to WT (Figure 4.3 C). Elevation of mitophagy during UPR^mt repair appears to be an active component of the UPR^mt that is redundantly regulated by each CHOP, ATF4 and ATF5, since elevated mitophagy occurs in all single transcription factor KO cells but not in TKO cells (Figure 6.2 A). This transcription factor dependent induction of mitophagy is specific to a proteostasis stress as OA induced mitochondrial damage does not replicate these mitophagy trends (Figure 6.4 B). These data reveal a previously unidentified signalling relationship that involves UPR^mt mediated induction of PINK1/Parkin mitophagy. Whether artificially elevated UPR^mt signalling could boost mitophagy activation is an interesting concept for future investigation that could have potential therapeutic effects.

It is mechanistically unclear how CHOP/ATF4/ATF5 are boosting PINK1/Parkin mitophagy. No TKO specific defects were observed in PINK1 accumulation, OA induced PINK1/Parkin mitophagy or PINK1/Parkin-independent mitophagy, indicating that the autophagy pathway is still

operating properly in TKO cells (Figures 6.3, 6.4). As mitophagy is not completely ablated in TKO cells and is still elevated above WT mitophagy levels at 24 h and 48 h recovery, the defect could lie in the ability of TKO cells to sustain high levels of mitophagy activity (Figure 6.2 A). Each transcription factor could be contributing to sustained mitophagy activation through additional transcription of the autophagy machinery. Due to the degradative nature of the autophagy process, continual replenishment of autophagy related proteins is required for sustained activation. However, most genes cumulatively lost in TKO cells were genes involved in autophagy regulation rather than structural autophagy genes (Figure 6.6). Of the transcripts lost in TKO cells, most were involved in the positive regulation of autophagy and in mTORC activation (Figure 6.6). While mTORC1 signalling is not required for PINK1/Parkin mitophagy activity, the elevated mitophagy rates with recovery may occur in part through an active upregulation of supporting autophagy processes (*65*). Forkhead-box class O1 (FOXO1) is a transcription factor that was decreased in expression specifically in TKO cells (Figure 6.6). Expression of FOXO1 has been shown to promote autophagy gene transcription in cardiomyocytes and facilitate PINK1 transcription in podocytes (*312, 313*). If FOXO1 is performing similar roles to those identified in primary murine cells in the context of the UPR^{mt} program, its expression in single transcription factor KO cells but not TKO cells suggests the levels of autophagy transcripts could still be a potential mechanism of the sustained mitophagy defect observed in TKO cells. The FOXO1 expression trends identified in Figure 6.6 may be having a delayed impact on transcription of structural autophagy proteins that was not captured at the 12 h G-TPP timepoint of the transcriptomic analysis. Analysis of the G-TPP induced transcriptome changes at later time points during the recovery stage of the UPR^{mt} may be required to identify the mechanistic cause of the failure to sustain mitophagy rates in TKO cells.

A small group of mitophagy related proteins (BCL2L13, UBE2L3, VCP) were decreased in expression in TKO cells but not in single transcription factor KO cells (Figures 6.5, 6.6). BCL2-like 13 (BCL2L13) has been identified as the mammalian homologue of the mitophagy protein Atg32 in *S. cerevisiae* (*314, 315*). While BCL2L13 was shown to function in mitophagy, it functions independently of the PINK1/Parkin mediated pathway (*314, 315*). On the other hand, both UBE2L3 and VCP have been identified as functioning in the PINK1/Parkin mitophagy pathway through facilitating Parkin recruitment in the context of UBE2L3, and in promoting mitophagy downstream of the PINK1 and Parkin initiation through VCP (*299-303*). TKO specific depletion of UBE2L3 and VCP transcripts could be decreasing the efficiency of PINK1/Parkin mitophagy, representing another potential mechanism though which PINK1/Parkin mitophagy activity is decreased in TKO cells. Further biochemical characterisation will be required to clarify

whether decreased levels of these PINK1/Parkin mitophagy specific proteins are causing the TKO specific defect in sustained mitophagy.

Previous publications have observed eIF2α phosphorylation with mitochondrial stress which can play a global role in shutting down translation (*101, 104*). Both PGAM5 cleavage and ATP levels analysed in Chapter 5 indicated that TKO cells experienced the most severe mitochondrial stress out of the transcription factor KO cells (Figures 5.2, 5.3). While eIF2α phosphorylation in response to G-TPP treatment hasn't been previously shown, if there is a more severe and prolonged global translational shutdown in TKO cells then a failure to adequately translate sufficient copies of structural autophagy transcripts could also be producing a TKO specific failure of sustained mitophagy rates. Analysis of autophagy protein levels in TKO cells during the recovery phase of the UPR^mt would help clarify whether the issue of sustained mitophagy lies in decreased protein production in TKO cells.

While the data in this thesis has not precisely clarified the mechanistic reason for the TKO specific mitophagy defect, it has pointed toward multiple different avenues in which a TKO-specific failure in sustained mitophagy could be occurring during G-TPP treatment. The scenarios produced from this data have provided multiple potential directions for follow up investigations into the mechanisms through which the UPR^mt is promoting PINK1/Parkin mitophagy activity.

6.7.3: Could ROS regulate PINK1/Parkin mitophagy induction during G-TPP treatment?

A curious phenomenon observed in the mitophagy data is the apparent regulatory switch between mild mitophagy induction in all cells during acute G-TPP treatment, and an elevation in mitophagy levels after G-TPP removal during the recovery phase (Figure 6.2 A). These trends contradict the proteostasis trends observed between these two phases of the UPR^mt program, meaning something other than proteostasis is likely mediating these dynamics (Chapter 4, Figure 4.3 C). PINK1 levels were seen at their highest in all cell lines at 12 h G-TPP treatment but mitophagy rates did not peak at that time point (Figures 6.2 A, 6.3). Accordingly, something must be supressing mitophagy activation during the acute stage, or facilitating further mitophagy activation in the repair phase that is altering PINK1 activity on mitochondria. PINK1 has been observed in HeLa cells to form a dimer in response to oxidation, which can inhibit PINK1 activity at high levels of oxidative stress (*316*). While it has not been established whether misfolded mitochondrial protein trigger excessive generation of reactive oxygen species (ROS), dysfunction of the OXPHOS machinery can to lead

to excessive ROS production (*317-320*). Significant OXPHOS dysfunction was observed at 12 h G-TPP treatment that was worsened in transcription factor KO cells (Chapter 5, Figures 5.3, 5.4). Potentially, an increase in ROS by 12 h G-TPP treatment through OXPHOS dysfunction is leading to the oxidation of PINK1 and inhibiting PINK1 activity during acute G-TPP treatment. ROS production mediated by OXPHOS dysfunction in literature involves assembled OXPHOS complexes that aren't operating correctly due to functional perturbations within the mitochondria (*317-320*). While CI aggregation in WT cells centred around the peripheral N- and Q- modules, transcription factor KO cells had aggregation of CI modules that sit close-to, and within the IMM, suggesting a more wide-spread structural collapse in CI (Chapter 4, Figures 4.8 B, 4.10). The OXPHOS machinery in transcription factor KO cells may reach a point where it is too severely damaged at a structural level to continue to produce excessive ROS. The subsequent elevation in mitophagy during the repair phase may be occurring through dissipation of the initial ROS produced coupled with the OXPHOS machinery being too damaged to produce ROS. Future investigations into G-TPP induced ROS production and the oxidation state of PINK1 during the acute stress and recovery stages of the UPR^{mt} will help further clarify this potential mechanism of mitophagy regulation. However, if ROS production and dissipation alone was modulating mitophagy dynamics, TKO cells which showed equally severe proteostasis defects and OXPHOS collapse should still show similar elevated mitophagy levels. The evident defect in mitophagy induction in the repair phase of the UPR^{mt} in TKO cells indicates that even if ROS production is contributing to mitophagy dynamics during the acute stress stage, it is not the sole regulatory factor of mitophagy activity in this context.

6.7.4: Does proteostasis repair require PINK1/Parkin mitophagy?

Typically, mitophagy is thought to respond to severe mitochondrial dysfunction to mitigate the release of cytotoxic factors. In contrast, UPR^{mt} mediated repair enables mildly dysfunctional mitochondria to remain in a cell and avoid mitophagy-mediated degradation. Identification of mitophagy activation in response to G-TPP induced proteostasis stress that triggers the UPR^{mt} program raises questions about what roles PINK1/Parkin mitophagy is playing in repairing the mitochondrial network. Potentially G-TPP treatment may exert a mosaic stress load across the mitochondrial network. Some mitochondria may be more severely damaged than others and unable to undergo repair, necessitating PINK1/Parkin mitophagy to remove those mitochondria. If mitophagy was only responding to severe mitochondrial damage, then a mild proteostasis stress may not trigger mitophagy.

Alternatively, PINK1/Parkin mitophagy may play an active role in restoring proteostasis by degrading mitochondria that are not severely damaged. It was noted in Chapter 4 that specific CI subunits in WT cells appeared resistant to UPR^mt mediated proteostasis repair, and these subunits corresponded to proteins previously observed to be accumulated in PINK1/Parkin mitophagy deficient samples (Figure 4.8 C) (*149, 196, 197*). Multiple other protein groups, including Ribosome assembly, tRNA-processing related, and Pyruvate metabolism related proteins also displayed repair-resistant aggregation trends in WT cells (Chapter 4, Figure 4.14). To date, these groups have not been linked to PINK1/Parkin mitophagy based regulation. However, since they follow similar trends to the CI proteins known to be turned over by PINK1/Parkin mitophagy, they could represent a novel subset of mitochondrial proteins that require PINK1/Parkin mitophagy for proteostasis maintenance. If there is indeed a subset of mitochondrial proteins that cannot be repaired by the UPR^mt alone, this could help explain the function of the UPR^mt-signalled mitophagy induction observed in this Chapter (See Chapter 6.7.2). An active role of the PINK1/Parkin mitophagy pathway in cleaning up protein aggregates within the mitochondrial network could represent new ways of cytotoxic mitochondrial dysfunction developing in neurons with impaired PINK1/Parkin mitophagy. To understand the role of PINK1/Parkin mitophagy in responding to proteostasis stress, it will be important to clarify how protein aggregation patterns change in cells with PINK1/Parkin mitophagy activity, particularly at the 48 h recovery time point in WT samples that saw incomplete proteostasis restoration through the UPR^mt alone. If PINK1/Parkin mitophagy is required to restore proteostasis of a subset of proteins that are perhaps particularly insensitive to chaperone and protease activity, it will be imperative to study these pathways in tandem in future studies assessing mitochondrial proteostasis.

6.7.5: UPR^mt activity is conserved in cortical neurons

While PINK1/Parkin mitophagy has been decisively linked to dopaminergic neuron degeneration, UPR^mt activity had not been shown in neuronal cells prior to this thesis. The detection of similar transcription factor signalling patterns to those seen in HeLa cells with G-TPP treatment has confirmed that the UPR^mt appears active in cortical neurons and is also tightly regulated with severe proteostatic stress leading to a shutdown of UPR^mt signalling. Understanding UPR^mt mediated contributions to mitochondrial health in neurons is important to facilitate our understanding of mitochondrial quality control in neurodegeneration. Whether boosted UPR^mt activity could protect against mitochondrial dysfunction in neurons, or if defects in unidentified UPR^mt components can contribute to neurodegeneration are interesting, important questions for

future analysis. Interestingly, it was observed that cortical neurons were much more sensitive to G-TPP treatment, requiring ~90x less G-TPP to induce detectable protein aggregation and UPR^{mt} signalling in neurons. More aggregation with less G-TPP treatment suggests neuronal mitochondria may have an inherently lower protein folding capacity buffer, and so mitochondrial protein aggregation may be much more pathological in nature in neurons than in other cell types. A more sensitive proteostasis system could mean certain physiological triggers may cause proteostasis stress in neurons that other cell types and tissues can tolerate. Accordingly, it will be important to contextualise proteostasis stress triggers in the context of a neuronal system when studying the biological role of the UPR^{mt} in protecting cellular health.

Analysis of transcriptome changes during the UPR^{mt} in HeLa cells indicated the conservation of UPR^{mt} mediated Wnt signalling and immune responses in mammalian cells, similar to those observed in *C. elegans* (*76, 246, 251*). Neurons within the brain are supported by the activities of multiple other cells, including astrocytes and microglia which are immune cells that mediate protection of the neuronal environment (*321*). Recently, evidence has started accumulating implicating neuroinflammation as a driving factor of neurodegeneration (*124, 322, 323*). The UPR^{mt} transcriptome characterised in this thesis present an interesting potential link between mitochondrial dysfunction and the neuro-immune system. If Wnt signalling is confirmed in future studies to facilitate the transmission of mitochondrial stress between cells in mammals, excessive UPR^{mt} activity may trigger a neuro-immune response by upregulating immune related processes in astrocytes and microglia. Whether a proteostasis-stress induced neuro-immune response is protective for neuronal health, or whether it would propagation of neuro-inflammation mediated neurodegeneration would require further analysis. The neuronal UPR^{mt} opens a new door into our analysis of mitochondrial quality control and stress dynamics in neurodegeneration and PD. While there are some similarities with UPR^{mt} activity in HeLa cells, the potentially unique proteostasis dynamics and regulatory signalling processes identified in cortical neurons necessitate future study of the neuronal UPR^{mt} to be also performed in a neuronal system. With the tools developed in this thesis, analysis of the neuronal UPR^{mt} is now feasible for future studies to tackle.

Chapter 7

Concluding remarks and future directions

7.1: Discussion

Mitochondrial function is an essential facet of cellular health which is maintained by the mitochondrial quality control machinery. Of the two major pathways that comprise the mitochondrial quality control machinery, the PINK1/Parkin mitophagy pathway has been comprehensively mapped out at a molecular level in recent years while our understanding of the UPR^{mt} has comparatively lagged behind. A combination of experimental limitations have factored into this large gap in literature. Firstly, there were few ways available to trigger an isolated protein folding stress within mitochondria. The techniques widely used involved exogenous protein expression or perturbation other aspects of mitochondrial function but not specifically the proteostasis machinery. These techniques produce compounding cellular stress signals that make it difficult to identify the signalling signatures of the UPR^{mt}. Additionally, no methods were available to analyse the proteostasis damage and repair of endogenous mitochondrial proteins, preventing study of the functional roles of the UPR^{mt} program.

This thesis started out with two main aims: first, to clarify the relationship between the three transcription factors that had been independently identified as functioning in the UPR^{mt} (CHOP, ATF4, ATF5), and second, to improve our understanding how PINK1/Parkin mitophagy and the UPR^{mt} interact when regulating mitochondrial health. Due to the technical advancements made in this thesis, the scope of study managed to extend past simply examining the transcription factor relationships. Instead, a broad characterisation of the functional activities of the UPR^{mt} were achieved to an unprecedented level. The in-depth characterisation of the UPR^{mt} program subsequently facilitated identification of a new role of the UPR^{mt} in maintaining sustained PINK1/Parkin mitophagy during proteostasis repair.

7.1.1: Current mechanistic understanding of the mammalian UPR[mt]

Prior to this thesis, we had a limited mechanistic understanding of the mammalian UPR[mt]. DELE1 was understood to be released from mitochondria through OMA1-mediated cleavage, which through interacting with the enzyme HRI led to the expression of CHOP, ATF4 and ATF5 (*104, 105*). Induction of these three transcription factors then boosted levels of mitochondrial chaperones and proteases, completing the UPR[mt] program (summarised in Figure 7.1) (*77, 95, 101*). How CHOP, ATF4 and ATF5 collectively contribute to the UPR[mt], what drives the mitochondrial specificity of the transcriptional program, and what happens on a functional level before, during and after the UPR[mt] was unknown. Information in this thesis has filled in multiple gaps in our mechanistic understanding of the UPR[mt] program, leading to the generation of a new, more detailed model that is summarised below.

Current understanding of the UPR[mt]:

Following G-TPP treatment, the protein folding capacity of mitochondria is reduced which leads to the accumulation of misfolded mitochondrial proteins. Specific subsets of mitochondrial proteins show elevated sensitivity to protein folding stress, including the mitochondrial ribosome, transcriptional machinery, and particularly CI of the OXPHOS machinery (Chapter 4). Collapse of the functional proteome with protein folding stress leads to a depletion of OXPHOS-generated ATP and a metabolic rewiring preferencing ATP production away from OXPHOS and towards glycolysis (Chapter 5). Following the accumulation of misfolded protein, DELE1 is cleaved by OMA1 and released to the cytosol (*104, 105*). DELE1 activation and release drives increased expression of CHOP, ATF4 and ATF5, either through elevated mRNA levels (CHOP, ATF4) or increased protein production/decreased protein turnover (ATF5) (Chapter 4). Each one of CHOP, ATF4 and ATF5 then induce transcriptional programs with mixed induction patterns comprising genes that require all three transcription factors for expression, two transcription factors for expression, one transcription factor for expression or that are redundantly expressed by each transcription factor (Chapter 5). The CHOP/ATF4/ATF5 regulated portion of the UPR[mt] accounts for ~ 56% of all UPR[mt]-driven transcriptional changes. The remaining 44% of transcriptional changes are driven by yet-unidentified signalling factors (Chapter 5). Collectively, these genetic changes increase the expression of the mitochondrial pathways including chaperone and protease system and folate and vitamin metabolism related genes, while decreasing expression of OXPHOS and transcription/translation related genes (Chapter 5). At a cellular level, significant transcriptional changes also occur through the UPR[mt], including increased expression of the

proteasomal system, cytosolic chaperones, immune related pathways, autophagy, and histone demethylation related genes. Decreased expression of histone methylation, cell cycle and transcription related genes are also observed (Chapter 5). The UPR^{mt} also drives sustained PINK1/Parkin mitophagy in the repair phase of the UPR^{mt} (Chapter 6). Collectively, these changes comprise the UPR^{mt} program. Following stress removal, the transcriptional changes driven by the UPR^{mt} lead to proteostasis repair. Different levels of UPR^{mt} mediated proteostasis protection and repair are seen across different groups in the mitochondrial proteome (Chapter 4). For example, OXPHOS proteins show only a small increase in aggregation during acute stress in UPR^{mt}-defective cells, but there are essentially no signs of proteostasis recovery in the absence of the UPR^{mt} (Figures 4.5, 4.6 B). The differential activities of the UPR^{mt} during acute stress and following stress removal position the UPR^{mt} as a bimodal program. The UPR^{mt} plays a role in protecting the mitochondrial proteome from proteostasis collapse during an acute stress, and then facilitates the recovery of the mitochondrial proteome during the repair phase of the UPR^{mt}. In cells with a functional UPR^{mt}, select proteins comprising subunits of CI, translation, tRNA processing and pyruvate metabolism were unable to be completely repaired through UPR^{mt} activity (Chapter 4). A schematic overview of our new understanding of the UPR^{mt} has been provided in Figure 7.1.

While significant advancements have been made in our mechanistic understanding of the UPR^{mt}, more remains to be discovered. Areas of future research include understanding what drives the mitochondrial specificity of the UPR^{mt} separate from DELE1, determining how protein folding stress specifically triggers OMA1 activation, and identifying the transcription factors that drive the CHOP/ATF4/ATF5 independent portion of the UPR^{mt} program.
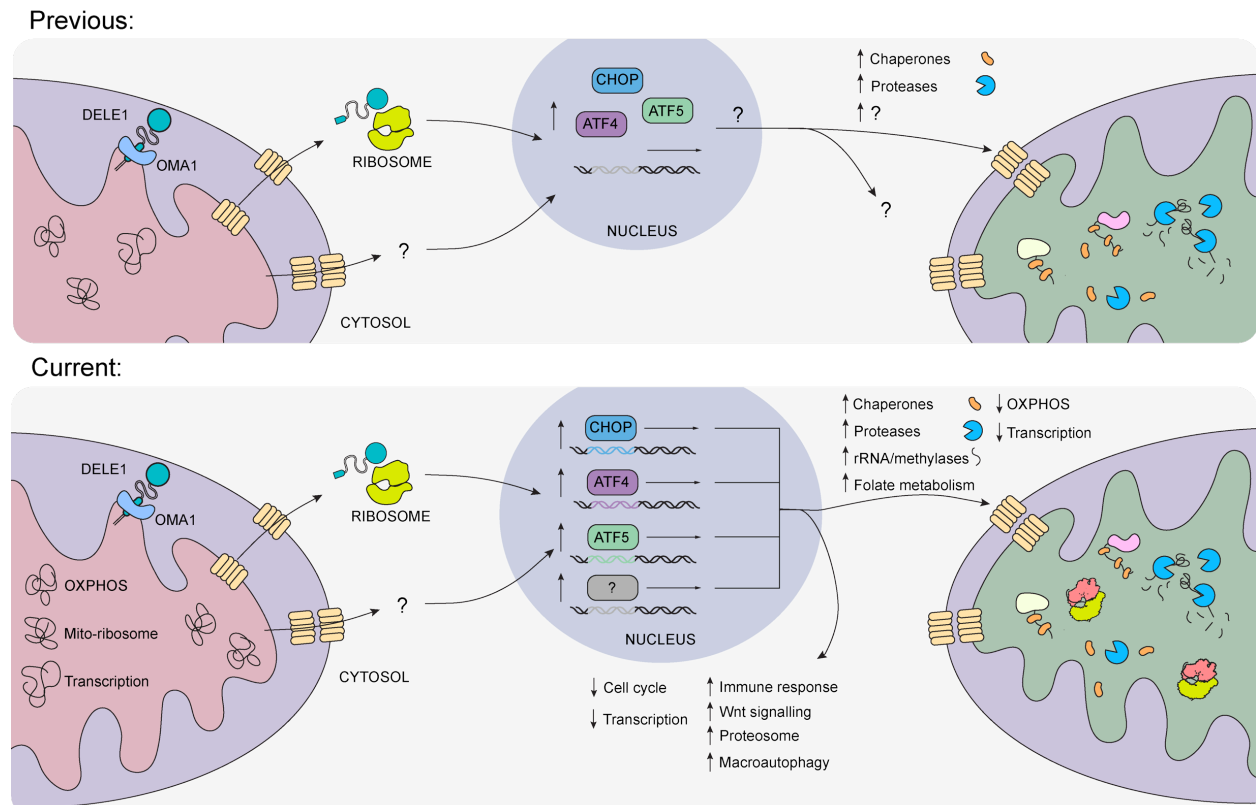
Figure 7.1 **Summary of our updated understanding of the mammalian UPR^{mt} based on the work in this thesis**. (*Previous*) Prior to the work in this thesis, the mammalian UPR^{mt} was understood to comprise the cleavage and release of DELE1 following the development of a protein folding stress. DELE1 then interacts with HRI, which causes phosphorylation of the ribosomal subunit eIF2α and an attenuation of cytosolic translation. This leads to the increased expression of CHOP, ATF4 and ATF5 that collectively drive a transcriptional program that boosts chaperone and protease expression, repairing mitochondrial health. (*Current*) A decreased mitochondrial protein folding capacity triggers a proteostasis collapse, strongly affecting components of the OXPHOS machinery, the mitochondrial ribosome and transcriptional machinery. Aggregation of these components of the mitochondrial proteome trigger DELE1 cleavage and release, which leads to the independent expression of CHOP, ATF4, ATF5 and other unidentified transcription factors. At a cellular level, these transcription factors drive an increase in expression of immune responses, Wnt signalling, the proteosome, macroautophagy pathways and the cytosolic chaperone system in addition to other gene pathways, while decreasing expression of cell cycle and transcription related genes. At a mitochondrial level, these transcription factors drive the increased expression of chaperones, proteases, folate metabolism and rRNA methylation related genes in addition to other gene groups (see Chapter 5), while increasing rRNA expression. Levels of OXPHOS and transcription related genes are reduced through UPR^{mt} activity. Collectively, these changes improve mitochondrial proteostasis and repair mitochondrial function. Each genetic program driven by CHOP, ATF4 and ATF5 is essential for UPR^{mt} mediated proteostasis protection and repair. Select cellular and mitochondrial pathways have been displayed in Figure 7.1; a more comprehensive list of genetic trends is found in Chapter 5.

7.1.2: Experimental toolbox to study the mammalian UPR^mt

Many of the advancements made in this thesis were made possible by establishing a comprehensive experimental workflow that allows for specific UPR^mt induction, and quantification of the functional changes to the mitochondrial proteome mediated by the UPR^mt.

An essential element to studying the UPR^mt which had proven problematic in earlier research is the ability to trigger a misfolded mitochondrial protein stress in isolation of other cellular stressors. While such a stressor may not necessarily reflect what would occur in a physiological setting, to understand the mechanisms and transcriptional changes behind the UPR^mt we must be able to isolate UPR^mt signalling from signalling produced by other stress response pathways. Shortly prior to the commencement of this work, G-TPP had been characterised as a method of inducing an isolated mitochondrial protein folding stress through pharmacological inhibition of mitochondrial HSP90 (*102, 142*). Work in this thesis has validated that G-TPP induces an acute protein folding stress that triggers isolated UPR^mt signalling and the induction of a transcriptional program that drives mitochondrial proteostasis repair (Chapters 3 – 5). Additionally, G-TPP can also be washed out of cells to remove the proteostasis stress on a short dynamic scale, allowing for study of both the protection and repair phases of the UPR^mt (Chapter 4). Varying transcriptional signatures have been produced in mitochondrial stress experiments performed across literature. Compared to the published transcriptomes available, the G-TPP induced UPR^mt transcriptional program analysed in Chapter 5 has produced more similarities to the well characterised *C. elegans* UPR^mt transcriptome changes than other previous studies (see Chapter 5.8.2). While some divergence would be expected due to the divergence in the signalling molecules driving these changes, G-TPP is highly specific at producing isolated mitochondrial protein folding stress. Similarities with the *C. elegans* program, which are unique to G-TPP treatment conditions compared to other less 'pure' methods of inducing proteostatic stress, suggest these similarities may be a point of conservation between the two programs. These similarities reinforce the essential need to use a highly specific method of proteostatic stress induction when studying the UPR^mt.

A somewhat unique aspect of the UPR^mt that has also hampered progress in study of the pathway lies in the nature of the stressor. Protein folding stress is specifically problematic to measure using standard analysis techniques as it does not necessarily alter protein levels within a cellular compartment. Instead, protein folding stress alters the levels of functional, properly assembled proteins that are available to a cell which can have severe phenotypic consequences. Measuring raw changes in protein abundance does not capture this additional dimension of protein function, meaning standard analytical assays such as whole lysate quantitative proteomics and western

blotting are not ideal readouts of UPR^{mt} activity. When the role of the UPR^{mt} is to repair damage from a protein folding stress, the proteostasis of an individual protein is the important quantitative metric when measuring effective UPR^{mt}-mediated repair, rather than changes in absolute protein levels. The mass spectrometry-based assay developed in this thesis addresses this fundamental problem in UPR^{mt} analysis (Chapter 3). The experimental pipeline developed in Chapter 3 allows for simultaneous quantification of the proteostasis of every detected mitochondrial protein. This allows not only for quantification of proteostasis damage at a specific point in time, but it also allows for the generation of a temporal measurement of the rate proteostasis repair, in addition to allowing for comparison of proteostasis across cell type, treatment conditions, or tissues. It is highly transferrable across different experimental systems and will be able to be utilised by other research groups to facilitate future study of the mammalian UPR^{mt}.

The analytical techniques developed in this thesis will not just be useful to the field of UPR^{mt} study. Although function is arguably the most critical aspect of a protein, it is frequently overlooked in many different types of analysis used in different fields of study since all standard quantitative proteomic assays and western blotting experiments miss this additional dimension of analysis. For UPR^{mt}-independent stress-related analysis, this poses a significant issue since cellular stressors could have confounding effects on proteostasis that need to be accounted for when interpreting results. For example, increased levels of the cytosolic ribosome would suggest increased translational capacity. However, if most of the cytosolic ribosome is aggregating, this would produce a very different phenotype of reduced cellular translation, highlighting the importance of considering protein function. Another area of study where functional analysis of proteins is particularly important is in signalling analysis. As signalling cascades often entail post-translational modification (PTM) changes, measuring only protein levels can miss signalling pathway activation. Work by the Picotti laboratory has made significant advancements in furthering functional proteomic analysis in the context of signalling cascades through generation of mass-spectrometry based pipelines that detect structural changes within proteins on a proteomic scale (*324*). The assay developed in this thesis provides a complimentary method to quantitatively analyse proteostasis, another component of protein function, to help further the field of functional proteomic analysis.

Collectively, the experimental tools characterised and developed in this thesis make accessible a field of study that was not sparse through a lack of interest, but through a lack of adequate analytical techniques. The G-TPP treatment, washout, and proteostasis analysis workflow will now allow us to monitor UPR^{mt} activity in other settings and physiological systems.

7.1.4: Integrating PINK1/Parkin mitophagy with the UPR^mt

As mentioned in the introductory writing of this thesis, the UPR^{mt} does not operate in isolation, and neither does PINK1/Parkin mitophagy (Chapter 1). To understand how each pathway contributes to maintaining mitochondrial health, particularly in the context of neuronal health, we must understand the interactions between these pathways.

While both PINK1/Parkin mitophagy and the UPR^{mt} respond to the same stimuli, work in this thesis has demonstrated that there is a unidirectional signalling relationship between the two pathways. PINK1/Parkin mitophagy activity does not influence UPR^{mt} signalling induction or shutdown during recovery. However, CHOP, ATF4 and ATF5 together regulate sustained mitophagy during the repair phase of the UPR^{mt} through a mechanism that was unable to be identified in the scope of this thesis (Chapter 6). The lack of influence of PINK1/Parkin mitophagy on UPR^{mt} signalling supports the idea that these pathways act in a somewhat linear manner, with the UPR^{mt} activated first in response to mild proteostasis stress, and PINK1/Parkin mitophagy activated second in response to sustained damage.

Initial data examining mitochondrial proteostasis in cells during the acute and recovery stage of the UPR^{mt} produced clusters of proteins that appeared resistant to proteostasis repair in WT cells (Chapter 4). Some of these proteins were CI subunits, which have been shown to be preferentially turned over by PINK1/Parkin mitophagy (Chapter 4). Whether PINK1/Parkin mitophagy plays a role in proteostasis repair is an important question to be answered in future research that will have strong implications on our understanding of the role of PINK1/Parkin mitophagy in protecting mitochondrial health (see Chapter 6.7.1).

While these relationships seem somewhat contradictory, the data in this thesis suggests both scenarios may be at play. PINK1/Parkin mitophagy may play a dual role in protecting mitochondria from a proteostasis stress through both removing protein aggregates from mitochondria comprised of proteins that are particularly resistant to chaperones and proteases, and also in removing mitochondria that are severely damaged beyond the scope of repair possible through the UPR^{mt}. A schematic summary of our current understanding of how both PINK1/Parkin mitophagy and the UPR^{mt} could integrate to respond to protein folding stress has been provided in Figure 7.2.
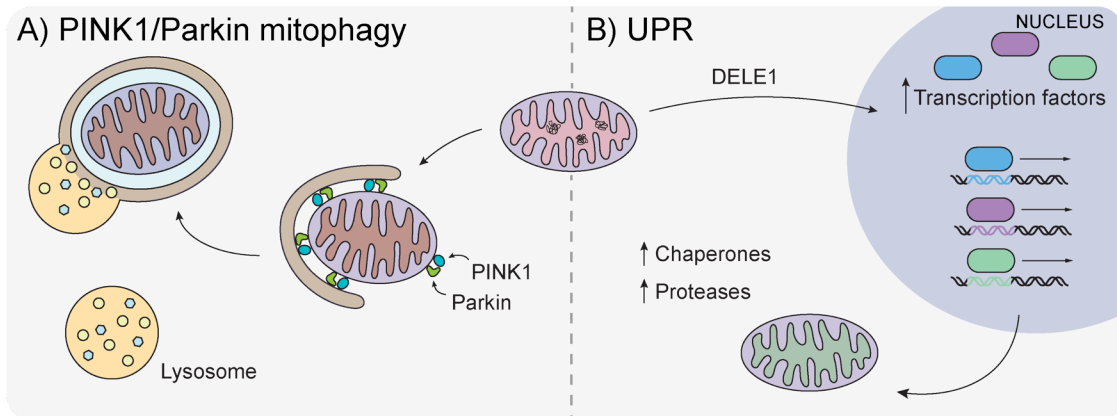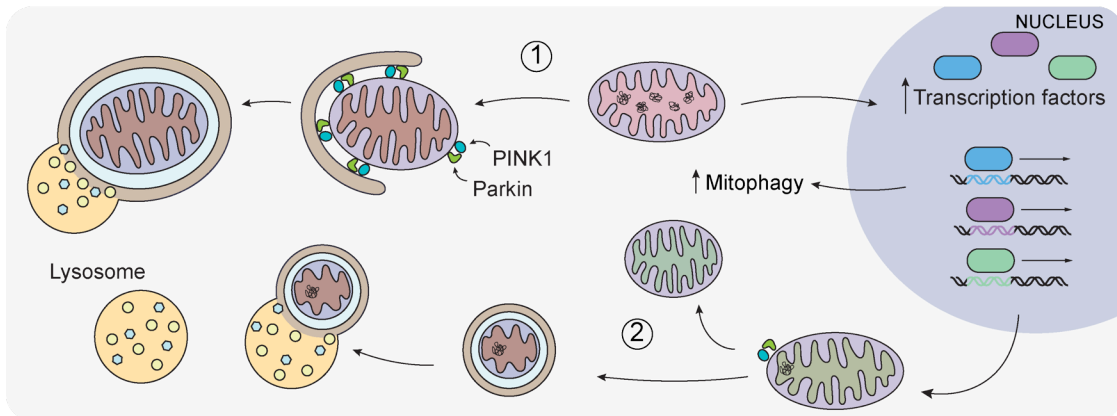
Figure 7.2 **Summary of our updated understanding of how PINK1/Parkin mitophagy and the UPR^mt interact during mitochondrial protein folding stress**. (*Previous*) While PINK1/Parkin mitophagy was known to respond to protein folding stress, interactions between PINK1/Parkin mitophagy and the UPR^mt had not been characterised. The most well characterised role of PINK1/Parkin mitophagy involves sequestering severely damaged mitochondria into an autophagosome prior to lysosomal degradation, while the UPR^mt repairs mitochondria experiencing mild mitochondrial stress. (*Current*) Work in this thesis has presented two possible roles of PINK1/Parkin mitophagy during protein folding stress. 1) PINK1/Parkin mitophagy may be degrading severely damaged mitochondria that may or may not contain incidental protein aggregates. 2) PINK1/Parkin mitophagy may be playing an active role in restoring proteostasis by sequestering and degrading select groups of proteins that are resistant to UPR^mt mediated repair. In addition to these roles in degrading mitochondria, PINK1/Parkin mitophagy activity is actively upregulated by the UPR^mt during recovery following a protein folding stress.

7.2: Future directions

7.2.1: Identifying additional UPR^{mt} signalling components

A clear and important area of future investigation is to identify the additional, unknown signalling components of the UPR^{mt}. It is still unknown what transmits mitochondrial specificity to the transcriptional program of the UPR^{mt} that is activated by DELE1. Additionally, it is unknown which transcription factors are driving the remaining ~44% of the UPR^{mt} program since CHOP, ATF4 and ATF5 were initially thought to regulate the full UPR^{mt} program (Chapter 5). Analysis in this thesis of transcriptional trends in the portion of the UPR^{mt} not regulated by CHOP, ATF4 and ATF5 produced a list of potential candidates that may regulate that portion of the UPR^{mt} program (Chapter 5). A genetic epistasis-based approach of generating transcription factor KO cell lines and validating the UPR^{mt} mediated transcriptional and proteostasis changes in response to G-TPP treatment will help clarify the roles of the transcriptional candidates generated in Chapter 5. In relation to the mitochondrial specificity of the UPR^{mt}, a promising area of study is in determining if there is a chromatin-modification program triggered by proteostatic stress that helps denote transcriptional specificity, as has been observed in *C. elegans*. Multiple histone-modification related genes were identified in the transcriptomics data that centred around the upregulation of histone acetylation and inhibition of histone methylation (Chapter 5). As mitochondria are known to provide substrate for histone acetylation marks, modulation of metabolite levels may serve as a method by which mitochondria tailor the generalised transcriptional changes triggered by DELE1 into the UPR^{mt} program (*260, 261*). Analysis of metabolic flux and the metabolome during G-TPP treatment will help determine the feasibility of metabolite-based signalling, while the histone modification factors identified in the UPR^{mt} transcriptomic analysis will provide candidates for genetic screening.

7.2.2: Characterising the role of PINK1/Parkin mitophagy in mediating proteostasis repair

Activation of PINK1/Parkin mitophagy in response to a protein folding stress has been robustly identified in both prior literature and in the mitophagy analysis conducted in this thesis (*11, 173*) (Chapter 6). The highest PINK1/Parkin mitophagy rates occur as the mitochondrial network is undergoing UPR^{mt} mediated repair following acute stress removal. While the activation of PINK1/Parkin mitophagy is not under contention, the biological role of mitophagy in this context is not yet understood. The most pressing line of investigation into the role of PINK1/Parkin

mitophagy will be establishing whether PINK1/Parkin mitophagy specifically degrades mitochondria harbouring insoluble protein aggregates during the UPR^{mt}, or whether only severely damaged mitochondria are targeted for removal. The next important area of investigation will be to clarify how PINK1/Parkin mitophagy affects functional repair and cellular health. Answering these questions collectively will help inform multiple areas of analysis. As PINK1/Parkin mitophagy did not affect UPR^{mt} signalling, understanding the cargo degraded by PINK1/Parkin mitophagy will clarify if protein aggregates propagate the UPR^{mt} signal. Further, if PINK1/Parkin mitophagy is responsible for degrading a subset of mitochondrial proteins to fully repair proteostasis, this could represent a yet-identified cellular phenotype of PINK1/Parkin mitophagy disruption.

7.2.3: Understanding how the UPR^{mt} influences PINK1/Parkin mitophagy

A key finding of the mitophagy-UPR^{mt} interaction analysis performed in Chapter 6 was that each CHOP, ATF4 and ATF5 are required for sustained mitophagy activation in the repair phase of the UPR^{mt}. Mechanistically how this occurs remains to be established. However, understanding how the UPR^{mt} facilitates sustained mitophagy is essential for understanding the molecular nature of the interactions between these two pathways. A relationship of this nature could present a potential new target that could be used to boost PINK1/Parkin mitophagy activity in a therapeutic setting. Multiple avenues of investigation could be pursued to address this question. While a broad assessment of the autophagy system was performed in Chapter 6, there are multiple parts of the autophagy pathway that were not encompassed in that initial analysis, including Parkin recruitment and PINK1 activity. Another possible investigative avenue involves measuring transcript and protein levels of autophagy related proteins in the repair phase of the UPR^{mt} to determine if there is a TKO specific depletion of autophagy related proteins. While the transcriptomic analysis at 12 h G-TPP treatment did not directly support this hypothesis, it does not rule out this hypothesis either as genes known to promote autophagy-related transcription were depleted in expression specifically in TKO cells (Figure 6.6). Transcriptome analysis at later timepoints during the recovery period may be required to see the effect of losing these positive autophagy regulators. Future studies should also involve examining the role of the three mitophagy-associated genes that were shown to be depleted specifically in TKO cells to determine if they play a role in driving G-TPP-mediated PINK1/Parkin mitophagy (Figure 6.6). Lastly, if the previously mentioned analysis routes still do not shed light on how the UPR^{mt} is driving mitophagy, exploring whether supplemental activation of PINK1/Parkin-independent mitophagy pathways occurs that could

have been co-detected in the mitophagy analysis performed in this thesis may provide some further directions for future research.

7.2.4: Long term changes to the mitochondrial proteome

A curious observation made when examining the temporal proteostasis trends of WT mitochondria was that some proteins improved in solubility following recovery from a G-TPP stress (Chapter 4). Combined with the chromatin remodelling related components that were present in the UPR^{mt} mediated transcriptome, and the mitochondrial RNA-methylation genes induced through the UPR^{mt} program, these changes suggest that there could be that long-standing modifications to the mitochondrial proteome that could facilitate a resistance to future proteostasis stress insults (Chapter 5). The concept of a long-term improvement in tolerance to stressors that change mitochondrial proteostasis raises a potential interesting mechanism of disease pathogenesis in neurodegeneration. If there are mutations in components of the UPR^{mt} program that prevent the development of long-term resistance to proteostasis stress, this could leave the mitochondrial network more susceptible to accumulating mitochondrial dysfunction that could exhaust the capacity of other quality control mechanisms such as PINK1/Parkin mitophagy. Long-standing epigenetic changes could also position UPR^{mt} activation as a potential therapeutic treatment to boost mitochondrial health in patients with defective mitochondrial function or defective mitochondrial quality control pathways. Analysis of mitochondrial proteostasis, UPR^{mt} program activation, and mitochondrial health in response to G-TPP retreatment will help us better understand this possible new function of the UPR^{mt}.

7.2.5: What physiological stressors trigger mitochondrial protein aggregation?

Substantial advancements in our understanding of the UPR^{mt} have been made through small molecule treatment of mitochondria with G-TPP. However, to date we have little information about what physiological stressors can result in mitochondrial protein folding stress. This issue has in part been created through our prior inability to measure endogenous mitochondrial protein aggregation. To be able to understand how UPR^{mt} activity and functional perturbations could lead to disease, it is imperative we determine how activation of the UPR^{mt} can occur in a physiological setting. The solubility assay developed in this thesis provides the technical means to begin interrogating mitochondrial protein solubility in different types of samples. Examining tissue samples from mouse models that have undergone a variety of physiological and genetic stressors,

in addition to disease patient samples will help us understand what causes mitochondrial protein folding stress in a physiological setting. In turn, this analysis will improve our understanding of the role of the UPR^mt in health and disease.

7.2.6: Does the UPR^mt contribute to the maintenance of neuronal health?

As PINK1/Parkin mitophagy dysfunction leads to neurodegeneration, understanding how the UPR^mt together with PINK1/Parkin mitophagy regulates mitochondrial health in neurons is essential for informing our understanding of how dysfunctional mitochondrial quality control can impact neuronal health. Neurons also are post-mitotic and cannot dilute mitochondrial protein aggregates through mitochondrial biogenesis triggered by cell division, meaning neurons may rely more heavily than other cell types on the UPR^mt to protect from mitochondrial proteostatic damage. Preliminary investigations into G-TPP mediated UPR^mt induction in primary cortical neurons indicated that neuronal mitochondria have different proteostasis sensitivities to HeLa cells (Chapter 6). Accordingly, the UPR^mt signalling pathway will need to be separately characterised in a neuronal system to understand UPR^mt function in neurons. Developing a comprehensive mechanistic understanding of the neuronal UPR^mt will facilitate future studies into the integrated role of the UPR^mt and PINK1/Parkin mitophagy in protecting neuronal health. Immune related signatures and Wnt signalling signatures were also observed in the UPR^mt transcriptomics data (Chapter 5). Experiments examining whether G-TPP-stressed neurons can activate a neuro-immune response in neighbouring microglia and astrocyte cells will help us understand whether dysfunctional mitochondrial proteostasis could contribute to the neuro-inflammation seen in PD.

An additional consideration is that mutations in components of the UPR^mt may in fact be causative for PD. A recent combinatorial review of GWAS studies focussing on identifying PD risk-loci identified ~90 genes with mutations that were attributed to ~ 25 – 35% of sporadic PD cases without a clear monogenic cause (*325*). Of these genes, 21 were altered in transcript expression with G-TPP treatment (Figure 7.3). Whether perturbed UPR^mt activity influences these genes to drive PD development, or whether there are monogenic components of the UPR^mt that are causative for a subset of PD development is a pertinent area of investigation. As a more detailed understanding of the signalling and effector molecules that drive the UPR^mt is developed (see Chapter 7.2.1), it will be important to refer back to genes known to be associated with PD to determine if mutated UPR^mt activity may be propagating a subset of sporadic PD cases.

	WT	CHOP KO	ATF4 KO	ATF5 KO	TKO
BAG3	2.16	1.08	0.51	0.60	0.79
DLG2	0.88	3.18	3.38	3.29	3.30
MBNL2	0.82	1.05	0.53	0.49	0.72
FYN	0.76	2.29	1.94	2.24	2.08
CHRNB1	0.75	1.04	0.05	0.34	0.93
MEX3C	0.74	0.43	-0.06	0.43	0.38
VAMP4	0.69	0.54	-0.11	0.33	0.74
CAMK2D	0.31	-0.75	-0.33	-0.87	-0.46
RAB29	0.24	-0.69	-0.70	-0.33	0.00
GBF1	-0.29	0.11	-0.05	-0.04	-0.02
IP6K2	-0.33	-0.16	0.42	0.10	0.19
FAM49B	-0.39	-0.44	0.80	0.37	0.07
NSF	-0.43	-0.43	-0.61	-0.48	-0.46
BRIP1	-0.45	-0.50	-1.47	-0.90	-0.97
SNCA	-0.48	-1.36	-0.39	-1.72	-0.64
UBAP2	-0.55	0.19	-0.06	0.20	-0.17
CAB39L	-0.58	-0.61	-0.43	-0.06	0.17
FAM171A2	-0.87	-1.33	-0.61	-0.51	-0.24
HIP1R	-0.94	0.52	0.41	0.85	0.31
KCNIP3	-0.98	-2.44	-1.36	-1.45	-1.93
KCNS3	-1.03	-2.61	-2.32	-2.99	-4.28

Key:
Log$_2$ fold change

Figure 7.3 **Heat map analysis of genes identified to be regulated by the UPR^{mt} that are also genes identified as risk-loci for Parkinson's disease development**. The transcriptomic data from Figure 5.8 of Chapter 5 was matched against the list of genes identified as risk-loci for PD development in a recent meta-analysis of GWAS studies (*325*). Genes identified in both the UPRmt transcriptome and risk-loci lists were isolated and displayed by heat map. Data was generated from 3 independent experiments.

7.2.7: Mitochondrial proteostasis and biomarker development

Although PD is the second most common neurological disease in Australia, it has proved difficult to diagnose at early stages of the disease owing to a lack of clear biomarkers. The severe symptomology of PD begins once ~31% of dopaminergic neurons in the substantia nigra have died (*326*). Diagnosis of PD once severe neuronal cell death has already occurred is incompatible from a therapeutic perspective. Therefore, in order to develop effective therapeutics to treat PD we must also find a way to diagnose PD much earlier.

A curious observation that has already been discussed at length in this thesis was the potential for PINK1/Parkin mitophagy to play an active role in repairing mitochondrial proteostasis. If future experimental validation does support a role for PINK1/Parkin mitophagy in maintaining proteostasis, mitochondrial proteostasis could function as an early-stage readout of mitochondrial dysfunction, and potentially as a biomarker of PD. Although cells have a different tolerance to

dysfunctional mitochondria, defective proteostasis may still be visible in patient-derived cell lines that can be collected as a part of a diagnostic program. Additionally, as ~ 95% of PD is currently classified as idiopathic without clear genetic causes, unidentified components of the UPR^{mt} may comprise some of these genetic drivers of PD. Screening for mitochondrial proteostasis changes may be a valuable tool in detecting pathogenic mutations of the UPR^{mt} prior to the presentation of neurodegenerative disease.

7.3: Conclusion

Given that mitochondrial quality control pathways play a vital role in protecting mitochondrial health, particularly in neurons, it is imperative that we understand at a mechanistic level the suite of pathways available to a cell to respond to mitochondrial dysfunction. The UPR^{mt} is a sparsely characterised pathway in mammals which mediates mitochondrial repair and responds to overlapping stimuli with PINK1/Parkin mitophagy, which is mutated in familial PD. Due to technical limitations, the mammalian UPR^{mt} has been a difficult pathway to study. This thesis aimed to improve our limited understanding of the mammalian UPR^{mt} and begin to untangle the interactions between the UPR^{mt} and PINK1/Parkin mitophagy. Investigations in this thesis have revealed that the UPR^{mt} functions as a bimodal program, driving protection of mitochondrial proteostasis during an acute stress and actively facilitating proteostasis repair. In particular, the UPR^{mt} facilitates protection of the mitochondrial ribosome, and facilitates protection and restoration of the OXPHOS machinery function, specifically complex I. Proteostasis protection mediated by the UPR^{mt} requires substantial rewiring of the cellular transcriptome, with multiple novel pathways identified to be altered through UPR^{mt} activation in this work. The three UPR^{mt} associated transcription factors, CHOP, ATF4 and ATF5 were found to play independent but equally essential roles in driving UPR^{mt} mediated proteostasis protection and repair but they performed these roles through a mosaic of interconnected signalling pathways with partial overlap. A novel role of the CHOP, ATF4 and ATF5 mediated arms of the UPR^{mt} in promoting sustained PINK1/Parkin mitophagy activity during proteostasis repair was also identified. These findings were made possible through the development of a novel experimental assay to measure the functional mitochondrial proteome through quantifying mitochondrial proteostasis. While significant advancements in our understanding of the UPR^{mt} and its interaction with PINK1/Parkin mitophagy have been made in this thesis, much more about these pathways remain to be discovered, and hopefully experimental tools developed in this thesis will now help accelerate future research into this important but largely untapped field.

Appendix

Appendix I

Plasmid	Addgene #	Enzymes used for cloning	Citation
pSpCas9(BB)-2A-GFP (PX458)	#48138	BbsI	pSpCas9(BB)-2A-GFP (PX458) was a gift from Feng Zhang (Addgene plasmid #48138; http://n2t.net/addgene:48138 ; RRID:Addgene_48138)
pBMN-YFP-Parkin	#59416	N/A	pBMN-YFP-Parkin was a gift from Richard Youle (Addgene plasmid # 59416 ; http://n2t.net/addgene:59416 ; RRID:Addgene_59416)
pCHAC-mt-mKeima	#72342	N/A	pCHAC-mt-mKeima was a gift from Richard Youle (Addgene plasmid # 72342 ; http://n2t.net/addgene:72342 ; RRID:Addgene_72342)
pGEM®-4Z	N/A	BamHI, HindIII	

Appendix I **Plasmids used for molecular cloning or protein expression in this work**.

Appendix II

Gene	Exon	Primer	Primer sequence (5' to 3') (bold: genomic DNA binding region)	PCR product (bp)
CHOP	1	Forward	GACCATCCTCTAGACTGCCGGATCCG**GATGGCAGCTGAGTCATTG**	650
		Reverse	GCGAGATTATAGAGATCCCAAGCTT**TCATGCTTGGTGCAGATTC**	
ATF4	2	Forward	ATGCGGATC**CCTCGATTCCAGCAAAGCACC**	742
		Reverse	ATGCAAGCTT**GCAGTGTAGTCTGGCTTCC**	
		Sequencing	**TGAGTGGGCCACCACCACATC**	N/A
ATF5	1	Forward	GCGCGGATCC**GTAGGTCTTCCACTTTCGCCTT**	338
		Reverse	GCGCAAGCTT**CTTCCACCTGCCCTTACCT**	

Appendix II **Genotyping primers used to sequence KO cell lines**.

Appendix III

Gene Symbol	Uniprot	GeneID /Location	Targeting location	TALEN or CRISPR gRNA (PAM)	Clone number used	Depth/detected Alleles	Mutation	Protein impact
CHOP	P35638	1649/NC_000012.12	Exon 1	Left arm: TCCTCATACCAGGCTTCC Right arm: TCCCGAAGGAGAAAGGCA	#1	10/2	c.[110_111insAACAACAC];c.[110_115delinsGGGTTAGGGTTAGGGTTAGGGTTAGGGTTAGGGTTAGGGTTAGGGTTAGGGTTAGGGTTAGGGTTAGGGTTAGGGTTAGGCCCTAGGGTTAGGGTTTTTTT]	p.[Y61Tfs*29];p.[T60Rfs*31]
ATF4	P18848	468/NC_000022.11	Exon 2	TTTGCAGAGGATGCCTTCTC<u>CGG</u>	#17	NA/4	c.[236_237insN];c.[231_244del];c.[234_247del];c.[237_250del]	P[F79*26];p.[A78Rfs*22];p.[F79Lfs*21];p.[F79Lfs*21]
ATF5	Q9Y2D1	22809/NC_000019.10	Exon 1	CATGTCACTCCTGGCGACCC<u>TGG</u>	#17	10/3	c.[16_17insG];c.[17_28del];c.[13_51del]	p.[T6Sfs*19];p.[T6K, L7_E10del];p.[A5_P17del]
CHOP/ATF4/ATF5 TKO								
ATF5	Q9Y2D1	22809/NC_000019.10	Exon 1	CATGTCACTCCTGGCGACCC<u>TGG</u>	#22 (made from CHOP KO #1)	10/2	c.[16del];c.[13_22del]	p.[T6Pfs*25];p.[A5_L7del]
ATF4	P18848	468/NC_000022.11	Exon 2	TTTGCAGAGGATGCCTTCTC<u>CGG</u>	#1 (made from CHOP/ATF5 DKO #22)	NA/5	c.[227+5_243del];c.[227+5_236del];c.[237_238del]; c.[227+4_244del]; c.[227+4_237del]	p.[?](affecting splicing);p.[?](affecting splicing);p.[S80Rfs*24];p.[?](affecting splicing);p.[?](affecting splicing)

Appendix III **CRISPR and TALEN sequences and genotyping results of the knockout cell lines generated in this study**

The indels for the targeted genes detected in the indicated knockout cell lines ("Mutation" column) and their translated proteins ("Protein impact" column) are formatted according to Human Genome Variation Society (HGVS; http://varnomen.hgvs.org/). Mutation positions within genes which have multiple splice variants are determined using the variant indicated as the canonical isoform in Uniprot. del = deletion; ins = insertion; c. = coding DNA; p. = protein; fs = frame shift; * = stop codon; [?] = affecting splicing; N= any nucleotide (A, C, T and G); X denotes one of the three amino acids A, T or S. The numbers following the asterisks denote the numbers of amino acids between the first amino acid changed after the mutation(s) and the first subsequent stop codon encountered

Appendix IV

A

Batch 1						Batch 2					
Cell line	Condition	Repeat	Fraction	Label	Sample #	Cell line	Condition	Repeat	Fraction	Label	Sample #
WT	DMSO	N1	P	127N	1	WT	DMSO	N1	S	127N	7
WT	DMSO	N2	P	128N	2	WT	DMSO	N2	S	128N	8
WT	DMSO	N3	P	129N	3	WT	DMSO	N3	S	129N	9
WT	12 h	N1	P	127C	4	WT	12 h	N1	S	127C	10
WT	12 h	N2	P	128C	5	WT	12 h	N2	S	128C	11
WT	12 h	N3	P	129C	6	WT	12 h	N3	S	129C	12
-	-	N1	P	130C	-	-	-	N1	S	130C	-
-	-	N2	P	131N	-	-	-	N2	S	131N	-
-	-	N3	P	131C	-	-	-	N3	S	131C	-

B

Batch 1

Cell line	Condition	Repeat	Fraction	Label	Sample #
WT	DMSO	N1	P	127N	1
WT	DMSO	N2	P	128N	2
WT	DMSO	N3	P	129N	3
WT	DMSO	N1	S	127C	4
WT	DMSO	N2	S	128C	5
WT	DMSO	N3	S	129C	6
CHOP KO	DMSO	N1	P	130C	7
CHOP KO	DMSO	N2	P	131N	8
CHOP KO	DMSO	N3	P	131C	9

Batch 2

Cell line	Condition	Repeat	Fraction	Label	Sample #
CHOP KO	DMSO	N1	S	127N	10
CHOP KO	DMSO	N2	S	128N	11
CHOP KO	DMSO	N3	S	129N	12
ATF4 KO	DMSO	N1	P	127C	13
ATF4 KO	DMSO	N2	P	128C	14
ATF4 KO	DMSO	N3	P	129C	15
ATF4 KO	DMSO	N1	S	130C	16
ATF4 KO	DMSO	N2	S	131N	17
ATF4 KO	DMSO	N3	S	131C	18

Batch 3

Cell line	Condition	Repeat	Fraction	Label	Sample #
ATF5 KO	DMSO	N1	P	127N	19
ATF5 KO	DMSO	N2	P	128N	20
ATF5 KO	DMSO	N3	P	129N	21
ATF5 KO	DMSO	N1	S	127C	22
ATF5 KO	DMSO	N2	S	128C	23
ATF5 KO	DMSO	N3	S	129C	24
TKO	DMSO	N1	P	130C	25
TKO	DMSO	N2	P	131N	26
TKO	DMSO	N3	P	131C	27

Batch 4

Cell line	Condition	Repeat	Fraction	Label	Sample #
TKO	DMSO	N1	S	127N	28
TKO	DMSO	N2	S	128N	29
TKO	DMSO	N3	S	129N	30
WT	12h	N1	P	127C	31
WT	12h	N2	P	128C	32
WT	12h	N3	P	129C	33
WT	12h	N1	S	130C	34
WT	12h	N2	S	131N	35
WT	12h	N3	S	131C	36

Batch 5

Cell line	Condition	Repeat	Fraction	Label	Sample #
CHOP KO	12h	N1	P	127N	37
CHOP KO	12h	N2	P	128N	38
CHOP KO	12h	N3	P	129N	39
CHOP KO	12h	N1	S	127C	40
CHOP KO	12h	N2	S	128C	41
CHOP KO	12h	N3	S	129C	42
ATF4 KO	12h	N1	P	130C	43
ATF4 KO	12h	N2	P	131N	44
ATF4 KO	12h	N3	P	131C	45

Batch 6

Cell line	Condition	Repeat	Fraction	Label	Sample #
ATF4 KO	12h	N1	S	127N	46
ATF4 KO	12h	N2	S	128N	47
ATF4 KO	12h	N3	S	129N	48
ATF5 KO	12h	N1	P	127C	49
ATF5 KO	12h	N2	P	128C	50
ATF5 KO	12h	N3	P	129C	51
ATF5 KO	12h	N1	S	130C	52
ATF5 KO	12h	N2	S	131N	53
ATF5 KO	12h	N3	S	131C	54

Batch 7

Cell line	Condition	Repeat	Fraction	Label	Sample #
TKO	12h	N1	P	127N	55
TKO	12h	N2	P	128N	56
TKO	12h	N3	P	129N	57
TKO	12h	N1	S	127C	58
TKO	12h	N2	S	128C	59
TKO	12h	N3	S	129C	60
WT	24h C	N1	P	130C	61
WT	24h C	N2	P	131N	62
WT	24h C	N3	P	131C	63

Batch 8

Cell line	Condition	Repeat	Fraction	Label	Sample #
WT	24h C	N1	S	127N	64
WT	24h C	N2	S	128N	65
WT	24h C	N3	S	129N	66
CHOP KO	24h C	N1	P	127C	67
CHOP KO	24h C	N2	P	128C	68
CHOP KO	24h C	N3	P	129C	69
CHOP KO	24h C	N1	S	130C	70
CHOP KO	24h C	N2	S	131N	71
CHOP KO	24h C	N3	S	131C	72

Batch 9

Cell line	Condition	Repeat	Fraction	Label	Sample #
ATF4 KO	24h C	N1	P	127N	73
ATF4 KO	24h C	N2	P	128N	74
ATF4 KO	24h C	N3	P	129N	75
ATF4 KO	24h C	N1	S	127C	76
ATF4 KO	24h C	N2	S	128C	77
ATF4 KO	24h C	N3	S	129C	78
ATF5 KO	24h C	N1	P	130C	79
ATF5 KO	24h C	N2	P	131N	80
ATF5 KO	24h C	N3	P	131C	81

Batch 10

Cell line	Condition	Repeat	Fraction	Label	Sample #
ATF5 KO	24h C	N1	S	127N	82
ATF5 KO	24h C	N2	S	128N	83
ATF5 KO	24h C	N3	S	129N	84
TKO	24h C	N1	P	127C	85
TKO	24h C	N2	P	128C	86
TKO	24h C	N3	P	129C	87
TKO	24h C	N1	S	130C	88
TKO	24h C	N2	S	131N	89
TKO	24h C	N3	S	131C	90

Batch 11

Cell line	Condition	Repeat	Fraction	Label	Sample #
WT	48h C	N1	P	127N	91
WT	48h C	N2	P	128N	92
WT	48h C	N3	P	129N	93
WT	48h C	N1	S	127C	94
WT	48h C	N2	S	128C	95
WT	48h C	N3	S	129C	96
CHOP KO	48h C	N1	P	130C	97
CHOP KO	48h C	N2	P	131N	98
CHOP KO	48h C	N3	P	131C	99

Batch 12

Cell line	Condition	Repeat	Fraction	Label	Sample #
CHOP KO	48h C	N1	S	127N	100
CHOP KO	48h C	N2	S	128N	101
CHOP KO	48h C	N3	S	129N	102
ATF4 KO	48h C	N1	P	127C	103
ATF4 KO	48h C	N2	P	128C	104
ATF4 KO	48h C	N3	P	129C	105
ATF4 KO	48h C	N1	S	130C	106
ATF4 KO	48h C	N2	S	131N	107
ATF4 KO	48h C	N3	S	131C	108

Batch 13

Cell line	Condition	Repeat	Fraction	Label	Sample #
ATF5 KO	48h C	N1	P	127N	109
ATF5 KO	48h C	N2	P	128N	110
ATF5 KO	48h C	N3	P	129N	111
ATF5 KO	48h C	N1	S	127C	112
ATF5 KO	48h C	N2	S	128C	113
ATF5 KO	48h C	N3	S	129C	114
TKO	48h C	N1	P	130C	115
TKO	48h C	N2	P	131N	116
TKO	48h C	N3	P	131C	117

Batch 14

| Cell line	Condition	Repeat	Fraction	Label	Sample #
TKO	48h C	N1	S	127N	118
TKO	48h C	N2	S	128N	119
TKO	48h C	N3	S	129N	120
WT	48h C	N1	P	127C	121
WT	48h C	N2	P	128C	122
WT	48h C	N3	P	129C	123
WT	48h C	N1	S	130C	124
WT	48h C	N2	S	131N	125
WT	48h C	N3	S	131C	126

Appendix IV **TMT batch labelling schematics**. **A**, **B**. TMT-10plex batch labelling schematics for (**A**) WT actute G-TPP treatment protein solubility experiment, and (**B**) G-TPP treatment and recovery protein solubility experiment (Chapter 4). Red = decoy sample included to fill the batch.

Appendix V
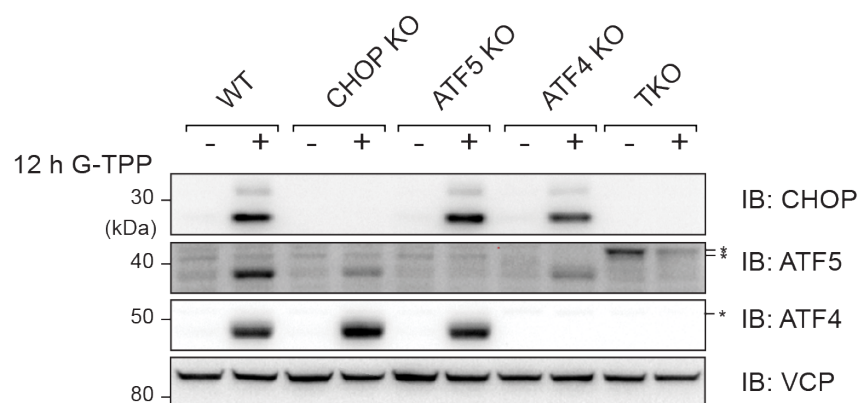
Appendix V **Validation of CHOP, ATF4, ATF5 and TKO cells.** WT, CHOP KO, ATF5 KO, ATF4 KO and CHOP/ATF4/ATF5 triple KO (TKO) cells were treated with DMSO or 9 μM G-TPP for 12 h, and levels of CHOP, ATF4 and ATF5 were analysed by immunoblot. * = non-specific band.

Appendix VI
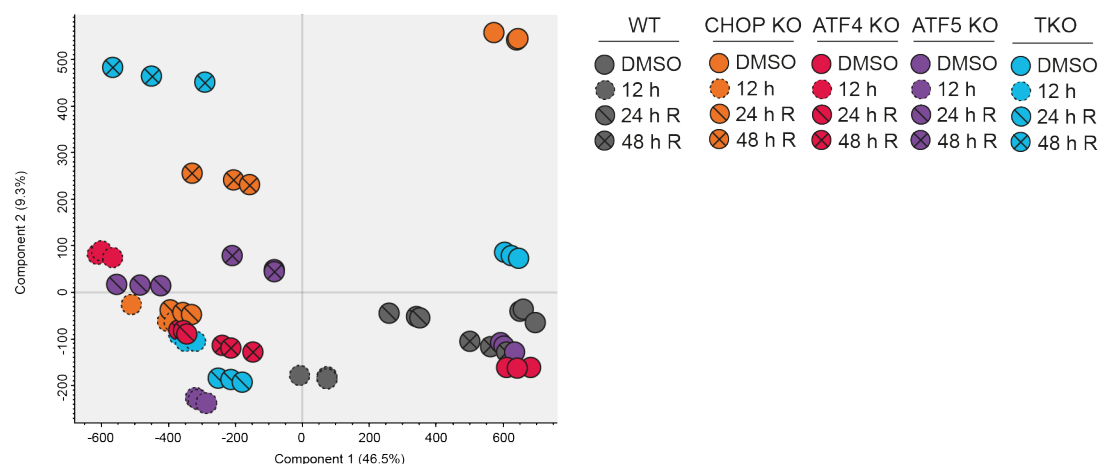
Appendix VI **Principle component analysis of mitochondrial protein solubility trends during acute G-TPP treatment and recovery**. Principal component analysis (PCA) was performed using the protein-specific solubility profiles of each WT, CHOP KO, ATF4 KO, ATF5 KO and TKO sample set generated from the data produced in Figure 4.2. PCA plots were generated using Perseus v1.6.15 (*165*).

References

[1]   Osellame LD, Blacker TS, Duchen MR. Cellular and molecular mechanisms of mitochondrial function. Best Practice & Research Clinical Endocrinology & Metabolism. 2012;26(6):711-23.

[2]   Ajioka RS, Phillips JD, Kushner JP. Biosynthesis of heme in mammals. Biochimica et Biophysica Acta (BBA) - Molecular Cell Research. 2006;1763(7):723-36.

[3]   Mesmin B. Mitochondrial lipid transport and biosynthesis: A complex balance. The Journal of Cell Biology. 2016;214(1):9-11.

[4]   Wang L. Mitochondrial purine and pyrimidine metabolism and beyond. Nucleosides, Nucleotides and Nucleic Acids. 2016;35(10-12):578-94.

[5]   Matilainen O, Quirós PM, Auwerx J. Mitochondria and Epigenetics – Crosstalk in Homeostasis and Stress. Trends in Cell Biology. 2017;27(6):453-63.

[6]   Weinberg Samuel E, Sena Laura A, Chandel Navdeep S. Mitochondria in the Regulation of Innate and Adaptive Immunity. Immunity. 2015;42(3):406-17.

[7]   Wang C, Youle RJ. The Role of Mitochondria in Apoptosis. Annual Review of Genetics. 2009;43(1):95-118.

[8]   Sorrentino V, Menzies KJ, Auwerx J. Repairing Mitochondrial Dysfunction in Disease. Annual Review of Pharmacology and Toxicology. 2018;58(1):353-89.

[9]   Tilokani L, Nagashima S, Paupe V, Prudent J. Mitochondrial dynamics: overview of molecular mechanisms. Essays In Biochemistry. 2018;62(3):341-60.

[10]   Byrne JJ, Soh MS, Chandhok G, Vijayaraghavan T, Teoh J-S, Crawford S, et al. Disruption of mitochondrial dynamics affects behaviour and lifespan in Caenorhabditis elegans. Cellular and Molecular Life Sciences. 2019;76(10):1967-85.

[11]   Burman JL, Pickles S, Wang C, Sekine S, Vargas JNS, Zhang Z, et al. Mitochondrial fission facilitates the selective mitophagy of protein aggregates. Journal of Cell Biology. 2017;216(10):3231-47.

[12]   Frey TG, Mannella CA. The internal structure of mitochondria. Trends in Biochemical Sciences. 2000;25(7):319-24.

[13]   Cogliati S, Enriquez JA, Scorrano L. Mitochondrial Cristae: Where Beauty Meets Functionality. Trends in Biochemical Sciences. 2016;41(3):261-73.

[14]   Jonckheere AI, Smeitink JAM, Rodenburg RJT. Mitochondrial ATP synthase: architecture, function and pathology. Journal of Inherited Metabolic Disease. 2012;35(2):211-25.

[15]   Andersson SGE, Zomorodipour A, Andersson JO, Sicheritz-Pontén T, Alsmark UCM, Podowski RM, et al. The genome sequence of Rickettsia prowazekii and the origin of mitochondria. Nature. 1998;396(6707):133-40.

[16]   Gustafsson CM, Falkenberg M, Larsson N-G. Maintenance and Expression of Mammalian Mitochondrial DNA. Annual Review of Biochemistry. 2016;85(1):133-60.

[17]   Greber BJ, Ban N. Structure and Function of the Mitochondrial Ribosome. Annual Review of Biochemistry. 2016;85(1):103-32.

[18]   Eilers M, Schatz G. Binding of a specific ligand inhibits import of a purified precursor protein into mitochondria. Nature. 1986;322(6076):228-32.

[19]   Rassow J, Hartl F-U, Guiard B, Pfanner N, Neupert W. Polypeptides traverse the mitochondrial envelope in an extended state. FEBS Letters. 1990;275(1-2):190-4.

[20]   Bousette N, Kislinger T, Fong V, Isserlin R, Hewel JA, Emili A, et al. Large-Scale Characterization and Analysis of the Murine Cardiac Proteome. Journal of Proteome Research. 2009;8(4):1887-901.

[21]   Abe Y, Shodai T, Muto T, Mihara K, Torii H, Nishikawa S-i, et al. Structural Basis of Presequence Recognition by the Mitochondrial Protein Import Receptor Tom20. Cell. 2000;100(5):551-60.

[22]   Vögtle FN, Wortelkamp S, Zahedi RP, Becker D, Leidhold C, Gevaert K, et al. Global Analysis of the Mitochondrial N-Proteome Identifies a Processing Peptidase Critical for Protein Stability. Cell. 2009;139(2):428-39.

[23]   Roise D, Horvath SJ, Tomich JM, Richards JH, Schatz G. A chemically synthesized pre-sequence of an imported mitochondrial protein can form an amphiphilic helix and perturb natural and artificial phospholipid bilayers. The EMBO Journal. 1986;5(6):1327-34.

[24]   Wiedemann N, Pfanner N. Mitochondrial Machineries for Protein Import and Assembly. Annual Review of Biochemistry. 2017;86(1):685-714.

[25]   Bauer MF, Sirrenberg C, Neupert W, Brunner M. Role of Tim23 as Voltage Sensor and Presequence Receptor in Protein Import into Mitochondria. Cell. 1996;87(1):33-41.

[26]   Pfanner N, Neupert W. Transport of proteins into mitochondria: a potassium diffusion potential is able to drive the import of ADP/ATP carrier. The EMBO Journal. 1985;4(11):2819-25.

[27]   Kang P-J, Ostermann J, Shilling J, Neupert W, Craig EA, Pfanner N. Requirement for hsp70 in the mitochondrial matrix for translocation and folding of precursor proteins. Nature. 1990;348(6297):137-43.

[28]   Horst M, Oppliger W, Rospert S, Schönfeld H-J, Schatz G, Azem A. Sequential action of two hsp70 complexes during protein import into mitochondria. The EMBO Journal. 1997;16(8):1842-9.

[29]   Hawlitschek G, Schneider H, Schmidt B, Tropschug M, Hartl F-U, Neupert W. Mitochondrial protein import: Identification of processing peptidase and of PEP, a processing enhancing protein. Cell. 1988;53(5):795-806.

[**30**]   Rüdiger S, Buchberger A, Bukau B. Interaction of Hsp70 chaperones with substrates. Nature Structural Biology. 1997;4(5):342-9.

[**31**]   Voos W. Chaperone–protease networks in mitochondrial protein homeostasis. Biochimica et Biophysica Acta (BBA) - Molecular Cell Research. 2013;1833(2):388-99.

[**32**]   Felts SJ, Owen BAL, Nguyen P, Trepel J, Donner DB, Toft DO. The hsp90-related Protein TRAP1 Is a Mitochondrial Protein with Distinct Functional Properties. Journal of Biological Chemistry. 2000;275(5):3305-12.

[**33**]   Altieri DC, Stein GS, Lian JB, Languino LR. TRAP-1, the mitochondrial Hsp90. Biochimica et Biophysica Acta (BBA) - Molecular Cell Research. 2012;1823(3):767-73.

[**34**]   Schubert U, Antón LC, Gibbs J, Norbury CC, Yewdell JW, Bennink JR. Rapid degradation of a large fraction of newly synthesized proteins by proteasomes. Nature. 2000;404(6779):770-4.

[**35**]   Koshiba T, Yasukawa K, Yanagi Y, Kawabata S-i. Mitochondrial Membrane Potential Is Required for MAVS-Mediated Antiviral Signaling. Science Signaling. 2011;4(158):ra7-ra.

[**36**]   Desler C, Lykke A, Rasmussen LJ. The Effect of Mitochondrial Dysfunction on Cytosolic Nucleotide Metabolism. Journal of Nucleic Acids. 2010;2010.

[**37**]   Yokota M, Hatakeyama H, Ono Y, Kanazawa M, Goto Y-i. Mitochondrial respiratory dysfunction disturbs neuronal and cardiac lineage commitment of human iPSCs. Cell Death &Amp; Disease. 2017;8:e2551.

[**38**]   Lin T-K, Cheng C-H, Chen S-D, Liou C-W, Huang C-R, Chuang Y-C. Mitochondrial Dysfunction and Oxidative Stress Promote Apoptotic Cell Death in the Striatum via Cytochrome c/ Caspase-3 Signaling Cascade Following Chronic Rotenone Intoxication in Rats. International Journal of Molecular Sciences. 2012;13(7):8722-39.

[**39**]   Silva JP, Köhler M, Graff C, Oldfors A, Magnuson MA, Berggren P-O, et al. Impaired insulin secretion and β-cell loss in tissue-specific knockout mice with mitochondrial diabetes. Nature Genetics. 2000;26(3):336-40.

[**40**]   Bhatti JS, Bhatti GK, Reddy PH. Mitochondrial dysfunction and oxidative stress in metabolic disorders — A step towards mitochondria based therapeutic strategies. Biochimica et Biophysica Acta (BBA) - Molecular Basis of Disease. 2017;1863(5):1066-77.

[**41**]   Boudina S, Sena S, O'Neill BT, Tathireddy P, Young ME, Abel ED. Reduced Mitochondrial Oxidative Capacity and Increased Mitochondrial Uncoupling Impair Myocardial Energetics in Obesity. Circulation. 2005;112(17):2686-95.

[**42**]   Cenini G, Rüb C, Bruderek M, Voos W. Amyloid β-peptides interfere with mitochondrial preprotein import competence by a coaggregation process. Molecular Biology of the Cell. 2016;27(21):3257-72.

[43]   Bratic A, Larsson N-G. The role of mitochondria in aging. J Clin Invest. 2013;123(3):951-7.

[44]   Gaude E, Frezza C. Tissue-specific and convergent metabolic transformation of cancer correlates with metastatic potential and patient survival. Nature Communications. 2016;7:13041.

[45]   Moussa C, Hebron M, Huang X, Ahn J, Rissman RA, Aisen PS, et al. Resveratrol regulates neuro-inflammation and induces adaptive immunity in Alzheimer's disease. Journal of Neuroinflammation. 2017;14(1):1.

[46]   Ryu D, Zhang H, Ropelle ER, Sorrentino V, Mázala DAG, Mouchiroud L, et al. NAD+ repletion improves muscle function in muscular dystrophy and counters global PARylation. Science Translational Medicine. 2016;8(361):361ra139-361ra139.

[47]   Narendra D, Tanaka A, Suen D-F, Youle RJ. Parkin is recruited selectively to impaired mitochondria and promotes their autophagy. The Journal of Cell Biology. 2008;183(5):795-803.

[48]   Lazarou M, Jin Seok M, Kane Lesley A, Youle Richard J. Role of PINK1 Binding to the TOM Complex and Alternate Intracellular Membranes in Recruitment and Activation of the E3 Ligase Parkin. Developmental Cell. 2012;22(2):320-33.

[49]   Greene AW, Grenier K, Aguileta MA, Muise S, Farazifard R, Haque ME, et al. Mitochondrial processing peptidase regulates PINK1 processing, import and Parkin recruitment. EMBO reports. 2012;13(4):378-85.

[50]   Jin SM, Lazarou M, Wang C, Kane LA, Narendra DP, Youle RJ. Mitochondrial membrane potential regulates PINK1 import and proteolytic destabilization by PARL. Journal of Cell Biology. 2010;191(5):933-42.

[51]   Kane LA, Lazarou M, Fogel AI, Li Y, Yamano K, Sarraf SA, et al. PINK1 phosphorylates ubiquitin to activate Parkin E3 ubiquitin ligase activity. The Journal of Cell Biology. 2014;205(2):143-53.

[52]   Shiba-Fukushima K, Arano T, Matsumoto G, Inoshita T, Yoshida S, Ishihama Y, et al. Phosphorylation of Mitochondrial Polyubiquitin by PINK1 Promotes Parkin Mitochondrial Tethering. PLOS Genetics. 2014;10(12):e1004861.

[53]   Kazlauskaite A, Martínez-Torres RJ, Wilkie S, Kumar A, Peltier J, Gonzalez A, et al. Binding to serine 65-phosphorylated ubiquitin primes Parkin for optimal PINK1-dependent phosphorylation and activation. EMBO reports. 2015;16(8):939-54.

[54]   Sauvé V, Lilov A, Seirafi M, Vranas M, Rasool S, Kozlov G, et al. A Ubl/ubiquitin switch in the activation of Parkin. The EMBO Journal. 2015;34(20):2492-505.

[55]   Wauer T, Simicek M, Schubert A, Komander D. Mechanism of phospho-ubiquitin-induced PARKIN activation. Nature. 2015;524:370.

[56]   Kumar A, Aguirre JD, Condos TE, Martinez-Torres RJ, Chaugule VK, Toth R, et al. Disruption of the autoinhibited state primes the E3 ligase parkin for activation and catalysis. The EMBO Journal. 2015;34(20):2506-21.

[**57**] Kazlauskaite A, Kondapalli C, Gourlay R, Campbell David G, Ritorto Maria S, Hofmann K, et al. Parkin is activated by PINK1-dependent phosphorylation of ubiquitin at Ser65. Biochemical Journal. 2014;460(1):127-41.

[**58**] Sarraf SA, Raman M, Guarani-Pereira V, Sowa ME, Huttlin EL, Gygi SP, et al. Landscape of the PARKIN-dependent ubiquitylome in response to mitochondrial depolarization. Nature. 2013;496:372.

[**59**] Ordureau A, Sarraf Shireen A, Duda David M, Heo J-M, Jedrychowski Mark P, Sviderskiy Vladislav O, et al. Quantitative Proteomics Reveal a Feedforward Mechanism for Mitochondrial PARKIN Translocation and Ubiquitin Chain Synthesis. Molecular Cell. 2014;56(3):360-75.

[**60**] Chan NC, Salazar AM, Pham AH, Sweredoski MJ, Kolawa NJ, Graham RLJ, et al. Broad activation of the ubiquitin–proteasome system by Parkin is critical for mitophagy. Human Molecular Genetics. 2011;20(9):1726-37.

[**61**] Yoshii SR, Kishi C, Ishihara N, Mizushima N. Parkin Mediates Proteasome-dependent Protein Degradation and Rupture of the Outer Mitochondrial Membrane. Journal of Biological Chemistry. 2011;286(22):19630-40.

[**62**] Gegg ME, Cooper JM, Chau K-Y, Rojo M, Schapira AHV, Taanman J-W. Mitofusin 1 and mitofusin 2 are ubiquitinated in a PINK1/parkin-dependent manner upon induction of mitophagy. Human Molecular Genetics. 2010;19(24):4861-70.

[**63**] Lazarou M, Sliter DA, Kane LA, Sarraf SA, Wang C, Burman JL, et al. The ubiquitin kinase PINK1 recruits autophagy receptors to induce mitophagy. Nature. 2015;524:309.

[**64**] Itakura E, Mizushima N. Characterization of autophagosome formation site by a hierarchical analysis of mammalian Atg proteins. Autophagy. 2010;6(6):764-76.

[**65**] Vargas JNS, Wang C, Bunker E, Hao L, Maric D, Schiavo G, et al. Spatiotemporal Control of ULK1 Activation by NDP52 and TBK1 during Selective Autophagy. Molecular Cell. 2019;74(2):347-62.e6.

[**66**] Russell RC, Tian Y, Yuan H, Park HW, Chang Y-Y, Kim J, et al. ULK1 induces autophagy by phosphorylating Beclin-1 and activating VPS34 lipid kinase. Nature Cell Biology. 2013;15:741.

[**67**] Axe EL, Walker SA, Manifava M, Chandra P, Roderick HL, Habermann A, et al. Autophagosome formation from membrane compartments enriched in phosphatidylinositol 3-phosphate and dynamically connected to the endoplasmic reticulum. The Journal of Cell Biology. 2008;182(4):685-701.

[**68**] Polson HEJ, de Lartigue J, Rigden DJ, Reedijk M, Urbé S, Clague MJ, et al. Mammalian Atg18 (WIPI2) localizes to omegasome-anchored phagophores and positively regulates LC3 lipidation. Autophagy. 2010;6(4):506-22.

[**69**] Dooley Hannah C, Razi M, Polson Hannah EJ, Girardin Stephen E, Wilson Michael I, Tooze Sharon A. WIPI2 Links LC3 Conjugation with PI3P, Autophagosome Formation, and Pathogen Clearance by Recruiting Atg12-5-16L1. Molecular Cell. 2014;55(2):238-52.

[70] Kabeya Y, Mizushima N, Ueno T, Yamamoto A, Kirisako T, Noda T, et al. LC3, a mammalian homologue of yeast Apg8p, is localized in autophagosome membranes after processing. The EMBO Journal. 2000;19(21):5720-8.

[71] Nguyen TN, Padman BS, Usher J, Oorschot V, Ramm G, Lazarou M. Atg8 family LC3/GABARAP proteins are crucial for autophagosome–lysosome fusion but not autophagosome formation during PINK1/Parkin mitophagy and starvation. Journal of Cell Biology. 2016;215(6):857-74.

[72] Padman BS, Nguyen TN, Uoselis L, Skulsuppaisarn M, Nguyen LK, Lazarou M. LC3/GABARAPs drive ubiquitin-independent recruitment of Optineurin and NDP52 to amplify mitophagy. Nature Communications. 2019;10(1):408.

[73] Diot A, Morten K, Poulton J. Mitophagy plays a central role in mitochondrial ageing. Mammalian Genome. 2016;27(7):381-95.

[74] Lin Y-F, Schulz AM, Pellegrino MW, Lu Y, Shaham S, Haynes CM. Maintenance and propagation of a deleterious mitochondrial genome by the mitochondrial unfolded protein response. Nature. 2016;533:416.

[75] Wilkening A, Rüb C, Sylvester M, Voos W. Analysis of heat-induced protein aggregation in human mitochondria. Journal of Biological Chemistry. 2018.

[76] Nargund AM, Pellegrino MW, Fiorese CJ, Baker BM, Haynes CM. Mitochondrial import efficiency of ATFS-1 regulates mitochondrial UPR activation. Science. 2012;337(6094):587-90.

[77] Zhao Q, Wang J, Levichkin IV, Stasinopoulos S, Ryan MT, Hoogenraad NJ. A mitochondrial specific stress response in mammalian cells. The EMBO Journal. 2002;21(17):4411-9.

[78] Haynes CM, Petrova K, Benedetti C, Yang Y, Ron D. ClpP Mediates Activation of a Mitochondrial Unfolded Protein Response in *C. elegans*. Developmental Cell. 2007;13(4):467-80.

[79] Haynes CM, Yang Y, Blais SP, Neubert TA, Ron D. The Matrix Peptide Exporter HAF-1 Signals a Mitochondrial UPR by Activating the Transcription Factor ZC376.7 in *C. elegans*. Molecular Cell. 2010;37(4):529-40.

[80] Tian Y, Garcia G, Bian Q, Steffen Kristan K, Joe L, Wolff S, et al. Mitochondrial Stress Induces Chromatin Reorganization to Promote Longevity and UPR^{mt}. Cell. 2016;165(5):1197-208.

[81] Nargund Amrita M, Fiorese Christopher J, Pellegrino Mark W, Deng P, Haynes Cole M. Mitochondrial and Nuclear Accumulation of the Transcription Factor ATFS-1 Promotes OXPHOS Recovery during the UPR^{mt}. Molecular Cell. 2015;58(1):123-33.

[82] Gao K, Li Y, Hu S, Liu Y. SUMO peptidase ULP-4 regulates mitochondrial UPR-mediated innate immunity and lifespan extension. eLife. 2019;8:e41792.

[**83**]   Houtkooper RH, Mouchiroud L, Ryu D, Moullan N, Katsyuba E, Knott G, et al. Mitonuclear protein imbalance as a conserved longevity mechanism. Nature. 2013;497:451.

[**84**]   Wu Z, Senchuk MM, Dues DJ, Johnson BK, Cooper JF, Lew L, et al. Mitochondrial unfolded protein response transcription factor ATFS-1 promotes longevity in a long-lived mitochondrial mutant through activation of stress response pathways. BMC Biology. 2018;16(1):147.

[**85**]   Bennett CF, Vander Wende H, Simko M, Klum S, Barfield S, Choi H, et al. Activation of the mitochondrial unfolded protein response does not predict longevity in Caenorhabditis elegans. Nature Communications. 2014;5:3483.

[**86**]   Aldridge JE, Horibe T, Hoogenraad NJ. Discovery of genes activated by the mitochondrial unfolded protein response (mtUPR) and cognate promoter elements. PloS one. 2007;2(9):e874-e.

[**87**]   Araki Y, Sugihara, H., & Hattori, T. In vitro effects of dextran sulfate sodium on a Caco-2 cell line and plausible mechanisms for dextran sulfate sodium-induced colitis. Oncology Reports. 2006(16):1357-62.

[**88**]   Deepa SS, Bhaskaran S, Ranjit R, Qaisar R, Nair BC, Liu Y, et al. Down-regulation of the mitochondrial matrix peptidase ClpP in muscle cells causes mitochondrial dysfunction and decreases cell proliferation. Free Radical Biology and Medicine. 2016;91:281-92.

[**89**]   Bhaskaran S, Pharaoh G, Ranjit R, Murphy A, Matsuzaki S, Nair BC, et al. Loss of mitochondrial protease ClpP protects mice from diet-induced obesity and insulin resistance. EMBO reports. 2018;19(3):e45009.

[**90**]   Seiferling D, Szczepanowska K, Becker C, Senft K, Hermans S, Maiti P, et al. Loss of CLPP alleviates mitochondrial cardiomyopathy without affecting the mammalian UPRmt. EMBO reports. 2016;17(7):953-64.

[**91**]   Yano M. ABCB10 depletion reduces unfolded protein response in mitochondria. Biochemical and Biophysical Research Communications. 2017;486(2):465-9.

[**92**]   Fu Z, Liu F, Liu C, Jin B, Jiang Y, Tang M, et al. Mutant huntingtin inhibits the mitochondrial unfolded protein response by impairing ABCB10 mRNA stability. Biochimica et Biophysica Acta (BBA) - Molecular Basis of Disease. 2019;1865(6):1428-35.

[**93**]   Yamamoto M, Arimura H, Fukushige T, Minami K, Nishizawa Y, Tanimoto A, et al. Abcb10 Role in Heme Biosynthesis *In Vivo*: Abcb10 Knockout in Mice Causes Anemia with Protoporphyrin IX and Iron Accumulation. Mol Cell Biol. 2014;34(6):1077-84.

[**94**]   Seguin A, Takahashi-Makise N, Yien YY, Huston NC, Whitman JC, Musso G, et al. Reductions in the mitochondrial ABC transporter Abcb10 affect the transcriptional profile of heme biosynthesis genes. Journal of Biological Chemistry. 2017;292(39):16284-99.

[**95**]   Fiorese Christopher J, Schulz Anna M, Lin Y-F, Rosin N, Pellegrino Mark W, Haynes Cole M. The Transcription Factor ATF5 Mediates a Mammalian Mitochondrial UPR. Current Biology. 2016;26(15):2037-43.

[96]   Oliveira AN, Hood DA. Effect of Tim23 knockdown in vivo on mitochondrial protein import and retrograde signaling to the UPR[mt] in muscle. American Journal of Physiology-Cell Physiology. 2018;315(4):C516-C26.

[97]   Benedetti C, Haynes CM, Yang Y, Harding HP, Ron D. Ubiquitin-Like Protein 5 Positively Regulates Chaperone Gene Expression in the Mitochondrial Unfolded Protein Response. Genetics. 2006;174(1):229-39.

[98]   Galande S, Purbey PK, Notani D, Kumar PP. The third dimension of gene regulation: organization of dynamic chromatin loopscape by SATB1. Current Opinion in Genetics & Development. 2007;17(5):408-14.

[99]   Yasui D, Miyano M, Cai S, Varga-Weisz P, Kohwi-Shigematsu T. SATB1 targets chromatin remodelling to regulate genes over long distances. Nature. 2002;419(6907):641-5.

[100]   Pakos-Zebrucka K, Koryga I, Mnich K, Ljujic M, Samali A, Gorman AM. The integrated stress response. EMBO reports. 2016;17(10):1374-95.

[101]   Quirós PM, Prado MA, Zamboni N, D'Amico D, Williams RW, Finley D, et al. Multi-omics analysis identifies ATF4 as a key regulator of the mitochondrial stress response in mammals. Journal of Cell Biology. 2017;216(7):2027-45.

[102]   Münch C, Harper JW. Mitochondrial unfolded protein response controls matrix pre-RNA processing and translation. Nature. 2016;534(7609):710-3.

[103]   Baker BM, Nargund AM, Sun T, Haynes CM. Protective Coupling of Mitochondrial Function and Protein Synthesis via the eIF2α Kinase GCN-2. PLOS Genetics. 2012;8(6):e1002760.

[104]   Guo X, Aviles G, Liu Y, Tian R, Unger BA, Lin Y-HT, et al. Mitochondrial stress is relayed to the cytosol by an OMA1–DELE1–HRI pathway. Nature. 2020;579(7799):427-32.

[105]   Fessler E, Eckl E-M, Schmitt S, Mancilla IA, Meyer-Bender MF, Hanf M, et al. A pathway coordinated by DELE1 relays mitochondrial stress to the cytosol. Nature. 2020;579(7799):433-7.

[106]   Donnelly N, Gorman AM, Gupta S, Samali A. The eIF2α kinases: their structures and functions. Cellular and Molecular Life Sciences. 2013;70(19):3493-511.

[107]   Harding HP, Novoa I, Zhang Y, Zeng H, Wek R, Schapira M, et al. Regulated Translation Initiation Controls Stress-Induced Gene Expression in Mammalian Cells. Molecular Cell. 2000;6(5):1099-108.

[108]   Sudhakar A, Ramachandran A, Ghosh S, Hasnain SE, Kaufman RJ, Ramaiah KVA. Phosphorylation of Serine 51 in Initiation Factor 2α (eIF2α) Promotes Complex Formation between eIF2α(P) and eIF2B and Causes Inhibition in the Guanine Nucleotide Exchange Activity of eIF2B. Biochemistry. 2000;39(42):12929-38.

[109]   Lu PD, Harding HP, Ron D. Translation reinitiation at alternative open reading frames regulates gene expression in an integrated stress response. The Journal of Cell Biology. 2004;167(1):27-33.

[110]   Zhou D, Palam LR, Jiang L, Narasimhan J, Staschke KA, Wek RC. Phosphorylation of eIF2 Directs ATF5 Translational Control in Response to Diverse Stress Conditions. Journal of Biological Chemistry. 2008;283(11):7064-73.

[111]   Wang X-Z, Kuroda M, Sok J, Batchvarova N, Kimmel R, Chung P, et al. Identification of novel stress-induced genes downstream of chop. The EMBO Journal. 1998;17(13):3619-30.

[112]   Averous J, Bruhat A, Jousse C, Carraro V, Thiel G, Fafournoux P. Induction of CHOP Expression by Amino Acid Limitation Requires Both ATF4 Expression and ATF2 Phosphorylation. Journal of Biological Chemistry. 2004;279(7):5288-97.

[113]   Pareek G, Thomas RE, Vincow ES, Morris DR, Pallanck LJ. Lon protease inactivation in Drosophila causes unfolded protein stress and inhibition of mitochondrial translation. Cell Death Discovery. 2018;4(1):51.

[114]   Baqri RM, Pietron AV, Gokhale RH, Turner BA, Kaguni LS, Shingleton AW, et al. Mitochondrial chaperone TRAP1 activates the mitochondrial UPR and extends healthspan in Drosophila. Mechanisms of Ageing and Development. 2014;141-142:35-45.

[115]   Dimos BA, Mahmud SA, Fuess LE, Mydlarz LD, Pellegrino MW. Uncovering a mitochondrial unfolded protein response in corals and its role in adapting to a changing world. Proceedings of the Royal Society B: Biological Sciences. 2019;286(1905):20190470.

[116]   Kelley DE, He J, Menshikova EV, Ritov VB. Dysfunction of Mitochondria in Human Skeletal Muscle in Type 2 Diabetes. Diabetes. 2002;51(10):2944-50.

[117]   Guerra F, Guaragnella N, Arbini AA, Bucci C, Giannattasio S, Moro L. Mitochondrial Dysfunction: A Novel Potential Driver of Epithelial-to-Mesenchymal Transition in Cancer. Frontiers in Oncology. 2017;7(295).

[118]   Curcio M, Bradke F. Axon Regeneration in the Central Nervous System: Facing the Challenges from the Inside. Annual Review of Cell and Developmental Biology. 2018;34(1):495-521.

[119]   Pathak D, Shields LY, Mendelsohn BA, Haddad D, Lin W, Gerencser AA, et al. The Role of Mitochondrially Derived ATP in Synaptic Vesicle Recycling. Journal of Biological Chemistry. 2015;290(37):22325-36.

[120]   Klein C, Westenberger A. Genetics of Parkinson's Disease. Cold Spring Harbor Perspectives in Medicine. 2012;2(1).

[121]   Matsuda N, Sato S, Shiba K, Okatsu K, Saisho K, Gautier CA, et al. PINK1 stabilized by mitochondrial depolarization recruits Parkin to damaged mitochondria and activates latent Parkin for mitophagy. The Journal of Cell Biology. 2010;189(2):211-21.

[**122**] Jenner P, Olanow CW. The pathogenesis of cell death in Parkinson's disease. Neurology. 2006;66(10 suppl 4):S24-S36.

[**123**] Pesah Y, Pham T, Burgess H, Middlebrooks B, Verstreken P, Zhou Y, et al. *Drosophila parkin* mutants have decreased mass and cell size and increased sensitivity to oxygen radical stress. Development. 2004;131(9):2183-94.

[**124**] Sliter DA, Martinez J, Hao L, Chen X, Sun N, Fischer TD, et al. Parkin and PINK1 mitigate STING-induced inflammation. Nature. 2018;561(7722):258-62.

[**125**] Heeman B, Van den Haute C, Aelvoet S-A, Valsecchi F, Rodenburg RJ, Reumers V, et al. Depletion of PINK1 affects mitochondrial metabolism, calcium homeostasis and energy maintenance. Journal of Cell Science. 2011;124(7):1115-25.

[**126**] Ramirez A, Heimbach A, Gründemann J, Stiller B, Hampshire D, Cid LP, et al. Hereditary parkinsonism with dementia is caused by mutations in ATP13A2, encoding a lysosomal type 5 P-type ATPase. Nature Genetics. 2006;38(10):1184-91.

[**127**] Li J-Q, Tan L, Yu J-T. The role of the LRRK2 gene in Parkinsonism. Molecular Neurodegeneration. 2014;9(1):47.

[**128**] Di Maio R, Hoffman EK, Rocha EM, Keeney MT, Sanders LH, De Miranda BR, et al. LRRK2 activation in idiopathic Parkinson's disease. Science Translational Medicine. 2018;10(451):eaar5429.

[**129**] Bonello F, Hassoun S-M, Mouton-Liger F, Shin YS, Muscat A, Tesson C, et al. LRRK2 impairs PINK1/Parkin-dependent mitophagy via its kinase activity: pathologic insights into Parkinson's disease. Human Molecular Genetics. 2019;28(10):1645-60.

[**130**] Schapansky J, Khasnavis S, DeAndrade MP, Nardozzi JD, Falkson SR, Boyd JD, et al. Familial knockin mutation of LRRK2 causes lysosomal dysfunction and accumulation of endogenous insoluble α-synuclein in neurons. Neurobiology of Disease. 2018;111:26-35.

[**131**] Casari G, De Fusco M, Ciarmatori S, Zeviani M, Mora M, Fernandez P, et al. Spastic Paraplegia and OXPHOS Impairment Caused by Mutations in Paraplegin, a Nuclear-Encoded Mitochondrial Metalloprotease. Cell. 1998;93(6):973-83.

[**132**] Mihaylova P, Murphy S, Walsh R. PO094 Spg7-related ataxia in the irish national ataxia clinic cohort. Journal of Neurology, Neurosurgery & Psychiatry. 2017;88(Suppl 1):A36-A.

[**133**] Pfeffer G, Pyle A, Griffin H, Miller J, Wilson V, Turnbull L, et al. SPG7 mutations are a common cause of undiagnosed ataxia. Neurology. 2015;84(11):1174-6.

[**134**] Peña S, Sherman T, Brookes PS, Nehrke K. The Mitochondrial Unfolded Protein Response Protects against Anoxia in Caenorhabditis elegans. PLOS ONE. 2016;11(7):e0159989.

[**135**] Strauss KM, Martins LM, Plun-Favreau H, Marx FP, Kautzmann S, Berg D, et al. Loss of function mutations in the gene encoding Omi/HtrA2 in Parkinson's disease. Human Molecular Genetics. 2005;14(15):2099-111.

[**136**] Patterson VL, Zullo AJ, Koenig C, Stoessel S, Jo H, Liu X, et al. Neural-Specific Deletion of Htra2 Causes Cerebellar Neurodegeneration and Defective Processing of Mitochondrial OPA1. PLOS ONE. 2014;9(12):e115789.

[**137**] Moisoi N, Klupsch K, Fedele V, East P, Sharma S, Renton A, et al. Mitochondrial dysfunction triggered by loss of HtrA2 results in the activation of a brain-specific transcriptional stress response. Cell Death Differ. 2008;16:449.

[**138**] Halterman MW, Gill M, DeJesus C, Ogihara M, Schor NF, Federoff HJ. The Endoplasmic Reticulum Stress Response Factor CHOP-10 Protects against Hypoxia-induced Neuronal Death. Journal of Biological Chemistry. 2010;285(28):21329-40.

[**139**] Silva RM, Ries V, Oo TF, Yarygina O, Jackson-Lewis V, Ryu EJ, et al. CHOP/GADD153 is a mediator of apoptotic death in substantia nigra dopamine neurons in an in vivo neurotoxin model of parkinsonism. Journal of Neurochemistry. 2005;95(4):974-86.

[**140**] Holtz WA, O'Malley KL. Parkinsonian Mimetics Induce Aspects of Unfolded Protein Response in Death of Dopaminergic Neurons. Journal of Biological Chemistry. 2003;278(21):19367-77.

[**141**] Horibe T, Hoogenraad NJ. The Chop Gene Contains an Element for the Positive Regulation of the Mitochondrial Unfolded Protein Response. PLOS ONE. 2007;2(9):e835.

[**142**] Fiesel FC, James ED, Hudec R, Springer W. Mitochondrial targeted HSP90 inhibitor Gamitrinib-TPP (G-TPP) induces PINK1/Parkin-dependent mitophagy. Oncotarget. 2017;8(63).

[**143**] Pickrell Alicia M, Huang C-H, Kennedy Scott R, Ordureau A, Sideris Dionisia P, Hoekstra Jake G, et al. Endogenous Parkin Preserves Dopaminergic Substantia Nigral Neurons following Mitochondrial DNA Mutagenic Stress. Neuron. 2015;87(2):371-81.

[**144**] Moisoi N, Fedele V, Edwards J, Martins LM. Loss of PINK1 enhances neurodegeneration in a mouse model of Parkinson's disease triggered by mitochondrial stress. Neuropharmacology. 2014;77:350-7.

[**145**] Oliveras-Salvá M, Macchi F, Coessens V, Deleersnijder A, Gérard M, Van der Perren A, et al. Alpha-synuclein-induced neurodegeneration is exacerbated in PINK1 knockout mice. Neurobiology of Aging. 2014;35(11):2625-36.

[**146**] Gispert S, Ricciardi F, Kurz A, Azizov M, Hoepken H-H, Becker D, et al. Parkinson Phenotype in Aged PINK1-Deficient Mice Is Accompanied by Progressive Mitochondrial Dysfunction in Absence of Neurodegeneration. PLOS ONE. 2009;4(6):e5777.

[**147**] Cooper JF, Machiela E, Dues DJ, Spielbauer KK, Senchuk MM, Van Raamsdonk JM. Activation of the mitochondrial unfolded protein response promotes longevity and dopamine neuron survival in Parkinson's disease models. Scientific Reports. 2017;7(1):16441.

[**148**] Kim H, Yang J, Kim MJ, Choi S, Chung J-R, Kim J-M, et al. Tumor Necrosis Factor Receptor-associated Protein 1 (TRAP1) Mutation and TRAP1 Inhibitor Gamitrinib-triphenylphosphonium (G-TPP) Induce a Forkhead Box O (FOXO)-dependent Cell

Protective Signal from Mitochondria. Journal of Biological Chemistry. 2016;291(4):1841-53.

[149] Pimenta de Castro I, Costa AC, Lam D, Tufi R, Fedele V, Moisoi N, et al. Genetic analysis of mitochondrial protein misfolding in Drosophila melanogaster. Cell Death Differ. 2012;19(8):1308-16.

[150] Papa L, Germain D. SirT3 Regulates the Mitochondrial Unfolded Protein Response. Mol Cell Biol. 2014;34(4):699-710.

[151] Jankovic J. Parkinson's disease: clinical features and diagnosis. Journal of Neurology, Neurosurgery & Psychiatry. 2008;79(4):368-76.

[152] Pickrell Alicia M, Youle Richard J. The Roles of PINK1, Parkin, and Mitochondrial Fidelity in Parkinson's Disease. Neuron. 2015;85(2):257-73.

[153] Gautier CA, Kitada T, Shen J. Loss of PINK1 causes mitochondrial functional defects and increased sensitivity to oxidative stress. Proceedings of the National Academy of Sciences. 2008;105(32):11364-9.

[154] Palacino JJ, Sagi D, Goldberg MS, Krauss S, Motz C, Wacker M, et al. Mitochondrial Dysfunction and Oxidative Damage in parkin-deficient Mice. Journal of Biological Chemistry. 2004;279(18):18614-22.

[155] Kitada T, Tong Y, Gautier CA, Shen J. Absence of nigral degeneration in aged parkin/DJ-1/PINK1 triple knockout mice. Journal of Neurochemistry. 2009;111(3):696-702.

[156] Dave KD, De Silva S, Sheth NP, Ramboz S, Beck MJ, Quang C, et al. Phenotypic characterization of recessive gene knockout rat models of Parkinson's disease. Neurobiology of Disease. 2014;70:190-203.

[157] Villeneuve LM, Purnell PR, Boska MD, Fox HS. Early Expression of Parkinson's Disease-Related Mitochondrial Abnormalities in PINK1 Knockout Rats. Molecular Neurobiology. 2016;53(1):171-86.

[158] Yang Y, Gehrke S, Imai Y, Huang Z, Ouyang Y, Wang J-W, et al. Mitochondrial pathology and muscle and dopaminergic neuron degeneration caused by inactivation of Drosophila Pink1 is rescued by Parkin. Proceedings of the National Academy of Sciences. 2006;103(28):10793-8.

[159] Whitworth AJ, Theodore DA, Greene JC, Beneš H, Wes PD, Pallanck LJ. Increased glutathione S-transferase activity rescues dopaminergic neuron loss in a Drosophila model of Parkinson's disease. Proceedings of the National Academy of Sciences. 2005;102(22):8024-9.

[160] Ran FA, Hsu PD, Wright J, Agarwala V, Scott DA, Zhang F. Genome engineering using the CRISPR-Cas9 system. Nature Protocols. 2013;8(11):2281-308.

[161] Livak KJ, Schmittgen TD. Analysis of relative gene expression data using real-time quantitative PCR and the 2(-Delta Delta C(T)) Method. Methods. 2001;25(4):402-8.

[162]   Winsor NJ, Killackey SA, Philpott DJ, Girardin SE. An optimized procedure for quantitative analysis of mitophagy with the mtKeima system using flow cytometry. BioTechniques. 2020;69(4):249-56.

[163]   Cox J, Mann M. MaxQuant enables high peptide identification rates, individualized p.p.b.-range mass accuracies and proteome-wide protein quantification. Nature Biotechnology. 2008;26(12):1367-72.

[164]   Plubell DL, Wilmarth PA, Zhao Y, Fenton AM, Minnier J, Reddy AP, et al. Extended Multiplexing of Tandem Mass Tags (TMT) Labeling Reveals Age and High Fat Diet Specific Proteome Changes in Mouse Epididymal Adipose Tissue. Molecular & Cellular Proteomics. 2017;16(5):873-90.

[165]   Tyanova S, Temu T, Sinitcyn P, Carlson A, Hein MY, Geiger T, et al. The Perseus computational platform for comprehensive analysis of (prote)omics data. Nature Methods. 2016;13(9):731-40.

[166]   Kuznetsova I, Lugmayr A, Rackham O, Filipovska A. OmicsVolcano: Software for intuitive visualization and interactive exploration of high-throughput biological data. STAR Protocols. 2021;2(1):100279.

[167]   Tsyganov K, James Perry A, Kenneth Archer S, Powell D. RNAsik: A Pipeline for complete and reproducible RNA-seq analysis that runs anywhere with speed and ease. The Journal of Open Source Software. 2018;3:583.

[168]   Kim J-E, Park H, Choi S-H, Kong M-J, Kang T-C. CDDO-Me Selectively Attenuates CA1 Neuronal Death Induced by Status Epilepticus via Facilitating Mitochondrial Fission Independent of LONP1. Cells. 2019;8(8):833.

[169]   Wang X-Y, Zhang X-H, Peng L, Liu Z, Yang Y-X, He Z-X, et al. Bardoxolone methyl (CDDO-Me or RTA402) induces cell cycle arrest, apoptosis and autophagy via PI3K/Akt/mTOR and p38 MAPK/Erk1/2 signaling pathways in K562 cells. Am J Transl Res. 2017;9(10):4652-72.

[170]   Qin D-J, Tang C-X, Yang L, Lei H, Wei W, Wang Y-Y, et al. Hsp90 Is a Novel Target Molecule of CDDO-Me in Inhibiting Proliferation of Ovarian Cancer Cells. PLOS ONE. 2015;10(7):e0132337.

[171]   Pollecker K, Sylvester M, Voos W. Proteomic analysis demonstrates the role of the quality control protease LONP1 in mitochondrial protein aggregation. Journal of Biological Chemistry. 2021;297(4):101134.

[172]   Moullan N, Mouchiroud L, Wang X, Ryu D, Williams Evan G, Mottis A, et al. Tetracyclines Disturb Mitochondrial Function across Eukaryotic Models: A Call for Caution in Biomedical Research. Cell Reports. 2015;10(10):1681-91.

[173]   Jin SM, Youle RJ. The accumulation of misfolded proteins in the mitochondrial matrix is sensed by PINK1 to induce PARK2/Parkin-mediated mitophagy of polarized mitochondria. Autophagy. 2013;9(11):1750-7.

[174]   Hansen KG, Herrmann JM. Transport of Proteins into Mitochondria. The Protein Journal. 2019;38(3):330-42.

[175] Weber RJM, Li E, Bruty J, He S, Viant MR. MaConDa: a publicly accessible mass spectrometry contaminants database. Bioinformatics. 2012;28(21):2856-7.

[176] Linares R, Tan S, Gounou C, Arraud N, Brisson AR. High-speed centrifugation induces aggregation of extracellular vesicles. J Extracell Vesicles. 2015;4:29509-.

[177] Sui X, Pires DEV, Ormsby AR, Cox D, Nie S, Vecchi G, et al. Widespread remodeling of proteome solubility in response to different protein homeostasis stresses. Proceedings of the National Academy of Sciences. 2020;117(5):2422-31.

[178] Pluskal T, Castillo S, Villar-Briones A, Orešič M. MZmine 2: Modular framework for processing, visualizing, and analyzing mass spectrometry-based molecular profile data. BMC Bioinformatics. 2010;11(1):395.

[179] Joshi A, Dai L, Liu Y, Lee J, Ghahhari NM, Segala G, et al. The mitochondrial HSP90 paralog TRAP1 forms an OXPHOS-regulated tetramer and is involved in mitochondrial metabolic homeostasis. BMC Biology. 2020;18(1):10.

[180] Bie AS, Cömert C, Körner R, Corydon TJ, Palmfeldt J, Hipp MS, et al. An inventory of interactors of the human HSP60/HSP10 chaperonin in the mitochondrial matrix space. Cell Stress and Chaperones. 2020;25(3):407-16.

[181] Wrobel L, Topf U, Bragoszewski P, Wiese S, Sztolsztener ME, Oeljeklaus S, et al. Mistargeted mitochondrial proteins activate a proteostatic response in the cytosol. Nature. 2015;524(7566):485-8.

[182] Kühl I, Miranda M, Atanassov I, Kuznetsova I, Hinze Y, Mourier A, et al. Transcriptomic and proteomic landscape of mitochondrial dysfunction reveals secondary coenzyme Q deficiency in mammals. eLife. 2017;6:e30952.

[183] Michel S, Canonne M, Arnould T, Renard P. Inhibition of mitochondrial genome expression triggers the activation of CHOP-10 by a cell signaling dependent on the integrated stress response but not the mitochondrial unfolded protein response. Mitochondrion. 2015;21:58-68.

[184] Luger A-L, Sauer B, Lorenz NI, Engel AL, Braun Y, Voss M, et al. Doxycycline Impairs Mitochondrial Function and Protects Human Glioma Cells from Hypoxia-Induced Cell Death: Implications of Using Tet-Inducible Systems. International journal of molecular sciences. 2018;19(5):1504.

[185] Sasaki K, Uchiumi T, Toshima T, Yagi M, Do Y, Hirai H, et al. Mitochondrial translation inhibition triggers ATF4 activation, leading to integrated stress response but not to mitochondrial unfolded protein response. Biosci Rep. 2020;40(11):BSR20201289.

[186] Kang BH, Plescia J, Song HY, Meli M, Colombo G, Beebe K, et al. Combinatorial drug design targeting multiple cancer signaling networks controlled by mitochondrial Hsp90. J Clin Invest. 2009;119(3):454-64.

[187] Cupo RR, Shorter J. Skd3 (human ClpB) is a potent mitochondrial protein disaggregase that is inactivated by 3-methylglutaconic aciduria-linked mutations. eLife. 2020;9:e55279.

[188] Pollecker K, Sylvester M, Voos W. Proteomic analysis demonstrates the role of the quality control protease LONP1 in mitochondrial protein aggregation. Journal of Biological Chemistry. 2021;297(4).

[189] Bogenhagen DF, Ostermeyer-Fay AG, Haley JD, Garcia-Diaz M. Kinetics and Mechanism of Mammalian Mitochondrial Ribosome Assembly. Cell reports. 2018;22(7):1935-44.

[190] Poveda-Huertes D, Taskin AA, Dhaouadi I, Myketin L, Marada A, Habernig L, et al. Increased mitochondrial protein import and cardiolipin remodelling upon early mtUPR. PLOS Genetics. 2021;17(7):e1009664.

[191] Anderson NS, Haynes CM. Folding the Mitochondrial UPR into the Integrated Stress Response. Trends in Cell Biology. 2020;30(6):428-39.

[192] Forsström S, Jackson CB, Carroll CJ, Kuronen M, Pirinen E, Pradhan S, et al. Fibroblast Growth Factor 21 Drives Dynamics of Local and Systemic Stress Responses in Mitochondrial Myopathy with mtDNA Deletions. Cell Metabolism. 2019;30(6):1040-54.e7.

[193] Huang da W, Sherman BT, Lempicki RA. Bioinformatics enrichment tools: paths toward the comprehensive functional analysis of large gene lists. Nucleic Acids Res. 2009;37(1):1-13.

[194] Huang da W, Sherman BT, Lempicki RA. Systematic and integrative analysis of large gene lists using DAVID bioinformatics resources. Nat Protoc. 2009;4(1):44-57.

[195] Formosa LE, Dibley MG, Stroud DA, Ryan MT. Building a complex complex: Assembly of mitochondrial respiratory chain complex I. Seminars in Cell & Developmental Biology. 2018;76:154-62.

[196] Vincow ES, Merrihew G, Thomas RE, Shulman NJ, Beyer RP, MacCoss MJ, et al. The PINK1–Parkin pathway promotes both mitophagy and selective respiratory chain turnover in vivo. Proceedings of the National Academy of Sciences. 2013;110(16):6400-5.

[197] Keeney PM, Xie J, Capaldi RA, Bennett JP. Parkinson's Disease Brain Mitochondrial Complex I Has Oxidatively Damaged Subunits and Is Functionally Impaired and Misassembled. The Journal of Neuroscience. 2006;26(19):5256-64.

[198] Kühlbrandt W. Structure and function of mitochondrial membrane protein complexes. BMC Biology. 2015;13(1):89.

[199] Pfeffer S, Woellhaf MW, Herrmann JM, Förster F. Organization of the mitochondrial translation machinery studied in situ by cryoelectron tomography. Nature Communications. 2015;6(1):6019.

[200] Wang T, Steel G, Milam AH, Valle D. Correction of ornithine accumulation prevents retinal degeneration in a mouse model of gyrate atrophy of the choroid and retina. Proceedings of the National Academy of Sciences. 2000;97(3):1224-9.

[201] van Karnebeek CDM, Ramos RJ, Wen X-Y, Tarailo-Graovac M, Gleeson JG, Skrypnyk C, et al. Bi-allelic GOT2 Mutations Cause a Treatable Malate-Aspartate Shuttle-Related Encephalopathy. The American Journal of Human Genetics. 2019;105(3):534-48.

[202] Lou X, Zhou X, Li H, Lu X, Bao X, Yang K, et al. Biallelic Mutations in ACACA Cause a Disruption in Lipid Homeostasis That Is Associated With Global Developmental Delay, Microcephaly, and Dysmorphic Facial Features. Frontiers in Cell and Developmental Biology. 2021;9(1966).

[203] García-Cazorla À, Verdura E, Juliá-Palacios N, Anderson EN, Goicoechea L, Planas-Serra L, et al. Impairment of the mitochondrial one-carbon metabolism enzyme SHMT2 causes a novel brain and heart developmental syndrome. Acta Neuropathologica. 2020;140(6):971-5.

[204] Frezza C. Mitochondrial metabolites: undercover signalling molecules. Interface Focus. 2017;7(2):20160100.

[205] Yoo HC, Yu YC, Sung Y, Han JM. Glutamine reliance in cell metabolism. Experimental & Molecular Medicine. 2020;52(9):1496-516.

[206] White PJ, McGarrah RW, Grimsrud PA, Tso S-C, Yang W-H, Haldeman JM, et al. The BCKDH Kinase and Phosphatase Integrate BCAA and Lipid Metabolism via Regulation of ATP-Citrate Lyase. Cell Metabolism. 2018;27(6):1281-93.e7.

[207] Ali EZ, Ngu L-H. Fourteen new mutations of BCKDHA, BCKDHB and DBT genes associated with maple syrup urine disease (MSUD) in Malaysian population. Molecular Genetics and Metabolism Reports. 2018;17:22-30.

[208] Yoneda T, Benedetti C, Urano F, Clark SG, Harding HP, Ron D. Compartment-specific perturbation of protein handling activates genes encoding mitochondrial chaperones. Journal of Cell Science. 2004;117(18):4055-66.

[209] Poveda-Huertes D, Matic S, Marada A, Habernig L, Licheva M, Myketin L, et al. An Early mtUPR: Redistribution of the Nuclear Transcription Factor Rox1 to Mitochondria Protects against Intramitochondrial Proteotoxic Aggregates. Molecular Cell. 2020;77(1):180-8.e9.

[210] Khan NA, Nikkanen J, Yatsuga S, Jackson C, Wang L, Pradhan S, et al. mTORC1 Regulates Mitochondrial Integrated Stress Response and Mitochondrial Myopathy Progression. Cell Metabolism. 2017;26(2):419-28.e5.

[211] Papa L, Germain D. Estrogen receptor mediates a distinct mitochondrial unfolded protein response. Journal of Cell Science. 2011;124(9):1396-402.

[212] Krishnamoorthy T, Pavitt GD, Zhang F, Dever TE, Hinnebusch AG. Tight binding of the phosphorylated alpha subunit of initiation factor 2 (eIF2alpha) to the regulatory subunits of guanine nucleotide exchange factor eIF2B is required for inhibition of translation initiation. Mol Cell Biol. 2001;21(15):5018-30.

[213] Shao L-W, Peng Q, Dong M, Gao K, Li Y, Li Y, et al. Histone deacetylase HDA-1 modulates mitochondrial stress response and longevity. Nature Communications. 2020;11(1):4639.

[214] Gyorgy AB, Szemes M, De Juan Romero C, Tarabykin V, Agoston DV. SATB2 interacts with chromatin-remodeling molecules in differentiating cortical neurons. European Journal of Neuroscience. 2008;27(4):865-73.

[215]   Bhaskara S, Jacques V, Rusche JR, Olson EN, Cairns BR, Chandrasekharan MB. Histone deacetylases 1 and 2 maintain S-phase chromatin and DNA replication fork progression. Epigenetics & Chromatin. 2013;6(1):27.

[216]   Oka Y, Varmark H, Vitting-Seerup K, Beli P, Waage J, Hakobyan A, et al. UBL5 is essential for pre-mRNA splicing and sister chromatid cohesion in human cells. EMBO reports. 2014;15(9):956-64.

[217]   Lee S, Kim S, Sun X, Lee J-H, Cho H. Cell cycle-dependent mitochondrial biogenesis and dynamics in mammalian cells. Biochemical and Biophysical Research Communications. 2007;357(1):111-7.

[218]   Stroud DA, Surgenor EE, Formosa LE, Reljic B, Frazier AE, Dibley MG, et al. Accessory subunits are integral for assembly and function of human mitochondrial complex I. Nature. 2016;538(7623):123-6.

[219]   Lazarou M, McKenzie M, Ohtake A, Thorburn DR, Ryan MT. Analysis of the Assembly Profiles for Mitochondrial- and Nuclear-DNA-Encoded Subunits into Complex I. Mol Cell Biol. 2007;27(12):4228-37.

[220]   Szczepanowska K, Senft K, Heidler J, Herholz M, Kukat A, Höhne MN, et al. A salvage pathway maintains highly functional respiratory complex I. Nature Communications. 2020;11(1):1643.

[221]   Dieteren CEJ, Koopman WJH, Swarts HG, Peters JGP, Maczuga P, van Gemst JJ, et al. Subunit-specific Incorporation Efficiency and Kinetics in Mitochondrial Complex I Homeostasis. Journal of Biological Chemistry. 2012;287(50):41851-60.

[222]   Scheper GC, van der Klok T, van Andel RJ, van Berkel CGM, Sissler M, Smet J, et al. Mitochondrial aspartyl-tRNA synthetase deficiency causes leukoencephalopathy with brain stem and spinal cord involvement and lactate elevation. Nature Genetics. 2007;39(4):534-9.

[223]   Galmiche L, Serre V, Beinat M, Assouline Z, Lebre A-S, Chretien D, et al. Exome sequencing identifies MRPL3 mutation in mitochondrial cardiomyopathy. Human Mutation. 2011;32(11):1225-31.

[224]   Alavi MV, Fuhrmann N. Dominant optic atrophy, OPA1, and mitochondrial quality control: understanding mitochondrial network dynamics. Molecular Neurodegeneration. 2013;8(1):32.

[225]   Gilkerson R, De La Torre P, St. Vallier S. Mitochondrial OMA1 and OPA1 as Gatekeepers of Organellar Structure/Function and Cellular Stress Response. Frontiers in Cell and Developmental Biology. 2021;9.

[226]   Sekine S, Kanamaru Y, Koike M, Nishihara A, Okada M, Kinoshita H, et al. Rhomboid Protease PARL Mediates the Mitochondrial Membrane Potential Loss-induced Cleavage of PGAM5. Journal of Biological Chemistry. 2012;287(41):34635-45.

[227]   Wai T, Saita S, Nolte H, Müller S, König T, Richter-Dennerlein R, et al. The membrane scaffold SLP2 anchors a proteolytic hub in mitochondria containing PARL and the i-AAA protease YME1L. EMBO reports. 2016;17(12):1844-56.

[228] Nargund AM, Pellegrino MW, Fiorese CJ, Baker BM, Haynes CM. Mitochondrial Import Efficiency of ATFS-1 Regulates Mitochondrial UPR Activation. Science. 2012;337(6094):587-90.

[229] Casas F, Rochard P, Rodier A, Cassar-Malek I, Marchal-Victorion S, Wiesner RJ, et al. A variant form of the nuclear triiodothyronine receptor c-ErbAalpha1 plays a direct role in regulation of mitochondrial RNA synthesis. Mol Cell Biol. 1999;19(12):7913-24.

[230] Cammarota M, Paratcha G, Bevilaqua LRM, De Stein ML, Lopez M, De Iraldi AP, et al. Cyclic AMP-Responsive Element Binding Protein in Brain Mitochondria. Journal of Neurochemistry. 1999;72(6):2272-7.

[231] Lee J, Kim C-H, Simon DK, Aminova LR, Andreyev AY, Kushnareva YE, et al. Mitochondrial Cyclic AMP Response Element-binding Protein (CREB) Mediates Mitochondrial Gene Expression and Neuronal Survival. Journal of Biological Chemistry. 2005;280(49):40398-401.

[232] Yoshida Y, Izumi H, Torigoe T, Ishiguchi H, Itoh H, Kang D, et al. p53 Physically Interacts with Mitochondrial Transcription Factor A and Differentially Regulates Binding to Damaged DNA. Cancer Research. 2003;63(13):3729-34.

[233] Bakhanashvili M, Grinberg S, Bonda E, Simon AJ, Moshitch-Moshkovitz S, Rahav G. p53 in mitochondria enhances the accuracy of DNA synthesis. Cell Death & Differentiation. 2008;15(12):1865-74.

[234] Gough DJ, Corlett A, Schlessinger K, Wegrzyn J, Larner AC, Levy DE. Mitochondrial STAT3 Supports Ras-Dependent Oncogenic Transformation. Science. 2009;324(5935):1713-6.

[235] Chen JQ, Delannoy M, Cooke C, Yager JD. Mitochondrial localization of ERα and ERβ in human MCF7 cells. American Journal of Physiology-Endocrinology and Metabolism. 2004;286(6):E1011-E22.

[236] Liu Z-P, Wu C, Miao H, Wu H. RegNetwork: an integrated database of transcriptional and post-transcriptional regulatory networks in human and mouse. Database. 2015;2015.

[237] Ge SX, Jung D, Yao R. ShinyGO: a graphical gene-set enrichment tool for animals and plants. Bioinformatics. 2019;36(8):2628-9.

[238] Eferl R, Wagner EF. AP-1: a double-edged sword in tumorigenesis. Nature Reviews Cancer. 2003;3(11):859-68.

[239] Hai T, Hartman MG. The molecular biology and nomenclature of the activating transcription factor/cAMP responsive element binding family of transcription factors: activating transcription factor proteins and homeostasis. Gene. 2001;273(1):1-11.

[240] Jung C, Higgins CMJ, Xu Z. Mitochondrial electron transport chain complex dysfunction in a transgenic mouse model for amyotrophic lateral sclerosis. Journal of Neurochemistry. 2002;83(3):535-45.

[241]   Menzies FM, Cookson MR, Taylor RW, Turnbull DM, Chrzanowska-Lightowlers ZMA, Dong L, et al. Mitochondrial dysfunction in a cell culture model of familial amyotrophic lateral sclerosis. Brain. 2002;125(7):1522-33.

[242]   Parker WD, Parks JK, Swerdlow RH. Complex I deficiency in Parkinson's disease frontal cortex. Brain Research. 2008;1189:215-8.

[243]   Schapira AHV, Cooper JM, Dexter D, Clark JB, Jenner P, Marsden CD. Mitochondrial Complex I Deficiency in Parkinson's Disease. Journal of Neurochemistry. 1990;54(3):823-7.

[244]   Dutta R, McDonough J, Yin X, Peterson J, Chang A, Torres T, et al. Mitochondrial dysfunction as a cause of axonal degeneration in multiple sclerosis patients. Annals of Neurology. 2006;59(3):478-89.

[245]   Campbell GR, Ziabreva I, Reeve AK, Krishnan KJ, Reynolds R, Howell O, et al. Mitochondrial DNA deletions and neurodegeneration in multiple sclerosis. Annals of Neurology. 2011;69(3):481-92.

[246]   Pellegrino MW, Nargund AM, Kirienko NV, Gillis R, Fiorese CJ, Haynes CM. Mitochondrial UPR-regulated innate immunity provides resistance to pathogen infection. Nature. 2014;516(7531):414-7.

[247]   Li TY, Sleiman MB, Li H, Gao AW, Mottis A, Bachmann AM, et al. The transcriptional coactivator CBP/p300 is an evolutionarily conserved node that promotes longevity in response to mitochondrial stress. Nature Aging. 2021;1(2):165-78.

[248]   Cochemé HM, Murphy MP. Complex I Is the Major Site of Mitochondrial Superoxide Production by Paraquat. Journal of Biological Chemistry. 2008;283(4):1786-98.

[249]   Durieux J, Wolff S, Dillin A. The Cell-Non-Autonomous Nature of Electron Transport Chain-Mediated Longevity. Cell. 2011;144(1):79-91.

[250]   Berendzen KM, Durieux J, Shao L-W, Tian Y, Kim H-e, Wolff S, et al. Neuroendocrine Coordination of Mitochondrial Stress Signaling and Proteostasis. Cell. 2016;166(6):1553-63.e10.

[251]   Zhang Q, Wu X, Chen P, Liu L, Xin N, Tian Y, et al. The Mitochondrial Unfolded Protein Response Is Mediated Cell-Non-autonomously by Retromer-Dependent Wnt Signaling. Cell. 2018;174(4):870-83.e17.

[252]   Sladowska M, Turek M, Kim M-J, Drabikowski K, Mussulini BHM, Mohanraj K, et al. Proteasome activity contributes to pro-survival response upon mild mitochondrial stress in Caenorhabditis elegans. PLOS Biology. 2021;19(7):e3001302.

[253]   Craig EA. Hsp70 at the membrane: driving protein translocation. BMC Biology. 2018;16(1):11.

[254]   Bannister AJ, Kouzarides T. Regulation of chromatin by histone modifications. Cell Research. 2011;21(3):381-95.

[255] Jambhekar A, Dhall A, Shi Y. Roles and regulation of histone methylation in animal development. Nature Reviews Molecular Cell Biology. 2019;20(10):625-41.

[256] Narlikar Geeta J, Sundaramoorthy R, Owen-Hughes T. Mechanisms and Functions of ATP-Dependent Chromatin-Remodeling Enzymes. Cell. 2013;154(3):490-503.

[257] Dzeja PP, Bortolon R, Perez-Terzic C, Holmuhamedov EL, Terzic A. Energetic communication between mitochondria and nucleus directed by catalyzed phosphotransfer. Proceedings of the National Academy of Sciences. 2002;99(15):10156-61.

[258] Imamura H, Huynh Nhat KP, Togawa H, Saito K, Iino R, Kato-Yamada Y, et al. Visualization of ATP levels inside single living cells with fluorescence resonance energy transfer-based genetically encoded indicators. Proceedings of the National Academy of Sciences. 2009;106(37):15651-6.

[259] Wright RHG, Lioutas A, Dily FL, Soronellas D, Pohl A, Bonet J, et al. ADP-ribose-derived nuclear ATP synthesis by NUDIX5 is required for chromatin remodeling. Science. 2016;352(6290):1221-5.

[260] Lozoya OA, Wang T, Grenet D, Wolfgang TC, Sobhany M, Ganini da Silva D, et al. Mitochondrial acetyl-CoA reversibly regulates locus-specific histone acetylation and gene expression. Life Science Alliance. 2019;2(1):e201800228.

[261] Martínez-Reyes I, Diebold Lauren P, Kong H, Schieber M, Huang H, Hensley Christopher T, et al. TCA Cycle and Mitochondrial Membrane Potential Are Necessary for Diverse Biological Functions. Molecular Cell. 2016;61(2):199-209.

[262] Metodiev MD, Lesko N, Park CB, Cámara Y, Shi Y, Wibom R, et al. Methylation of 12S rRNA Is Necessary for In Vivo Stability of the Small Subunit of the Mammalian Mitochondrial Ribosome. Cell Metabolism. 2009;9(4):386-97.

[263] Laptev I, Shvetsova E, Levitskii S, Serebryakova M, Rubtsova M, Bogdanov A, et al. Mouse Trmt2B protein is a dual specific mitochondrial metyltransferase responsible for m5U formation in both tRNA and rRNA. RNA Biology. 2020;17(4):441-50.

[264] Metodiev MD, Spåhr H, Loguercio Polosa P, Meharg C, Becker C, Altmueller J, et al. NSUN4 Is a Dual Function Mitochondrial Protein Required for Both Methylation of 12S rRNA and Coordination of Mitoribosomal Assembly. PLOS Genetics. 2014;10(2):e1004110.

[265] Shi Z, Xu S, Xing S, Yao K, Zhang L, Xue L, et al. Mettl17, a regulator of mitochondrial ribosomal RNA modifications, is required for the translation of mitochondrial coding genes. The FASEB Journal. 2019;33(11):13040-50.

[266] Haute LV, Hendrick AG, D'Souza AR, Powell CA, Rebelo-Guiomar P, Harbour ME, et al. METTL15 introduces N4-methylcytidine into human mitochondrial 12S rRNA and is required for mitoribosome biogenesis. Nucleic Acids Research. 2019;47(19):10267-81.

[267] Rorbach J, Boesch P, Gammage PA, Nicholls TJJ, Pearce SF, Patel D, et al. MRM2 and MRM3 are involved in biogenesis of the large subunit of the mitochondrial ribosome. Molecular Biology of the Cell. 2014;25(17):2542-55.

[**268**]   Shi Y, He C, Ma C, Yu T, Cong Y, Cai W, et al. Smad nuclear interacting protein 1 (SNIP1) inhibits intestinal inflammation through regulation of epithelial barrier function. Mucosal Immunology. 2018;11(3):835-45.

[**269**]   Kim RH, Wang D, Tsang M, Martin J, Huff C, de Caestecker MP, et al. A novel Smad nuclear interacting protein, SNIP1, suppresses p300-dependent TGF-β signal transduction. Genes & Development. 2000;14(13):1605-16.

[**270**]   Di Marcantonio D, Martinez E, Kanefsky JS, Huhn JM, Gabbasov R, Gupta A, et al. ATF3 coordinates serine and nucleotide metabolism to drive cell cycle progression in acute myeloid leukemia. Molecular Cell. 2021;81(13):2752-64.e6.

[**271**]   Kool J, Hamdi M, Cornelissen-Steijger P, van der Eb AJ, Terleth C, van Dam H. Induction of ATF3 by ionizing radiation is mediated via a signaling pathway that includes ATM, Nibrin1, stress-induced MAPkinases and ATF-2. Oncogene. 2003;22(27):4235-42.

[**272**]   Wang C-M, Brennan VC, Gutierrez NM, Wang X, Wang L, Yang W-H. SUMOylation of ATF3 alters its transcriptional activity on regulation of TP53 gene. Journal of Cellular Biochemistry. 2013;114(3):589-98.

[**273**]   Zhang Z-B, Ruan C-C, Chen D-R, Zhang K, Yan C, Gao P-J. Activating transcription factor 3 SUMOylation is involved in angiotensin II-induced endothelial cell inflammation and dysfunction. Journal of Molecular and Cellular Cardiology. 2016;92:149-57.

[**274**]   Chikka Madhusudana R, Anbalagan C, Dvorak K, Dombeck K, Prahlad V. The Mitochondria-Regulated Immune Pathway Activated in the C. elegans Intestine Is Neuroprotective. Cell Reports. 2016;16(9):2399-414.

[**275**]   Frank SR, Schroeder M, Fernandez P, Taubert S, Amati B. Binding of c-Myc to chromatin mediates mitogen-induced acetylation of histone H4 and gene activation. Genes & development. 2001;15(16):2069-82.

[**276**]   Xu D, Popov N, Hou M, Wang Q, Björkholm M, Gruber A, et al. Switch from Myc/Max to Mad1/Max binding and decrease in histone acetylation at the telomerase reverse transcriptase promoter during differentiation of HL60 cells. Proceedings of the National Academy of Sciences. 2001;98(7):3826-31.

[**277**]   Chinenov Y, Kerppola TK. Close encounters of many kinds: Fos-Jun interactions that mediate transcription regulatory specificity. Oncogene. 2001;20(19):2438-52.

[**278**]   Zhou H, Zarubin T, Ji Z, Min Z, Zhu W, Downey JS, et al. Frequency and Distribution of AP-1 Sites in the Human Genome. DNA Research. 2005;12(2):139-50.

[**279**]   Norwitz ER, Xu S, Xu J, Spiryda LB, Park JS, Jeong K-H, et al. Direct Binding of AP-1 (Fos/Jun) Proteins to a SMAD Binding Element Facilitates Both Gonadotropin-releasing Hormone (GnRH)- and Activin-mediated Transcriptional Activation of the Mouse GnRH Receptor Gene. Journal of Biological Chemistry. 2002;277(40):37469-78.

[**280**]   Zhang Y, Feng X-H, Derynck R. Smad3 and Smad4 cooperate with c-Jun/c-Fos to mediate TGF-β-induced transcription. Nature. 1998;394(6696):909-13.

[281] Ly LL, Yoshida H, Yamaguchi M. Nuclear transcription factor Y and its roles in cellular processes related to human disease. Am J Cancer Res. 2013;3(4):339-46.

[282] Yamanaka T, Miyazaki H, Oyama F, Kurosawa M, Washizu C, Doi H, et al. Mutant Huntingtin reduces HSP70 expression through the sequestration of NF-Y transcription factor. The EMBO Journal. 2008;27(6):827-39.

[283] Yamanaka T, Tosaki A, Kurosawa M, Matsumoto G, Koike M, Uchiyama Y, et al. NF-Y inactivation causes atypical neurodegeneration characterized by ubiquitin and p62 accumulation and endoplasmic reticulum disorganization. Nature Communications. 2014;5(1):3354.

[284] Cunningham JT, Rodgers JT, Arlow DH, Vazquez F, Mootha VK, Puigserver P. mTOR controls mitochondrial oxidative function through a YY1–PGC-1α transcriptional complex. Nature. 2007;450(7170):736-40.

[285] Blättler SM, Verdeguer F, Liesa M, Cunningham JT, Vogel RO, Chim H, et al. Defective Mitochondrial Morphology and Bioenergetic Function in Mice Lacking the Transcription Factor Yin Yang 1 in Skeletal Muscle. Mol Cell Biol. 2012;32(16):3333-46.

[286] Liu W, Guo Q, Zhao H. Oxidative stress-elicited YY1 potentiates antioxidative response via enhancement of NRF2-driven transcriptional activity: A potential neuronal defensive mechanism against ischemia/reperfusion cerebral injury. Biomedicine & Pharmacotherapy. 2018;108:698-706.

[287] Denison SR, Wang F, Becker NA, Schüle B, Kock N, Phillips LA, et al. Alterations in the common fragile site gene Parkin in ovarian and other cancers. Oncogene. 2003;22(51):8370-8.

[288] Pawlyk AC, Giasson BI, Sampathu DM, Perez FA, Lim KL, Dawson VL, et al. Novel Monoclonal Antibodies Demonstrate Biochemical Variation of Brain Parkin with Age. Journal of Biological Chemistry. 2003;278(48):48120-8.

[289] Katayama H, Kogure T, Mizushima N, Yoshimori T, Miyawaki A. A Sensitive and Quantitative Technique for Detecting Autophagic Events Based on Lysosomal Delivery. Chemistry & Biology. 2011;18(8):1042-52.

[290] Nguyen TN, Padman BS, Lazarou M. Deciphering the Molecular Signals of PINK1/Parkin Mitophagy. Trends in Cell Biology. 2016;26(10):733-44.

[291] Lőrincz P, Juhász G. Autophagosome-Lysosome Fusion. Journal of Molecular Biology. 2020;432(8):2462-82.

[292] Chen Y, Yu L. Recent progress in autophagic lysosome reformation. Traffic. 2017;18(6):358-61.

[293] Deas E, Plun-Favreau H, Gandhi S, Desmond H, Kjaer S, Loh SHY, et al. PINK1 cleavage at position A103 by the mitochondrial protease PARL. Human Molecular Genetics. 2010;20(5):867-79.

[**294**]   Meissner C, Lorenz H, Weihofen A, Selkoe DJ, Lemberg MK. The mitochondrial intramembrane protease PARL cleaves human Pink1 to regulate Pink1 trafficking. Journal of Neurochemistry. 2011;117(5):856-67.

[**295**]   Allen GFG, Toth R, James J, Ganley IG. Loss of iron triggers PINK1/Parkin-independent mitophagy. EMBO reports. 2013;14(12):1127-35.

[**296**]   Hara Y, Yanatori I, Tanaka A, Kishi F, Lemasters JJ, Nishina S, et al. Iron loss triggers mitophagy through induction of mitochondrial ferritin. EMBO reports. 2020;21(11):e50202.

[**297**]   Klionsky DJ, Abdel-Aziz AK, Abdelfatah S, Abdellatif M, Abdoli A, Abel S, et al. Guidelines for the use and interpretation of assays for monitoring autophagy (4th edition)[1]. Autophagy. 2021;17(1):1-382.

[**298**]   Bordi M, De Cegli R, Testa B, Nixon RA, Ballabio A, Cecconi F. A gene toolbox for monitoring autophagy transcription. Cell Death & Disease. 2021;12(11):1044.

[**299**]   Hasson SA, Kane LA, Yamano K, Huang C-H, Sliter DA, Buehler E, et al. High-content genome-wide RNAi screens identify regulators of parkin upstream of mitophagy. Nature. 2013;504(7479):291-5.

[**300**]   Fiesel FC, Moussaud-Lamodière EL, Ando M, Springer W. A specific subset of E2 ubiquitin-conjugating enzymes regulate Parkin activation and mitophagy differently. Journal of Cell Science. 2014;127(16):3488-504.

[**301**]   Geisler S, Vollmer S, Golombek S, Kahle PJ. The ubiquitin-conjugating enzymes UBE2N, UBE2L3 and UBE2D2/3 are essential for Parkin-dependent mitophagy. Journal of Cell Science. 2014;127(15):3280-93.

[**302**]   Tanaka A, Cleland MM, Xu S, Narendra DP, Suen D-F, Karbowski M, et al. Proteasome and p97 mediate mitophagy and degradation of mitofusins induced by Parkin. Journal of Cell Biology. 2010;191(7):1367-80.

[**303**]   Kim Nam C, Tresse E, Kolaitis R-M, Molliex A, Thomas Ruth E, Alami Nael H, et al. VCP Is Essential for Mitochondrial Quality Control by PINK1/Parkin and this Function Is Impaired by VCP Mutations. Neuron. 2013;78(1):65-80.

[**304**]   Wang Y, Xu E, Musich PR, Lin F. Mitochondrial dysfunction in neurodegenerative diseases and the potential countermeasure. CNS Neuroscience & Therapeutics. 2019;25(7):816-24.

[**305**]   Kitada T, Asakawa S, Hattori N, Matsumine H, Yamamura Y, Minoshima S, et al. Mutations in the parkin gene cause autosomal recessive juvenile parkinsonism. Nature. 1998;392(6676):605-8.

[**306**]   Valente EM, Abou-Sleiman PM, Caputo V, Muqit MMK, Harvey K, Gispert S, et al. Hereditary Early-Onset Parkinson's Disease Caused by Mutations in PINK1. Science. 2004;304(5674):1158-60.

[**307**]   Deneris ES, Hobert O. Maintenance of postmitotic neuronal cell identity. Nature Neuroscience. 2014;17(7):899-907.

[308] Dörrbaum AR, Kochen L, Langer JD, Schuman EM. Local and global influences on protein turnover in neurons and glia. eLife. 2018;7:e34202.

[309] Wang Z, Ying Z, Bosy-Westphal A, Zhang J, Schautz B, Later W, et al. Specific metabolic rates of major organs and tissues across adulthood: evaluation by mechanistic model of resting energy expenditure. The American Journal of Clinical Nutrition. 2010;92(6):1369-77.

[310] Hyder F, Rothman DL, Bennett MR. Cortical energy demands of signaling and nonsignaling components in brain are conserved across mammalian species and activity levels. Proceedings of the National Academy of Sciences. 2013;110(9):3549-54.

[311] Sugawara T, Lewén A, Gasche Y, Yu F, Chan PH. Overexpression of SOD1 protects vulnerable motor neurons after spinal cord injury by attenuating mitochondrial cytochrome c release. The FASEB Journal. 2002;16(14):1997-9.

[312] Sengupta A, Molkentin JD, Yutzey KE. FoxO Transcription Factors Promote Autophagy in Cardiomyocytes. Journal of Biological Chemistry. 2009;284(41):28319-31.

[313] Li W, Du M, Wang Q, Ma X, Wu L, Guo F, et al. FoxO1 Promotes Mitophagy in the Podocytes of Diabetic Male Mice via the PINK1/Parkin Pathway. Endocrinology. 2017;158(7):2155-67.

[314] Otsu K, Murakawa T, Yamaguchi O. BCL2L13 is a mammalian homolog of the yeast mitophagy receptor Atg32. Autophagy. 2015;11(10):1932-3.

[315] Murakawa T, Yamaguchi O, Hashimoto A, Hikoso S, Takeda T, Oka T, et al. Bcl-2-like protein 13 is a mammalian Atg32 homologue that mediates mitophagy and mitochondrial fragmentation. Nature Communications. 2015;6(1):7527.

[316] Gan ZY, Callegari S, Cobbold SA, Cotton TR, Mlodzianoski MJ, Schubert AF, et al. Activation mechanism of PINK1. Nature. 2022;602(7896):328-35.

[317] Ramsay RR, Singer TP. Relation of superoxide generation and lipid peroxidation to the inhibition of NADH-Q oxidoreductase by rotenone, piericidin A, and MPP+. Biochemical and Biophysical Research Communications. 1992;189(1):47-52.

[318] Starkov AA, Fiskum G. Myxothiazol Induces H2O2 Production from Mitochondrial Respiratory Chain. Biochemical and Biophysical Research Communications. 2001;281(3):645-50.

[319] Siebels I, Dröse S. Q-site inhibitor induced ROS production of mitochondrial complex II is attenuated by TCA cycle dicarboxylates. Biochimica et Biophysica Acta (BBA) - Bioenergetics. 2013;1827(10):1156-64.

[320] McLennan HR, Esposti MD. The Contribution of Mitochondrial Respiratory Complexes to the Production of Reactive Oxygen Species. Journal of Bioenergetics and Biomembranes. 2000;32(2):153-62.

[321] Matejuk A, Ransohoff RM. Crosstalk Between Astrocytes and Microglia: An Overview. Frontiers in Immunology. 2020;11.

[**322**] Matheoud D, Cannon T, Voisin A, Penttinen A-M, Ramet L, Fahmy AM, et al. Intestinal infection triggers Parkinson's disease-like symptoms in Pink1−/− mice. Nature. 2019;571(7766):565-9.

[**323**] Matheoud D, Sugiura A, Bellemare-Pelletier A, Laplante A, Rondeau C, Chemali M, et al. Parkinson's Disease-Related Proteins PINK1 and Parkin Repress Mitochondrial Antigen Presentation. Cell. 2016;166(2):314-27.

[**324**] Cappelletti V, Hauser T, Piazza I, Pepelnjak M, Malinovska L, Fuhrer T, et al. Dynamic 3D proteomes reveal protein functional alterations at high resolution *in situ*. Cell. 2021;184(2):545-59.e22.

[**325**] Nalls MA, Blauwendraat C, Vallerga CL, Heilbron K, Bandres-Ciga S, Chang D, et al. Identification of novel risk loci, causal insights, and heritable risk for Parkinson's disease: a meta-analysis of genome-wide association studies. The Lancet Neurology. 2019;18(12):1091-102.

[**326**] Fearnley JM, Lees AJ. Ageing and Parkinson's Disease: Substancia Nigra Regional Selectivity. Brain. 1991;114(5):2283-301.